NASA TECHNICAL NOTE

NASA TN D-6886

NASA TN D-6886

EFFECTS OF AN IN-FLIGHT THRUST REVERSER ON THE STABILITY AND CONTROL CHARACTERISTICS OF A SINGLE-ENGINE FIGHTER AIRPLANE MODEL

by Charles E. Mercer and Donald L. Maiden

Langley Research Center
Hampton, Va. 23365

NATIONAL AERONAUTICS AND SPACE ADMINISTRATION • WASHINGTON, D. C. • SEPTEMBER 1972

NASA TN D-6886

SEPTEMBER 1972

1. Report No.	2. Government Accession No.	3. Recipient's Catalog No.
NASA TN D-6886		

4. Title and Subtitle	5. Report Date
EFFECTS OF AN IN-FLIGHT THRUST REVERSER ON THE STABILITY AND CONTROL CHARACTERISTICS OF A SINGLE-ENGINE FIGHTER AIRPLANE MODEL	September 1972
	6. Performing Organization Code

7. Author(s)	8. Performing Organization Report No.
Charles E. Mercer and Donald L. Maiden	L-8395
	10. Work Unit No. 501-17-01-11
9. Performing Organization Name and Address	11. Contract or Grant No.
NASA Langley Research Center Hampton, Va. 23365	
	13. Type of Report and Period Covered
12. Sponsoring Agency Name and Address	Technical Note
National Aeronautics and Space Administration Washington, D.C. 20546	14. Sponsoring Agency Code

15. Supplementary Notes

16. Abstract

This investigation was conducted at the Langley 16-foot transonic tunnel at Mach numbers from 0.23 to 1.30. The purpose of the investigation was to establish changes in thrust-minus-drag performance as well as longitudinal and directional stability and control characteristics attributable to an in-flight thrust reverser of the blocker-deflector door type. The longitudinal and directional stability and control characteristics are presented in this report. Test conditions simulated landing-approach conditions as well as high-speed maneuvering such as may be required for combat or steep descent from high altitude. The results indicate that the longitudinal stability of the model would be slightly reduced with the thrust control unit in the stowed position; however, in the deployed reverse thrust positions, significant disturbances to the longitudinal stability occur. The directional stability and control characteristics were also significantly degraded by reverse thrust operation.

17. Key Words (Suggested by Author(s))	18. Distribution Statement
In-flight thrust reverser Maneuvering device	Unclassified – Unlimited

19. Security Classif. (of this report)	20. Security Classif. (of this page)	21. No. of Pages	22. Price*
Unclassified	Unclassified	236	$3.00

*For sale by the National Technical Information Service, Springfield, Virginia 22151

EFFECTS OF AN IN-FLIGHT THRUST REVERSER ON THE STABILITY AND CONTROL CHARACTERISTICS OF A SINGLE-ENGINE FIGHTER AIRPLANE MODEL

By Charles E. Mercer and Donald L. Maiden
Langley Research Center

SUMMARY

A wind-tunnel investigation has been conducted in the Langley 16-foot transonic tunnel on a 1/7.5-scale, powered, single-engine fighter airplane model fitted with an in-flight thrust control unit (TCU). The purpose of the investigation was to determine the changes in propulsion performance characteristics as well as changes in stability and control attributed to the installation of the TCU. This report presents only the results of the stability and control analysis. The investigation was conducted through a Mach number range of 0.23 to 1.30 at angles of attack from -3° to 15° and at angles of sideslip from -2° to 10°. The primary-nozzle jet-total-pressure ratio was varied from 1.0 (jet off) to approximately 5. The model wings were configured for the cruise and the landing-approach conditions. Six exhaust-deflector-door configurations and six blocker-door positions from stowed to fully deployed conditions were tested.

The results of the investigation indicate a small nose-down pitching-moment increment could be attributed to the TCU installation in the stowed position; the TCU installation in the stowed position that had aerodynamic characteristics nearest those of the basic model had the upper deflector doors set at the closed position and the lower door set at the faired (partially open $\approx 2^{\circ}$) position; exhaust-deflector-door deployment for the TCU installation in reverse-thrust mode generally produced a nose-up pitch increment for most Mach numbers; and reversed thrust decreased stabilizer effectiveness, directional stability, and control at most subsonic Mach numbers. A potentially hazardous operating condition can occur at Mach 0.23 and 0.34 with blocker doors closed more than 75 to 80 percent.

INTRODUCTION

An in-flight thrust reverser is a device intended to be used to modulate the thrust of a jet-powered airplane without impairing the flying qualities of the aircraft. Such a device has been investigated analytically and experimentally since the early 1950's. During this time, the complexity of the hardware, adverse stability and control influences, and engine

operating limitations have made the use of in-flight thrust reversers impractical. (See refs. 1 to 8.) However, continued increases in the thrust-weight ratio of the modern air superiority fighter, combined with advances in thrust reverser technology, have renewed interest in the use of in-flight thrust reversers. (See refs. 9 to 13.)

The anticipated improvements in maneuverability and STOL capability for tactical aircraft which may be achieved by use of thrust modulation have resulted in a program for the development of an in-flight thrust reverser for a single-engine fighter airplane. As part of this program, an investigation has been conducted in the Langley 16-foot transonic tunnel on a blocker-deflector door thrust control unit fitted to an existing single-engine fighter airplane model described in reference 3. The history of development for the thrust control unit used in the present investigation is given in reference 10.

The purpose of the present investigation was to determine the influence of the thrust control unit on performance, stability, and control of a single-engine fighter airplane model. Reference 14 presents the results of the performance characteristics of the investigation. This report presents the results of the effect of the in-flight thrust reverser on the stability and control characteristics of the model.

The investigation was conducted through the Mach number range from 0.23 to 1.30 at angles of attack from -3° to 15° and at angles of sideslip from -2° to 10°. A hydrogen-peroxide gas generator was used to provide hot gas for the engine-exhaust simulation. The primary-nozzle jet-total-pressure ratio was varied from 1.0 (jet off) to approximately 5.

SYMBOLS

A_u area of upper exhaust port, meters^2

AR aspect ratio

b wing span, 1.2924 meters

$C_{(F-D)}$ jet (gross) thrust minus fuselage-empennage drag coefficient, $\frac{F - D}{qS}$

C_L fuselage-empennage lift coefficient, $\frac{L}{qS}$

C_l fuselage-empennage rolling-moment coefficient, $\frac{M_X}{qSb}$

C_m fuselage-empennage pitching-moment coefficient, $\frac{M_Y}{qS\bar{c}}$

C_n	fuselage-empennage yawing-moment coefficient, $\frac{M_Z}{qSb}$
C_Y	fuselage-empennage side-force coefficient, $\frac{Y}{qS}$
ΔC_L	lift coefficient increment, $C_{L,TCU} - C_{L,basic}$
ΔC_m	pitching-moment coefficient increment, $C_{m,TCU} - C_{m,basic}$
ΔC_l	rolling-moment coefficient increment, $C_{l,TCU} - C_{l,basic}$
ΔC_n	yawing-moment coefficient increment, $C_{n,TCU} - C_{n,basic}$
ΔC_Y	side-force coefficient increment, $C_{Y,TCU} - C_{Y,basic}$
$\frac{\partial C_m}{\partial \delta_h}$	longitudinal control effectiveness
$\frac{\partial C_l}{\partial \beta}$	effective dihedral
$\frac{\partial C_n}{\partial \beta}$	directional stability derivative
$\frac{\partial C_n}{\partial \delta_r}$	directional control effectiveness
δC_L	adjusted lift coefficient, $C_{L,\beta\neq0} - C_{L,\beta=0}$
δC_m	adjusted pitching-moment coefficient, $C_{m,\beta\neq0} - C_{m,\beta=0}$
δC_l	adjusted rolling-moment coefficient, $C_{l,\beta\neq0} - C_{l,\beta=0}$
δC_n	adjusted yawing-moment coefficient, $C_{n,\beta\neq0} - C_{n,\beta=0}$
δC_Y	adjusted side-force coefficient, $C_{Y,\beta\neq0} - C_{Y,\beta=0}$
c	wing chord, meters
$\bar{c}$	wing mean aerodynamic chord, 0.3332 meter
c_r	wing root chord, meters

c_t	wing tip chord, meters
D	fuselage-empennage aerodynamic drag, newtons
d	diameter, meters
F	jet (gross) thrust, positive toward nose, newtons
g	acceleration due to gravity, m/sec^2
L	fuselage-empennage aerodynamic lift, newtons
M	free-stream Mach number
M_X	fuselage-empennage aerodynamic rolling moment, m-N
M_Y	fuselage-empennage aerodynamic pitching moment, m-N
M_Z	fuselage-empennage aerodynamic yawing moment, m-N
$p_{t,p}$	primary-nozzle jet total pressure, N/m^2
$p_{t,s}$	secondary-cooling-air total pressure, N/m^2
p_∞	free-stream static pressure, N/m^2
q	free-stream dynamic pressure, N/m^2
r	radius, meters
S	wing (reference) area, 0.4125 $meter^2$
$T_{t,p}$	primary-nozzle jet total temperature, kelvins
$T_{t,s}$	secondary-cooling-air total temperature, kelvins
Y	fuselage-empennage aerodynamic side force, newtons
α	angle of attack, degrees

β angle of aideslip, degrees

δ_b TCU blocker-door position, percent blockage

δ_{dl} TCU lower deflector-door angle, positive from reference line parallel to thrust center line, degrees

δ_{du} TCU upper deflector-door angle, positive from reference line parallel to thrust center line, degrees

δ_f wing-trailing-edge flap deflection angle, positive upward, degrees

δ_h horizontal-tail deflection angle, positive leading edge upward, degrees

δ_r rudder deflection angle, positive trailing edge right, degrees

δ_s wing-leading-edge slat deflection angle, positive upward, degrees

Λ sweep angle, degrees

Subscript:

∞ free-stream conditions

Abbreviations:

A/B afterburning

MIL military

TCU thrust control unit

APPARATUS AND METHODS

Wind Tunnel

The Langley 16-foot transonic tunnel is a single-return atmospheric wind tunnel with an octagonal slotted-throat test section and continuous air exchange. The tunnel has a continuously variable speed range from Mach 0.20 to 1.30. A description of the Langley 16-foot transonic tunnel is given in references 15 and 16.

Model and Support System

The test model was a 1/7.5-scale model of a single-engine fighter airplane. Except where noted, the model was in a clean configuration; that is, wing-flap and slat deflection angles were 0°. For a Mach number of 0.23, a landing-approach configuration was simulated where wing-flap and slat deflection angles were -30° and -20°, respectively. Figure 1 shows the basic unmodified airplane configuration installed in the Langley 16-foot transonic tunnel. Corresponding views of the model with a thrust control unit (TCU) are presented in figure 2.

The model was supported at the wing tip on a bifurcated sting-support system as shown in figure 3. A more detailed description of this type of support system is given in reference 17. Geometric characteristics of the model are also given in the figure. The wing formed an integral part of the support system and provided a fixture for the six-component balance. The fuselage was mounted on the balance so that all fuselage-empennage and thrust-drag forces could be measured. Since the wing was part of the support system, wing forces were not measured; however, wing-body flow interference effects are included in the measurements.

Except for a fiber-glass nose section, the model was constructed principally of steel and was powered by a hydrogen peroxide turbojet-engine simulator similar to that described in reference 18. Two engine simulators, one representing a convergent nozzle at the military power setting and the other representing a convergent nozzle at the afterburning power setting, were used to produce a hot jet exhaust with physical characteristics closely matching the exhaust of a turbojet engine.

The jet-engine simulator was enveloped by a secondary-cooling-air ejector. Metered air, simulating secondary cooling air, was supplied through high-pressure air lines inside the right wing. (See fig. 3.) Two afterbody-ejector configurations were used in the investigation: one was the basic airplane configuration, and the second was the airplane modified to incorporate an in-flight TCU. (See fig. 4.)

The in-flight TCU used in this investigation was a shrouded blocker-deflector door type combined with a tertiary-air ejector and was fitted aft of the convergent nozzle (figs. 4 and 5). The tertiary-air inlets also serve as reverse-thrust exhaust ports as indicated by the deflected exhaust shown in figure 5. Three external deflection doors in a Y-orientation (fig. 4(a)) were utilized to vary the exhaust-port area from that required for the optimum thrust-minus-drag performance in the forward-thrust mode to the larger port area required for exhaust during the reverse-thrust model. Six sets of fixed brackets were utilized to provide deflector-door annular positions from fully closed (however, a small clearance exists on either side of the deflector doors) to maximum deployment $(\delta_{du} = \delta_{dl} = 60^{\circ})$. Six sets of exhaust-gas blocker doors were used to represent six

blocker-door positions simulating a deployment sequence from fully stowed to fully deployed. (See figs. 5 and 6.)

Instrumentation

A six-component strain-gage balance was used to measure forces and moments on the fuselage and empennage of the model. (See fig. 3.) As explained in the previous section, forces and moments on the wing were not measured but the wing-body flow interference effects were included.

Pressure transducers were used to measure the primary-nozzle jet total pressure and the secondary-cooling-air static and total pressures. Thermocouples were used to measure the primary-nozzle jet and secondary-cooling-air total temperatures. (See fig. 4.)

The angle of attack of the fuselage was measured by a calibrated attitude indicator mounted in the canopy. The angle of sideslip was obtained by use of yaw knuckles built into the model support system. Two electronic turbine flowmeters were used to measure the mass flow rate of hydrogen peroxide to the primary nozzle and the average value was used. A calibrated venturi was used to measure the secondary-cooling-air flow rate.

Tests

Tests were conducted in the Langley 16-foot transonic tunnel at Mach numbers from 0.23 to 1.30 with angles of attack and sideslip varied from -3° to 15° and -2° to 10°, respectively. In the clean configuration, horizontal-tail deflections of -1.5° and -4° and rudder deflections of 0° and -5° were tested, whereas, for the approach configuration, horizontal-tail deflections of -1.5°, -4°, and -10° and rudder deflections of 0° and -15° were tested. Two engine simulators representing convergent nozzles at either military power setting or afterburning power setting were tested. The primary-nozzle jet-total-pressure ratio was varied from 1.0 (jet off) to approximately 5. The secondary-cooling-air mass flow rate remained constant during variations of the primary total-pressure ratio but was changed with Mach number from approximately 0.054 kg/sec to 0.099 kg/sec.

PRESENTATION OF RESULTS

Changes in test conditions for figures 7 to 40 are noted in table I. The results of the investigation are presented in the following figures:

TABLE I.- EFFECT OF PRESSURE RATIO ON AERODYNAMIC CHARACTERISTICS

(a) Basic model

β, deg	δ_h, deg	δ_r, deg	Power setting	Figure
Clean configuration (flaps and slats stowed)				
0	-1.5	0	MIL and A/B	7
	-4		MIL	8
	Off			9
	-1.5	-5		10
2		0		11
-2				12
5				13
5		-5		14
Landing-approach configuration (flaps deflected -30° and slats deflected -20°)				
0	-1.5	0	MIL	15(a)
0	-10			15(b)
2				15(c)
2		-15		15(d)
-2		0		15(e)
10		0		15(f)
10		-15		15(g)

TABLE I.- EFFECT OF PRESSURE RATIO ON AERODYNAMIC CHARACTERISTICS – Concluded

(b) Model with the thrust control unit (TCU)

β, deg	δ_h, deg	δ_r, deg	δ_{du}, deg	δ_{dl}, deg	δ_b, percent	Remarks	Power setting	Figure
Landing-approach configuration								
0	-1.5	0	32.5	52.5	0		MIL	16(a)
0	-10	↓	↓	↓	↓		↓	16(b)
10	↓	↓	↓	↓	↓		↓	16(c)
10	↓	-15	↓	↓	↓		↓	16(d)
0	-1.5	0	↓	↓	25		↓	16(e)
↓	-10	↓	↓	↓	25		↓	16(f)
↓	-1.5	↓	↓	↓	50		↓	16(g)
↓	-10	↓	↓	↓	50		↓	16(h)
↓	-1.5	↓	↓	↓	75		↓	16(i)
↓	-4	↓	↓	↓	↓		↓	16(j)
↓	-10	↓	↓	↓	↓		↓	16(k)
2	↓	↓	↓	↓	↓		↓	16(l)
2	↓	-15	↓	↓	↓		↓	16(m)
-2	↓	0	↓	↓	↓		↓	16(n)
10	↓	0	↓	↓	↓		↓	16(o)
↓	↓	-15	↓	↓	↓		↓	16(p)
↓	↓	-15	↓	↓	↓	δ_{du} with side plates	↓	16(q)
0	-1.5	0	↓	↓	90		↓	16(r)
0	-10	0	↓	↓	90		↓	16(s)
Clean configuration								
0	-1.5	0	Faired; 2°	Faired; 2°	0		MIL and A/B	17
↓	↓	↓	Closed	Closed	↓		MIL and A/B	18
↓	↓	↓	Closed	Faired	↓		MIL	19
↓	↓	↓	Faired	28.5	↓		↓	20
↓	↓	↓	32.5	52.5	↓		↓	21
5	↓	↓	↓	↓	↓		↓	22
5	↓	-5	↓	↓	↓		↓	23
0	↓	0	↓	↓	25		↓	24
↓	↓	↓	↓	↓	50		↓	25
↓	↓	↓	↓	↓	75		↓	26
↓	↓	↓	↓	↓	90		↓	27
↓	↓	↓	↓	↓	100		↓	28
↓	-4	↓	↓	↓	↓		↓	29(a) to 29(c)
↓	Off	↓	↓	↓	↓		↓	29(d)
↓	-1.5	-5	↓	↓	↓		↓	30
↓	↓	0	↓	↓	↓	δ_{du} with side plates	↓	31
↓	↓	↓	↓	↓	↓	A_u decreased 14 percent	↓	32
2	↓	↓	↓	↓	↓		↓	33
-2	↓	↓	↓	↓	↓		↓	34
5	↓	↓	↓	↓	↓		↓	35
↓	↓	-5	↓	↓	↓		↓	36
↓	↓	↓	↓	↓	↓	δ_{du} with side plates	↓	37
0	↓	0	43.5	43.5	↓		↓	38
0	↓	↓	28	60	↓		↓	39
0	↓	↓	60	60	↓		↓	40

RESULTS AND DISCUSSION

The aerodynamic characteristics of the model are presented as a function of jet-total-pressure ratio for several angles of attack, angles of sideslip, and Mach numbers. These characteristics show the forces and moments of the fuselage-tail combination and include the wing-body flow interference effects. The data are presented for the basic model and with the TCU installed with the wings in the clean configuration (flaps and slats retracted) and in the landing-approach configuration (flaps deflected -30° and slats deflected -20°). The absolute levels of the aerodynamic forces and moments (figs. 7 to 40) are of little significance to this paper since the purpose of the basic model was to provide a reference with which to compare the effects of installing the TCU. The following discussion is directed to the study of the longitudinal and directional stability and control of the model equipped with the TCU for flight conditions during which reverse thrust could be employed.

The aerodynamic forces and moments on the basic model for both wing configurations (clean and landing approach) shown in figures 7 to 15 are affected by jet operation which indicates that the jet exhaust influences the region surrounding the aft fuselage-tail part of the model especially at the lower Mach numbers ($M \leq 0.60$). These jet effects are similar to those presented in reference 17.

Installation of the TCU in the forward-thrust mode ($\delta_b = 0$ percent) and for both wing conditions generally produced aerodynamic forces and moments that had trends similar to those of the basic model (figs. 16(a) and 17 compared with figs. 15(a) and 7, respectively). The variation with pressure ratio was consistent, only small changes in C_m and C_L being noted. At low thrust modulation ($\delta_b = 25$ percent), variation with pressure ratio again showed small changes in the forces and moments (figs. 16(e) and 24 compared with figs. 16(a) and 21, respectively). For high thrust modulation ($\delta_b \geq 50$ percent), both C_m and C_L showed increasing nonlinearities with pressure ratio variation as δ_b increased. At the largest blocker-door settings both coefficients displayed reversals with pressure ratio variation. Lateral characteristics showed large and nonlinear variations whenever laterally unsymmetrical flow existed, $\beta \neq 0^{\circ}$, with increases in pressure ratio (figs. 16(g) to 16(s) and figs. 25 to 40 compared with figs. 16(a) and 21).

Longitudinal Stability and Control

The variations of the estimated engine operating-pressure ratio $p_{t,p}/p_{\infty}$ with Mach number for a typical turbojet engine for military and afterburning power settings are presented in figure 41. All comparisons between the various configurations will generally be made at these operating-pressure ratios.

Forward thrust.- The effect of the TCU installation on the pitching moment of the basic model in the forward-thrust mode over the investigated Mach number range is shown in figure 42. The ΔC_m represents the difference in pitching-moment characteristics between the TCU configuration and the basic model. The pitching-moment increments are shown for military and afterburning nozzle power settings. The data indicate that the TCU modification to the model produced a small nose-down pitching-moment increment ($\Delta C_m \approx 0.02$ maximum). Based on the results presented in reference 19, this increment would represent about a 1^o change in horizontal-tail setting. The data of figure 42 show that this largest nose-down increment occurs when the deflector doors were positioned in the faired door setting ($\delta_{du} = \delta_{dl}$ = Faired = 2^o). Closing the deflector doors down ($\delta_{du} = \delta_{dl}$ = Closed) or deploying the doors open ($\delta_{du} = 32.5^o$; $\delta_{dl} = 52.5^o$) decreased the nose-down increment and indicated that for some combination of deflector-door settings, an arrangement might be obtained which would retain the basic model longitudinal stability characteristics.

In an attempt to minimize the effects of the TCU installation, several other deflector-door combinations were tested. Shown in figure 43 are the effects of deflector-door position on the lift and pitching-moment increments as a function of angle of attack for several Mach numbers and military power engine operation. For all deflector-door combinations, the data show that with changes in angle of attack, the changes in slope of ΔC_m were small (slight nose-down trend) except for $M = 1.3$ where a large nose-down moment slope occurs. At subsonic speeds and jet-on operation, a nose-down pitching-moment increment generally occurred for most combinations of deflector-door settings except for the configuration with a door combination of δ_{du} = Closed and δ_{dl} = Faired. This configuration, when compared with the basic model, generally produced a small change or no change in pitch, and at $M = 1.3$ it provided the smallest nose-down pitching moment for all deflector-door combinations.

Reverse thrust.- The effect of deflector-door position on the lift and pitching-moment increments for the TCU (δ_b = 100 percent, clean configuration) is presented in figure 44. At jet-off engine operation, the data generally show a slight nose-up pitch increment which tended to increase with increasing changes in angle of attack at most test conditions, with an exception to be noted at $M = 1.30$. These results are opposite to those obtained with the blocker doors stowed (δ_b = 0 percent) as shown by the previous figure.

The effect of full reverse-thrust operation (δ_b = 100 percent) on the lift and pitching-moment coefficient increments for the various deflector-door settings is large at all Mach numbers and seemingly inconsistent increments are shown to occur at several Mach numbers. (For example, see figs. 44(a) and 44(c).) At a Mach number of 0.34 and for the lower values of upper deflector-doors position, $\delta_{du} \leq 32.5^o$, a large nose-down pitch increment is present; whereas, for the higher door settings, $\delta_{du} > 32.5^o$, a large nose-up pitch increment is observed. A possible cause for the difference in direction ΔC_m for

the deflector-door combination is the resultant normal-thrust vector obtained with the different door combinations. Any analysis of the aerodynamic coefficients presented must consider the vector thrust forces from the TCU as well as the aerodynamic forces induced on the model.

The magnitude of the resultant normal-force vector (aerodynamic lift plus thrust) varies with deflector-door setting combinations and angle of attack. This variation causes significant changes to ΔC_L at a Mach number of 0.34 where ΔC_L is shown to decrease with increased upper deflector-door angular setting relative to the lower door setting; however, a reversal in direction is noted for the deflector-door setting of $\delta_{du} = 60^o$. This reversal indicates that a maximum decrease in ΔC_L would occur for some value of door setting between $\delta_{du} = 43.5^o$ and $\delta_{du} = 60^o$. In addition, ΔC_L is shown to decrease with increasing angle of attack. In one case it is believed, based on reference 14, the increase in deflector-door angular setting for the upper reverse ports increased the normal component of the thrust vector. In the angle-of-attack case, the back pressure to the reverse-thrust port or nozzle increased significantly for the lower port as the lower reversed exhaust was directed more upstream. This change of back pressure restricted the amount of flow through the lower port and caused the upper reverse-thrust ports to pass more flow; thus, a decrease in ΔC_L with increase in angle of attack resulted.

The axial location of the resultant normal-force vector also varies with deflector-door combinations. All deflector-door combinations in figure 44(a) appear to have a point at which $\Delta C_L = 0$. That $\Delta C_L = 0$ at this point does not necessarily mean that the normal vector of reverse thrust is zero, but that the resultant normal-force vector (aerodynamic lift on model plus thrust) on the model equipped with the TCU is equal to the normal force on the basic model. Thus, ΔC_m shown at $\Delta C_L = 0$ at Mach 0.34 (fig. 44(a)) is primarily caused by the shift in axial location of the resultant normal-force vector. The shift in axial location is probably caused by a change in the center of pressure on the model due to the resultant flow interference of reverse thrust which shifts the location of the aerodynamic force, and by the normal-thrust component of reverse thrust imposed on the aft end of the model. At equal values of lift ($\Delta C_L = 0$), a change in pitching moment (fig. 44(a)) occurs with nose-down pitching-moment increments (rearward shift of resultant normal force) attributed to the smaller upper deflector-door angular settings and conversely nose-up pitching-moment increments (forward shift at resultant normal force) attributed to the large upper deflector-door angular settings.

At the other Mach numbers presented in figures 44(b) to 44(d), an increase in deflector-door setting resulted in large nose-up pitch increments for jet-on operation. Angle of attack produced a positive pitching-moment slope at all Mach numbers except $M = 1.3$. The order of the increments in ΔC_m is not consistent with deflector-door setting for different Mach numbers. On the average over the subsonic speed range, the deflector-door angular positions that provided pitch increments which would require the

least amount of change in control setting ($\delta_h \pm 2^o$, ref. 19) were $\delta_{du} = 32.5^o$ and $\delta_{dl} = 52.5^o$. These deflector-door settings, $\delta_{du} = 32.5^o$ and $\delta_{dl} = 52.5^o$, based on these data are not the optimum settings, but exhibit better lift and pitch characteristics than the other deflector-door angular combinations which were investigated. For full reverse thrust it could be estimated that deflector-door combinations of $\delta_{du} \approx 35^o$ to 45^o and $\delta_{dl} \approx 45^o$ to 55^o with a 10^o difference between the upper and lower deflector-door angular settings would minimize the change in pitching moment with TCU installation.

Modulated thrust.- The effect of blocker-door closure (modulated thrust) on the lift and pitching-moment increments is presented in figures 45 and 46 as a function of angle of attack for various Mach numbers and at scheduled jet-total-pressure ratios. Angle of attack normally had only moderate effects ($\Delta C_m \approx 0.04$ maximum) on the pitching-moment increments except for $\delta_b \geqq 75$ percent at $M = 0.23$. (See fig. 45.) As was mentioned in connection with figure 44 where for the low subsonic Mach numbers unsystematical forces and moments occurred for the configurations having the lower values of upper deflector-door settings, $\delta_{du} \leqq 32.5^o$, and maximum blocker-door closure, $\delta_b = 100$ percent, the same trend is seen to occur for blocker-door closures less than full open (for example, $\delta_b \geqq 75$ percent) at Mach 0.23 and 0.34. (See figs. 45(a) and 45(b).)

Figure 46 summarizes the effects of blocker-door deployment on the pitching-moment increment for several Mach numbers at selected angles of attack. For most Mach numbers up to about 50-percent closure of the blocker doors ($\delta_b \approx 50$ percent), a slight nose-down pitching moment is shown to diminish with increasing blocker-door closure. After about 50-percent closure, a nose-up pitching moment is incurred. This nose-up pitching moment is shown to increase rapidly after 60-percent blockage up to a maximum ΔC_m at about 75- to 90-percent blockage, depending on Mach number. At Mach 0.23 and 0.34, large nose-down pitching moments occur after the maximum nose-up pitch increments are incurred at 75- to 80-percent blockage. This rapid change in pitching moment will significantly affect longitudinal stability and could cause an uncontrollable situation. Therefore, it is recommended that caution be exercised so that blocker-door closures greater than 70 percent could not occur for Mach numbers below about 0.60.

Stabilizer effectiveness.- The effect of horizontal-tail deflection on the incremental lift and pitching-moment coefficients of the TCU (reverse-thrust mode) as a function of angle of attack is shown in figure 47. With deflection of the horizontal tail from the normal flight setting, $\delta_h = -1.5^o$, in the presence of the TCU installation, a further decrease (more nose down) in pitching-moment increment is shown to occur at all test conditions except for $M = 0.23$, $\delta_b = 50$ percent and $M = 0.34$, $\delta_b = 100$ percent. Also complete removal of the horizontal tail produced a more negative pitching-moment increment when compared with the two tail-on settings (see fig. 47(c), $M = 0.90$, $\delta_b = 100$ percent). Angle-of-attack change has negligible effect on the pitching-moment increments at each

tail setting except for $M = 0.23$ and $\delta_b = 90$ percent where an increasing negative slope occurs with increased angles of attack.

Stabilizer effectiveness of the basic model and TCU as a function of Mach number for typical operating conditions is presented in figure 48. Also presented in this figure is information shown in reference 19 which reveals the stabilizer effectiveness of the complete model (fuselage-tails-wings without jet simulation). Comparing the results of reference 19 with those of the present paper indicates close agreement at all test conditions for the basic model. Modification of the model to incorporate the TCU in the reverse-thrust mode ($\delta_b = 75$ percent or $\delta_b = 100$ percent) revealed that stabilizer effectiveness would be reduced by about 30 to 40 percent through the Mach number range except near $M = 0.34$ where a slight increase in tail control is noted. Inasmuch as the increase in tail effectiveness occurred at scheduled engine operating-pressure ratio, operation of the TCU at a slightly reduced value of $p_{t,p}/p_\infty$ would have revealed stabilizer effectiveness to be similar to that observed at the other subsonic Mach numbers. A possible cause for this inconsistency in tail effectiveness with engine throttle position might be seen in figures 28(a) and 29(a) where the pitching-moment coefficient of the TCU with $\delta_h = -1.5^\circ$ is seen to be effected more by increasing engine throttle than the TCU with $\delta_h = -4^\circ$ (steeper slope at the higher pressure ratios). This result indicates that the flow-field interference effects are less at the higher horizontal-tail settings.

Presented in figure 49 is the effect of modulating reverse thrust on the stabilizer effectiveness at $M = 0.23$ (landing-approach configuration). For the blocker-door closures below 50 percent, stabilizer effectiveness is slightly degraded (approximately 20 percent depending on angle of attack) whereas for closures greater than 50 percent, tail effectiveness is reduced by about 40 percent. The reduction in tail effectiveness is caused by the increase of reverse-thrust exhaust which disturbs the flow field around the tail.

A schedule of acceleration forces due to horizontal-tail deflection for the basic airplane is shown in figure 50. This information is reproduced from data presented in reference 19 and shows that for most Mach numbers the horizontal-tail deflection would generate acceleration forces acceptable for normal flight conditions except through the sonic speed range ($M = 0.90$ to $M = 1.0$). For example, at $M = 0.9$ a change in δ_h from -0.8° (steady flight, $g = 0$) to -1.4° would induce acceleration forces approaching 5g and this change was only 0.6°. The results of figure 48 show the stabilizer effectiveness of the TCU ($\delta_b = 100$ percent) to be $\frac{\partial C_m}{\partial \delta_h} \approx 0.014$ at $M = 0.90$. In reverse-thrust operation of the TCU as shown in figure 46(b), a maximum change in pitching moment of $\Delta C_m = 0.037$ occurs at Mach 0.9 for approximately 80-percent blocker-door closure. In order to maintain near-zero pitch increment with this deployment of blocker doors, a change of horizontal-tail setting of approximately 2.6° would be required. If the change in horizontal-tail setting is not performed as rapidly as the blocker doors close, the airplane

could experience acceleration forces substantially in excess of 5g. Because of the high acceleration forces which will be encountered at $M = 0.90$ and reverse-thrust operation, it is recommended that the pilot be very cautious during reverse-thrust operation at the higher Mach numbers.

Directional Stability and Control

Directional stability.- The effect of angle of attack on the incremental aerodynamic characteristics of the TCU for several angles of sideslip is presented in figure 51. The model has the deflector doors open ($\delta_{du} = 32.5^{o}$; $\delta_{dl} = 52.5^{o}$) and the blocker doors either stowed (forward-thrust mode, $\delta_b = 0$ percent) or deployed (reversed-thrust mode, $\delta_b =$ 75 percent for $M = 0.23$ and $\delta_b = 100$ percent for $M \geq 0.34$) for this comparison.

The data for the TCU with blocker doors stowed ($\delta_b = 0$ percent) show that increasing the angle of sideslip from 0^{o} to 5^{o} had very little effect on the yawing-moment increment, ΔC_n. The trend was to decrease slightly (has negative slope) with increased Mach number (figs. 51(a) to 51(e)). With deployment of the blocker doors ($\delta_b = 75$ percent or 100 percent, depending on Mach number) and operation at scheduled total-pressure ratios, increases in angle of sideslip generally produced a loss in yawing-moment increment (ΔC_n is negative) at all subsonic Mach numbers especially for $\beta = 10^{o}$. Angle of attack generally had no appreciable effect on ΔC_n except for $M = 0.23$ where an increase in negative slope is noted for increased angles of attack and positive angles of sideslip. (See fig. 51(f).)

In order to more readily distinguish effects of sideslip on the aerodynamic coefficients, they have all been adjusted so that they must pass through the origin; thus, slope changes are readily discernible. The variation of the adjusted aerodynamic coefficients with angle of sideslip for both the basic and TCU models is shown in figure 52. The basic model data are also presented to provide trends with which comparison of the TCU might be made. The data show the adjusted force and moment coefficients on the model in the clean configuration to be fairly linear with increased angles of sideslip; however, a nonlinearity occurred in pitching moment of the model in the landing-approach configuration at $M = 0.23$. Since this abnormality occurs for both the basic and TCU models, it is apparently a configuration characteristic and warrants no further explanation.

Directional stability derivatives (fuselage-tail combination) for the basic model and the TCU are presented in figure 53. The TCU with blocker door stowed, $\delta_b = 0$ percent, improved directional stability $\partial C_n / \partial \beta$ by about 10 percent of that for the basic model over the Mach range tested. (See fig. 53(a).) The TCU with the blocker doors deployed ($\delta_b = 75$ percent) and wings configured for landing-approach conditions ($M = 0.23$) showed a reduction in directional stability from about 10 percent at an angle of attack of 6^{o} to 50 percent at 12^{o}. At subsonic Mach numbers greater than 0.23 (clean configuration),

reversed thrust (δ_b = 100 percent) reduced the directional stability up to 40 percent; however, no change in $\partial C_n/\partial\beta$ was seen to occur at M = 1.30 (fig. 53(a)). For Mach numbers greater than 0.23, angle of attack had no appreciable effect on $\partial C_n/\partial\beta$; therefore, an average value was used in the comparisons of figure 53.

Presented in figure 53(b) is the effective dihedral comparison of the basic and TCU models. As was seen previously in the directional stability comparison (fig. 53(a)), the TCU with blocker doors stowed (δ_b = 0 percent) also had little apparent effect on the rolling-moment characteristics whereas with blocker doors deployed (δ_b = 75 percent or 100 percent), a decrease in the rolling-moment derivatives occurred at most Mach numbers and angles of attack.

Rudder effectiveness.- The incremental aerodynamic characteristics of the TCU due to rudder deflection are presented as a variation with angle of attack in figures 54 and 55. At the scheduled pressure ratio rudder deflection had little to no influence on the incremental force and moment coefficients of the TCU with blocker doors stowed, δ_b = 0 percent. (See fig. 54.) Whereas for the TCU with blocker doors deployed, $\delta_b \geqq 75$ percent (fig. 55), rudder deflection resulted in a negative ΔC_n at all subsonic Mach numbers and at scheduled engine operating-pressure ratios; whereas at Mach 1.30 (fig. 55(g)) a slight increase in ΔC_n was observed. Rudder deflection caused a slight increase in ΔC_l at subsonic speeds and a slight loss at M = 1.30. Very little effect on pitching-moment increment resulted from deflection of the rudder at most conditions, the trend being a nose-up increment especially at the lower Mach numbers.

Rudder effectiveness of the basic and TCU models (fig. 56) showed that the TCU with blocker doors stowed (δ_b = 0 percent) caused a negligible loss in rudder power but the reverse-thrust mode, $\delta_b \geqq 75$ percent, produced a reduction in rudder power from 20 to 40 percent at subsonic speeds and a small increase in rudder effectiveness at M = 1.30.

Alternate Configurations

In an attempt to decrease the unfavorable pitching-moment increments and to decrease or eliminate the loss in directional stability caused by the installation of the TCU (reverse-thrust mode), two alternate configurations were tested. One configuration had small side plates attached to the upper deflector doors that created a scoop design whereas the second configuration reduced by 14 percent the open area of the upper exhaust ports (see fig. 5(b)). The results from the tests of these two configurations are shown in figure 57.

At the scheduled jet-total-pressure ratios the addition of the side plates had a favorable influence (with respect to the TCU without side plates) on both the pitching-moment increment ($+\Delta C_m$) and yawing-moment increment ($+\Delta C_n$) at all subsonic test conditions except for $\beta = 5^\circ$ and M = 0.34 and 0.60 where a nose-down pitch increment was

observed. The increase in pitch and yaw increments is probably due to the channeled flow caused by the side plates being directed forward into the external flow field which generate disturbances that produce a favorable effect on the aft fuselage tail surfaces.

Reduction of the port area provided by the upper deflector doors by 14 percent had no appreciable effect on either ΔC_m or ΔC_n at these test conditions. This result indicates that restriction of the amount of exhaust flow through the upper ports was either too small or that the restricted flow had no influence on the external flow field acting on the aft section of the model.

SUMMARY OF RESULTS

A wind-tunnel investigation has been conducted in the Langley 16-foot transonic tunnel on a single-engine fighter model with and without a thrust control unit (TCU) with blocker and deflector doors. The investigation was conducted through the 0.23 to 1.30 Mach number range at angles of attack from -3° to 15° and angles of sideslip from -2° to 10°. The primary-nozzle jet-total-pressure ratio was varied from 1.0 (jet off) to approximately 5.

The results of the investigation indicate the following:

1. A small nose-down pitching-moment increment requiring approximately a 1° change in horizontal-tail setting to obtain zero increment was produced by the TCU installation in the stowed position for both military and afterburning power settings.

2. The TCU in the stowed position closest approaching the characteristics of the basic model in longitudinal stability and control was configured so that the upper deflector doors were in the closed position and the lower deflector door was in the faired position.

3. Deflector-door deployment with TCU in reverse-thrust mode (blocker-door closure, 100 percent) at military power generally produced a nose-up pitching-moment increment for most Mach numbers (exception $M = 0.34$).

4. Deflector-door annular positions of 32.5° for the upper doors and 52.5° for the lower door required the smallest change in longitudinal-control setting to maintain zero pitching-moment increments during full reverse thrust.

5. A small nose-up pitching-moment increment ($\Delta C_m = 0.02$) was incurred for blocker-door deployment from stowed to about 50-percent closure; however, a large pitch-up moment was incurred with a maximum at about 75- to 90-percent closure which was followed by a severe nose-down pitching moment at blocker-door closures greater than 80 percent particularly at $M = 0.23$ and 0.34. This condition presented potentially hazardous operation.

6. Reversed thrust decreased stabilizer effectiveness by approximately 30 to 40 percent at all subsonic Mach numbers except $M = 0.34$ where it caused a slight increase in tail effectiveness.

7. The TCU modification in reverse-thrust mode produced a significant loss in directional stability and control at subsonic Mach numbers.

Langley Research Center,
National Aeronautics and Space Administration,
Hampton, Va., June 22, 1972.

REFERENCES

1. Polak, I. P.: Development of Turbo-Jet Engine Thrust Destroying and Reversing Nozzle No. AEL 102. Rep. No. AEL-1108 (Project TED Nos. NAM-PP-375 and NAM-04614), Naval Air Material Center, NAES (Philadelphia), Jan. 13, 1950.

2. Povolny, John H.; Steffen, Fred W.; and McArdle, Jack G.: Summary of Scale-Model Thrust-Reverser Investigation. NACA Rep. 1314, 1957. (Supersedes NACA TN 3664.)

3. Swihart, John M.: Effect of Target-Type Thrust Reverser on Transonic Aerodynamic Characteristics of a Single-Engine Fighter Model. NACA RM L57J16, 1958.

4. Kohl, Robert C.; and Algranti, Joseph S.: Investigation of a Full-Scale, Cascade-Type Thrust Reverser. NACA TN 3975, 1957.

5. Kohl, Robert C.: Performance and Operational Studies of a Full-Scale Jet-Engine Thrust Reverser. NACA TN 3665, 1956.

6. Tolhurst, William H., Jr.; Kelly, Mark W.; and Greif, Richard K.: Full-Scale Wind-Tunnel Investigation of the Effects of a Target-Type Thrust Reverser on the Low-Speed Aerodynamic Characteristics of a Single-Engine Jet Airplane. NASA TN D-72, 1959.

7. Kelly, Mark W.; Greif, Richard K.; and Tolhurst, William H., Jr.: Full-Scale Wind-Tunnel Tests of a Swept-Wing Airplane With a Cascade-Type Thrust Reverser. NASA TN D-311, 1960.

8. Falarski, Michael D.; and Mort, Kenneth W.: Full-Scale Wind-Tunnel Investigation of a Target-Type Thrust Reverser on the A-37B Airplane. NASA TM X-1985, 1970.

9. Weiss, D. C.; and McGuigan, W. M.: Inflight Thrust Control for Fighter Aircraft. AIAA Paper No. 70-513, Mar. 1970.

10. Linderman, D. L.; and Mount, J. S.: Development of an In-Flight Thrust Reverser for Tactical/Attack Aircraft. AIAA Paper No. 70-699, June 1970.

11. Taylor, John W. R., ed.: Jane's All The World's Aircraft. McGraw-Hill Book Co., c.1970.

12. Bruner, Georges: Les Avions Etrangers, Autres que Soviétiques, au Salon de Bourget. L'Aéronautique et L'Astronautique, vol. 1970-1, no. 17, 1970, pp. 39-49.

13. Aronson, Robert, ed.: European Fighter Aircraft. Mach. Des., vol. 41, no. 24, Oct. 16, 1969, pp. 44-50.

14. Maiden, Donald L.; and Mercer, Charles E.: Performance Characteristics of a Single-Engine Fighter Model Fitted With an In-Flight Thrust Reverser. NASA TN D-6460, 1971.

15. Schaefer, William T., Jr.: Characteristics of Major Active Wind Tunnels at the Langley Research Center. NASA TM X-1130, 1965.

16. Ward, Vernon G.; Whitcomb, Charles F.; and Pearson, Merwin D.: Air-Flow and Power Characteristics of the Langley 16-Foot Transonic Tunnel With Slotted Test Section. NACA RM L52E01, 1952.

17. Swihart, John M.; Norton, Harry T., Jr.; and Schmeer, James W.: Effect of Several Afterbody Modifications Including Terminal Fairings on the Drag of a Single-Engine Fighter Model With Hot-Jet Exhaust. NASA MEMO 10-29-58L, 1958.

18. Runckel, Jack F.; and Swihart, John M.: A Hydrogen Peroxide Hot-Jet Simulator for Wind-Tunnel Tests of Turbojet-Exit Models. NASA MEMO 1-10-59L, 1959.

19. Cuffe, A. G.; and Trott, W. C.: Static and Dynamic Stability and Control Data for the F9F-9 Airplane. Pt. II.- Longitudinal Stability and Control. Rep. No. XA98-B-3.6-II, Grumman Aircraft Eng. Corp., Feb. 1955.

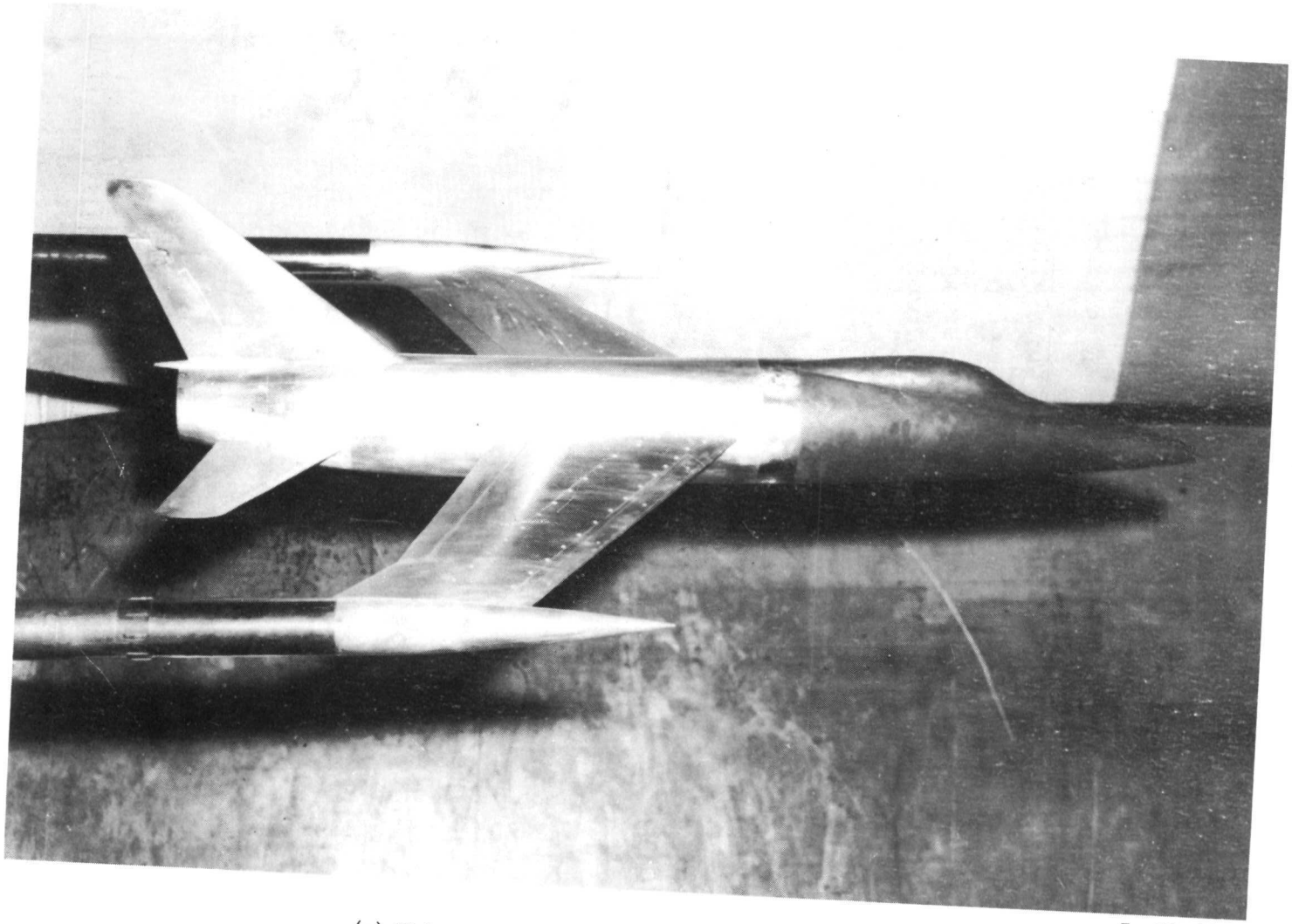

L-69-6345

(a) Side view of model with basic afterbody.

Figure 1.- Single-engine fighter model installed in Langley 16-foot transonic tunnel.

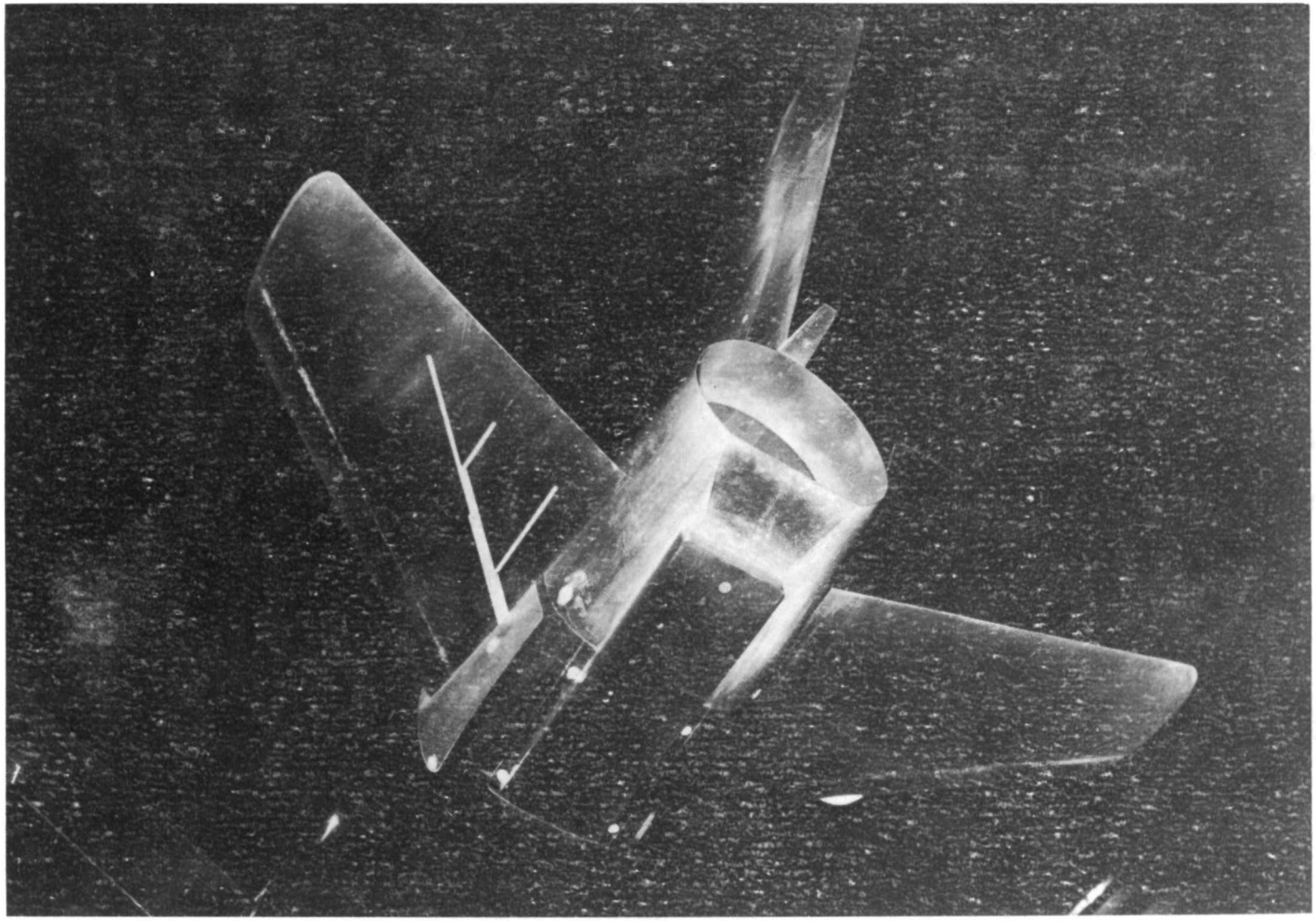

L-71-683

(b) Rear view of basic afterbody.

Figure 1.- Continued.

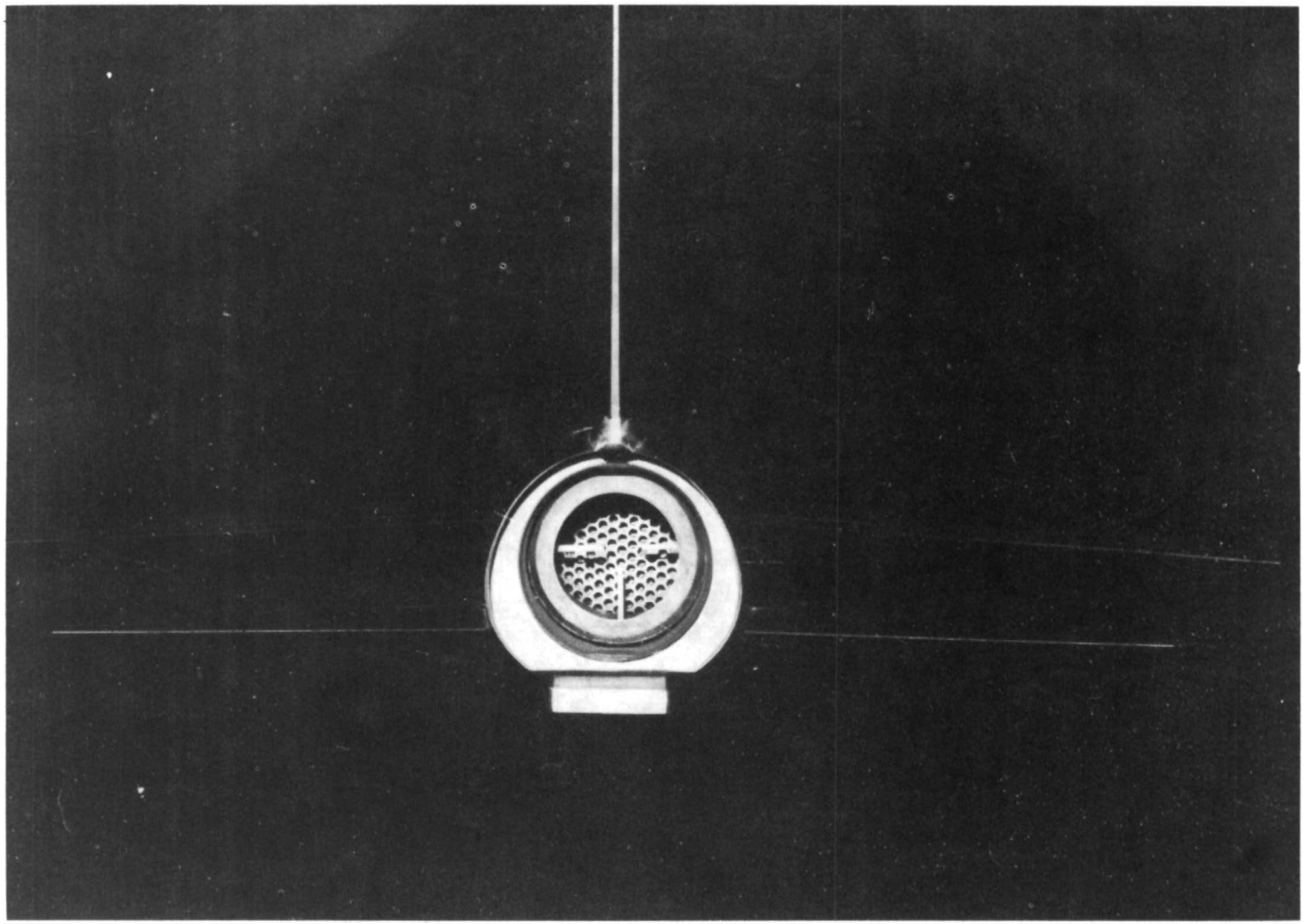

L-71-684

(c) Aft end view of basic afterbody nozzle arrangement.

Figure 1.- Concluded.

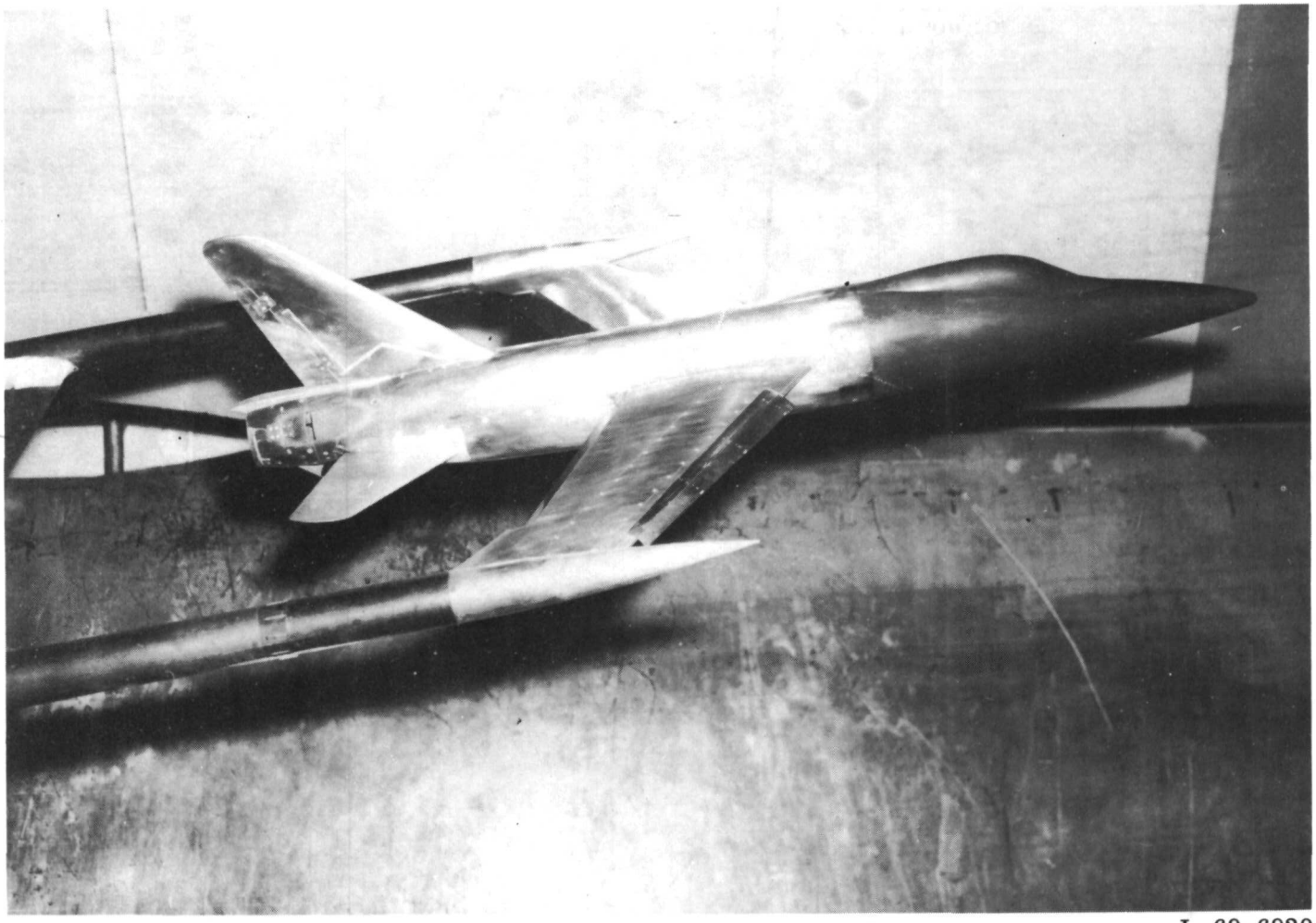

L-69-6920

(a) Approach configuration with thrust control unit deployed.

Figure 2.- Retrofit thrust control unit mounted on a single-engine fighter model installed in Langley 16-foot transonic tunnel.

L-71-685

(b) Stowed configuration (δ_{du} = δ_{dl} = Closed) of thrust control unit.

Figure 2.- Continued.

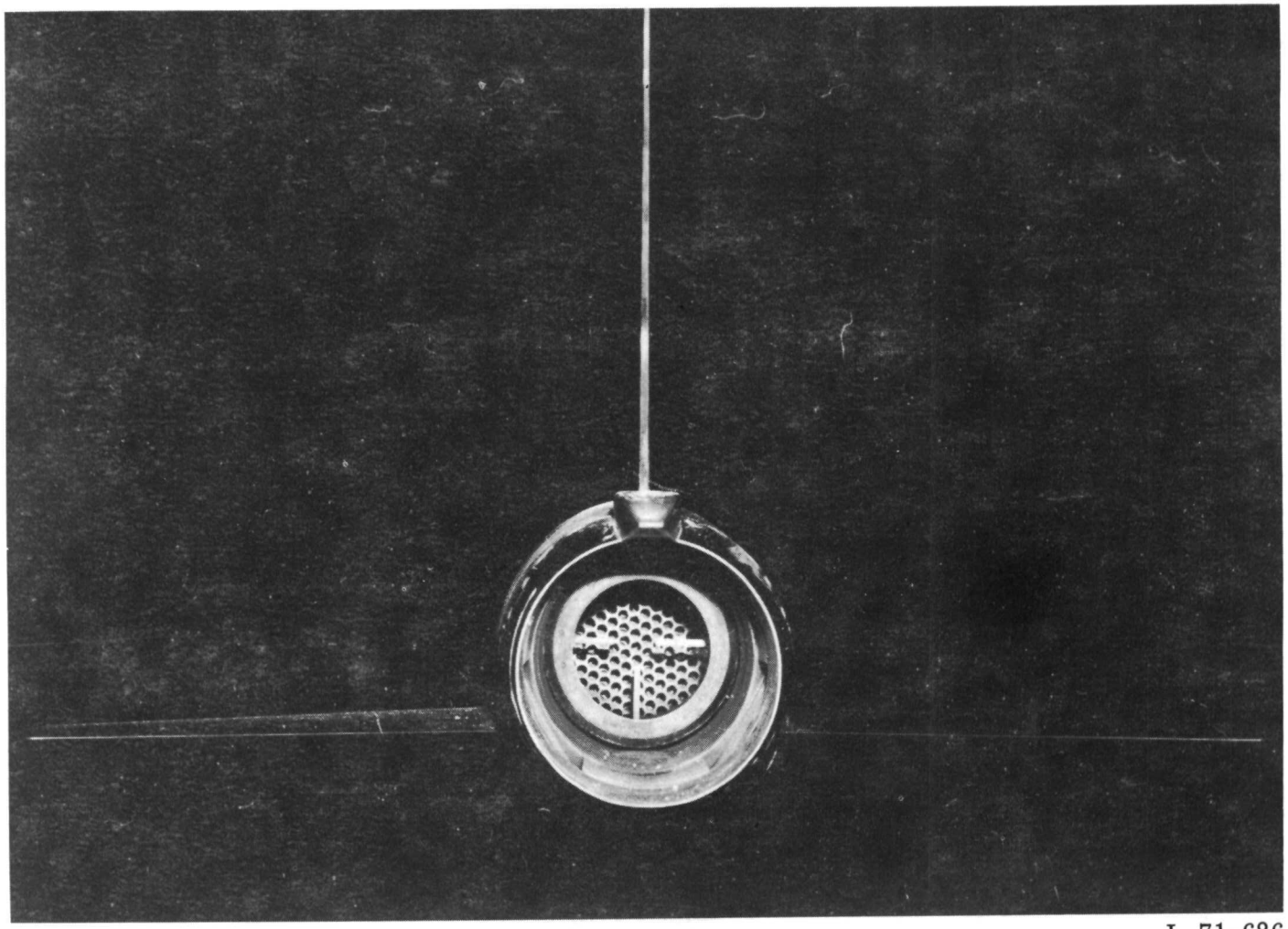

L-71-686

(c) Aft end view of stowed thrust control unit nozzle arrangement.

Figure 2.- Continued.

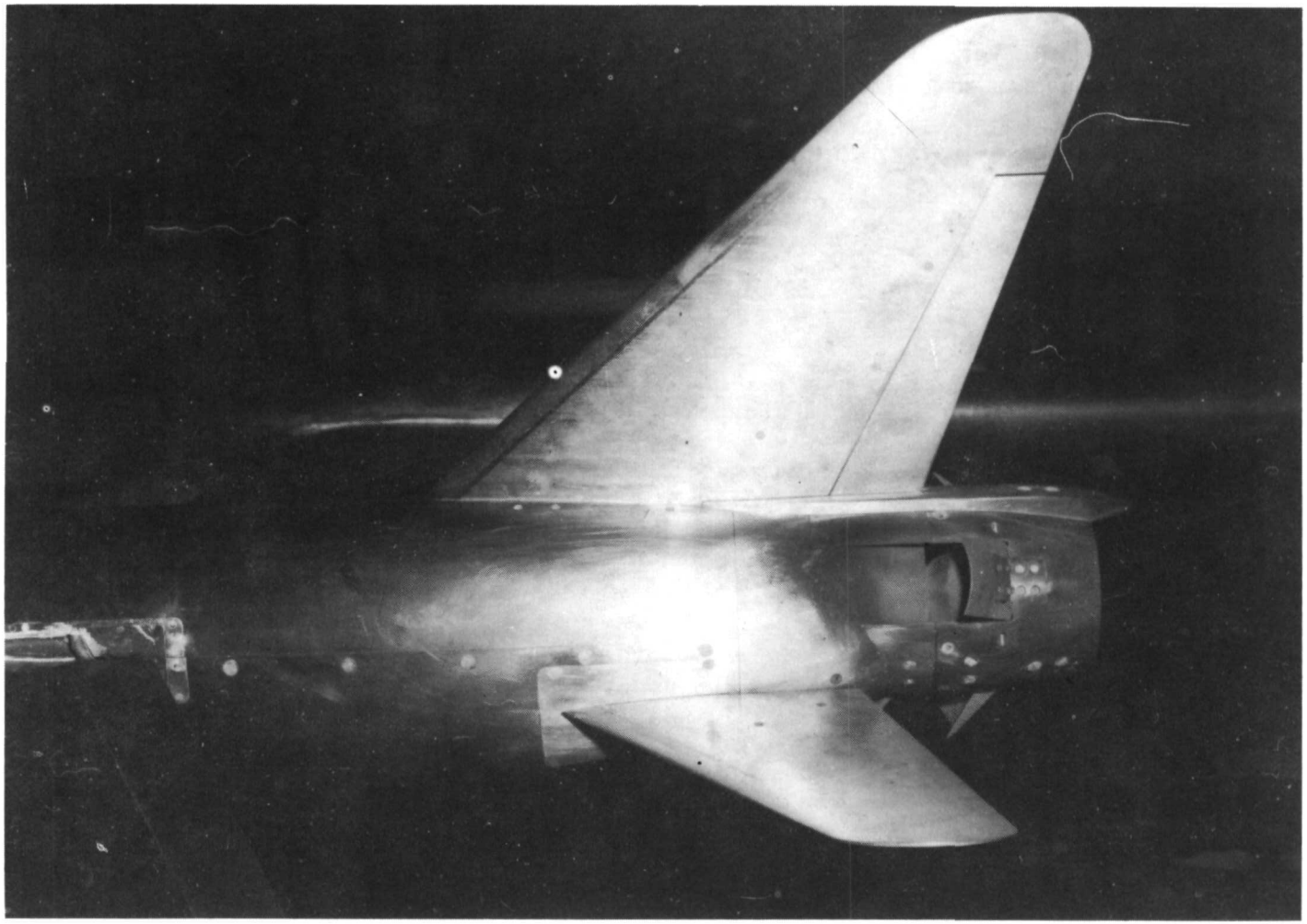

L-69-6398

(d) Deployed configuration of thrust control unit. δ_b = 100 percent; $\delta_{du} = 32.5^o$; and $\delta_{dl} = 52.5^o$.

Figure 2.- Continued.

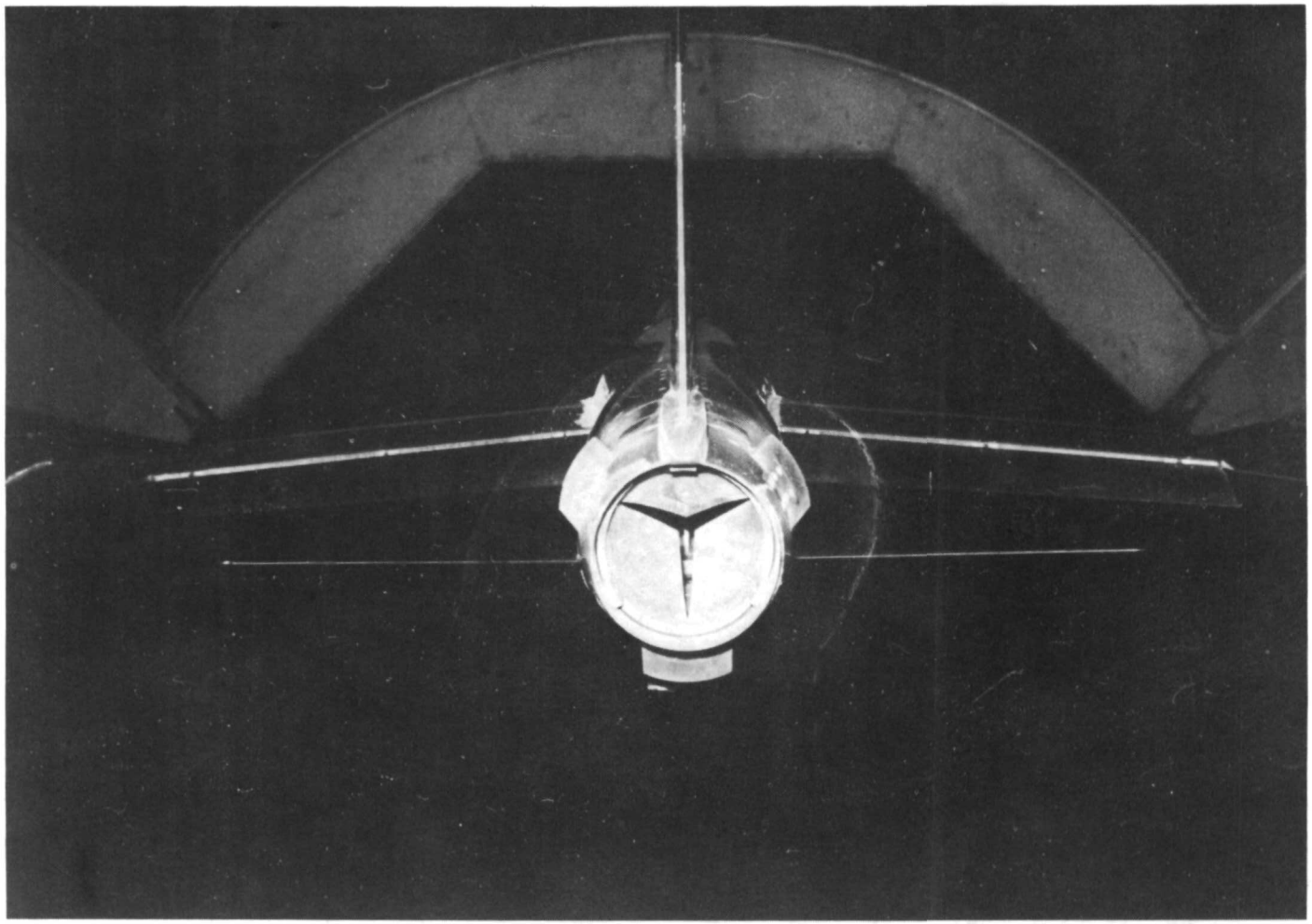

L-71-687

(e) Aft end view of deployed thrust control unit (δ_b = 90 percent).

Figure 2.- Continued.

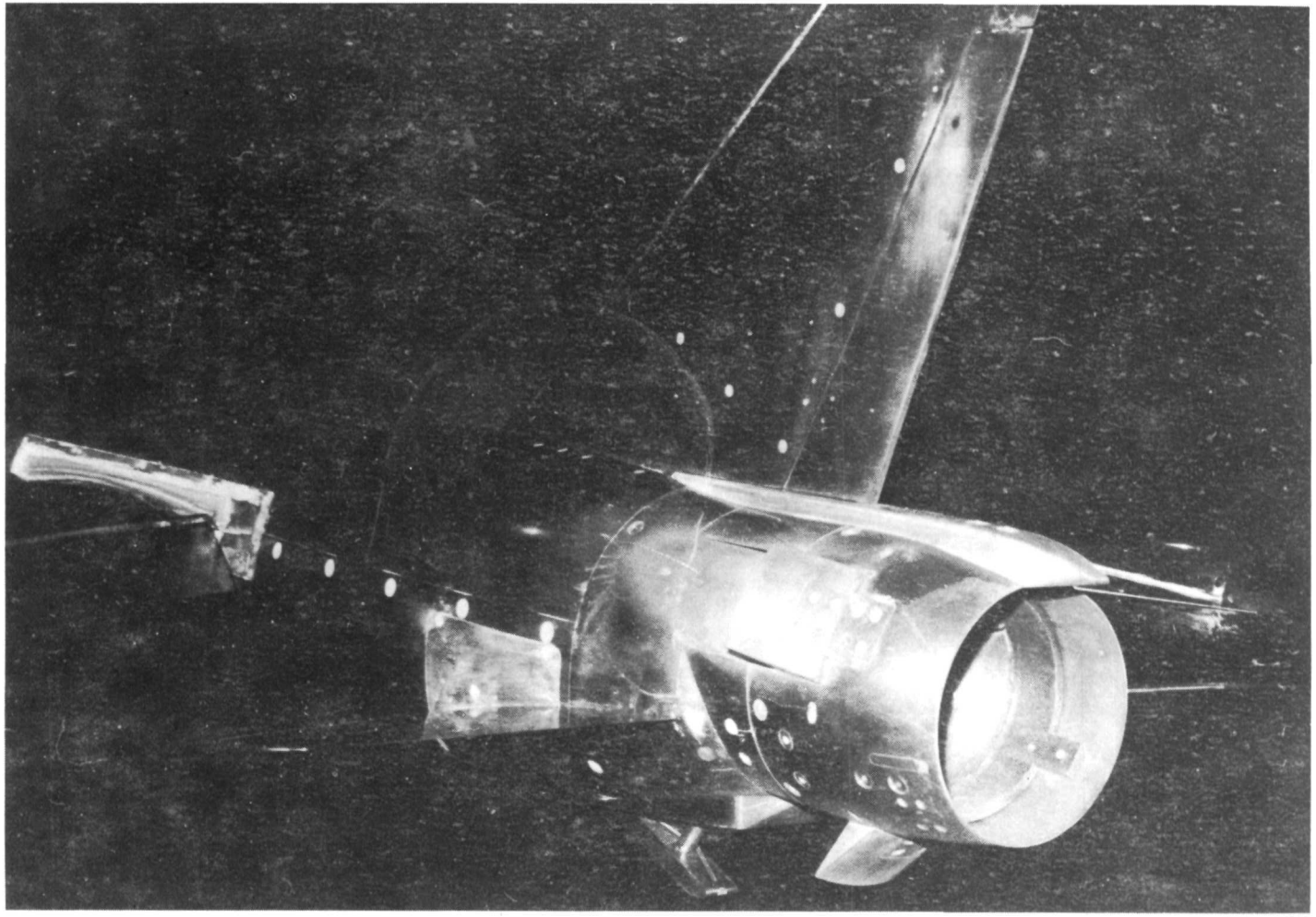

L-71-688

(f) Approach configuration with thrust control unit.

Figure 2.- Concluded.

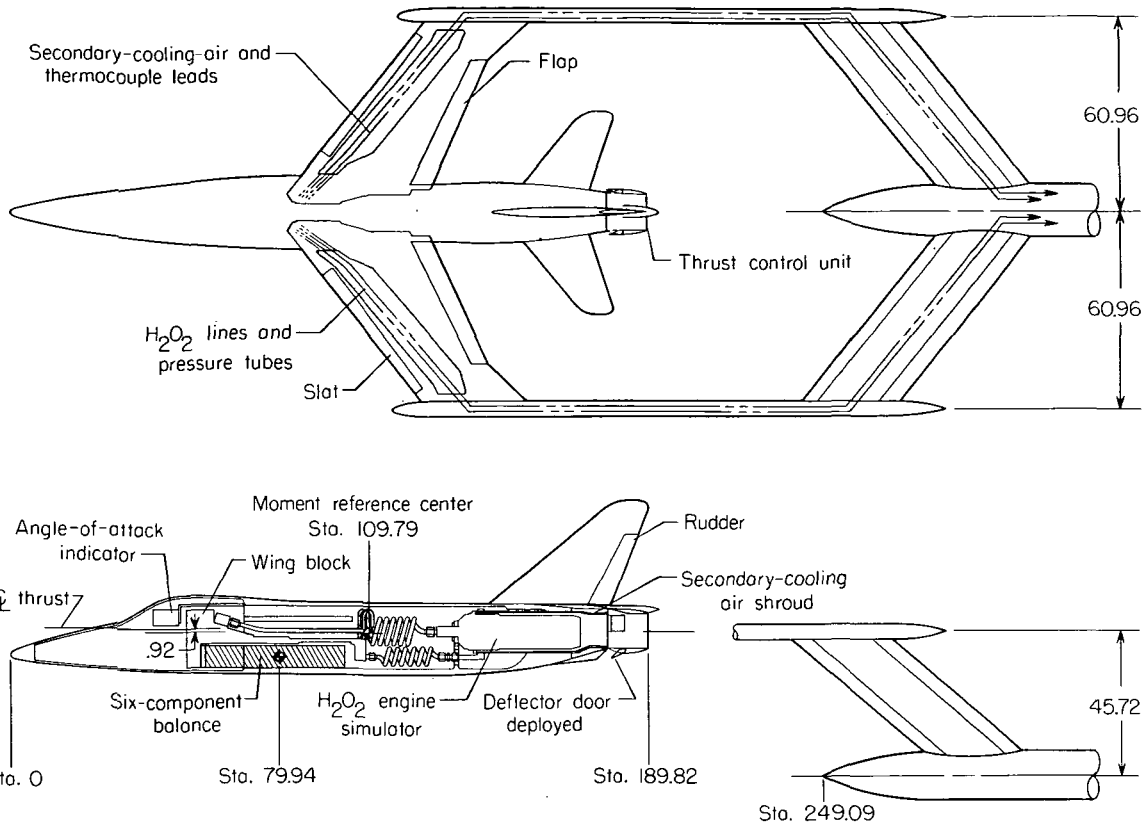

Wing	
Area (nominal)	0.4125 m^2
AR	4.00
Λ at c/4	35°
Cathedral	2.50°
Root section	NACA 65A006 modified
Tip section	NACA 65A006 modified
c_r	43.87 cm
c_t	21.94 cm
Taper ratio	0.50

Horizontal tail	
Area (total exposed)	0.0720 m^2
AR	3.50
Λ at c/4	35°
Root section	NACA 65A006
Tip section	NACA 65A004
c_r	25.13 cm
c_t	10.06 cm
Taper ratio	0.40

Engine	
Dry nozzle diameter	7.15 cm
A/B nozzle diameter	8.89 cm
Dry nozzle area	0.0040 m^2
A/B nozzle area	0.0062 m^2

Vertical tail	
Fin area (including rudder)	0.0729 m^2
Rudder area	0.0110 m^2
Λ at c/4	45°35'
Root section	NACA 0006
Tip section	NACA 0006

Figure 3.- Schematic of modified model with retrofit thrust control unit and bifurcated sting support. All dimensions are in centimeters unless otherwise noted.

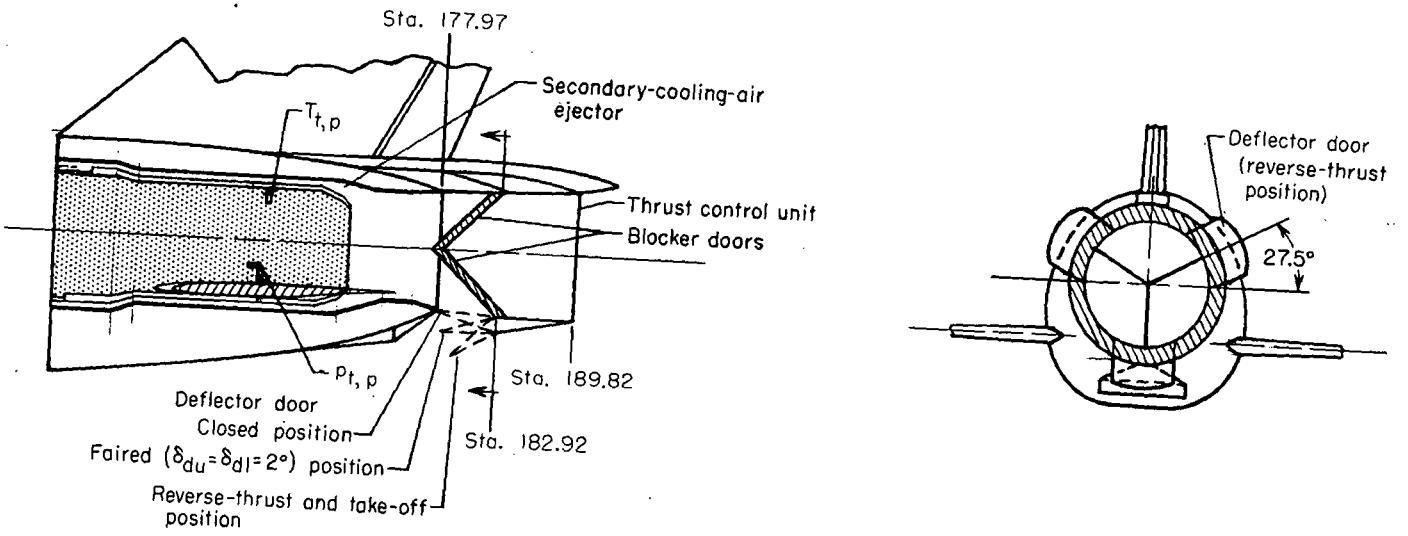

(a) Modified afterbody and ejector with thrust control unit (TCU).

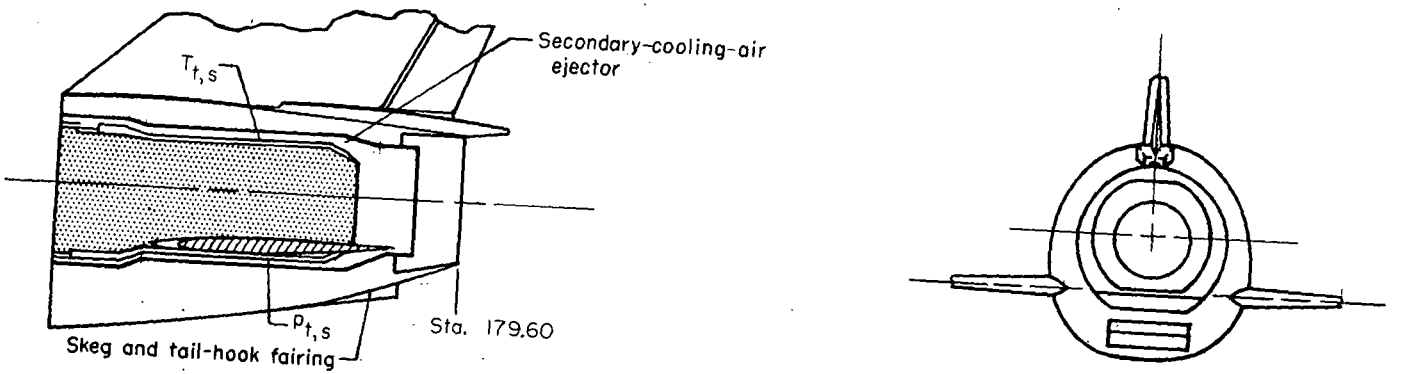

(b) Reference afterbody and ejector (basic).

Figure 4.- Schematic showing basic afterbody and modified afterbody with thrust control unit. All dimensions are in centimeters unless otherwise noted.

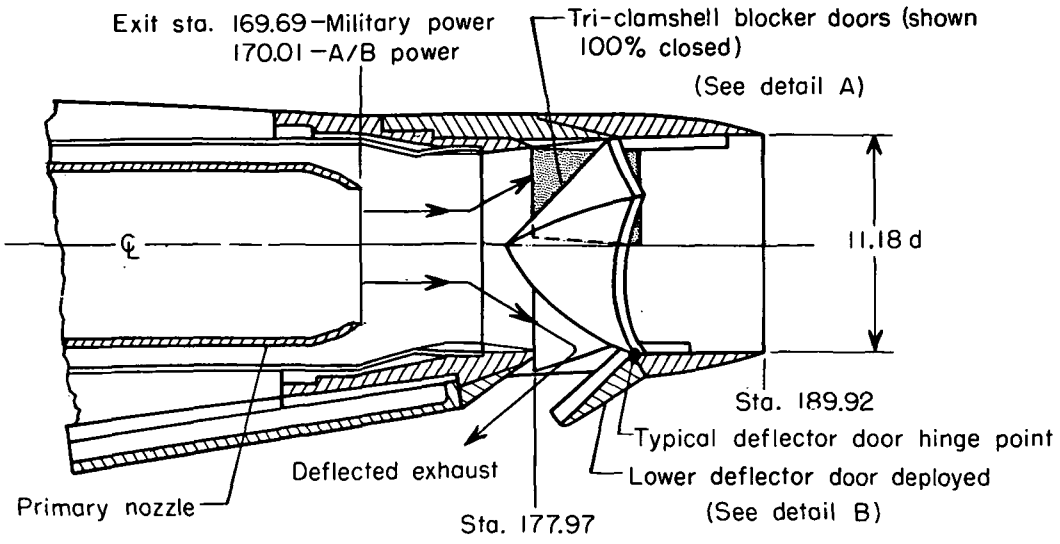

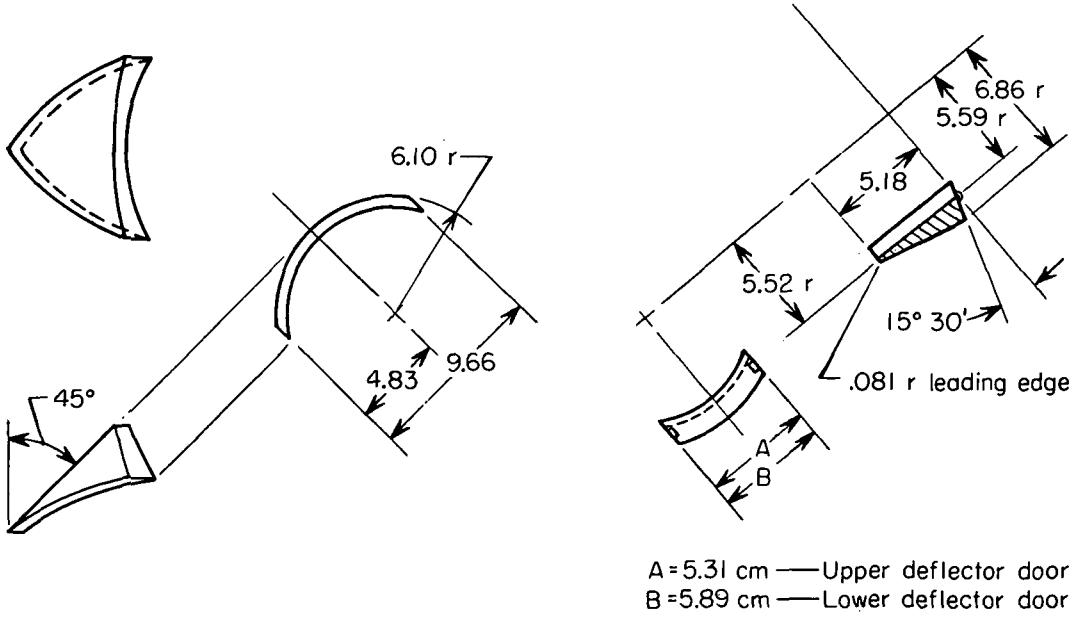

Detail A—Typical clamshell geometry

Detail B—Deflector-door details

(a) Schematic of aft fuselage cutaway showing tri-clamshell in 100-percent closed position. (δ_b = 100 percent.)

Figure 5.- Details of blocker- and deflector-door geometry. All dimensions are in centimeters unless otherwise noted.

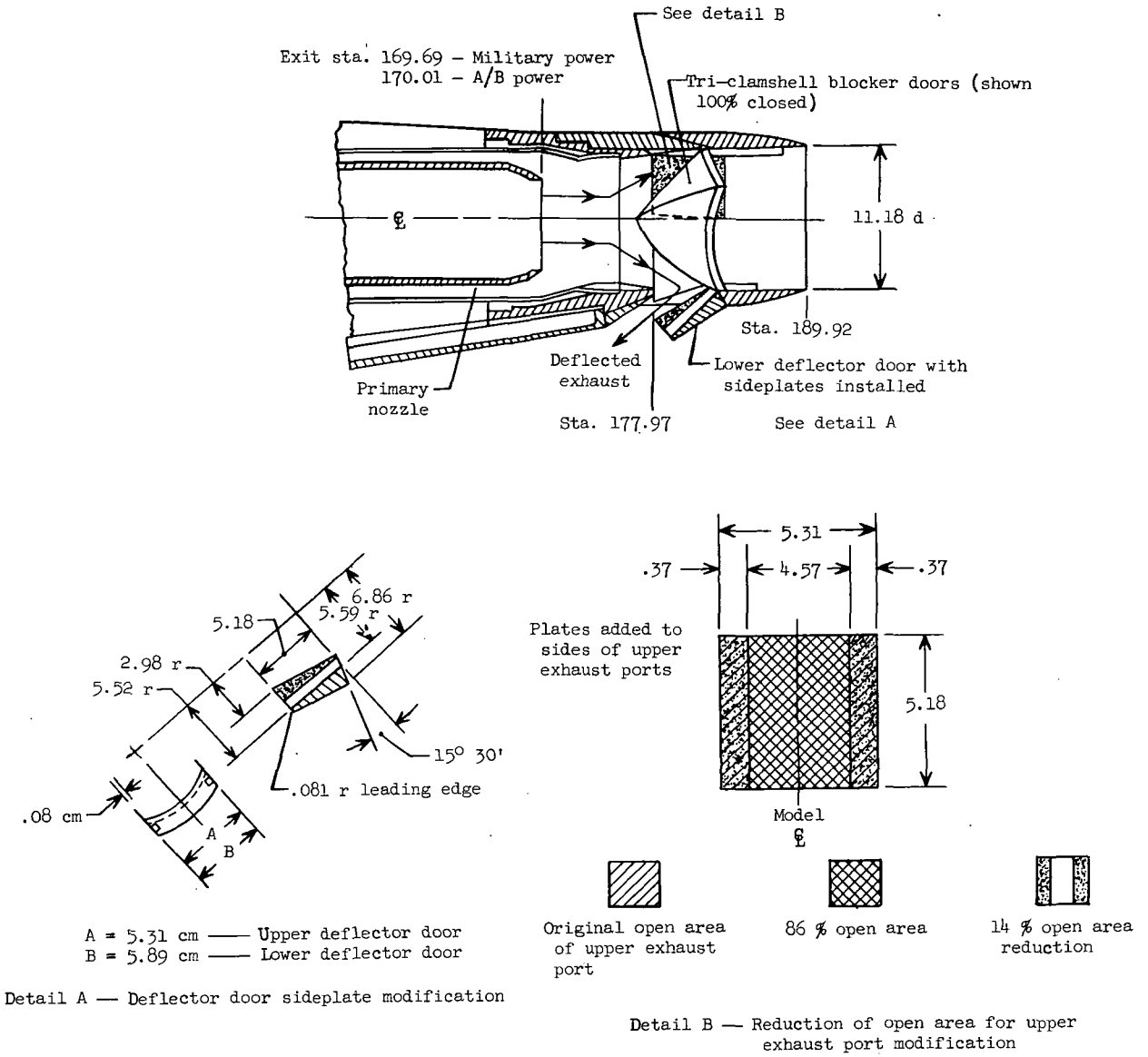

(b) Schematic of alternate configurations.

Figure 5.- Concluded.

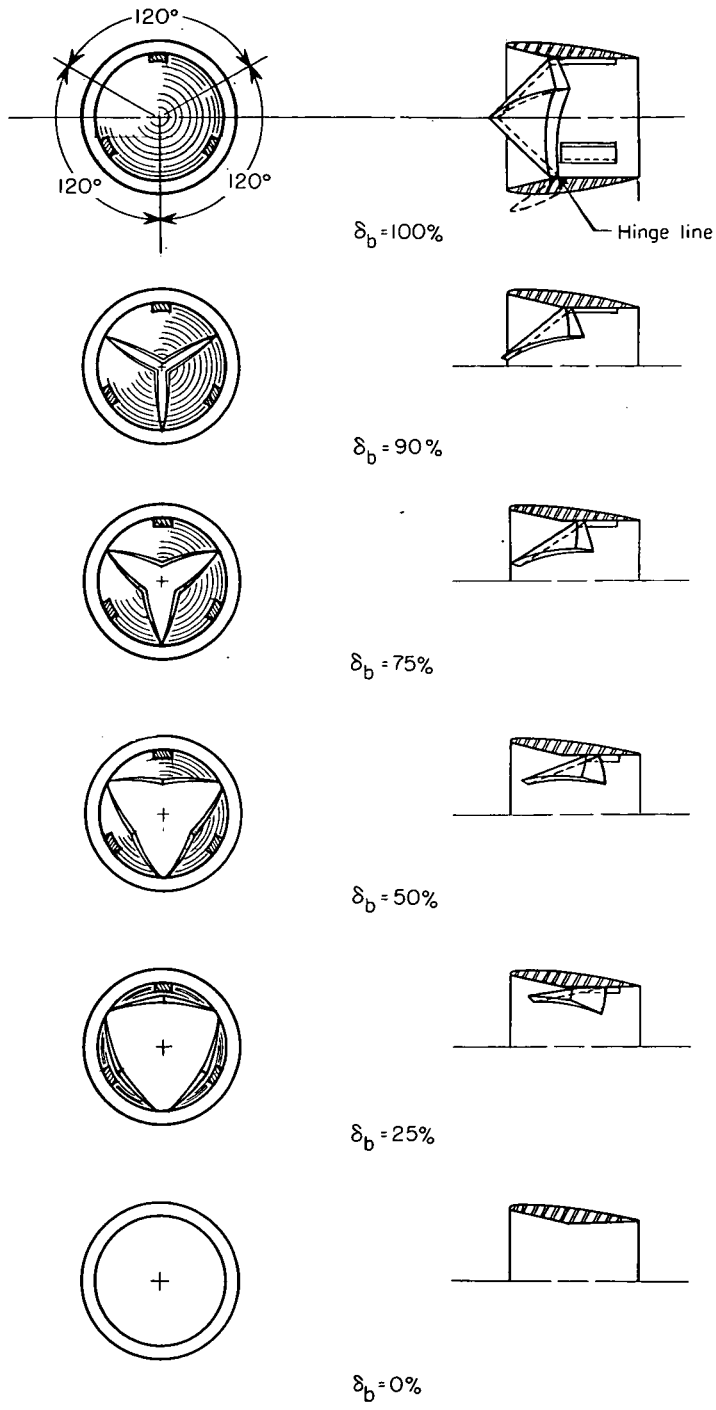

Figure 6.- Thrust control unit blocker-door configurations.

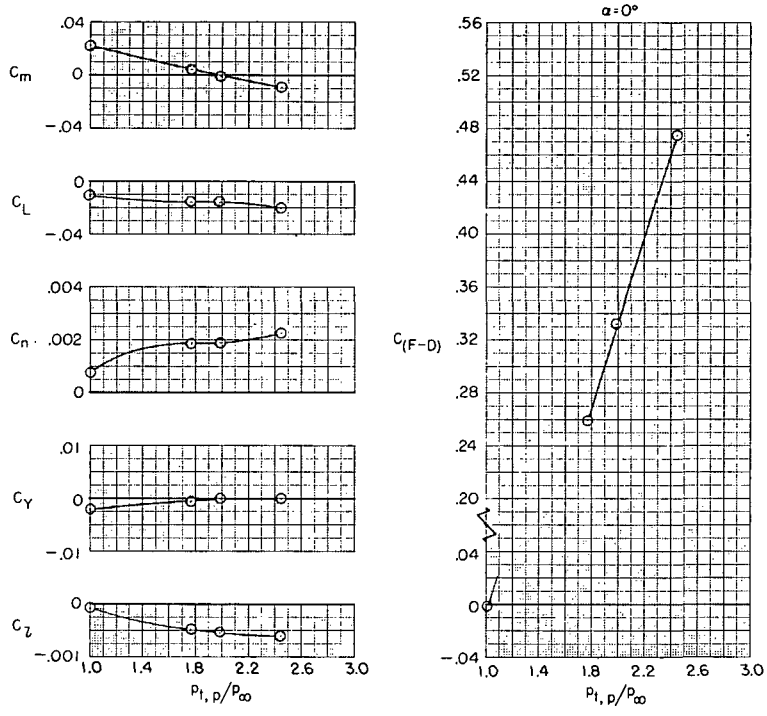

(a) M = 0.24; military power.

Figure 7.- Effect of jet-total-pressure ratio on aerodynamic characteristics of basic model for several angles of attack and Mach numbers. $\beta = 0^o$; $\delta_f = 0^o$; $\delta_s = 0^o$; $\delta_h = -1.5^o$; and $\delta_r = 0^o$.

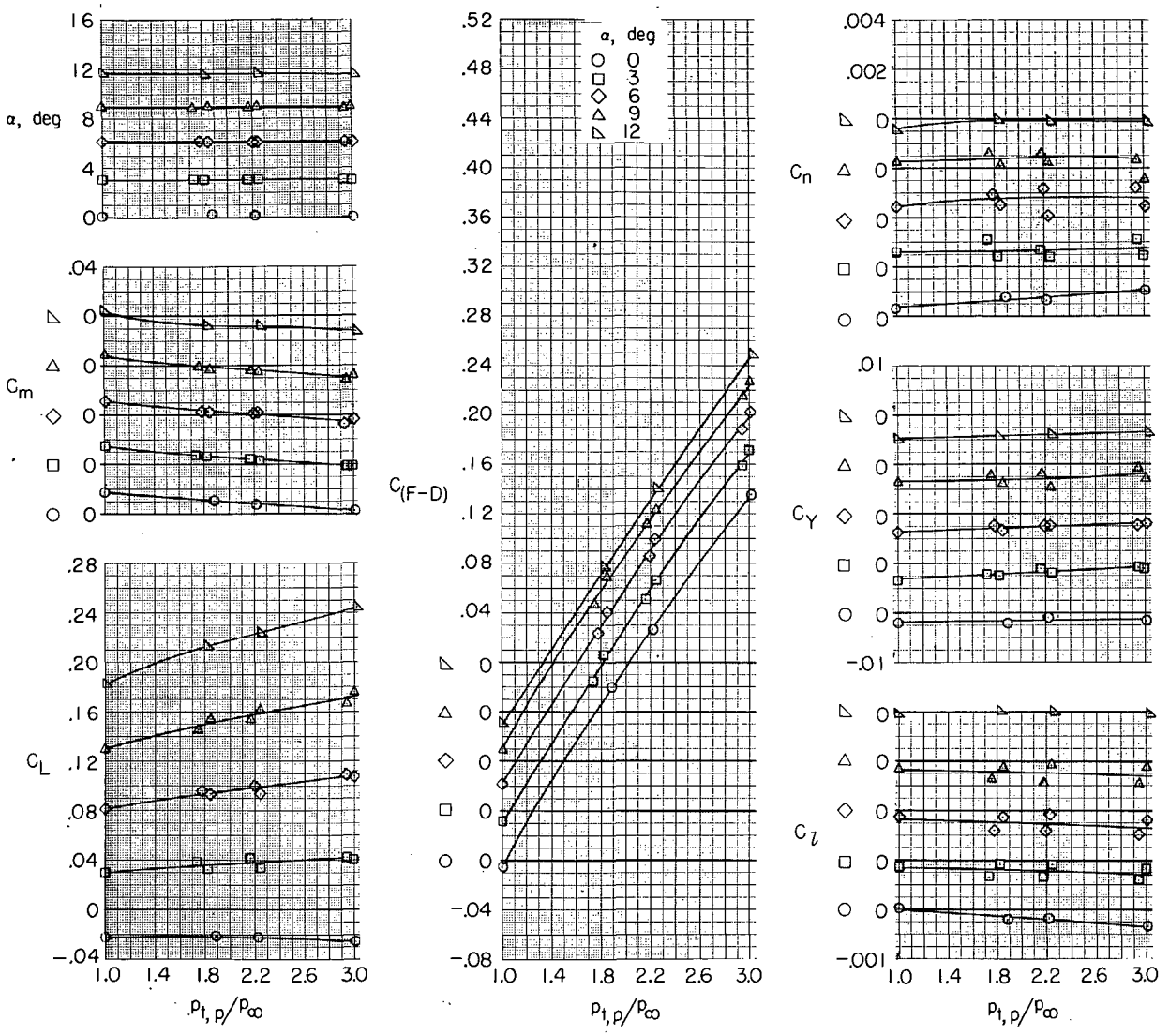

(b) M = 0.35; military power.

Figure 7.- Continued.

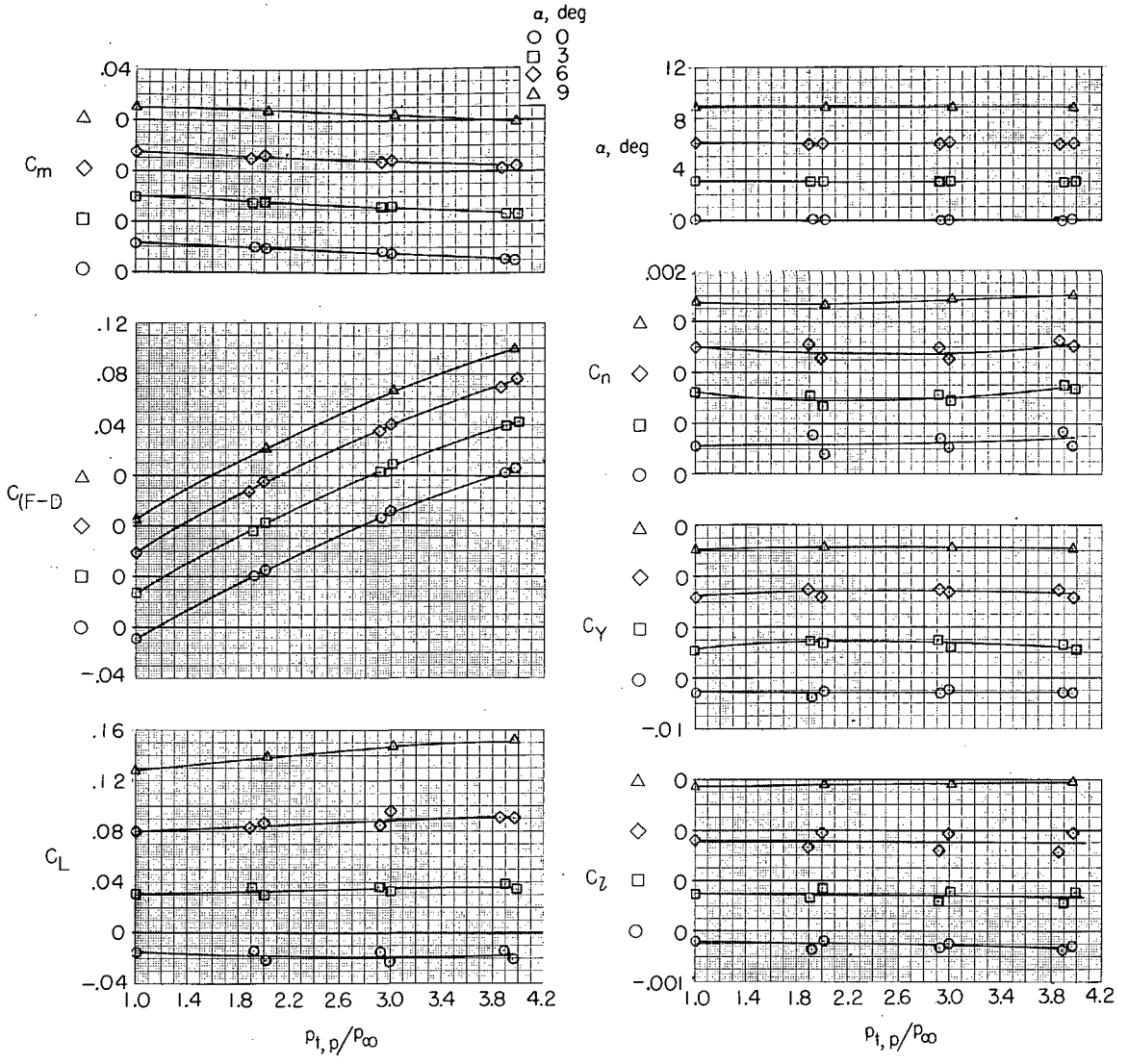

(c) M = 0.60; military power.

Figure 7.- Continued.

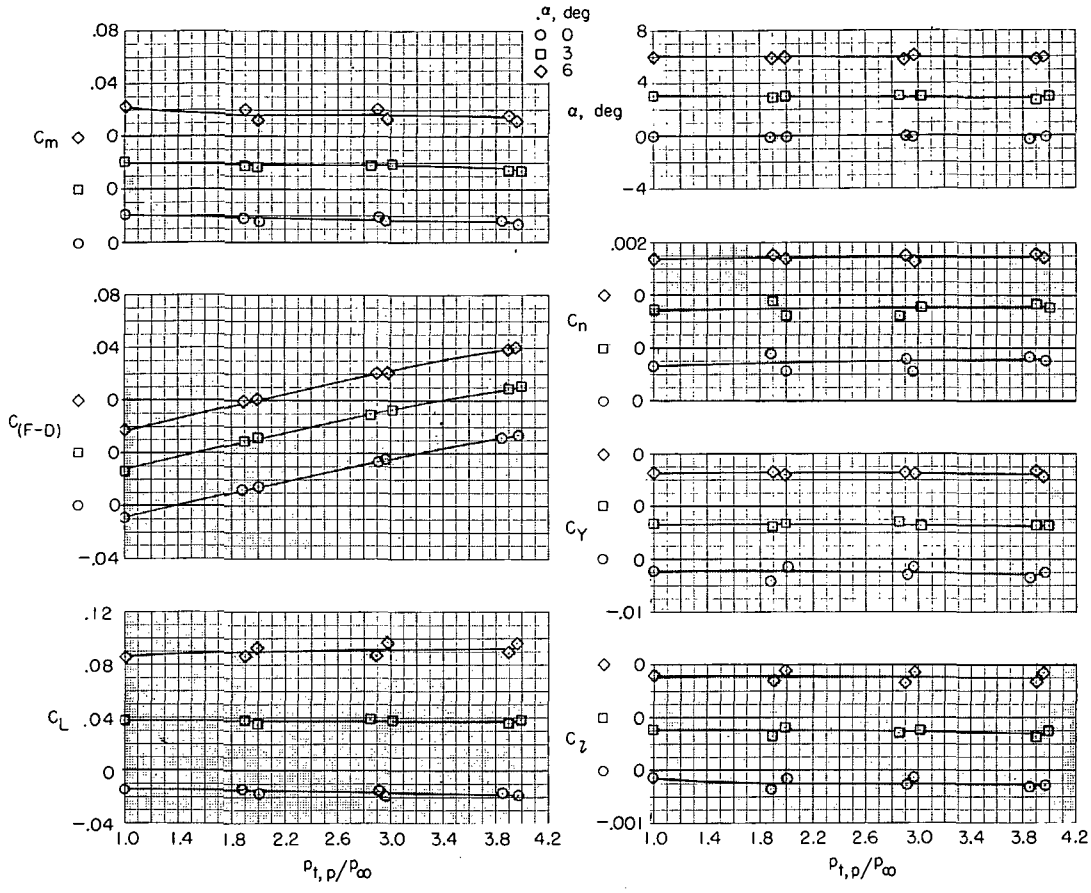

(d) M = 0.90; military power.

Figure 7.- Continued.

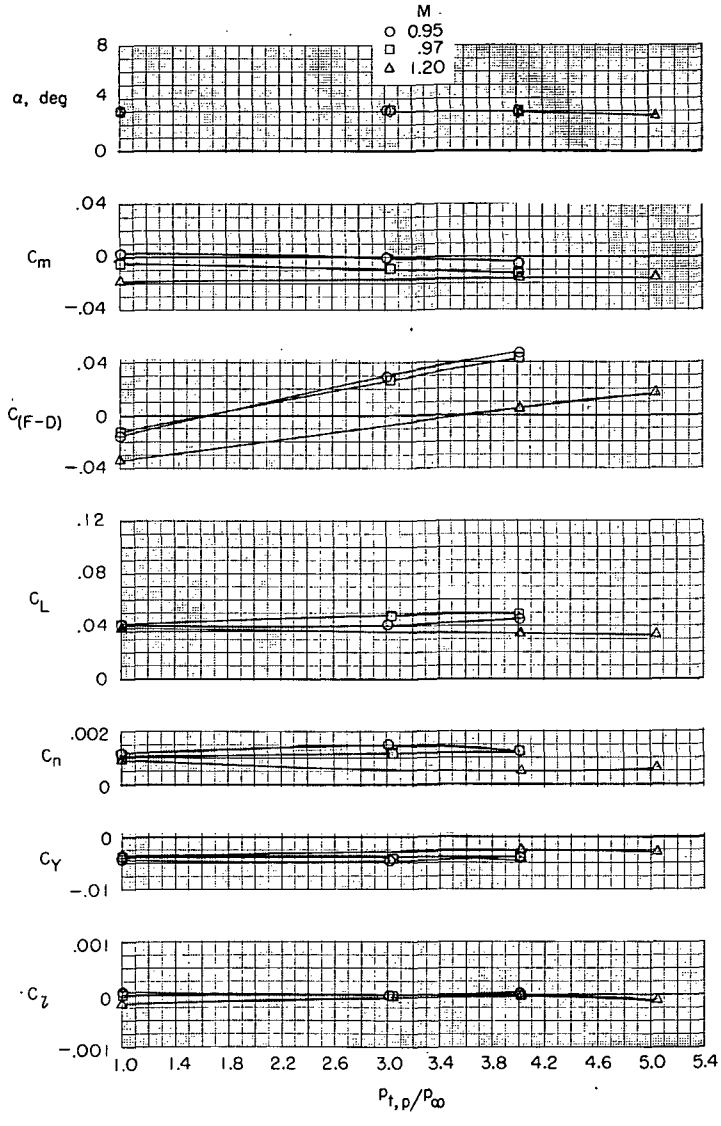

(e) M = 0.95 to 1.20; military power.

Figure 7.- Continued.

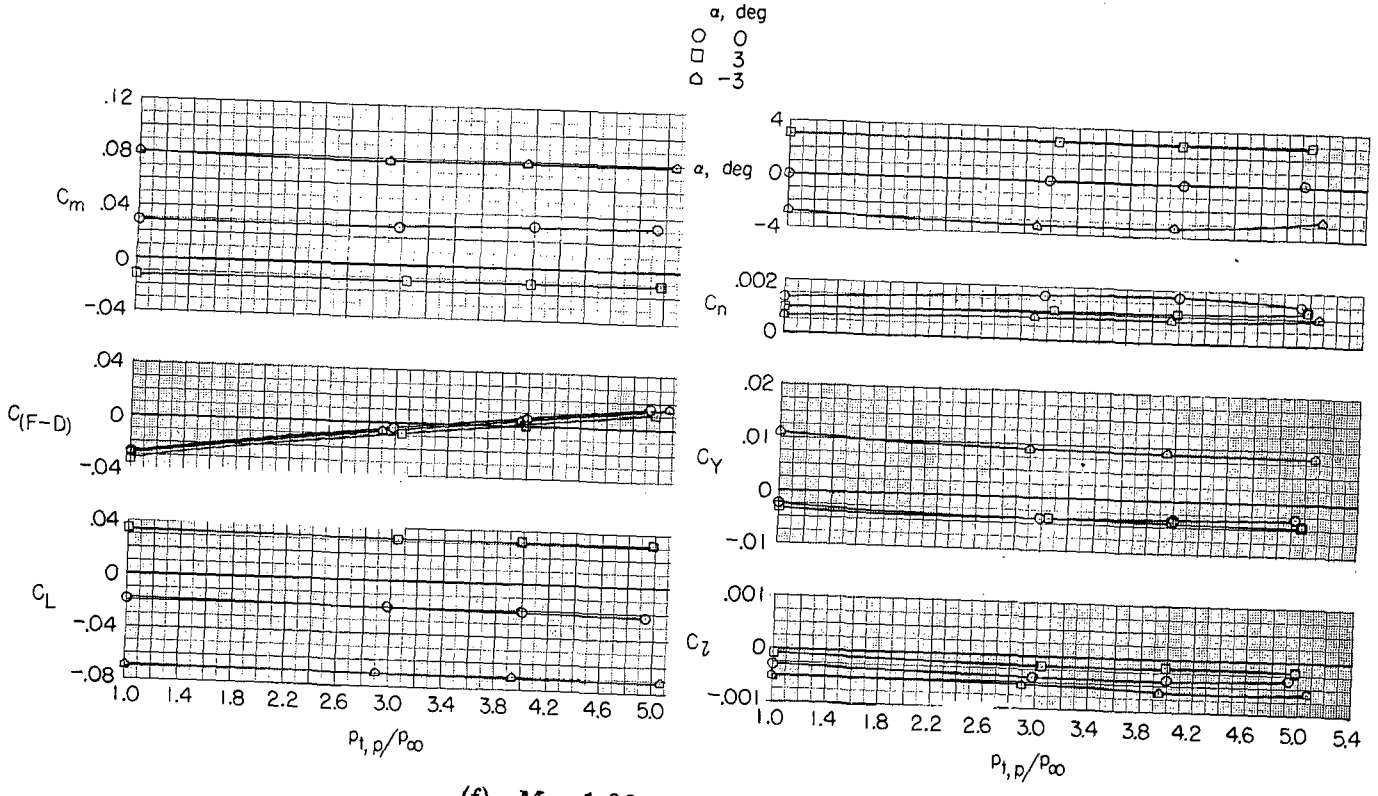

(f) M = 1.30; military power.

Figure 7.- Continued.

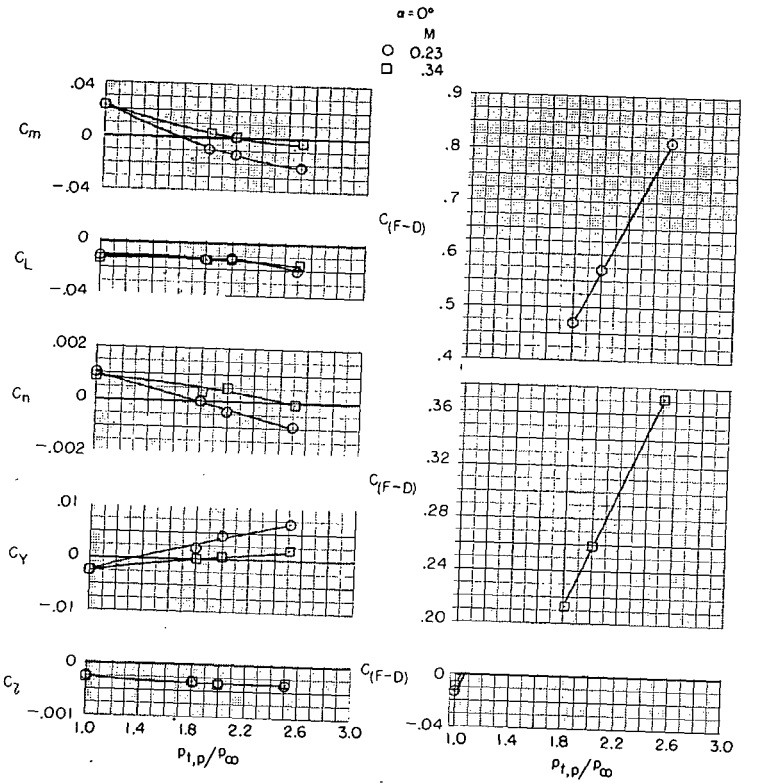

(g) M = 0.23 and 0.34; afterburning power.

Figure 7.- Continued.

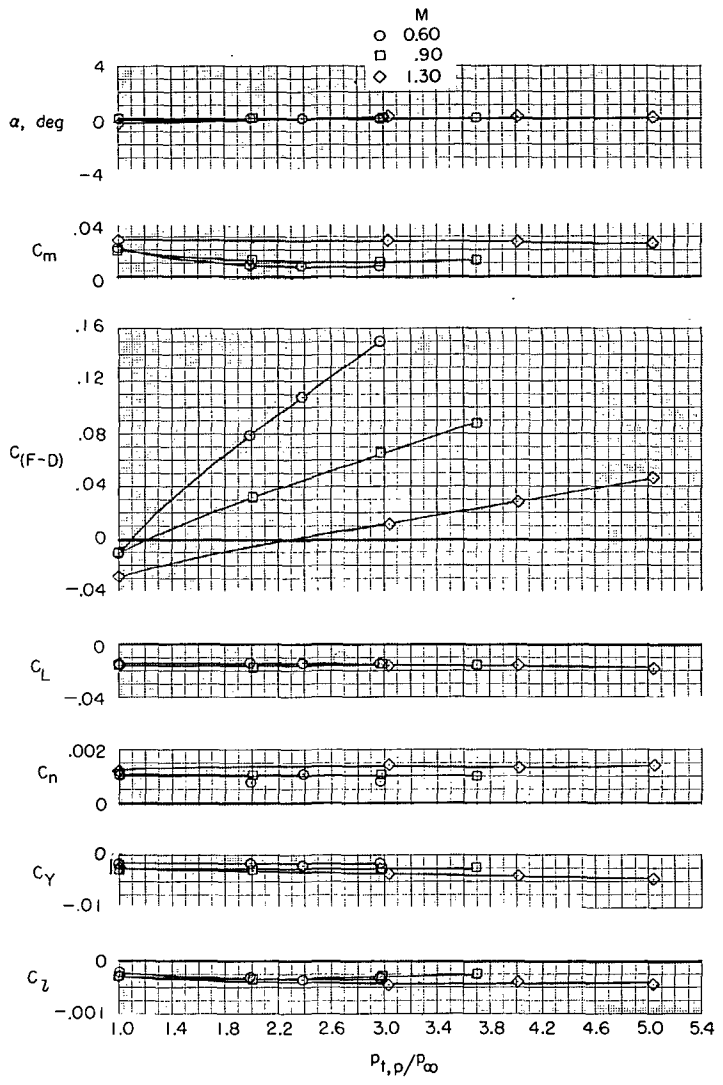

(h) M = 0.60, 0.90, and 1.30; afterburning power.

Figure 7.- Concluded.

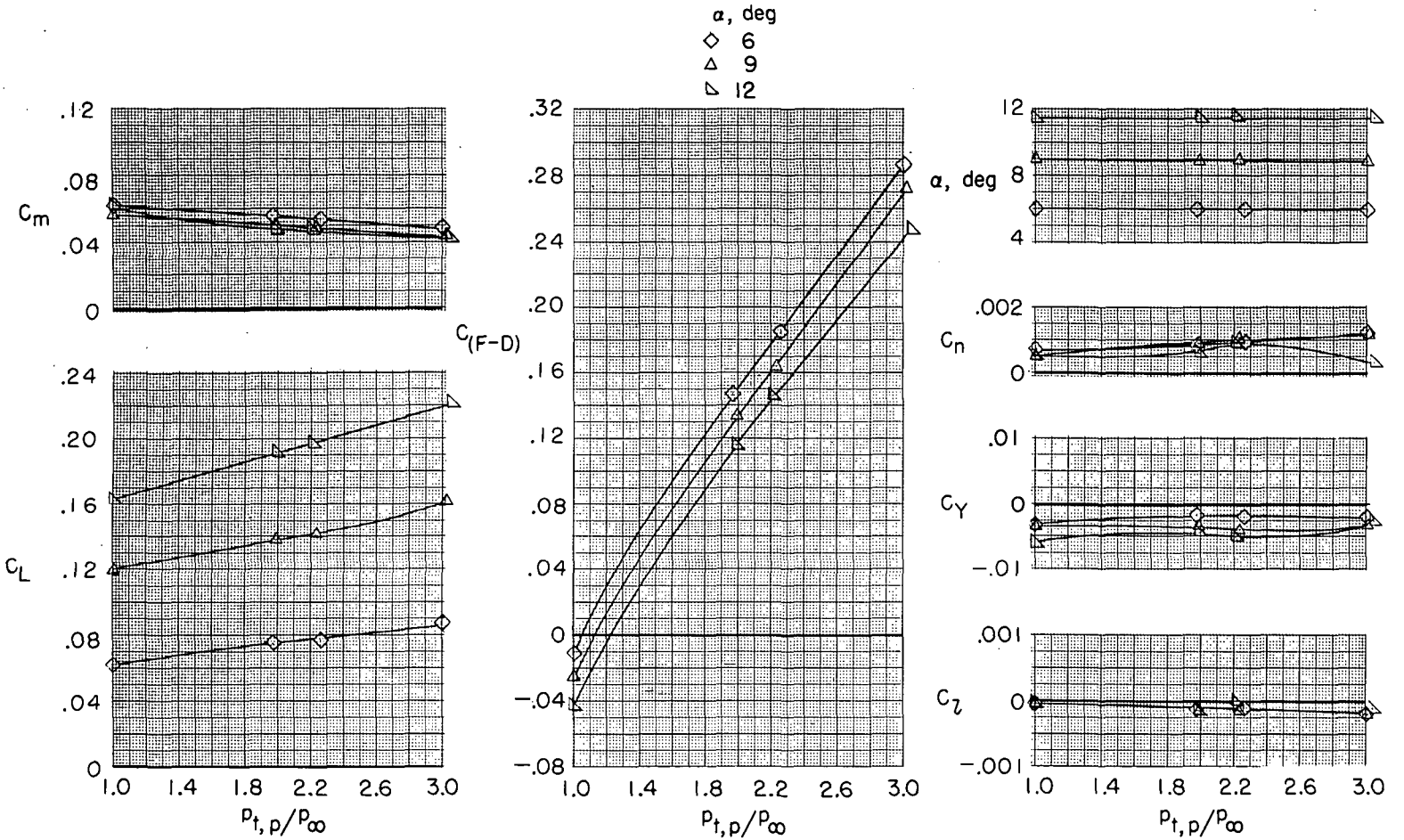

(a) M = 0.35.

Figure 8.- Effect of jet-total-pressure ratio on aerodynamic characteristics of basic model for several angles of attack and Mach numbers. $\beta = 0^o$; $\delta_f = 0^o$; $\delta_s = 0^o$; $\delta_h = -4^o$; $\delta_r = 0^o$; and military power.

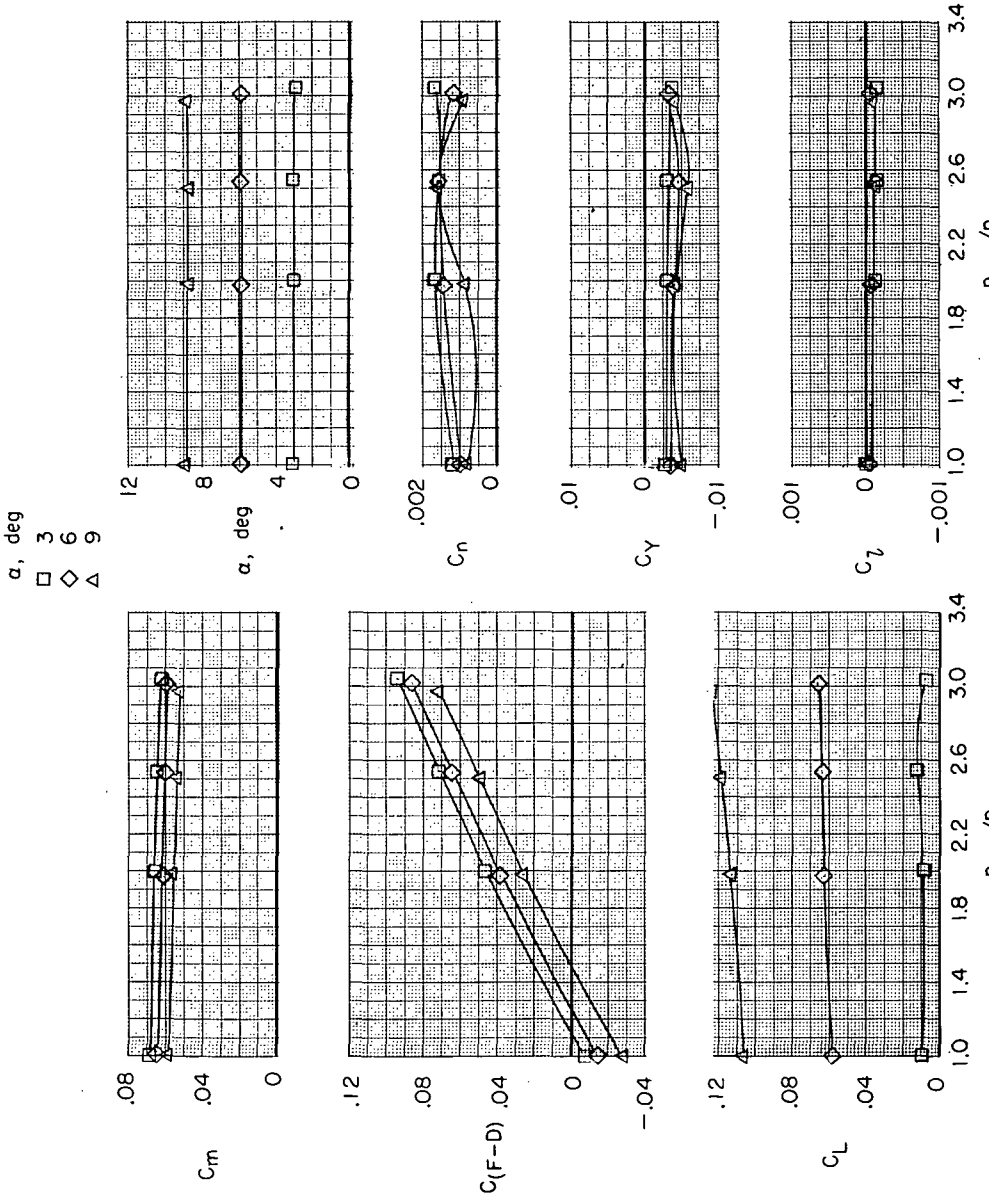

(b) M = 0.60.

Figure 8.- Continued.

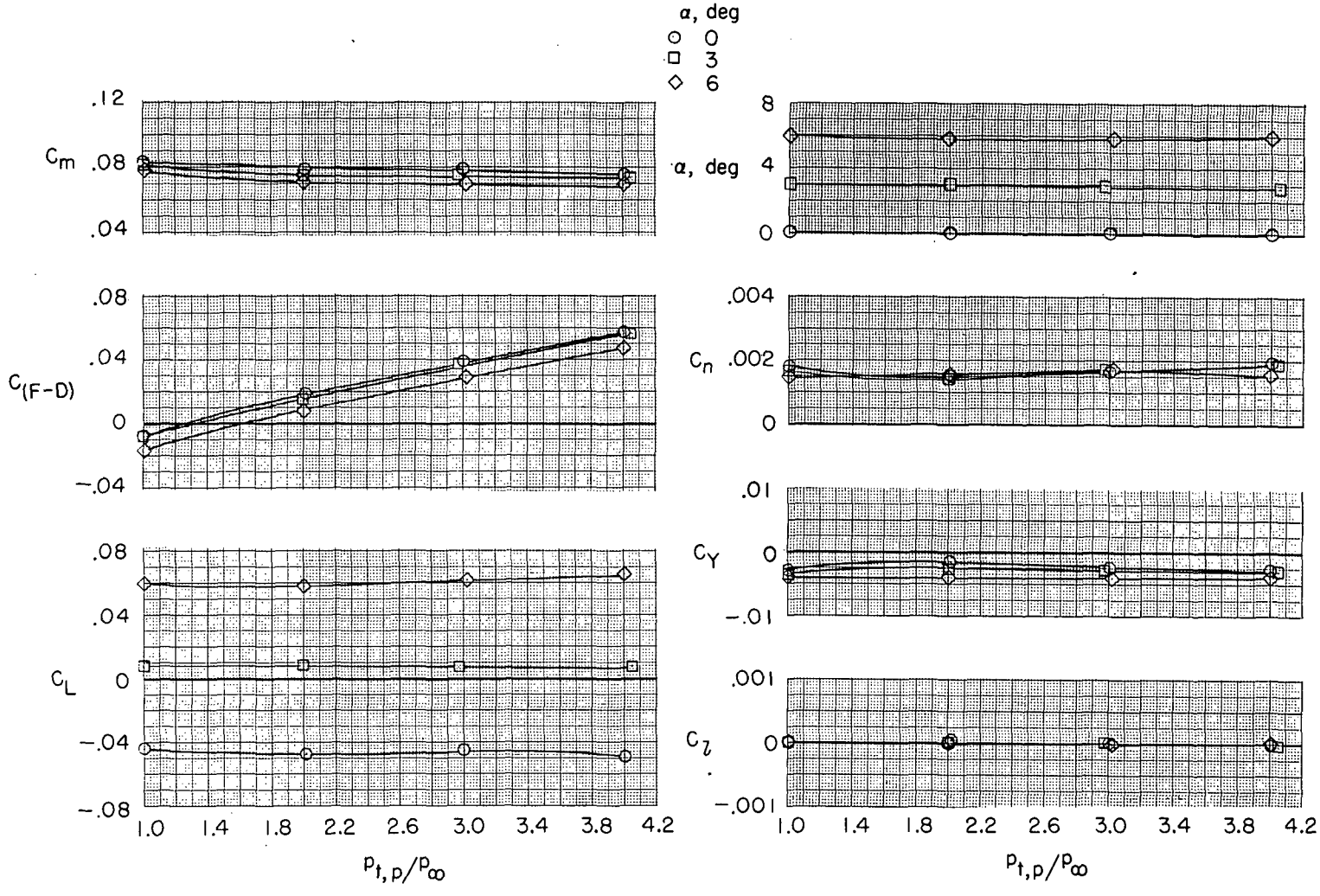

(c) M = 0.90.

Figure 8.- Concluded.

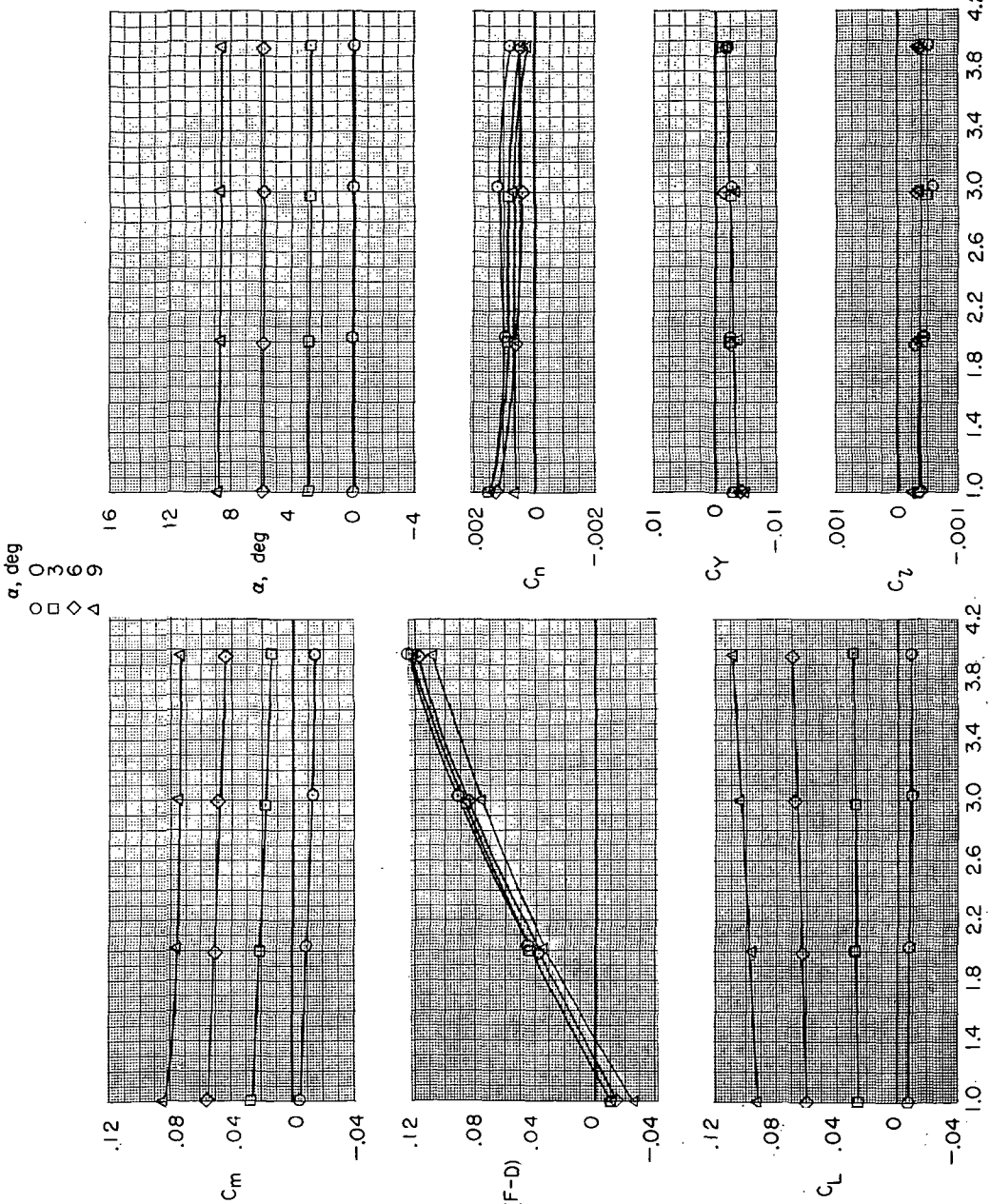

(b) M = 0.60.

Figure 9.- Continued.

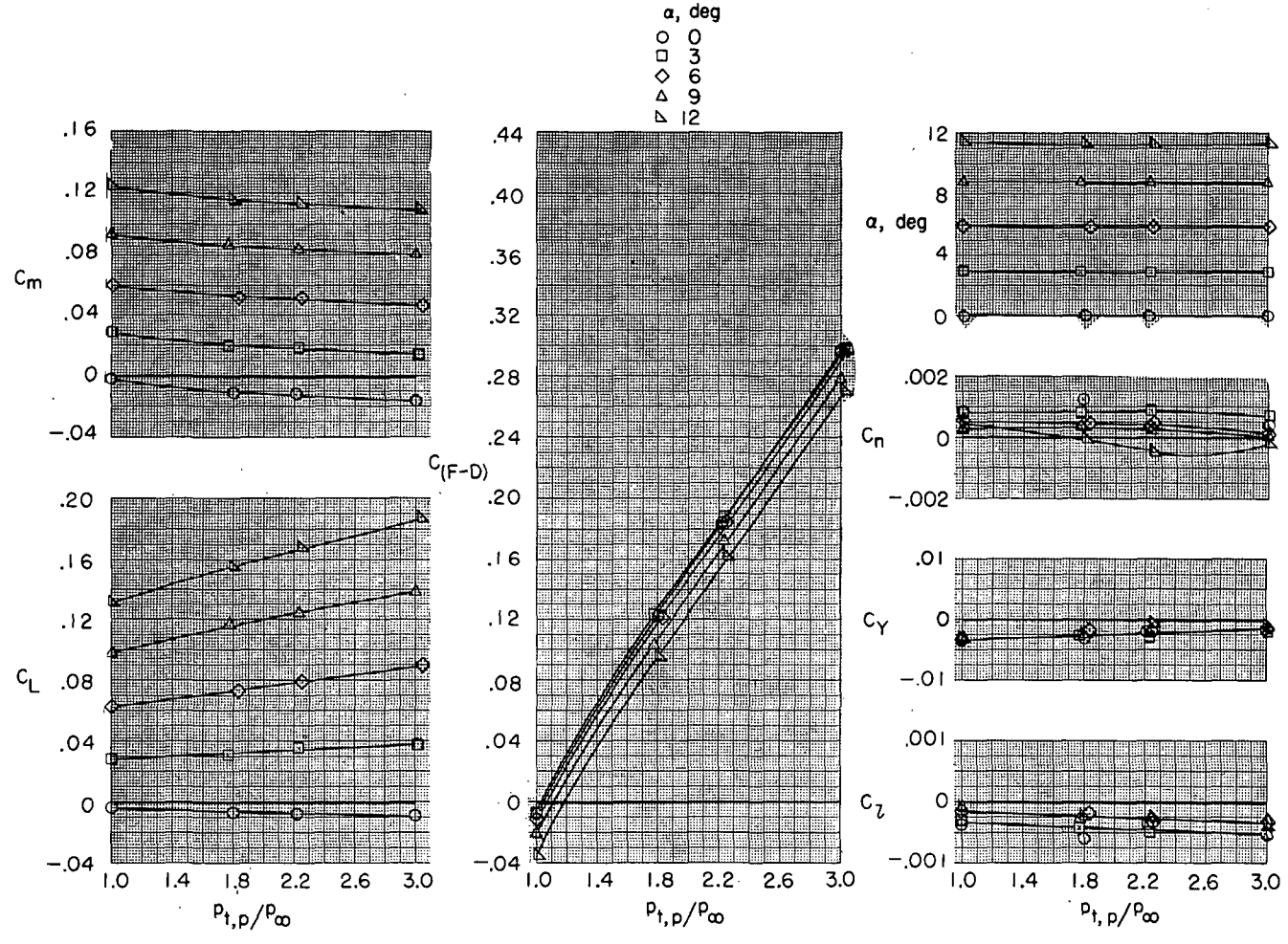

(a) M = 0.34.

Figure 9.- Variation of aerodynamic characteristics of basic model with jet-total-pressure ratio for several angles of attack and Mach numbers. $\beta = 0^o$; $\delta_f = 0^o$; $\delta_s = 0^o$; δ_h = Off; $\delta_r = 0^o$; and military power.

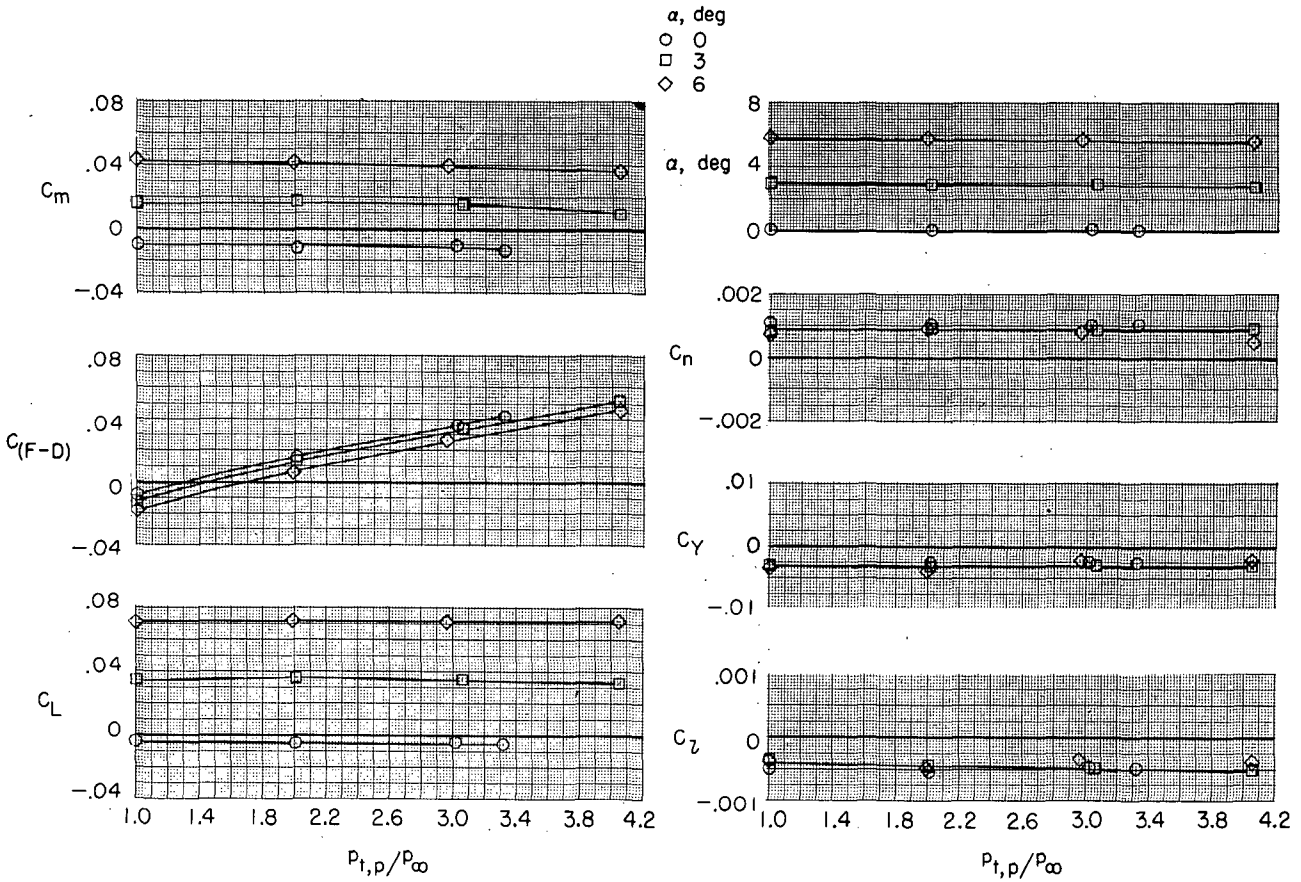

(c) M = 0.90.

Figure 9.- Continued.

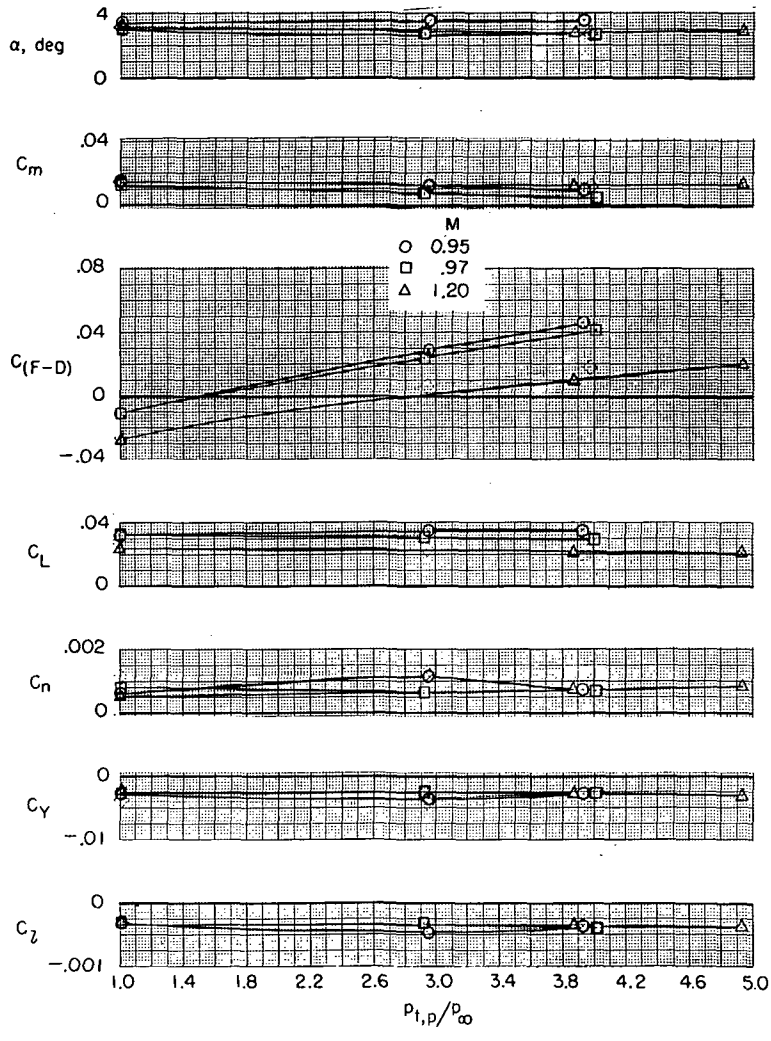

(d) M = 0.95 to 1.20.

Figure 9.- Continued.

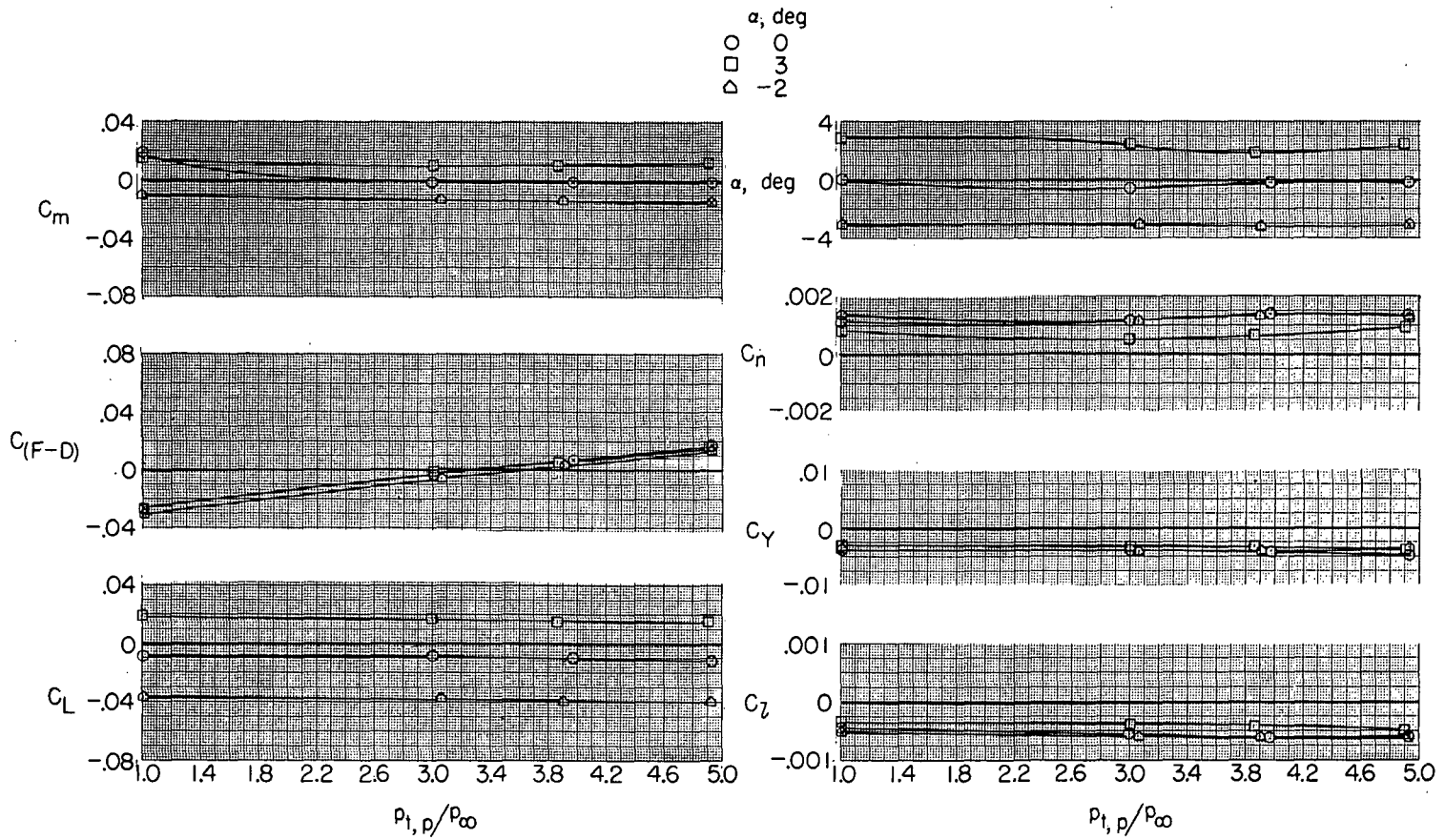

(e) M = 1.30.

Figure 9.- Concluded.

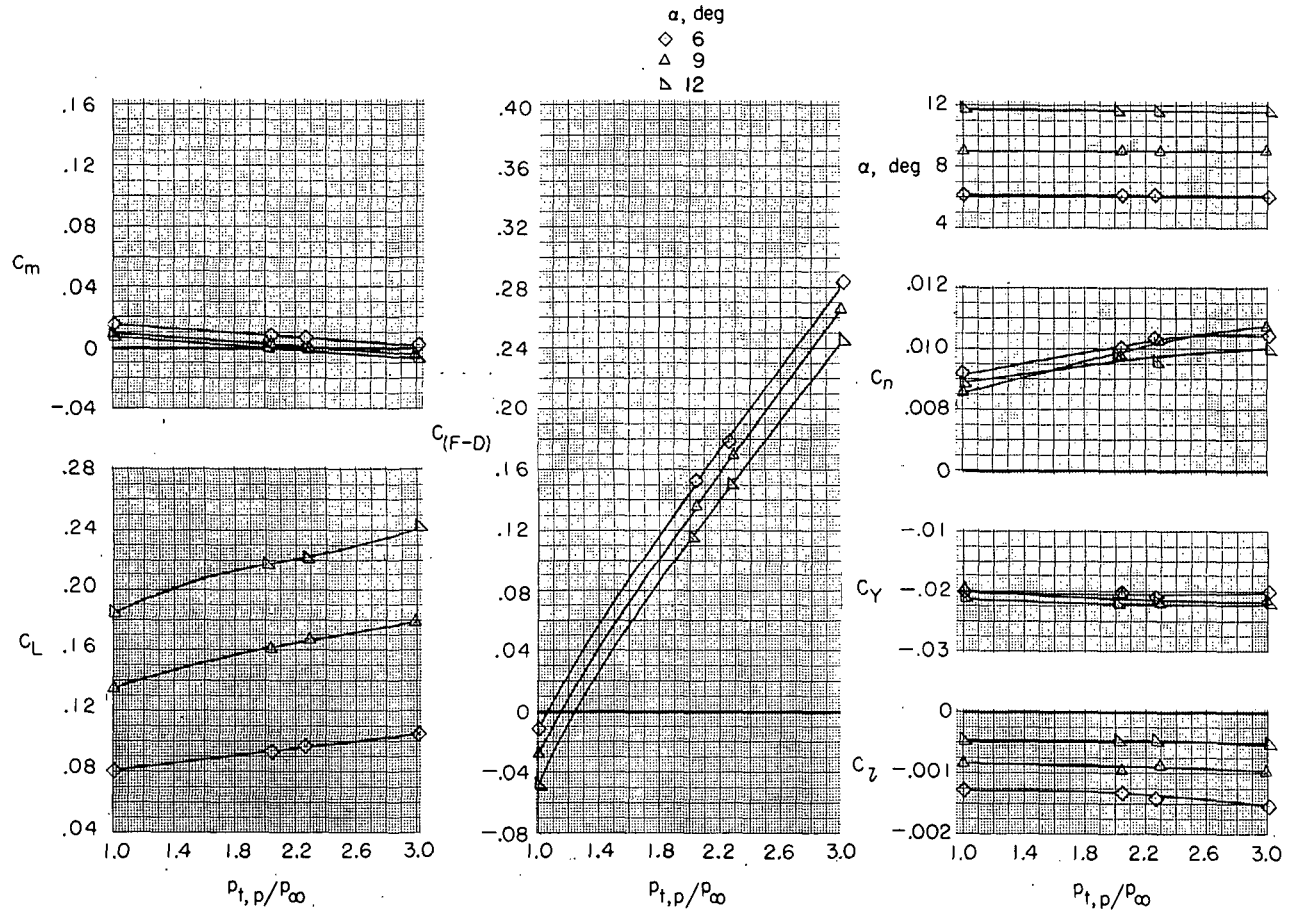

(a) M = 0.35.

Figure 10.- Variation of aerodynamic characteristics of basic model with jet-total-pressure ratio for several angles of attack and Mach numbers. $\beta = 0^o$; $\delta_f = 0^o$; $\delta_s = 0^o$; $\delta_h = -1.5^o$; $\delta_r = -5^o$; and military power.

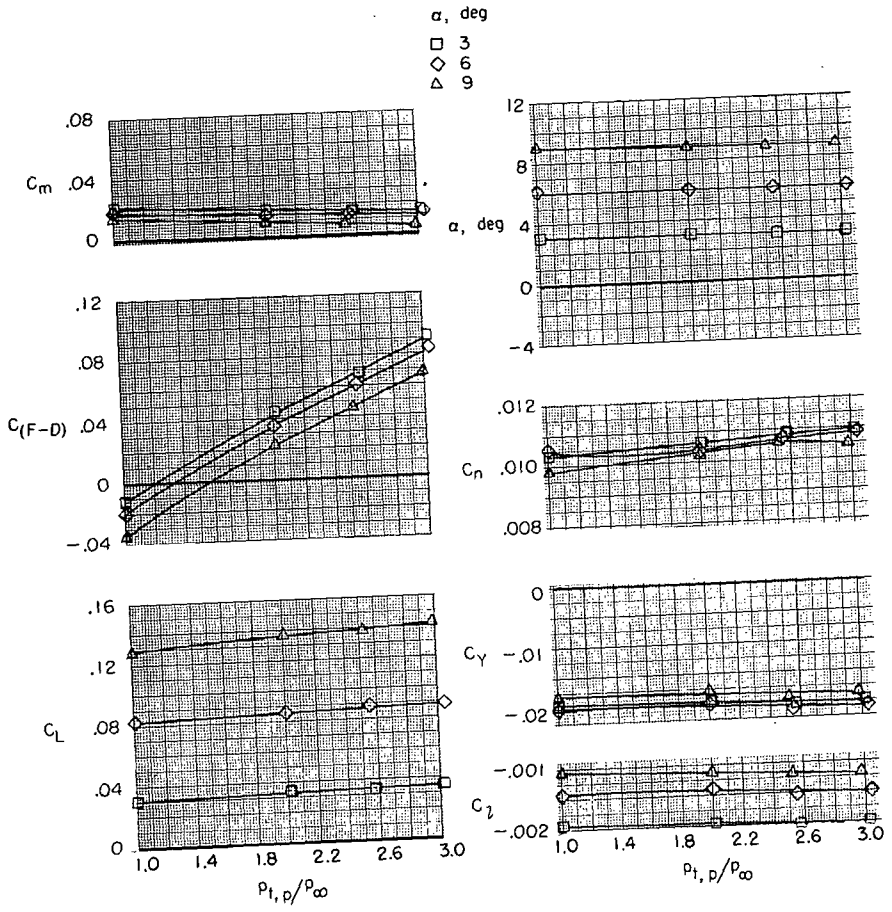

(b) M = 0.60.

Figure 10.- Continued.

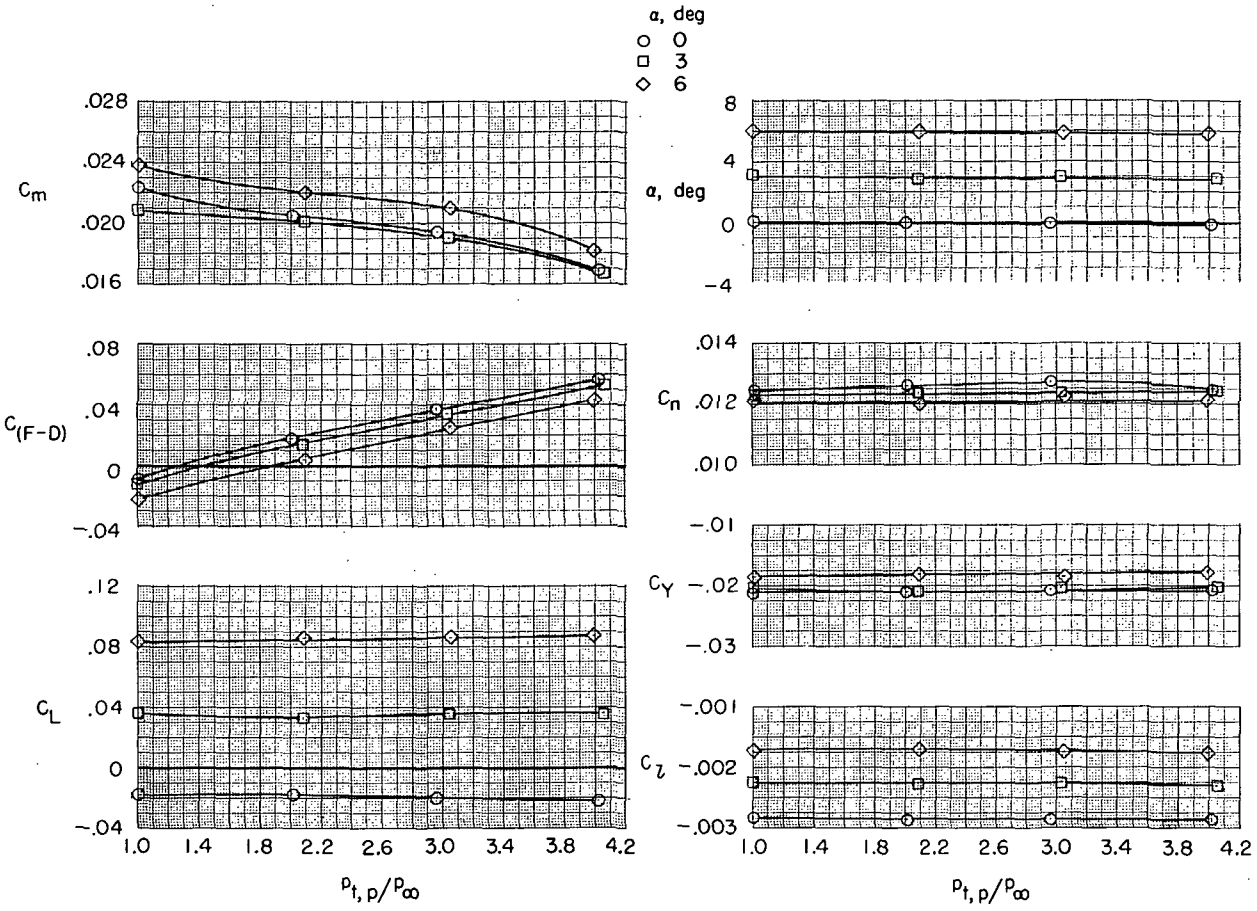

(c) M = 0.90.

Figure 10.- Continued.

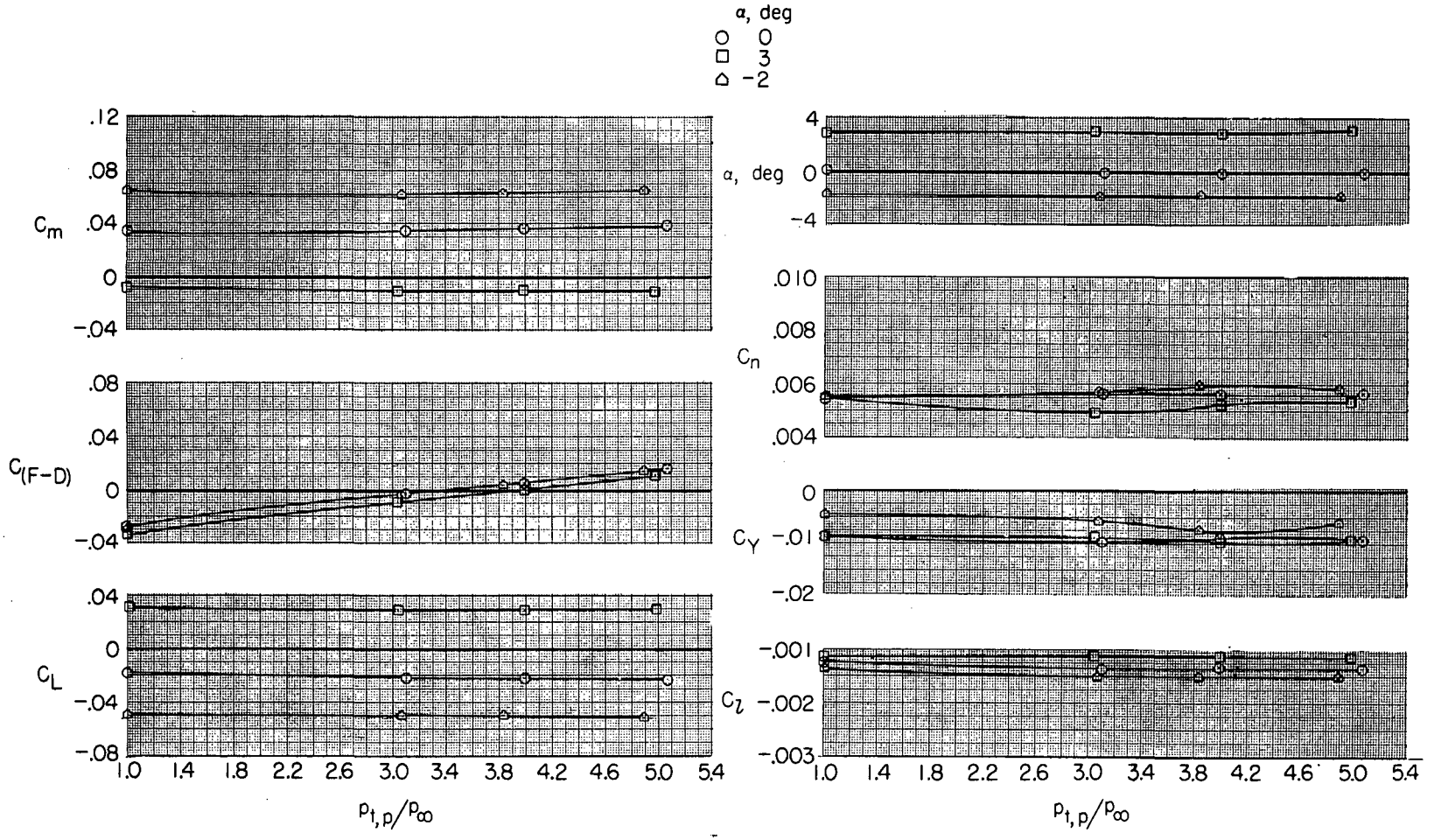

(d) M = 1.30.

Figure 10.- Concluded.

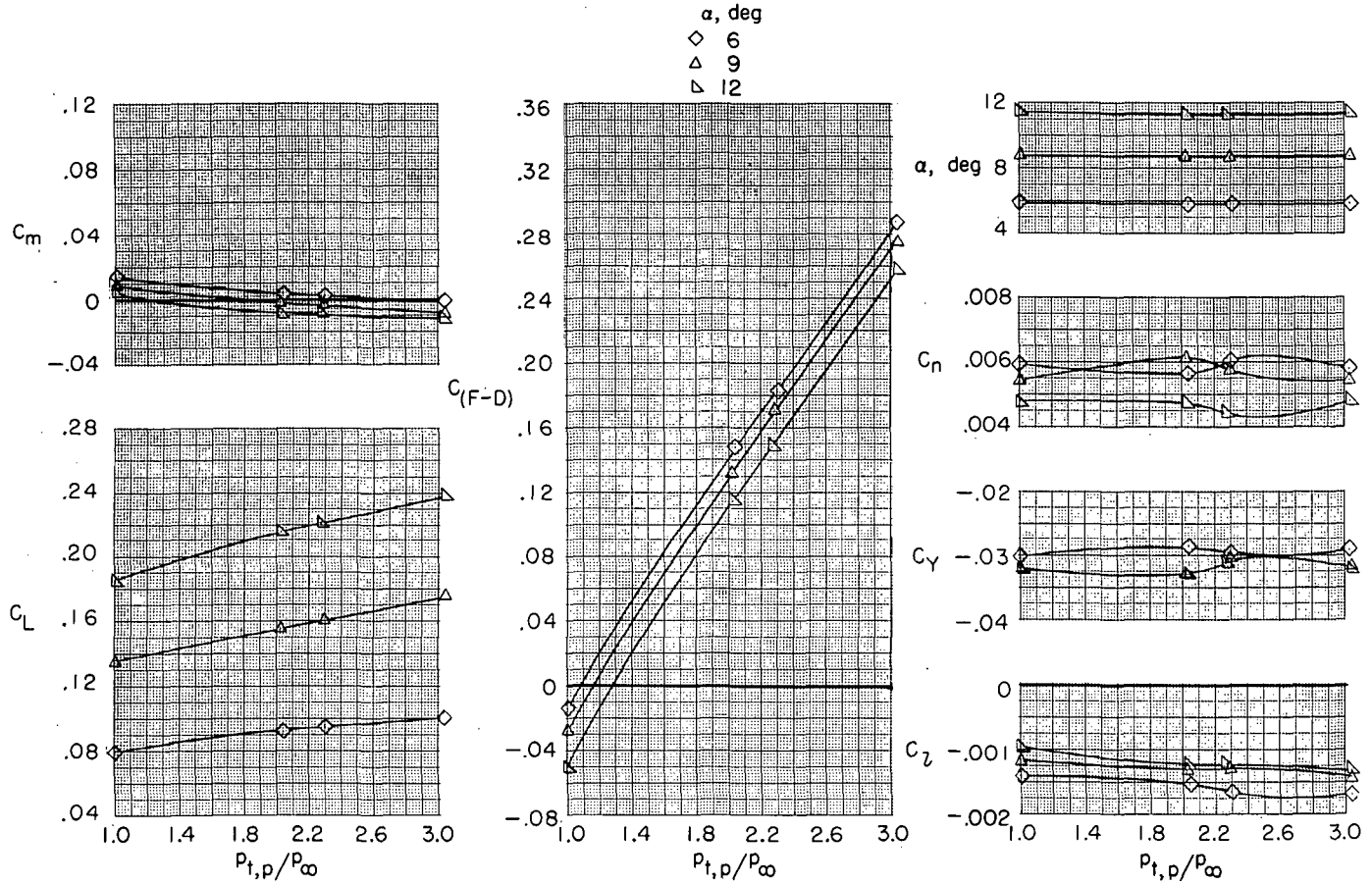

(a) M = 0.34.

Figure 11.- Effect of jet-total-pressure ratio on aerodynamic characteristics of basic model for several angles of attack and Mach numbers. $\beta = 2^o$; $\delta_f = 0^o$; $\delta_s = 0^o$; $\delta_h = -1.5^o$; $\delta_r = 0^o$; and military power.

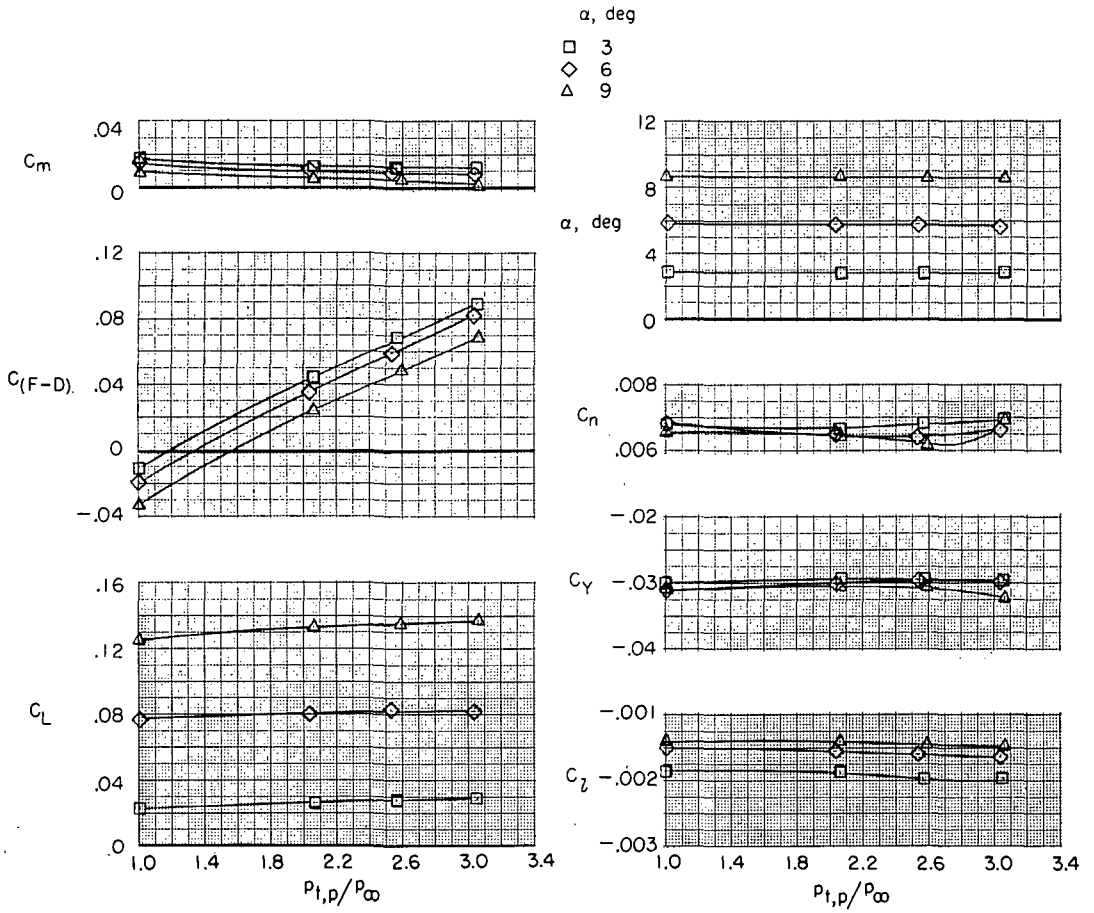

(b) M = 0.60.

Figure 11.- Continued.

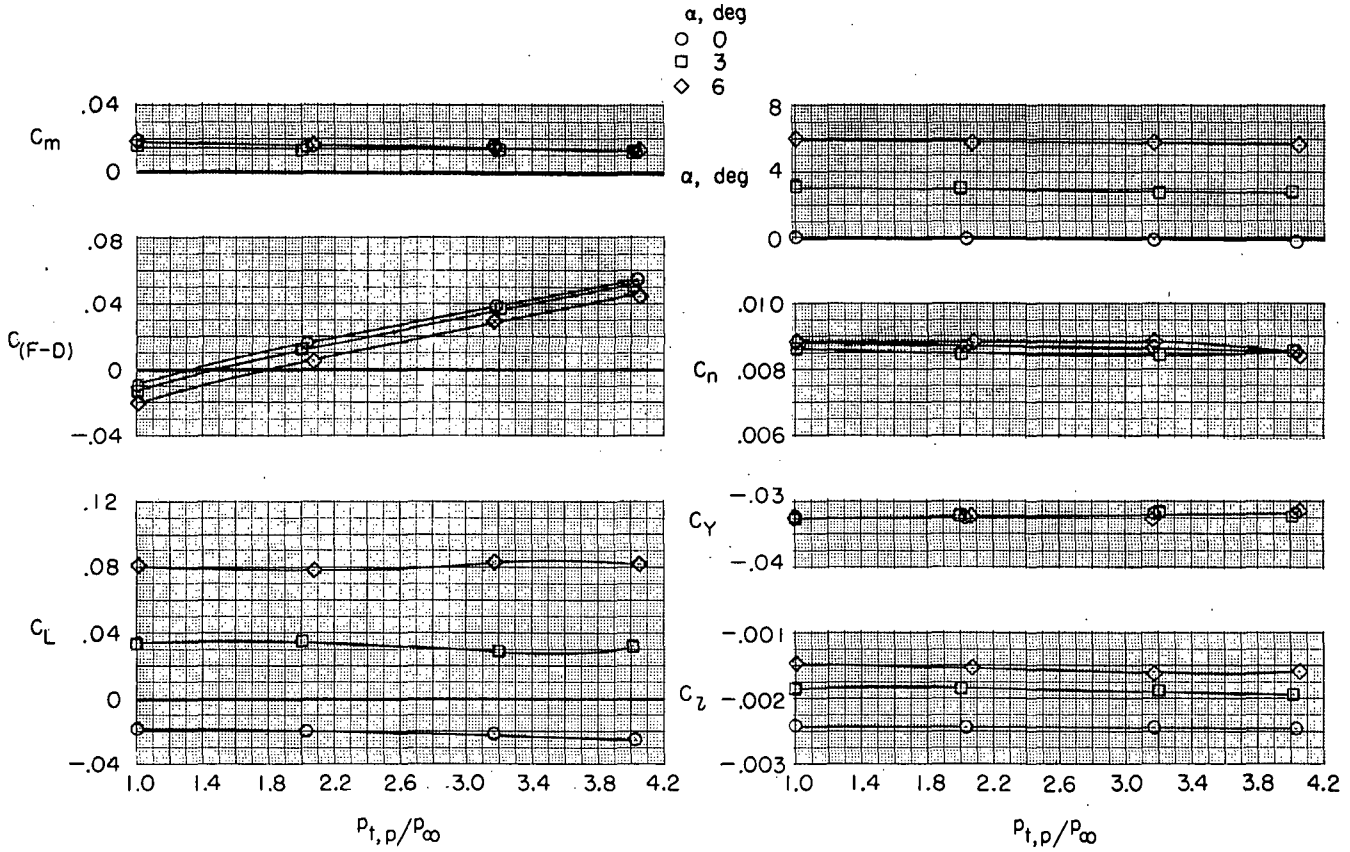

(c) M = 0.90.

Figure 11.- Continued.

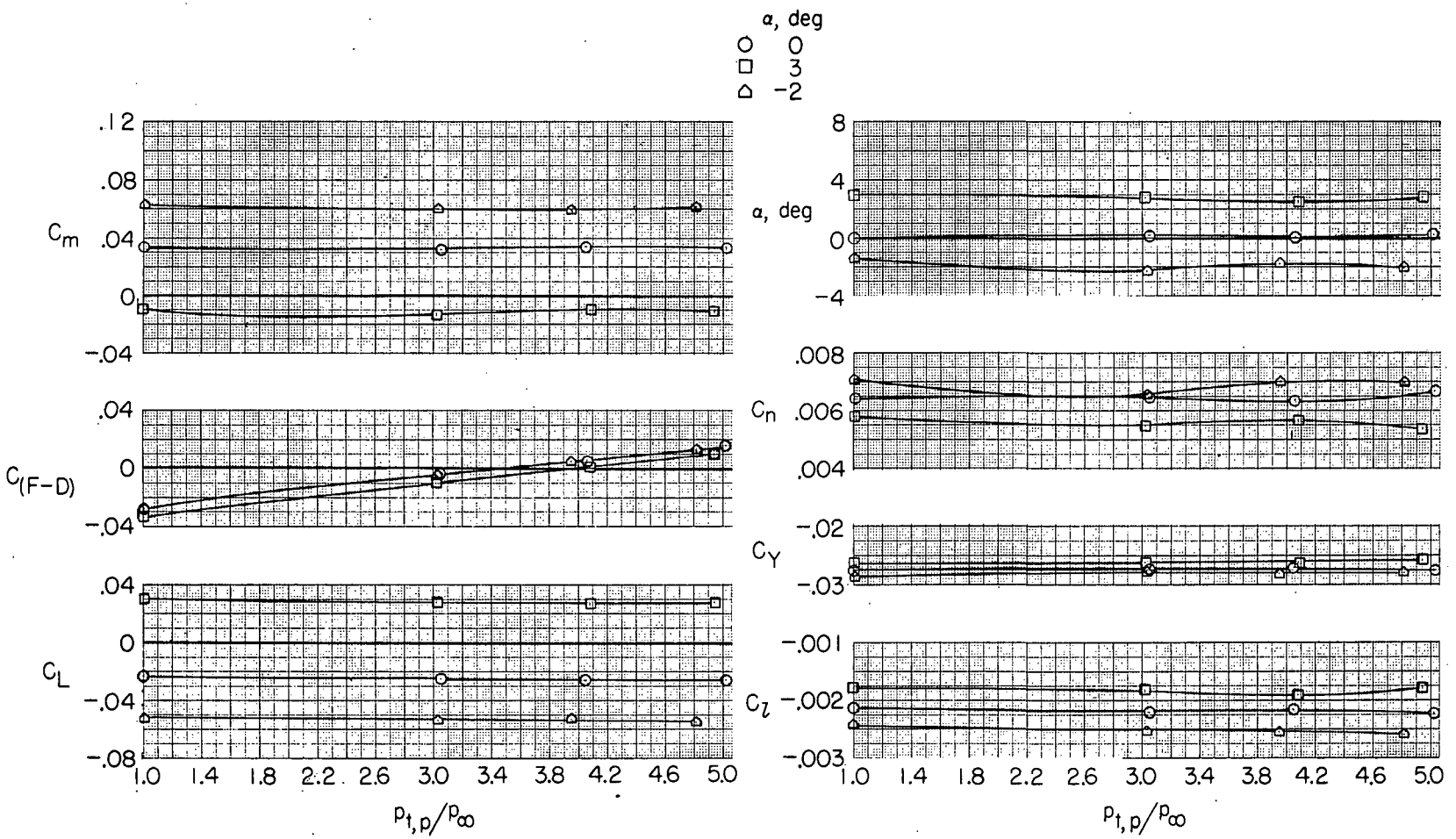

(d) M = 1.30.

Figure 11.- Concluded.

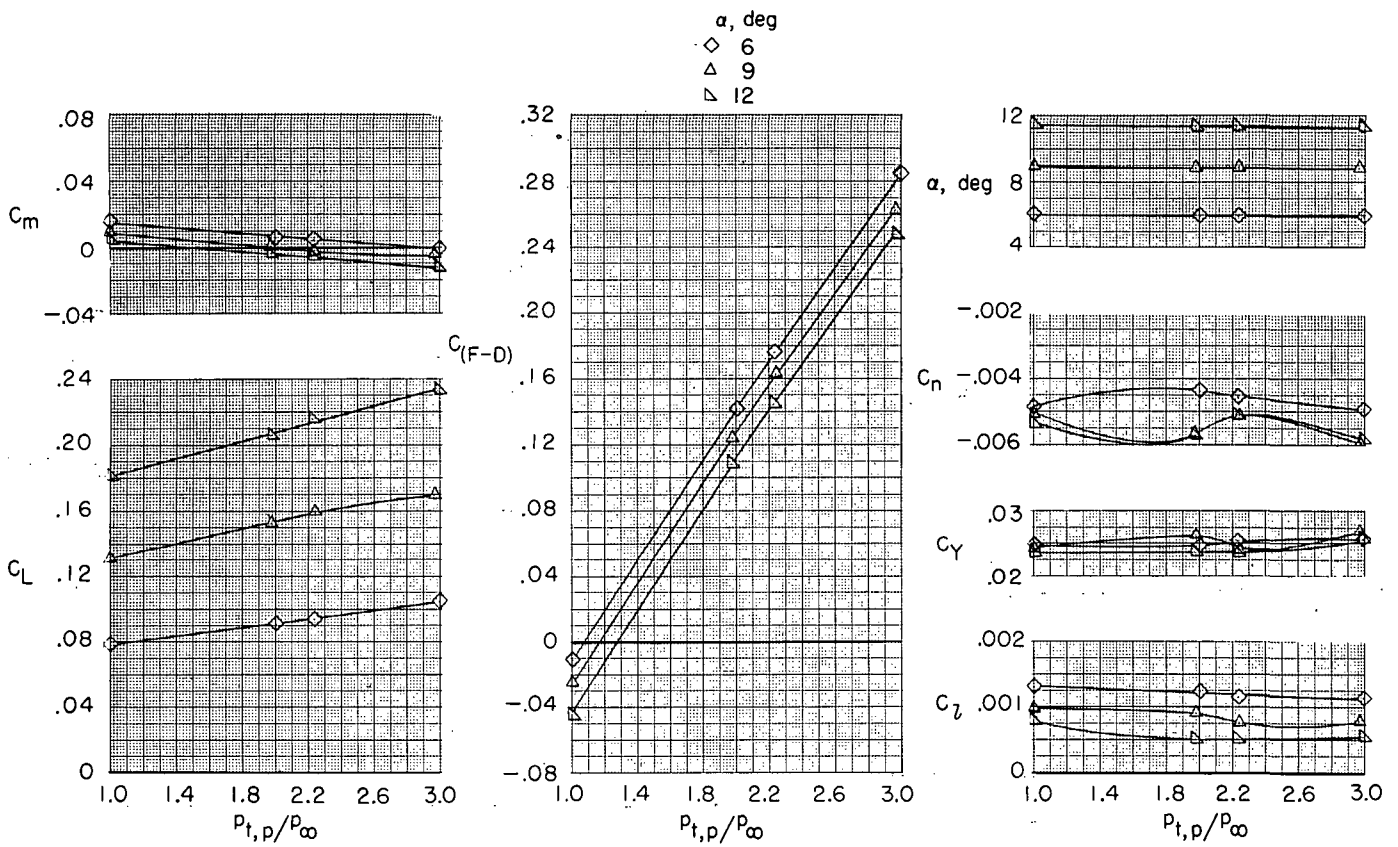

(a) M = 0.34.

Figure 12.- Effect of jet-total-pressure ratio on aerodynamic characteristics of basic model for several angles of attack and Mach numbers. $\beta = -2^o$; $\delta_f = 0^o$; $\delta_s = 0^o$; $\delta_h = -1.5^o$; $\delta_r = 0^o$; and military power.

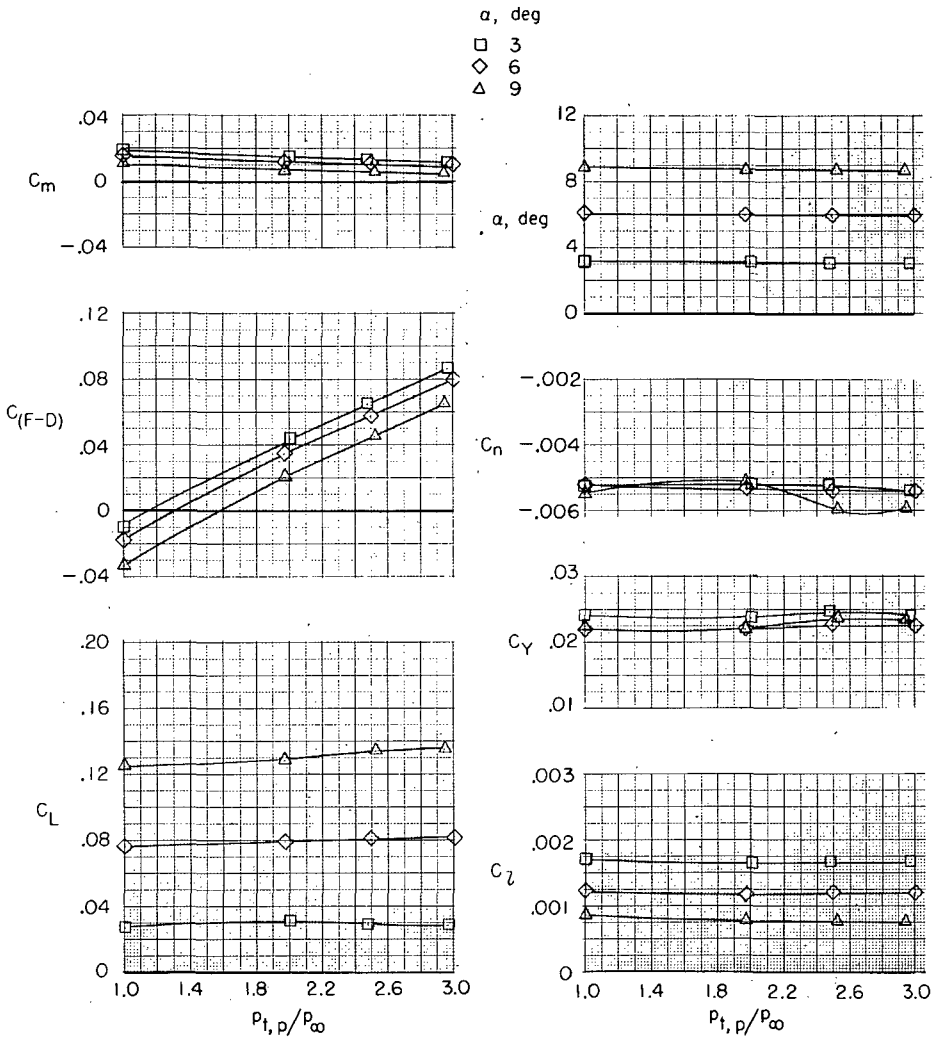

(b) M = 0.60.

Figure 12.- Continued.

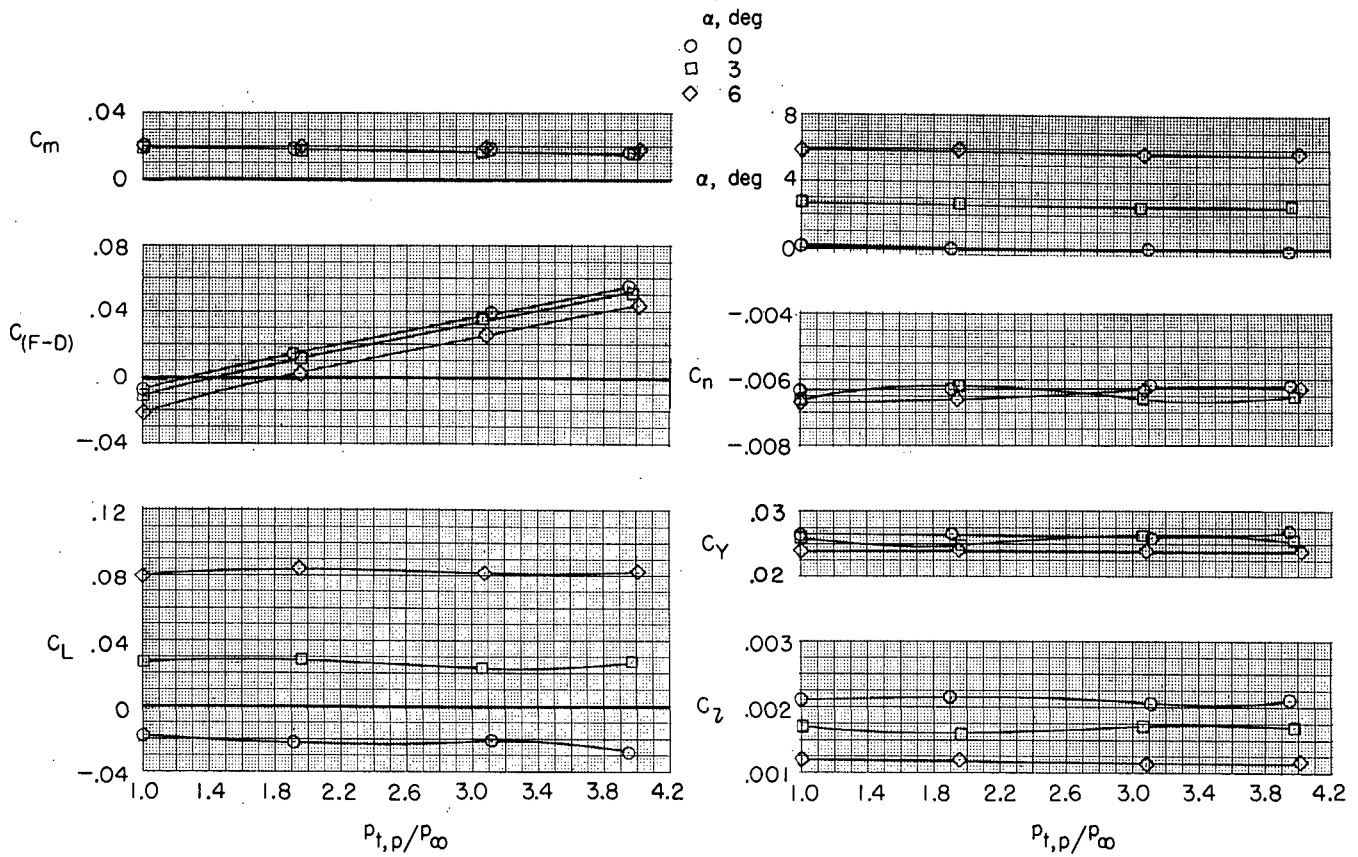

(c) M = 0.90.

Figure 12.- Continued.

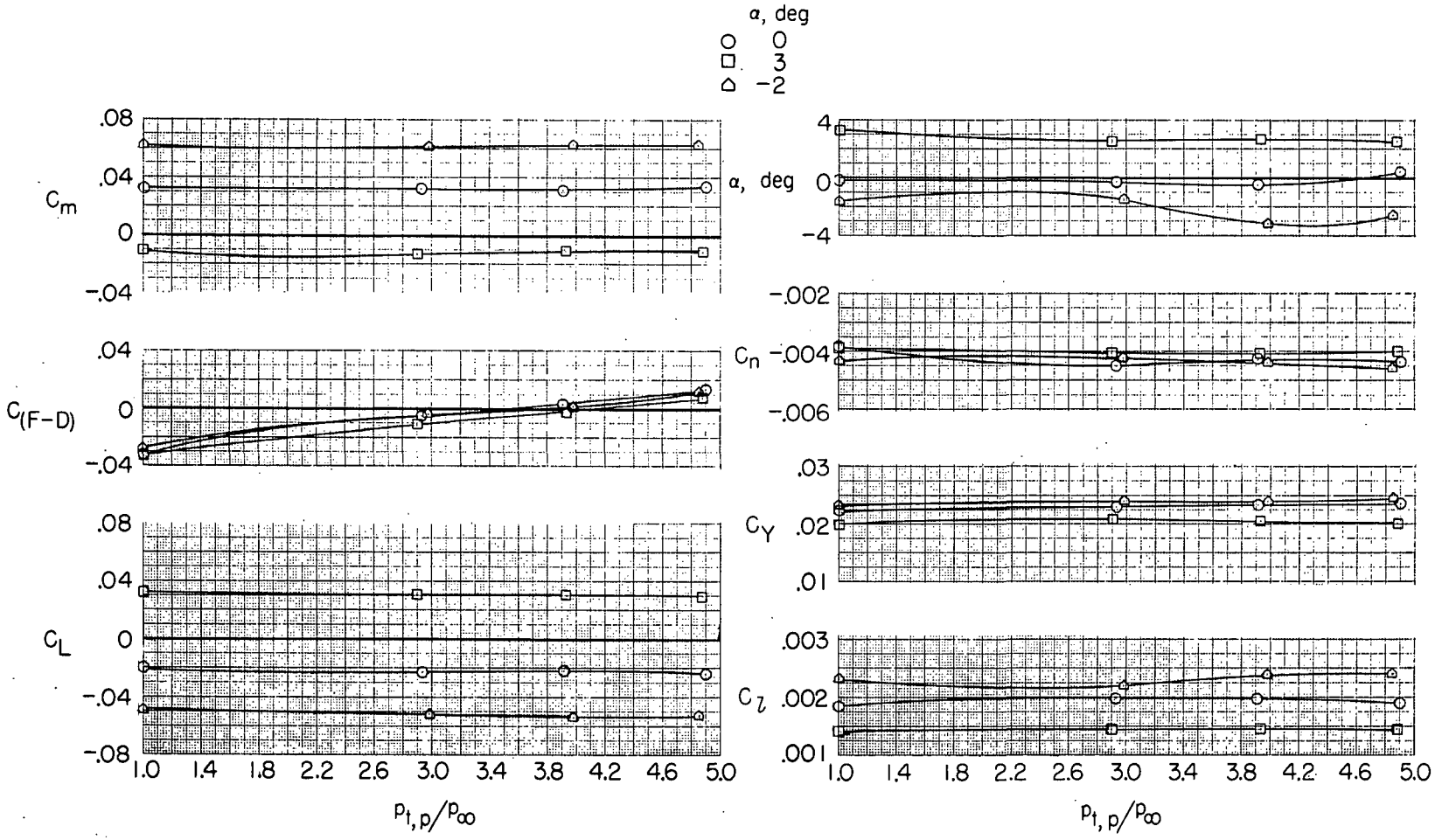

(d) M = 1.30.

Figure 12.- Concluded.

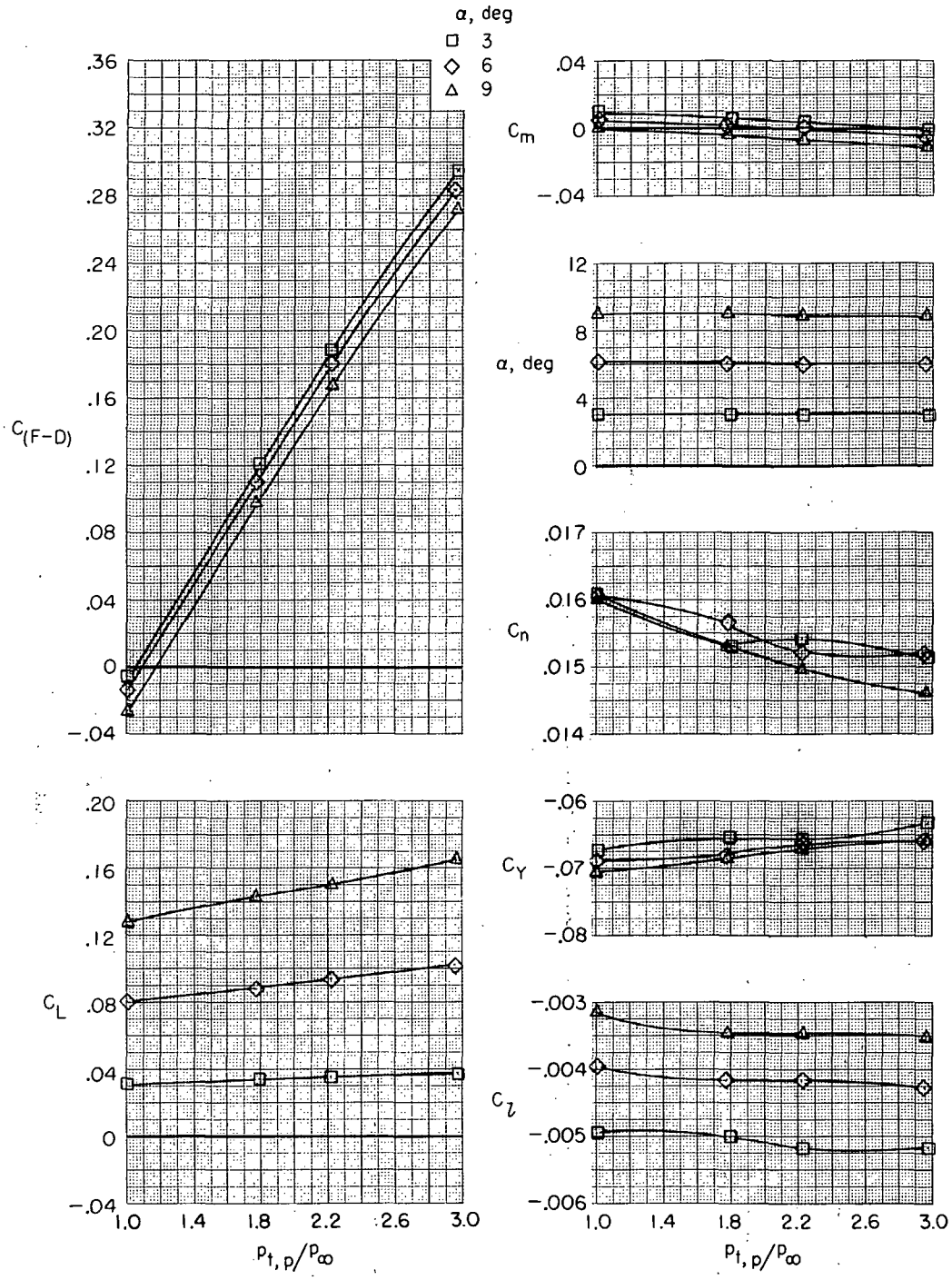

(a) M = 0.34.

Figure 13.- Effect of jet-total-pressure ratio on aerodynamic characteristics of basic model for several angles of attack and Mach numbers. $\beta = 5^{o}$; $\delta_f = 0^{o}$; $\delta_s = 0^{o}$; $\delta_h = -1.5^{o}$; $\delta_r = 0^{o}$; and military power.

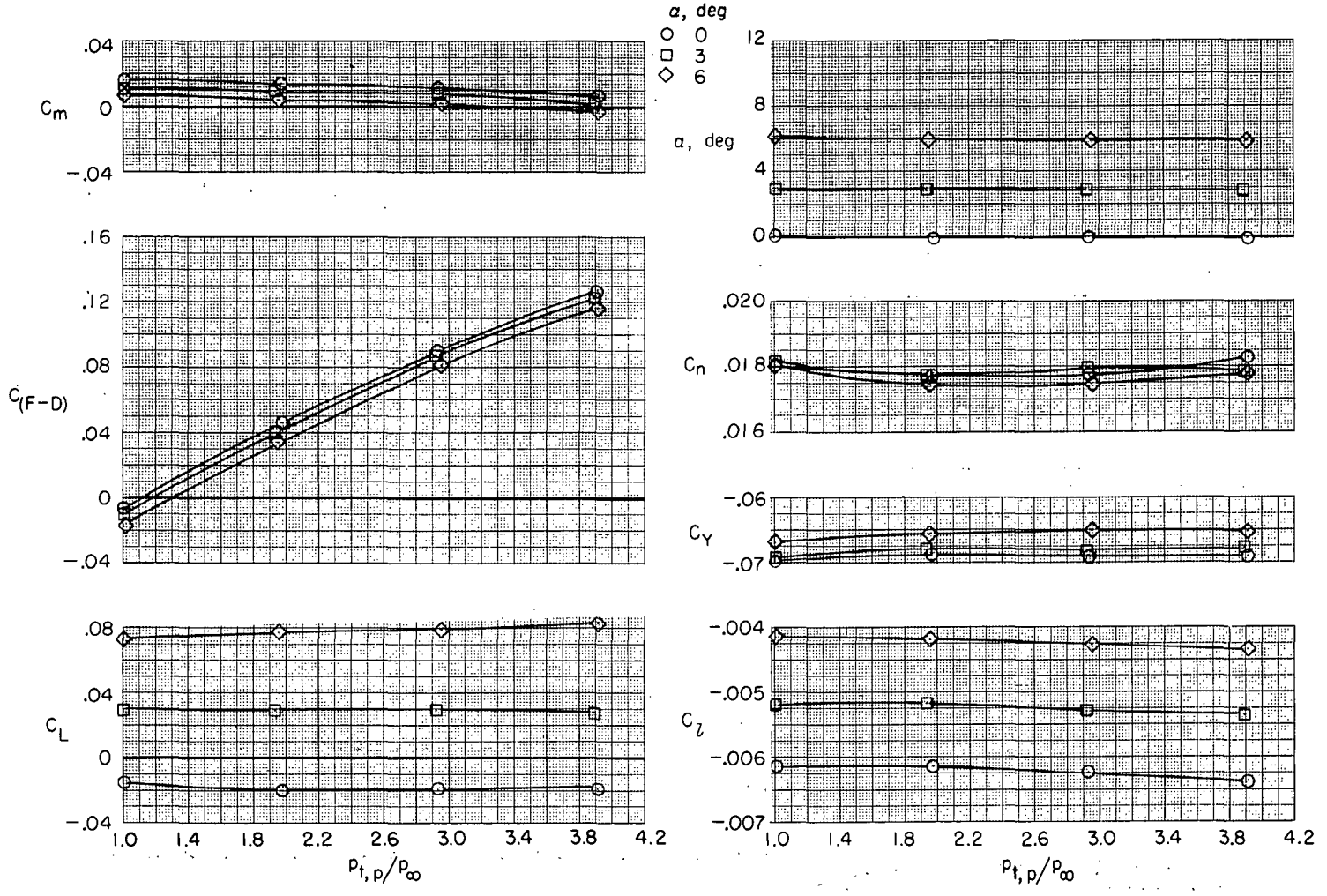

(b) M = 0.60.

Figure 13.- Continued.

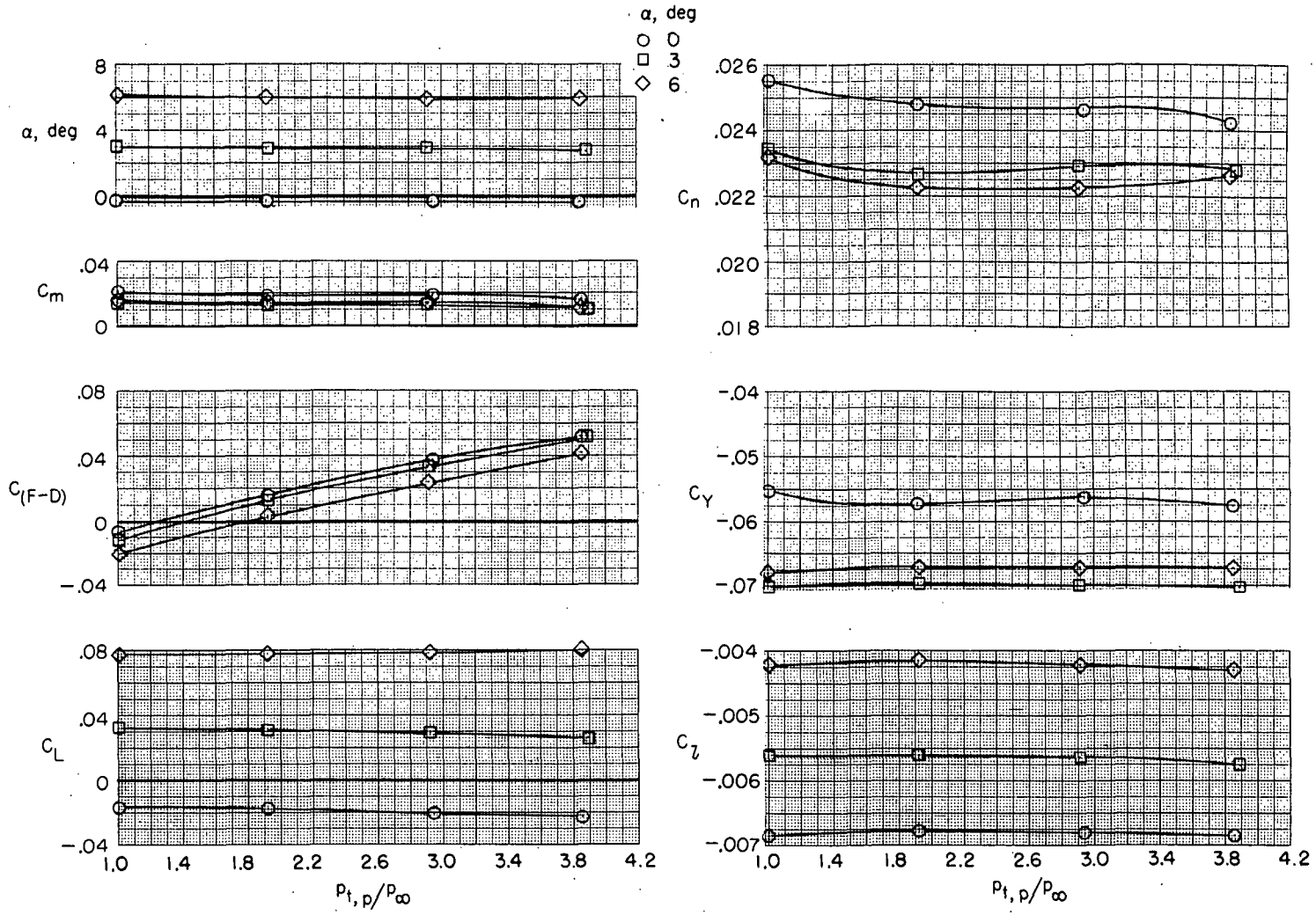

(c) M = 0.90.

Figure 13.- Concluded.

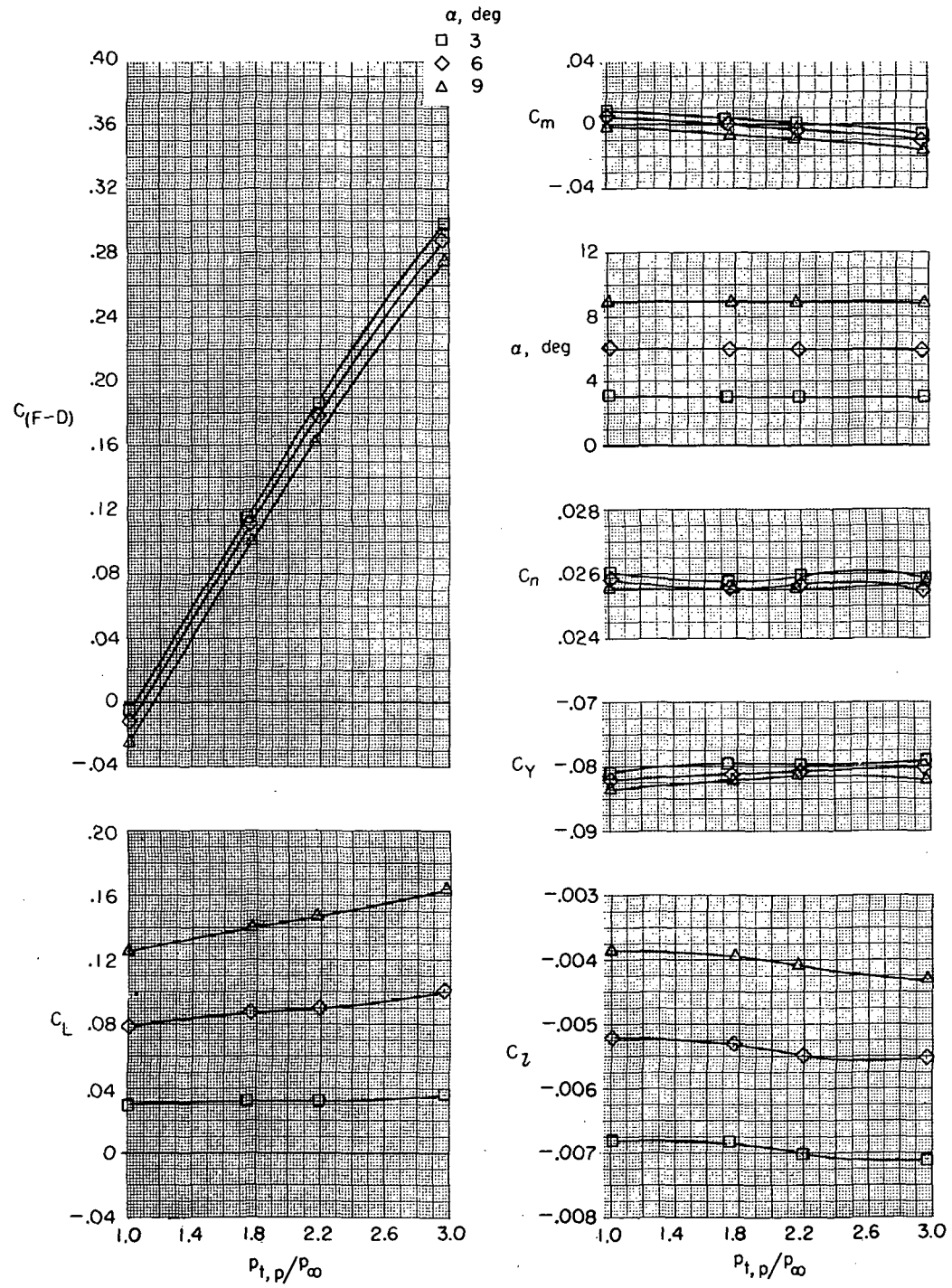

(a) M = 0.34.

Figure 14.- Effect of jet-total-pressure ratio on aerodynamic characteristics of basic model for several angles of attack and Mach numbers. $\beta = 5^{o}$; $\delta_f = 0^{o}$; $\delta_s = 0^{o}$; $\delta_h = -1.5^{o}$; $\delta_r = -5^{o}$; and military power.

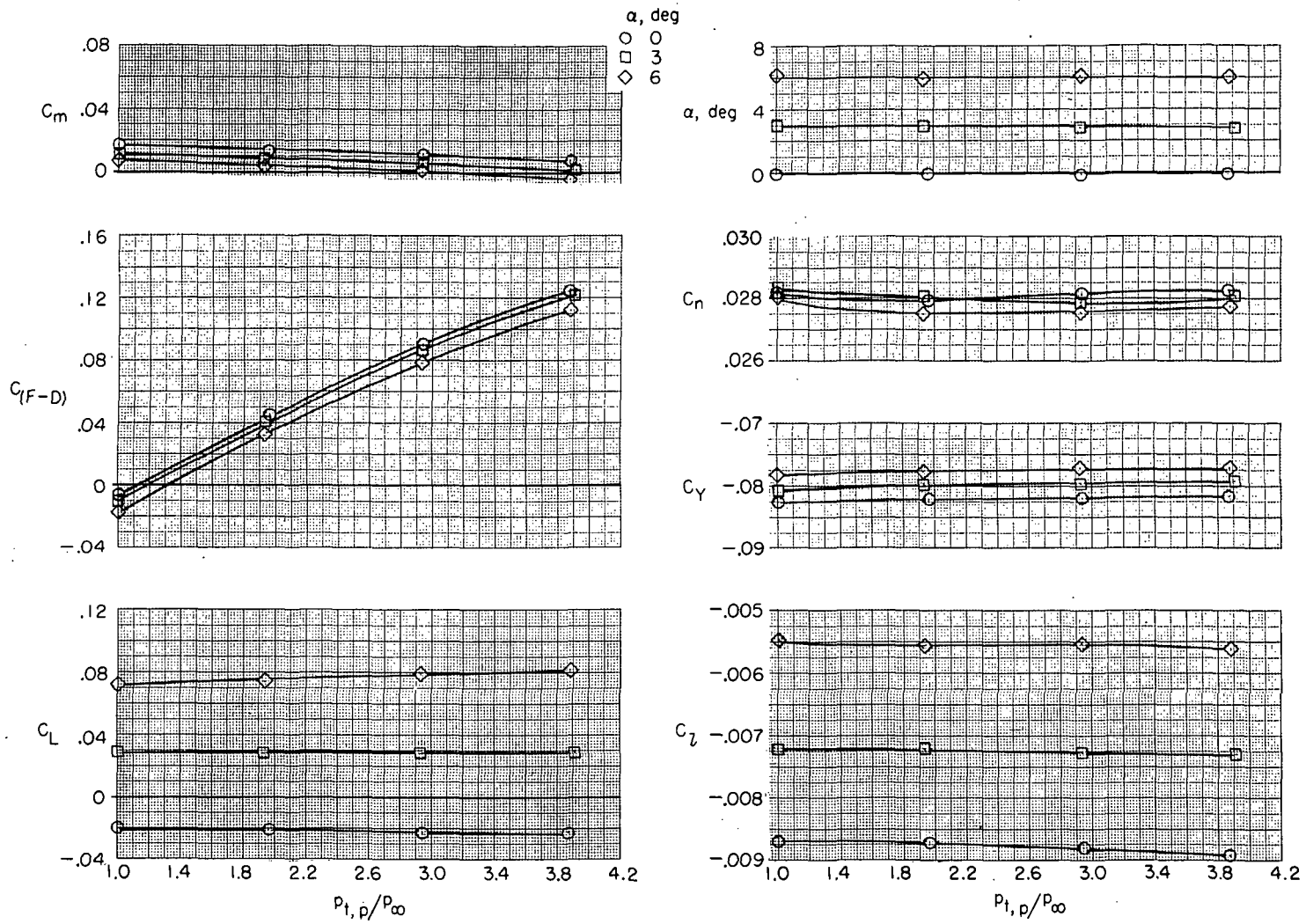

(b) M = 0.60.

Figure 14.- Concluded.

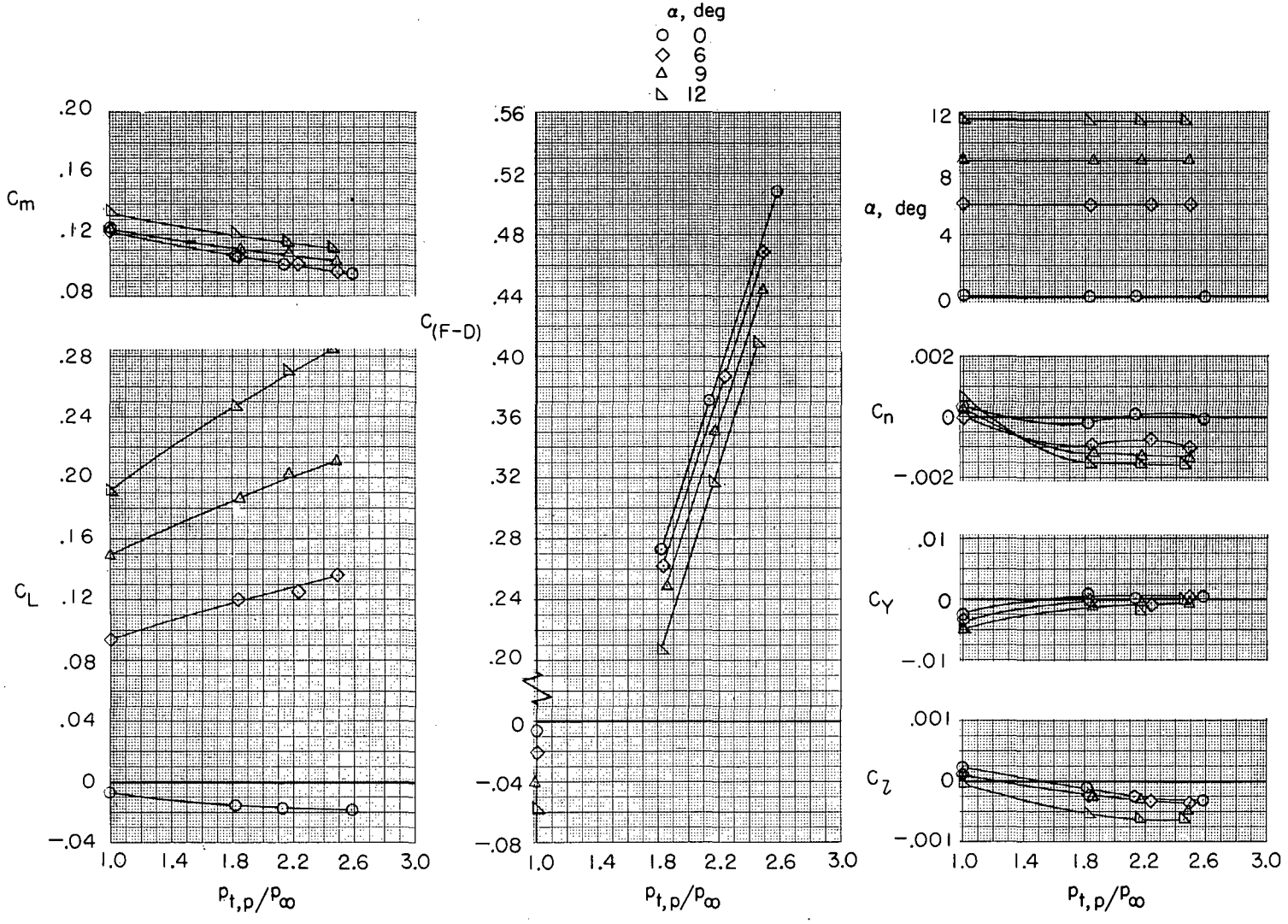

(a) $\beta = 0^o$; $\delta_h = -1.5^o$; $\delta_r = 0^o$.

Figure 15.- Effect of jet-total-pressure ratio on aerodynamic characteristics of basic model in approach configuration for several angles of attack. M = 0.23; $\delta_f = -30^o$; $\delta_s = -20^o$; and military power.

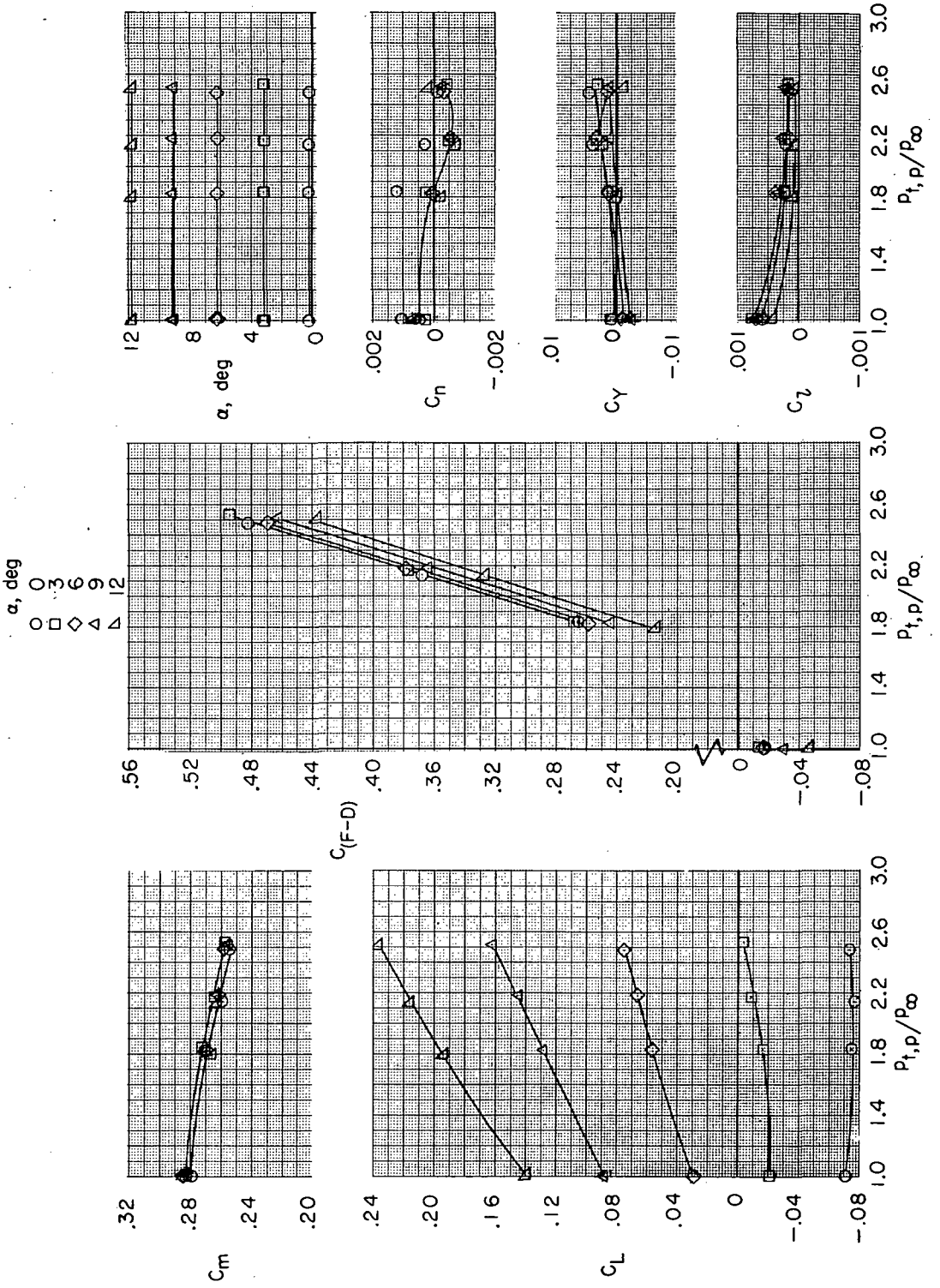

(b) $\beta = 0^\circ$; $\delta_h = -10^\circ$; $\delta_r = 0^\circ$.

Figure 15.- Continued.

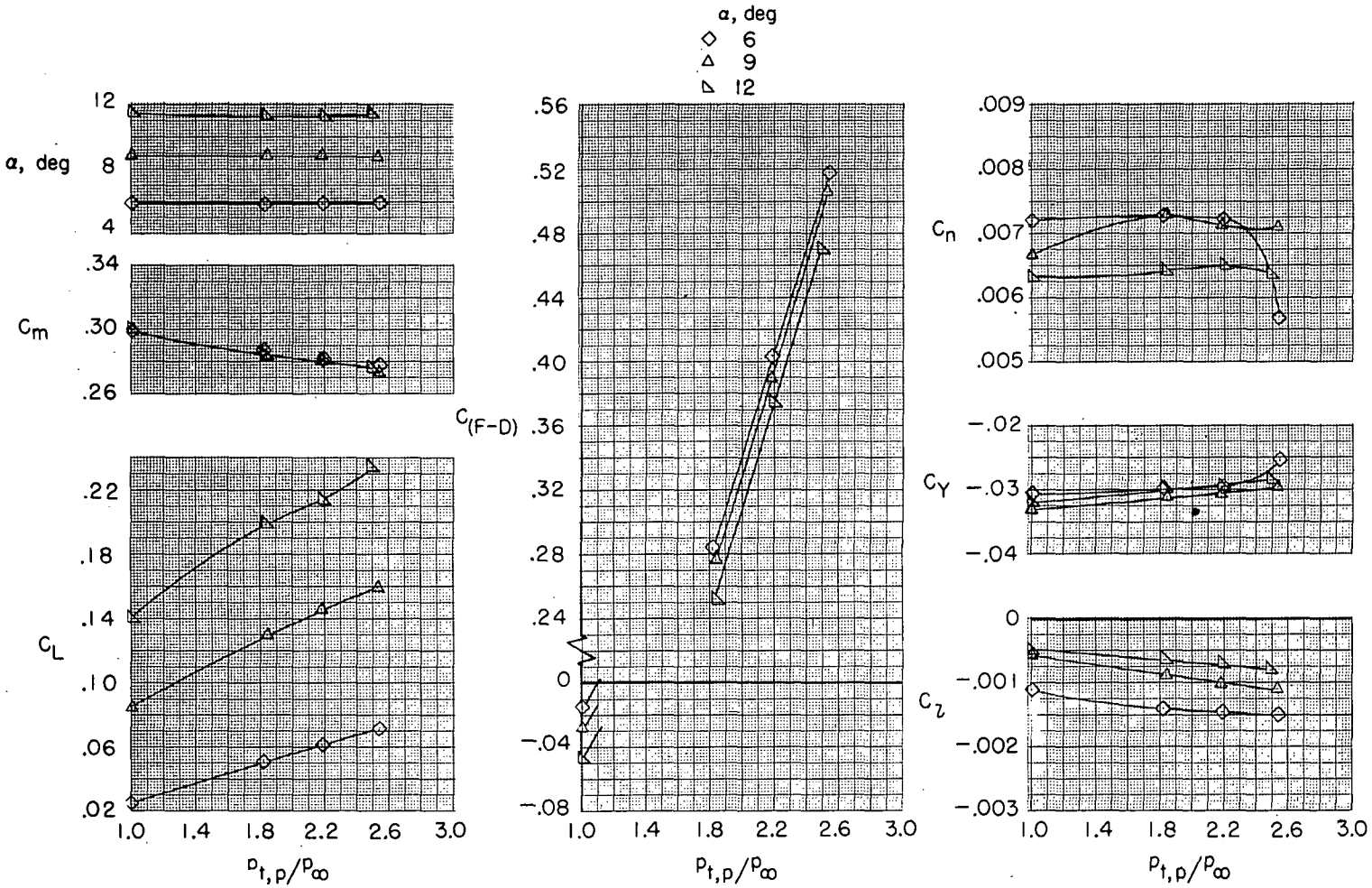

(c) $\beta = 2^o$; $\delta_h = -10^o$; $\delta_r = 0^o$.

Figure 15.- Continued.

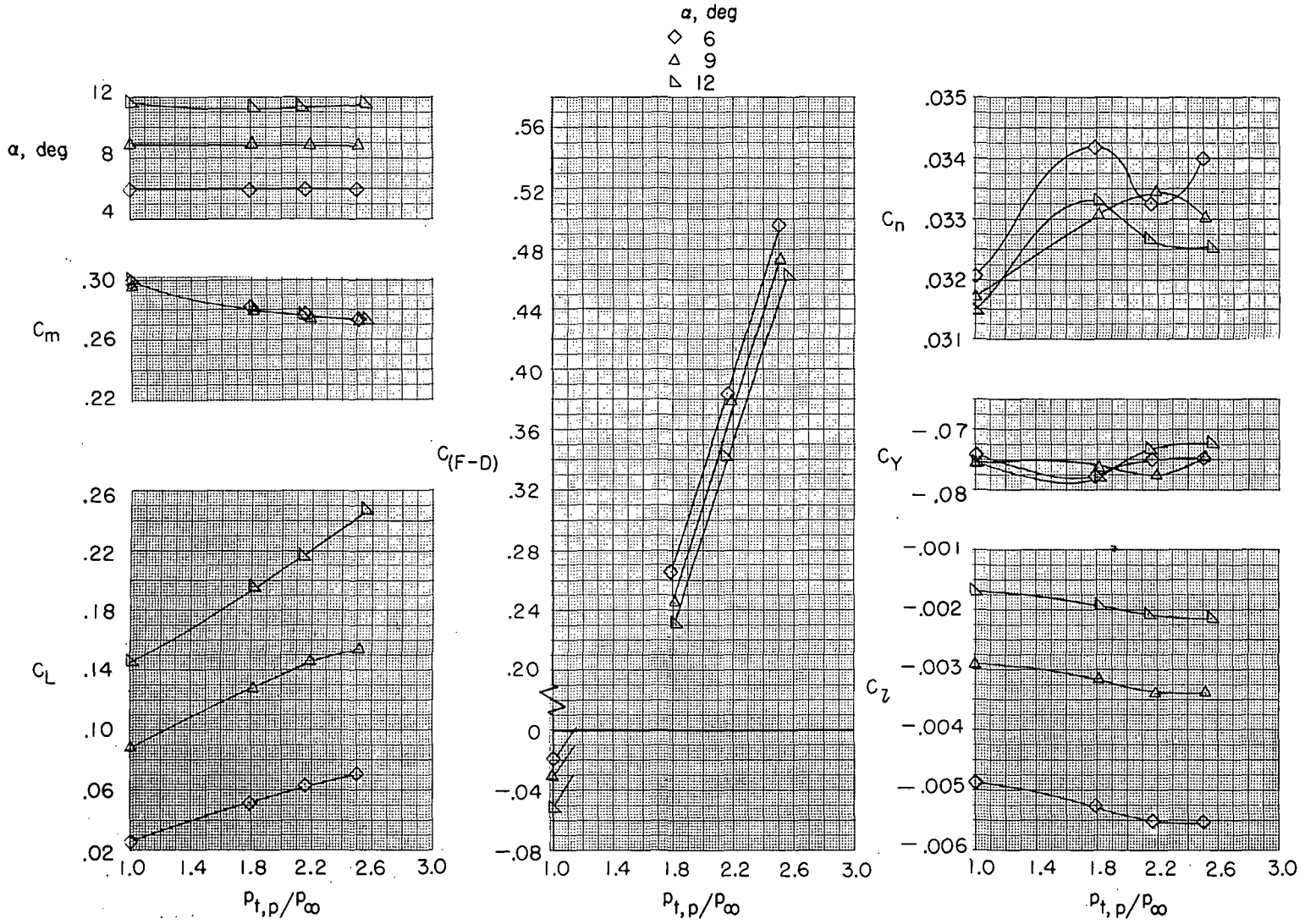

(d) $\beta = 2^o$; $\delta_h = -10^o$; $\delta_r = -15^o$.

Figure 15.- Continued.

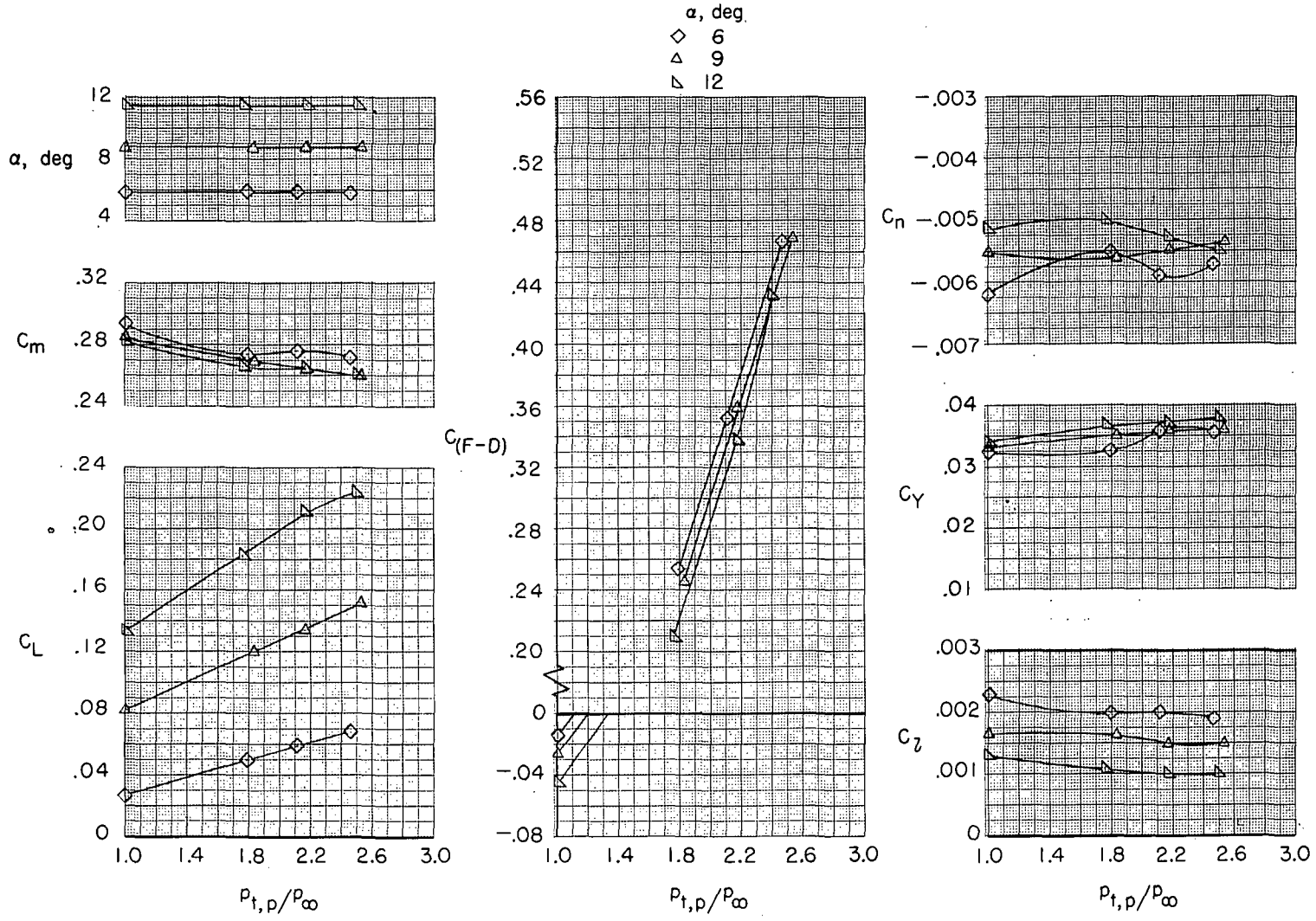

(e) $\beta = -2^o$; $\delta_h = -10^o$; $\delta_r = 0^o$.

Figure 15.- Continued.

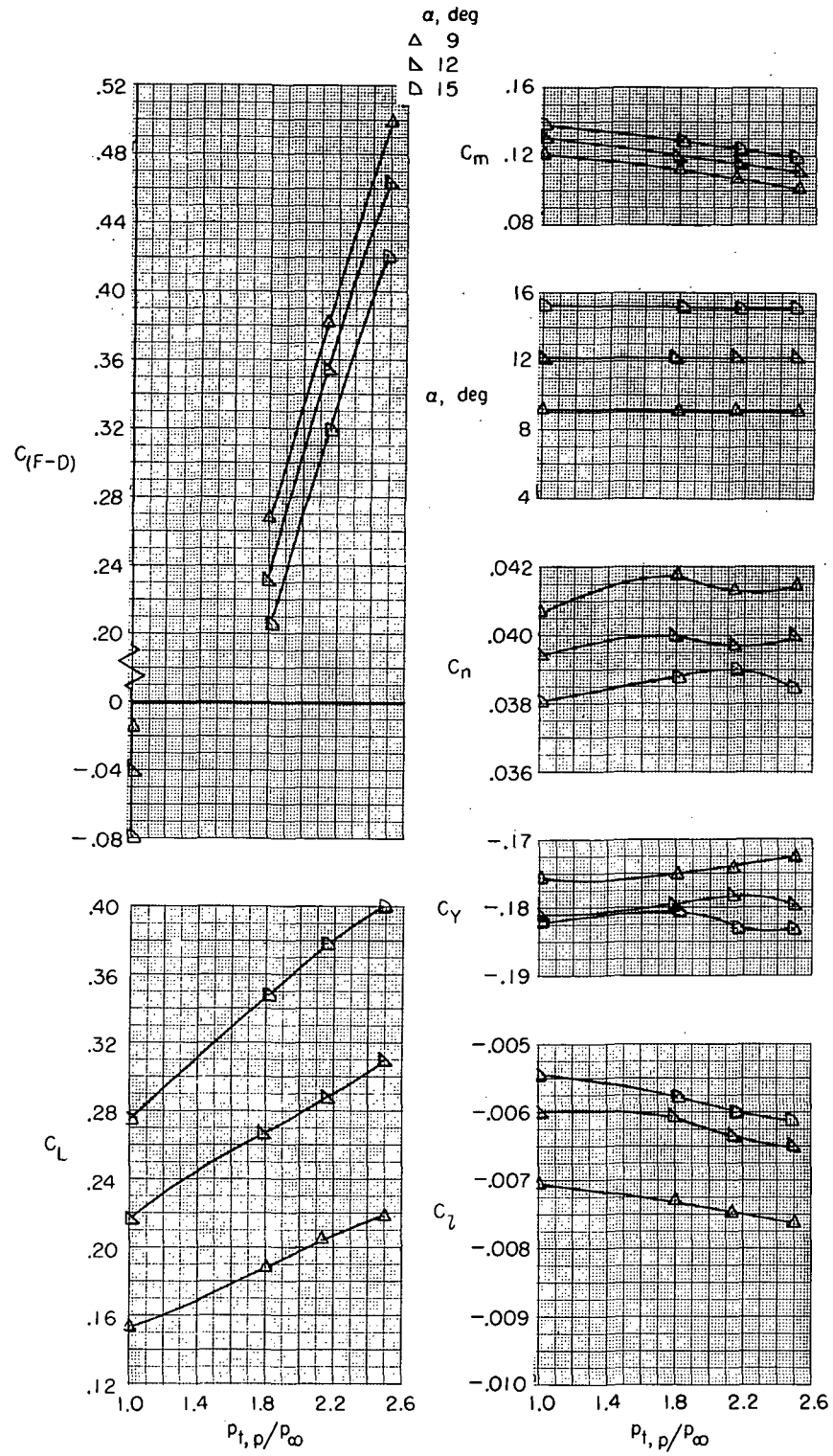

(f) $\beta = 10^{o}$; $\delta_{h} = -10^{o}$; $\delta_{r} = 0^{o}$.

Figure 15.- Continued.

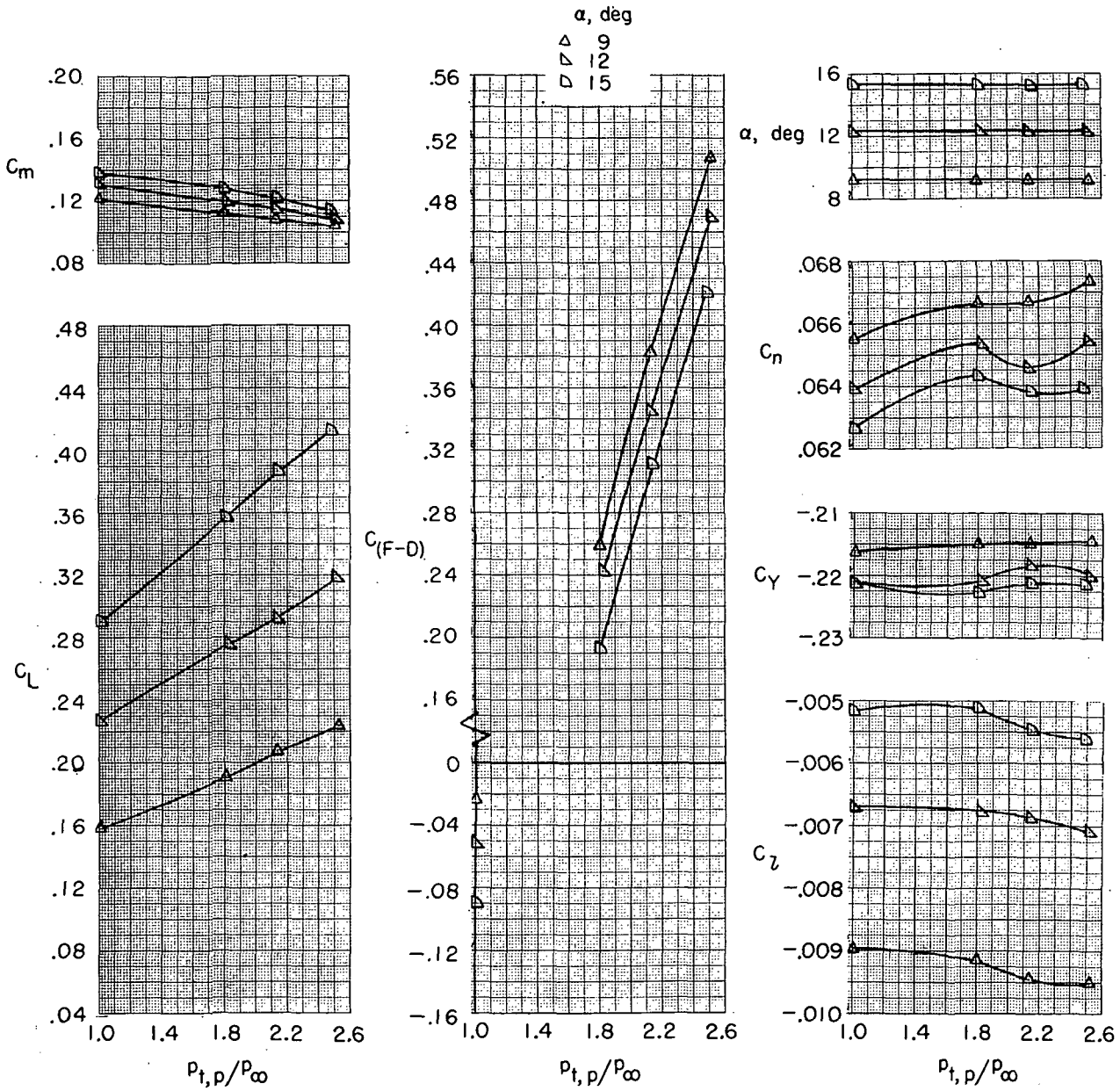

(g) $\beta = 10^o$; $\delta_h = -10^o$; $\delta_r = -15^o$.

Figure 15.- Concluded.

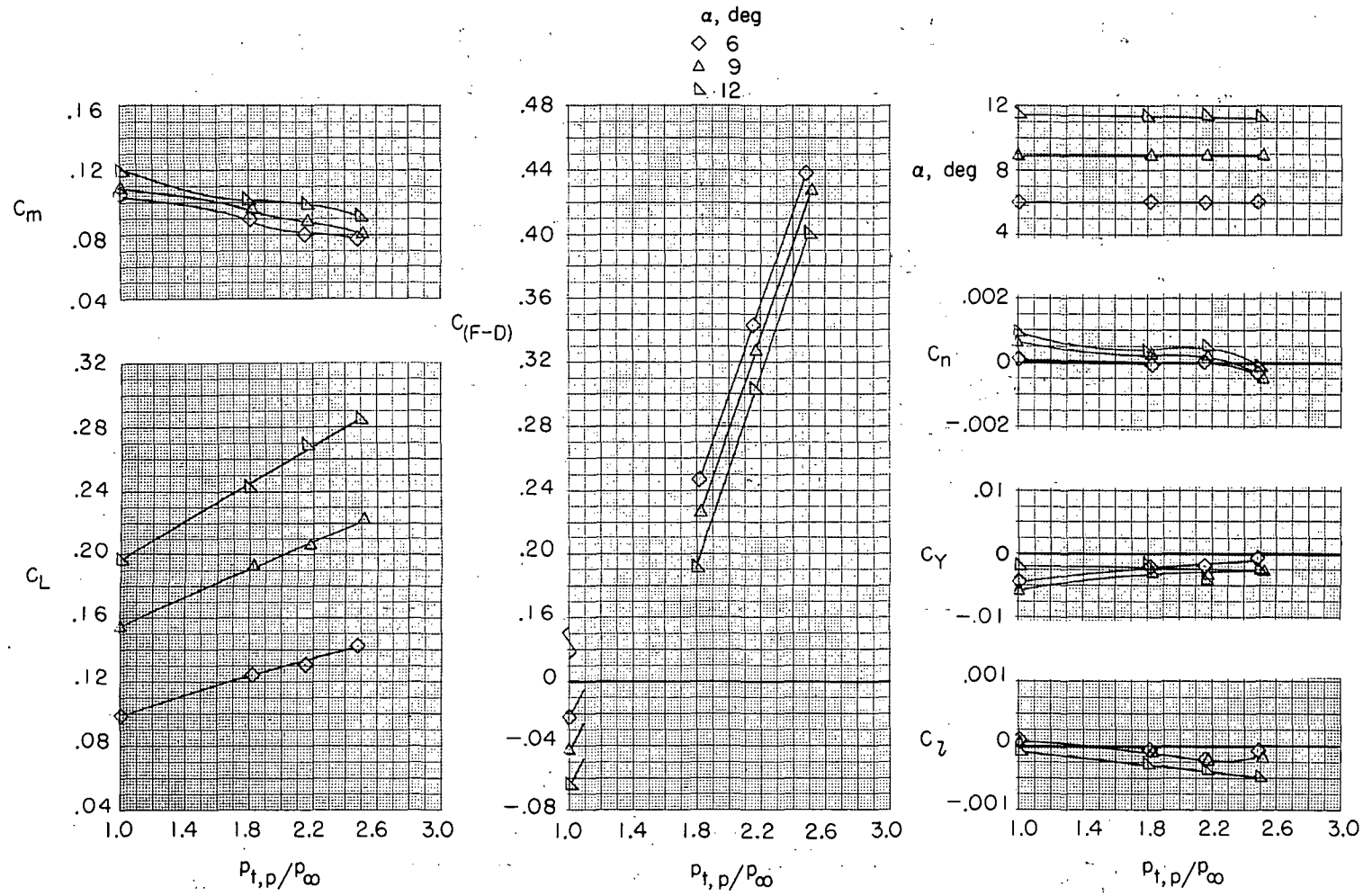

(a) $\beta = 0^o$; $\delta_b = 0$ percent; $\delta_h = -1.5^o$; $\delta_r = 0^o$.

Figure 16.- Effect of jet-total-pressure ratio on aerodynamic characteristics of model in approach configuration with thrust control unit (TCU) for several angles of attack. M = 0.23; $\delta_f = -30^o$; $\delta_s = -20^o$; $\delta_{du} = 32.5^o$; $\delta_{dl} = 52.5^o$; and military power.

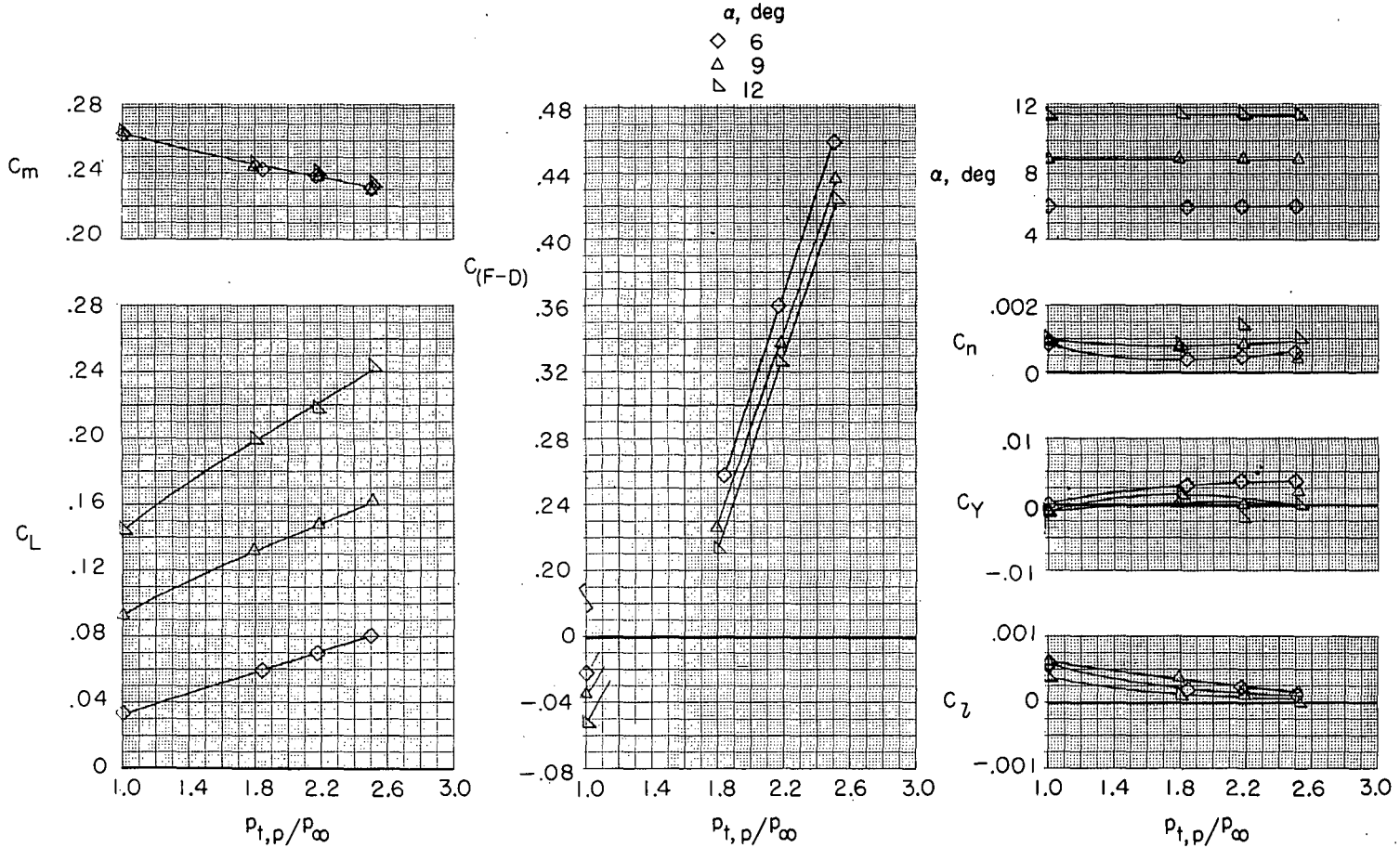

(b) $\beta = 0^o$; $\delta_b = 0$ percent; $\delta_h = -10^o$; $\delta_r = 0^o$.

Figure 16.- Continued.

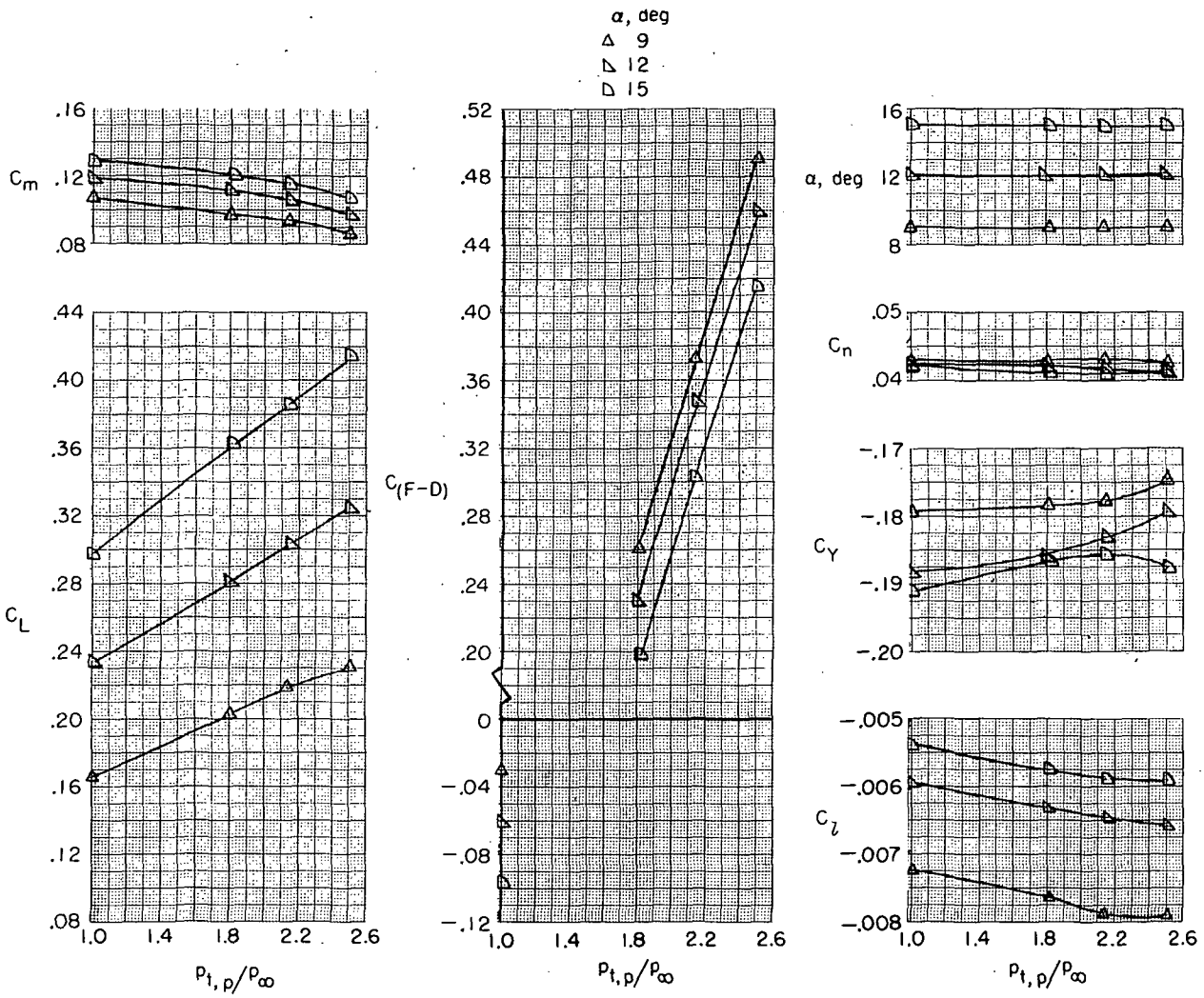

(c) $\beta = 10^o$; $\delta_b = 0$ percent; $\delta_h = -10^o$; $\delta_r = 0^o$.

Figure 16.- Continued.

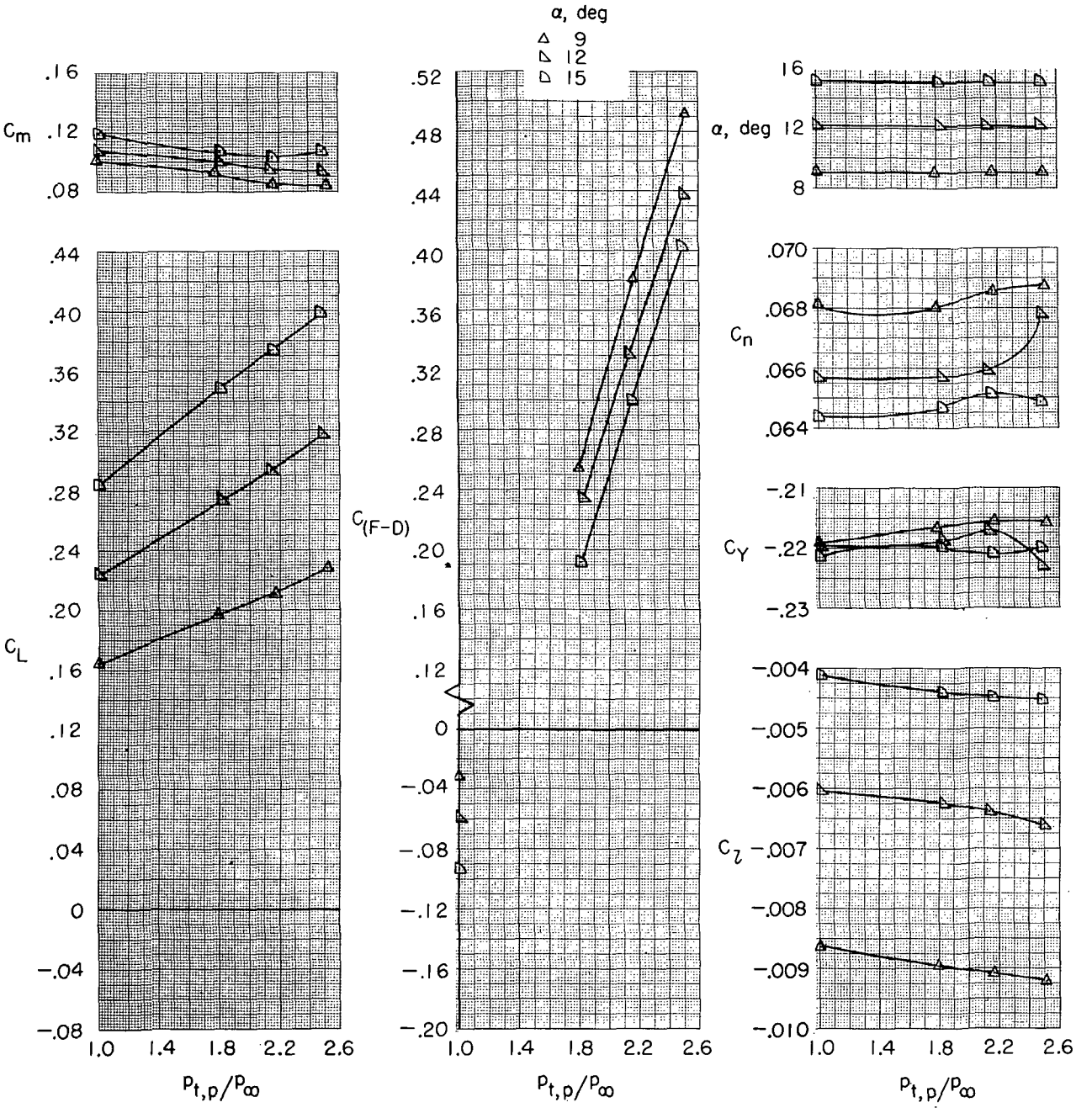

(d) $\beta = 10^o$; $\delta_b = 0$ percent; $\delta_h = -10^o$; $\delta_r = -15^o$.

Figure 16.- Continued.

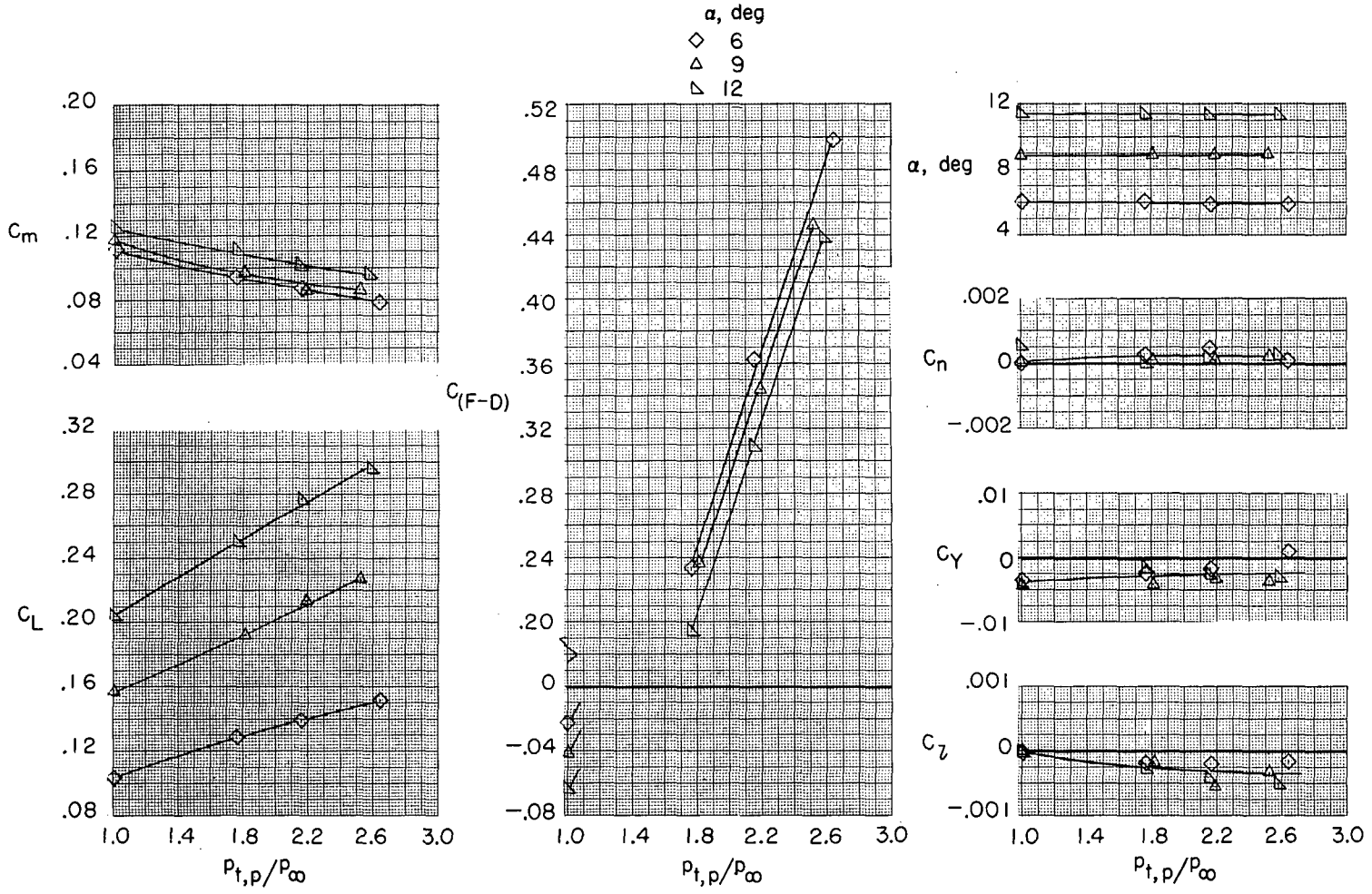

(e) $\beta = 0^o$; $\delta_b = 25$ percent; $\delta_h = -1.5^o$; $\delta_r = 0^o$.

Figure 16.- Continued.

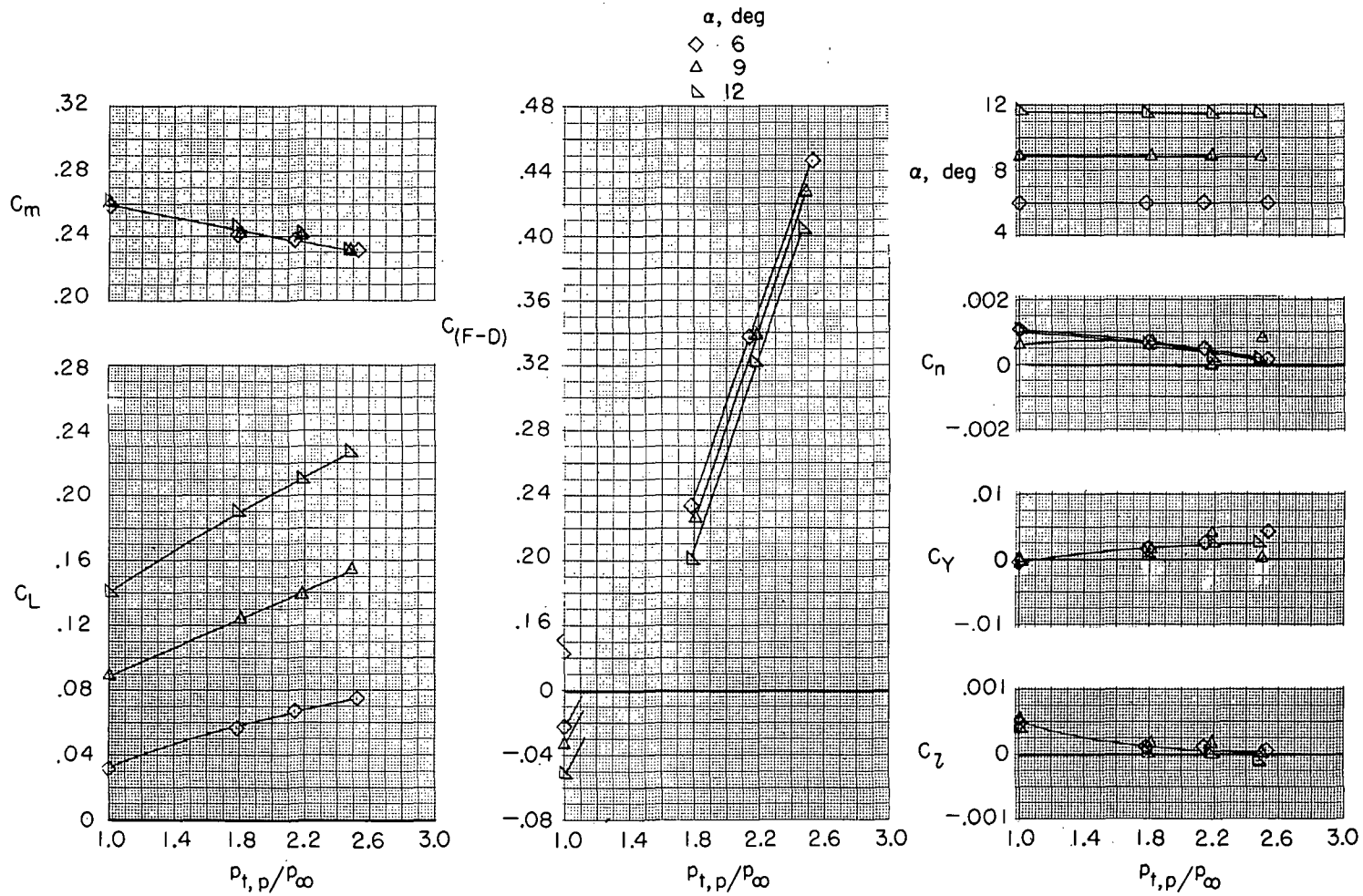

(f) $\beta = 0^o$; $\delta_b = 25$ percent; $\delta_h = -10^o$; $\delta_r = 0^o$.

Figure 16.- Continued.

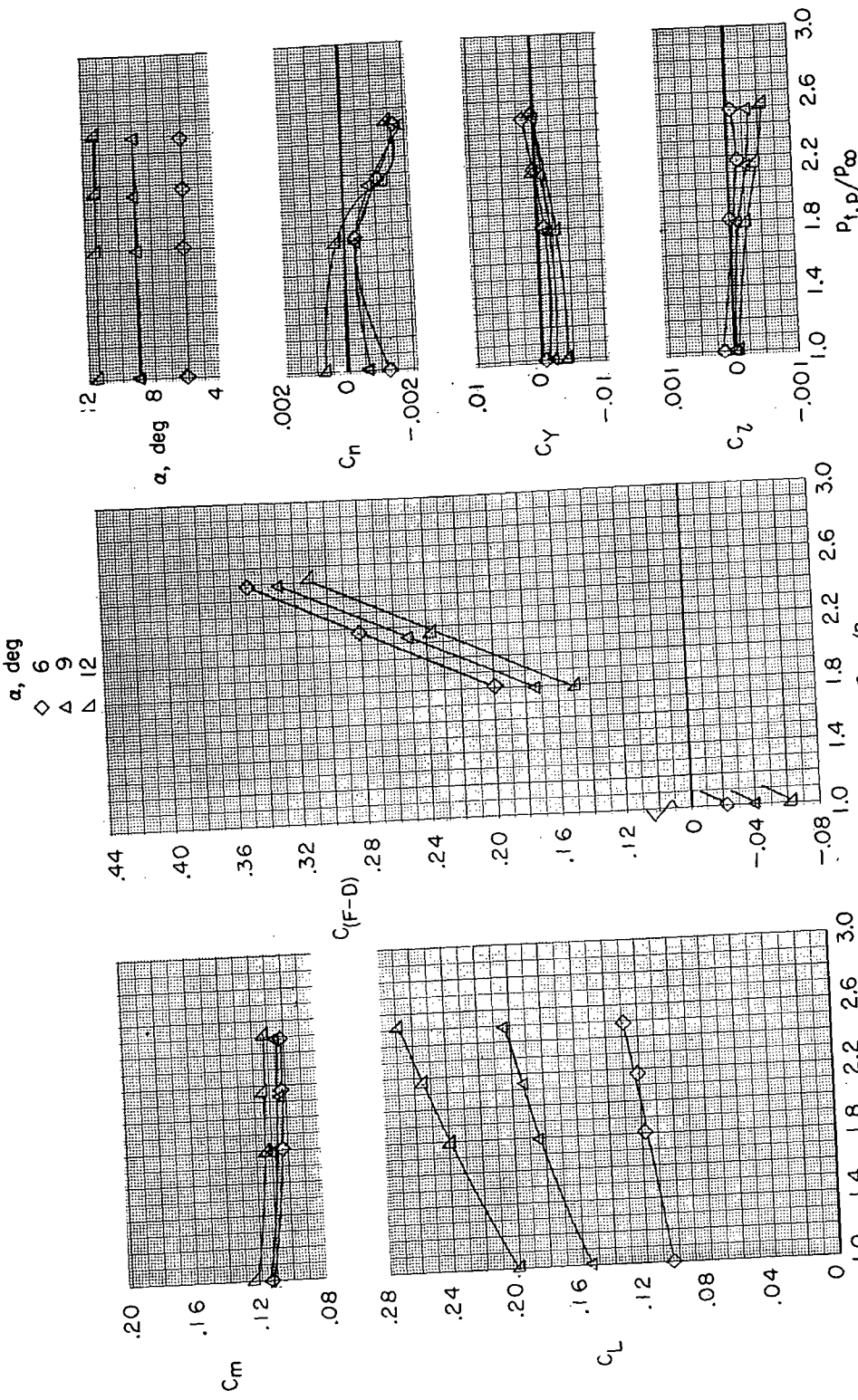

(g) $\beta = 0^o$; $\delta_b = 50$ percent; $\delta_h = -1.5^o$; $\delta_r = 0^o$.

Figure 16.- Continued.

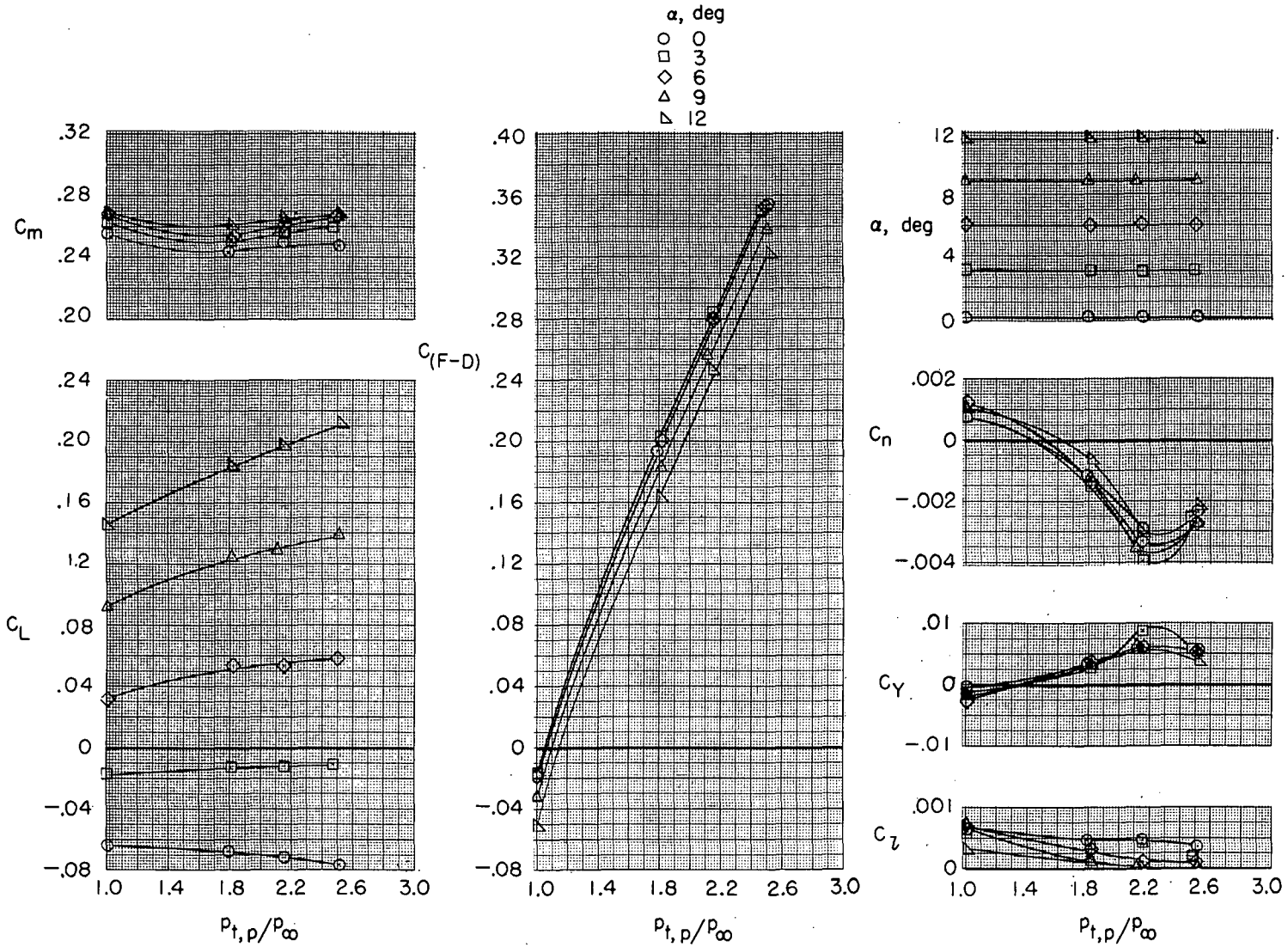

(h) $\beta = 0^o$; $\delta_b = 50$ percent; $\delta_h = -10^o$; $\delta_r = 0^o$.

Figure 16.- Continued.

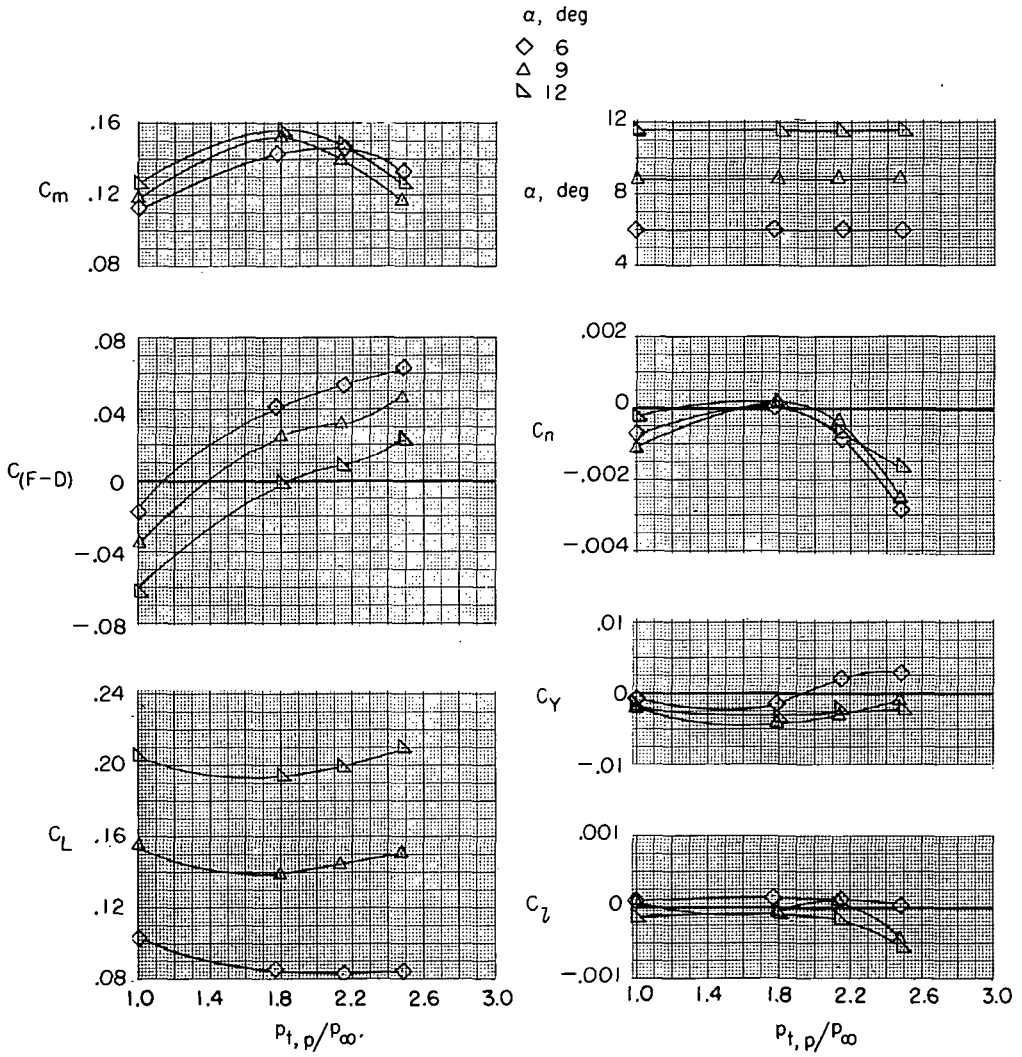

(i) $\beta = 0^o$; $\delta_b = 75$ percent; $\delta_h = -1.5^o$; $\delta_r = 0^o$.

Figure 16.- Continued.

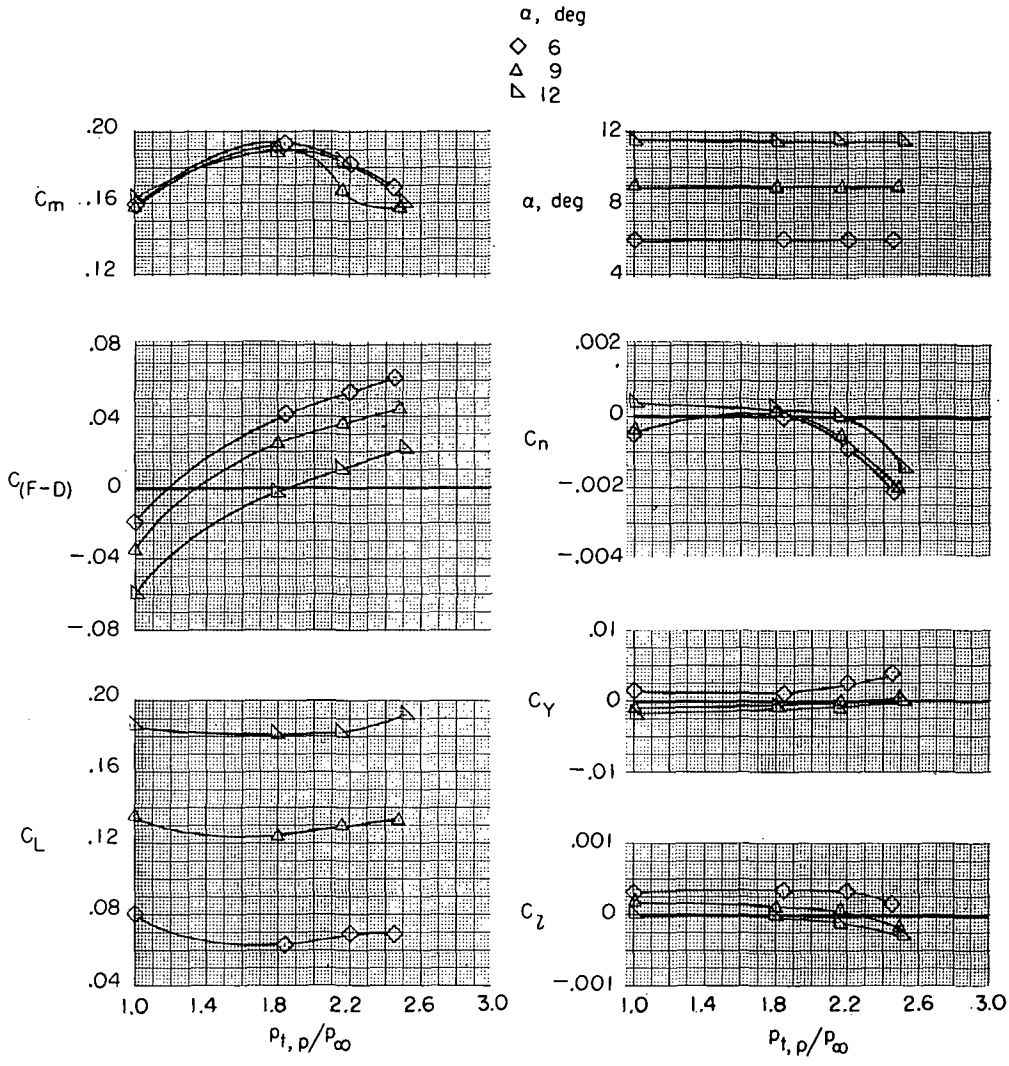

(j) $\beta = 0^o$; $\delta_b = 75$ percent; $\delta_h = -4^o$; $\delta_r = 0^o$.

Figure 16.- Continued.

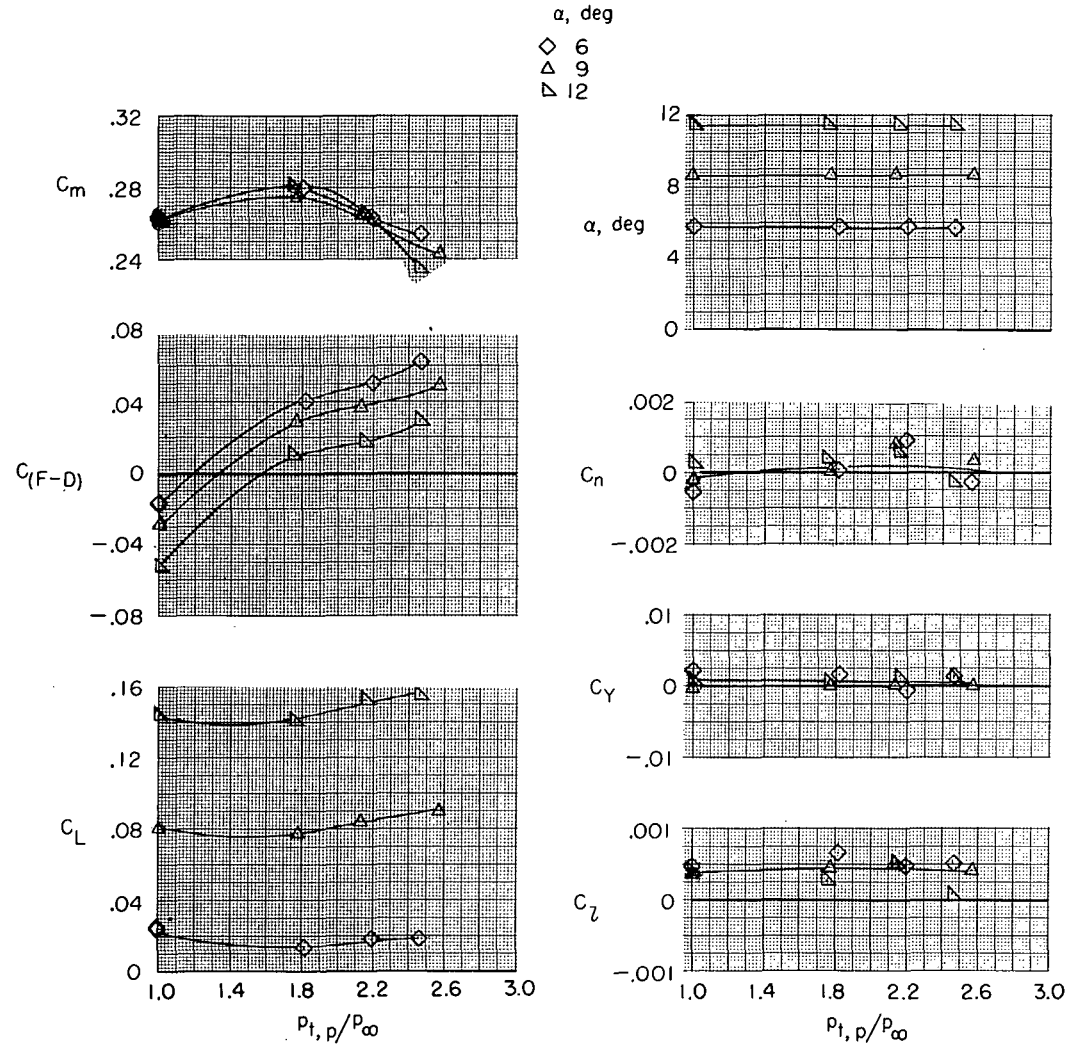

(k) $\beta = 0^o$; $\delta_b = 75$ percent; $\delta_h = -10^o$; $\delta_r = 0^o$.

Figure 16.- Continued.

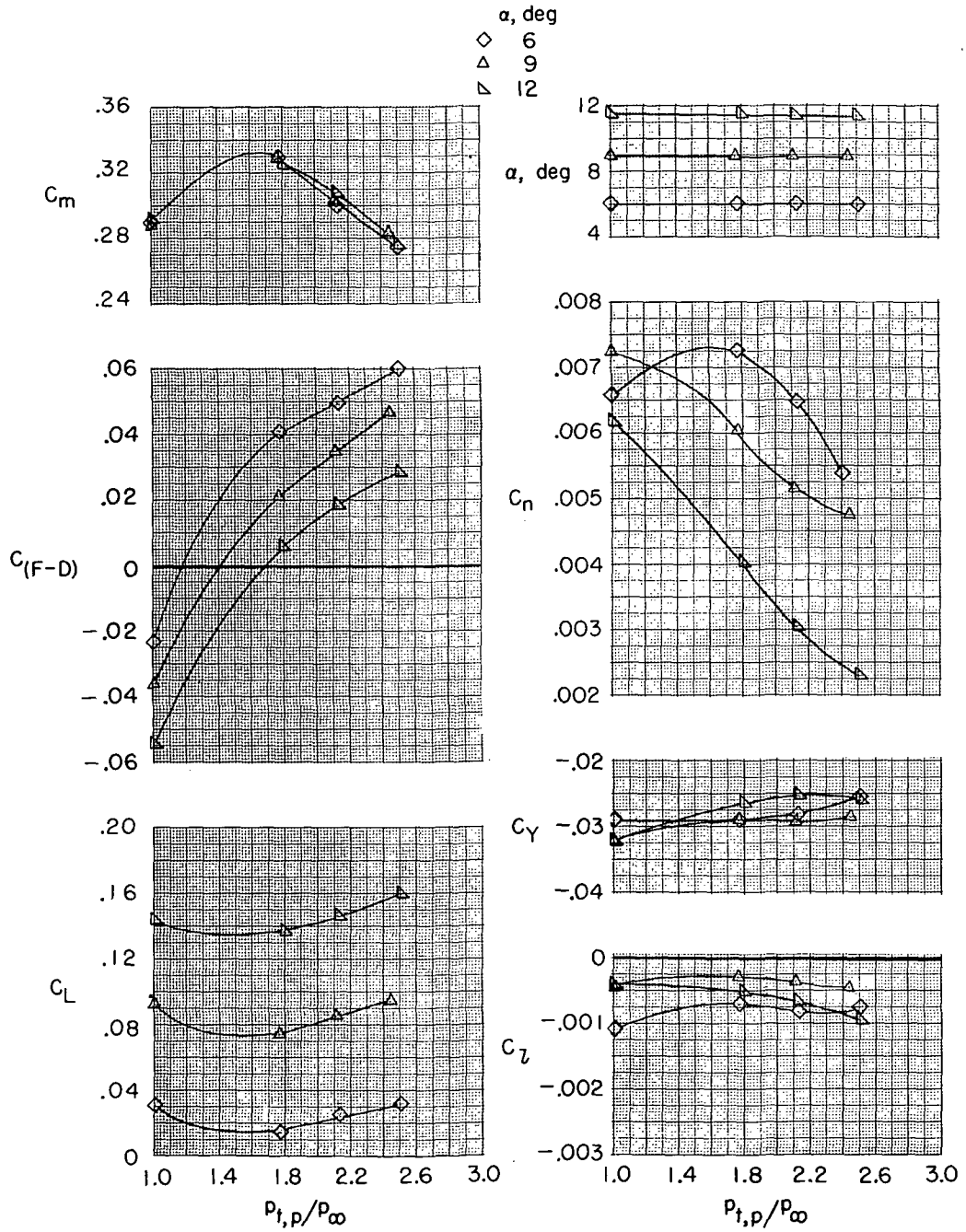

(l) $\beta = 2^o$; $\delta_b = 75$ percent; $\delta_h = -10^o$; $\delta_r = 0^o$.

Figure 16.- Continued.

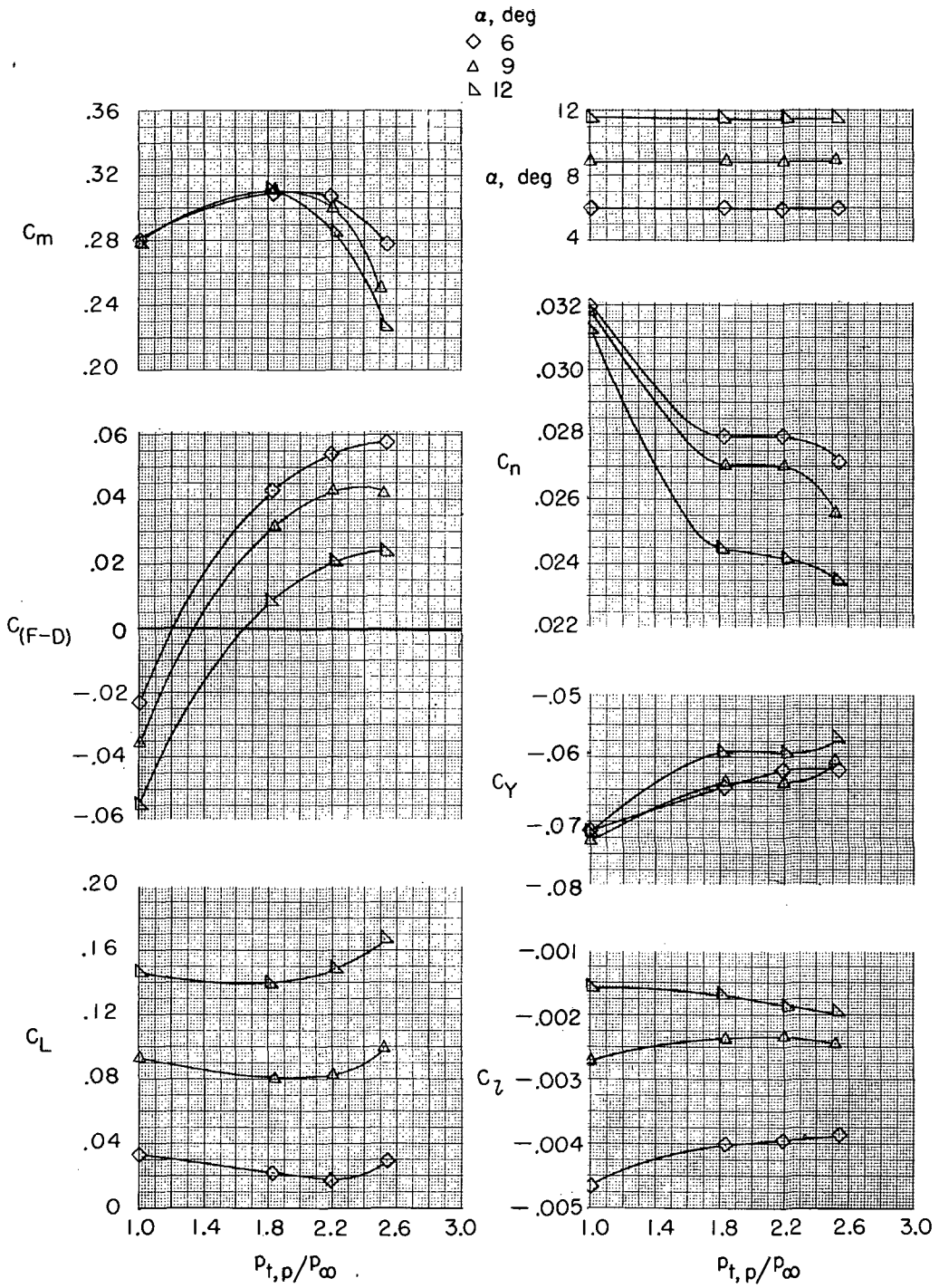

(m) $\beta = 2^o$; $\delta_b = 75$ percent; $\delta_h = -10^o$; $\delta_r = -15^o$.

Figure 16.- Continued.

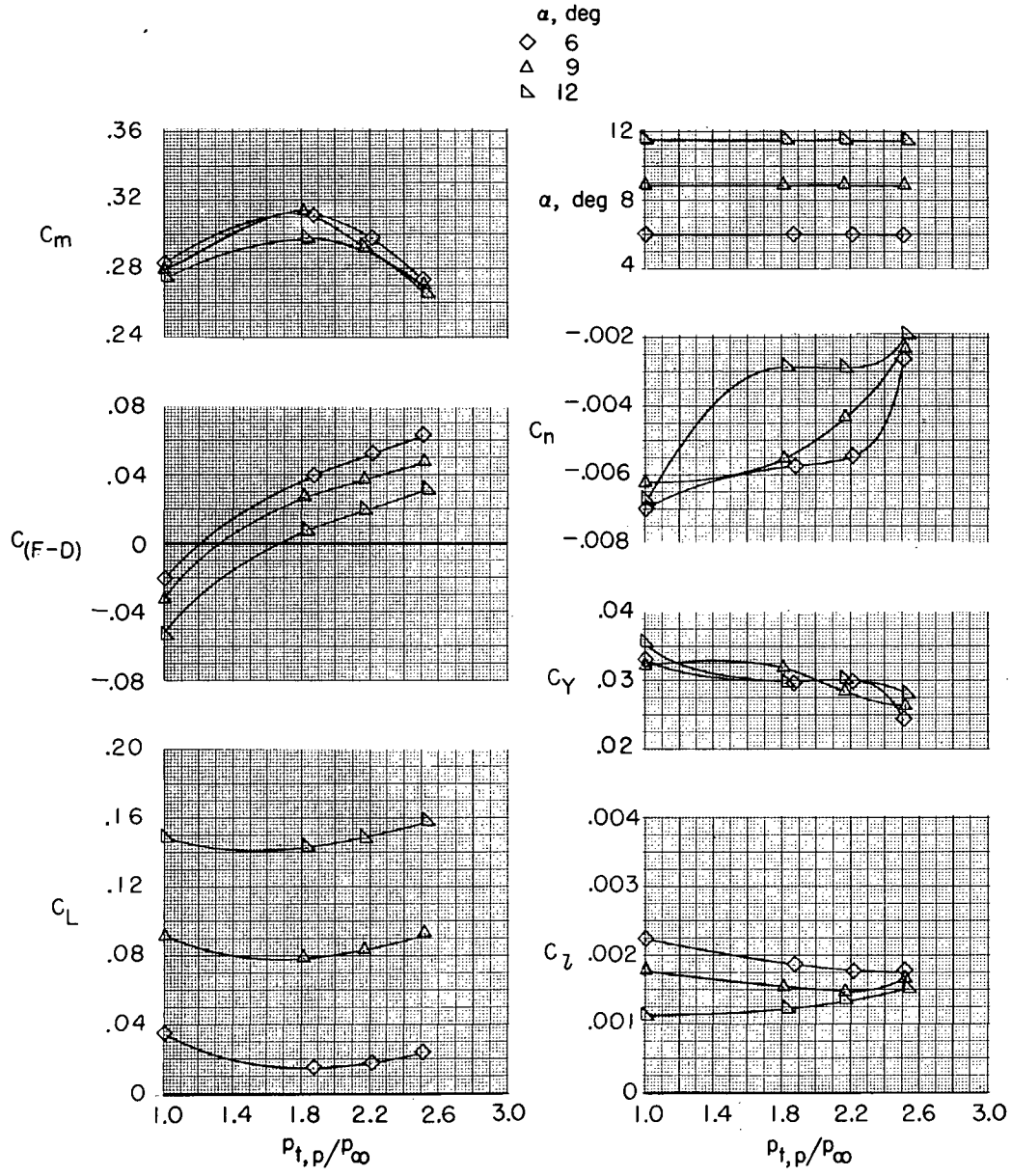

(n) $\beta = -2^o$; $\delta_b = 75$ percent; $\delta_h = -10^o$; $\delta_r = 0^o$.

Figure 16.- Continued.

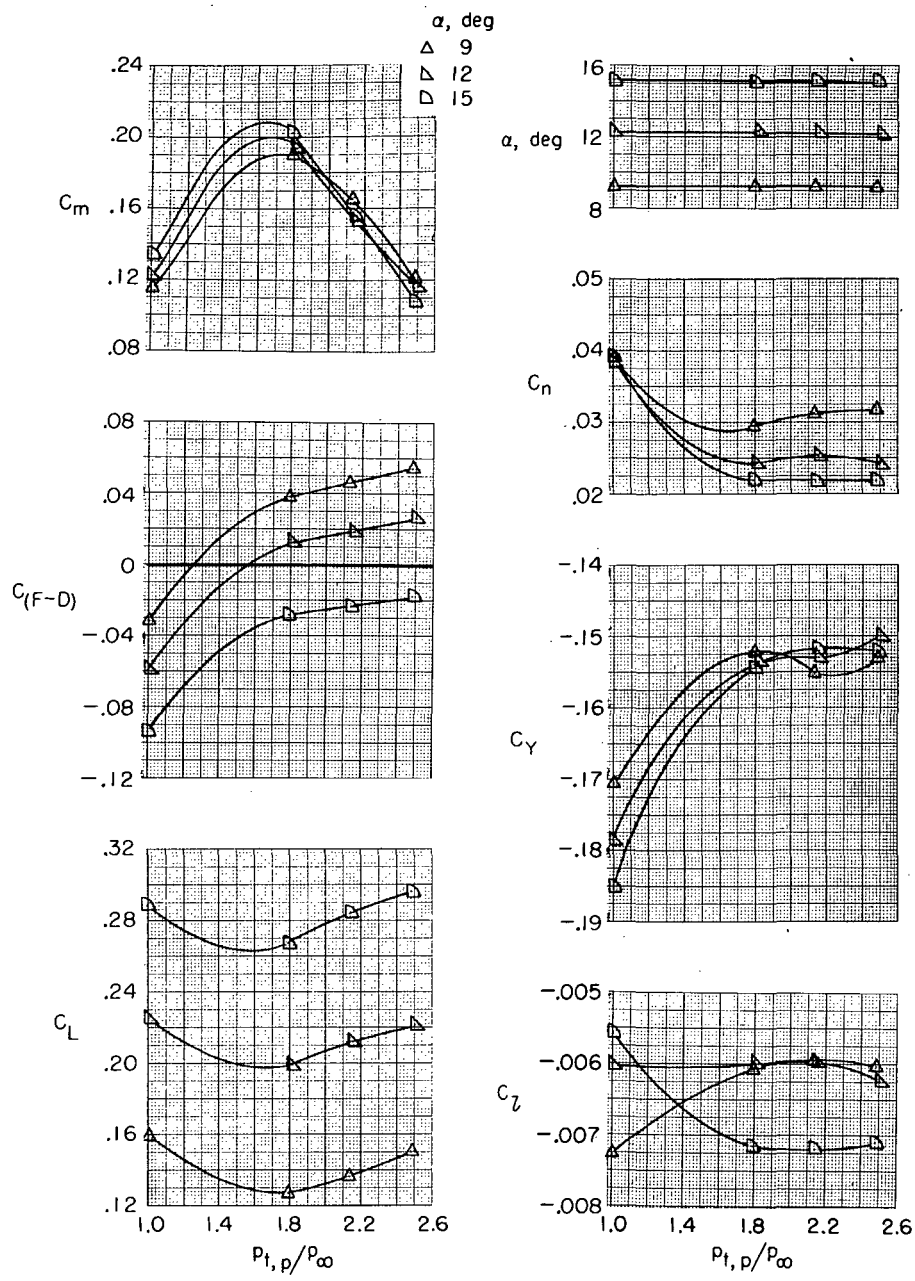

(o) $\beta = 10^o$; $\delta_b = 75$ percent; $\delta_h = -10^o$; $\delta_r = 0^o$.

Figure 16.- Continued.

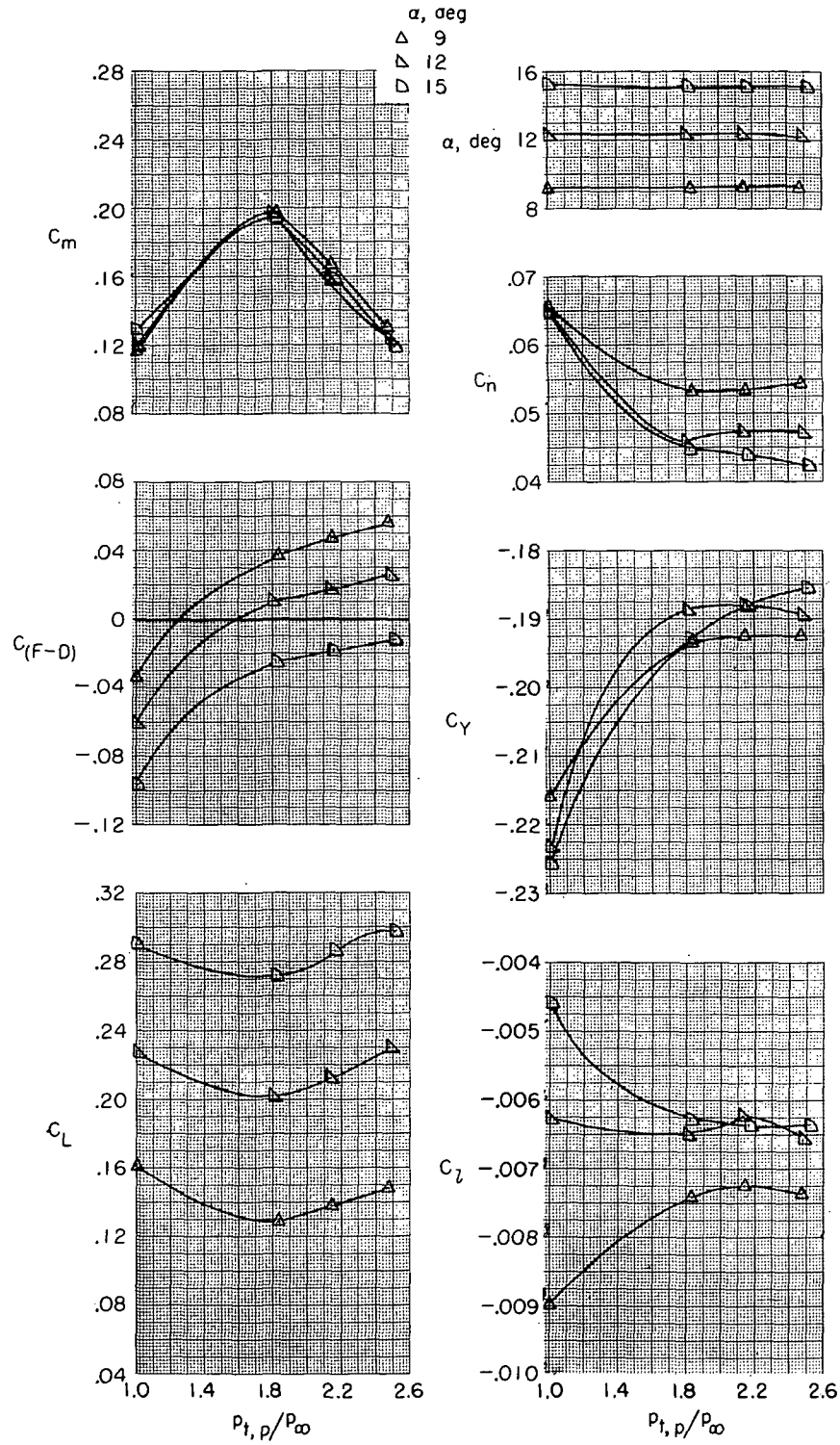

(p) $\beta = 10^o$; $\delta_b = 75$ percent; $\delta_h = -10^o$; $\delta_r = -15^o$.

Figure 16.- Continued.

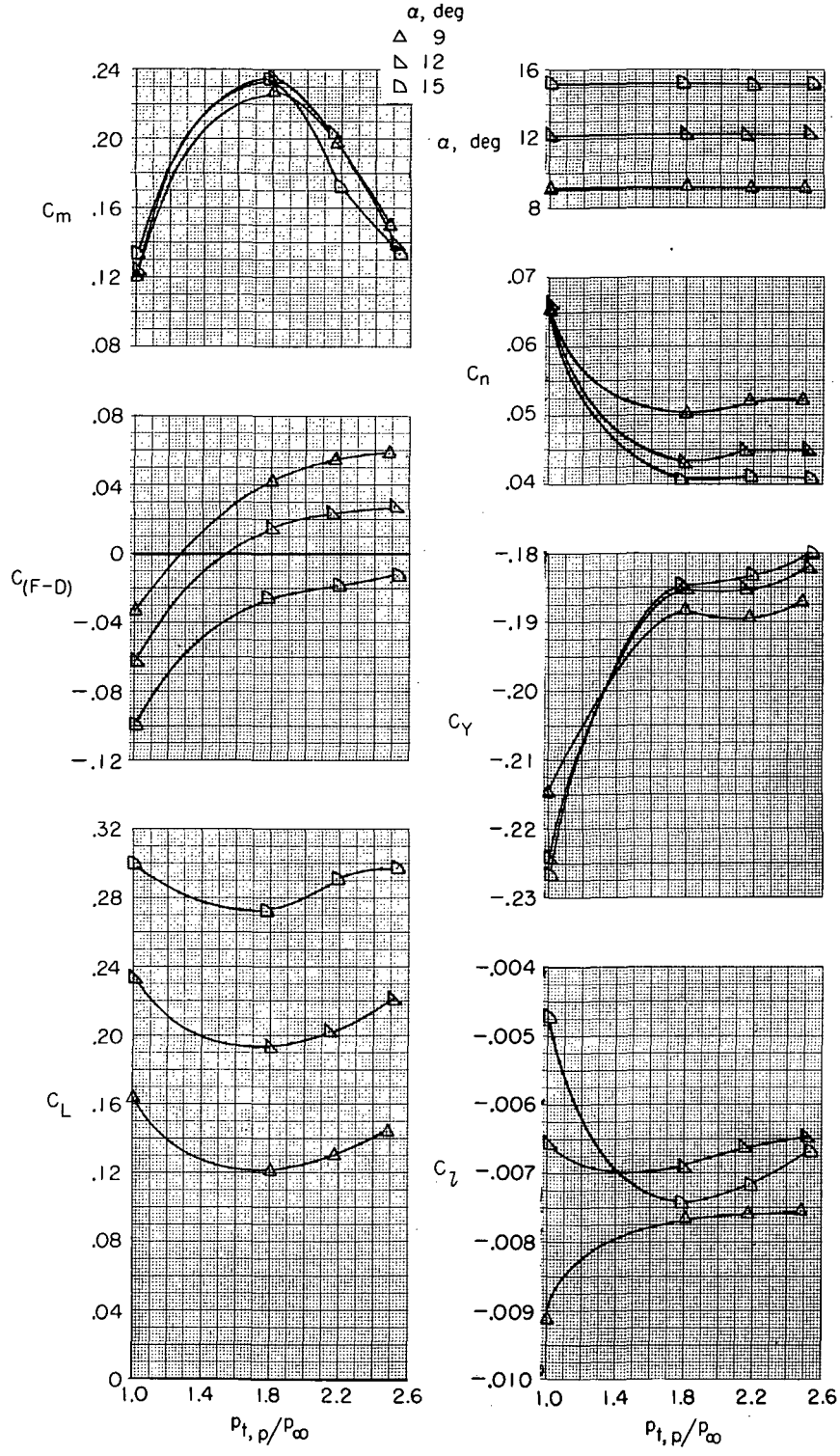

(q) $\beta = 10^o$; $\delta_b = 75$ percent; $\delta_h = -10^o$; $\delta_r = -15^o$; δ_{du} with side plates.

Figure 16.- Continued.

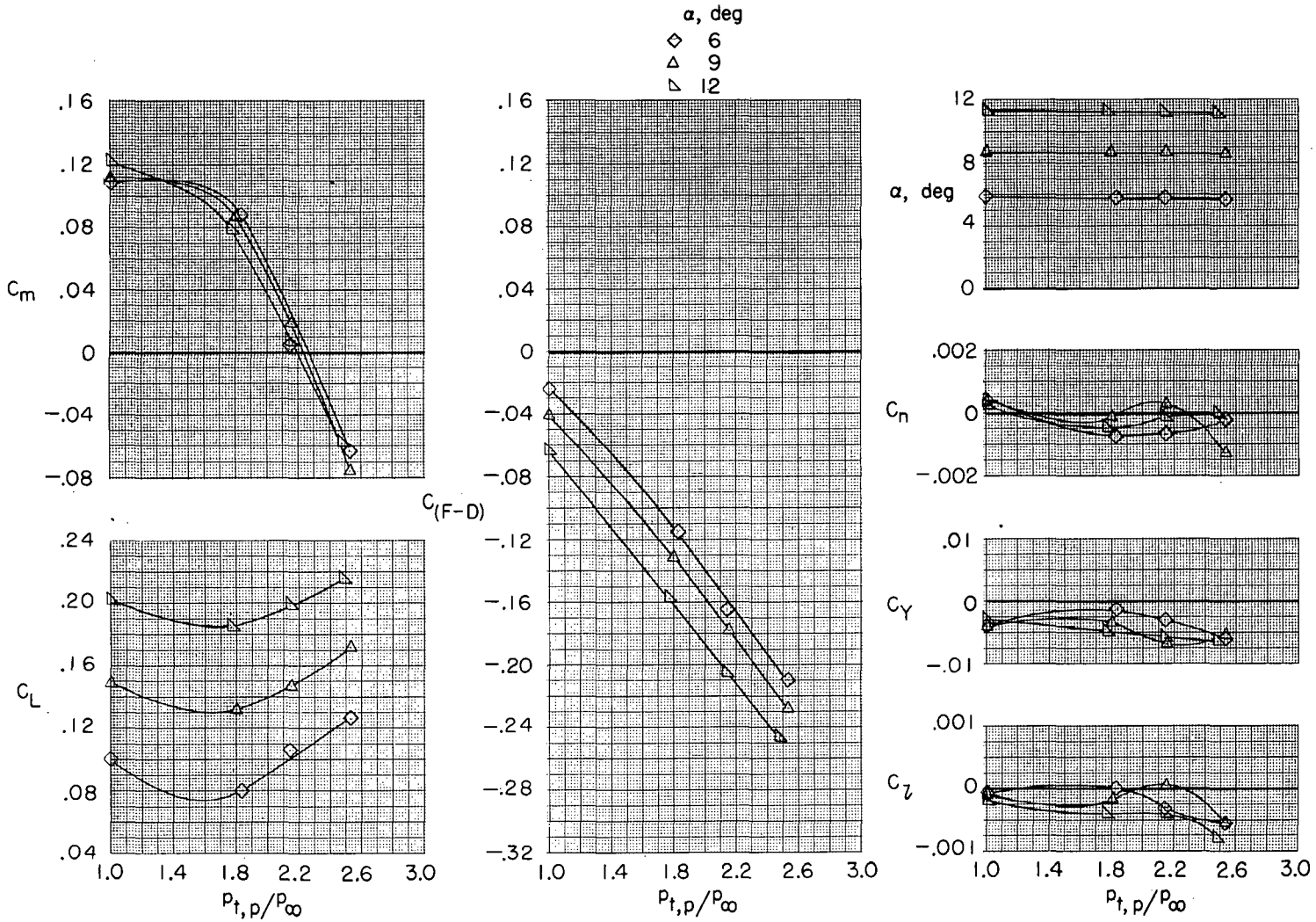

(r) $\beta = 0^o$; δ_b = 90 percent; $\delta_h = -1.5^o$; $\delta_r = 0^o$.

Figure 16.- Continued.

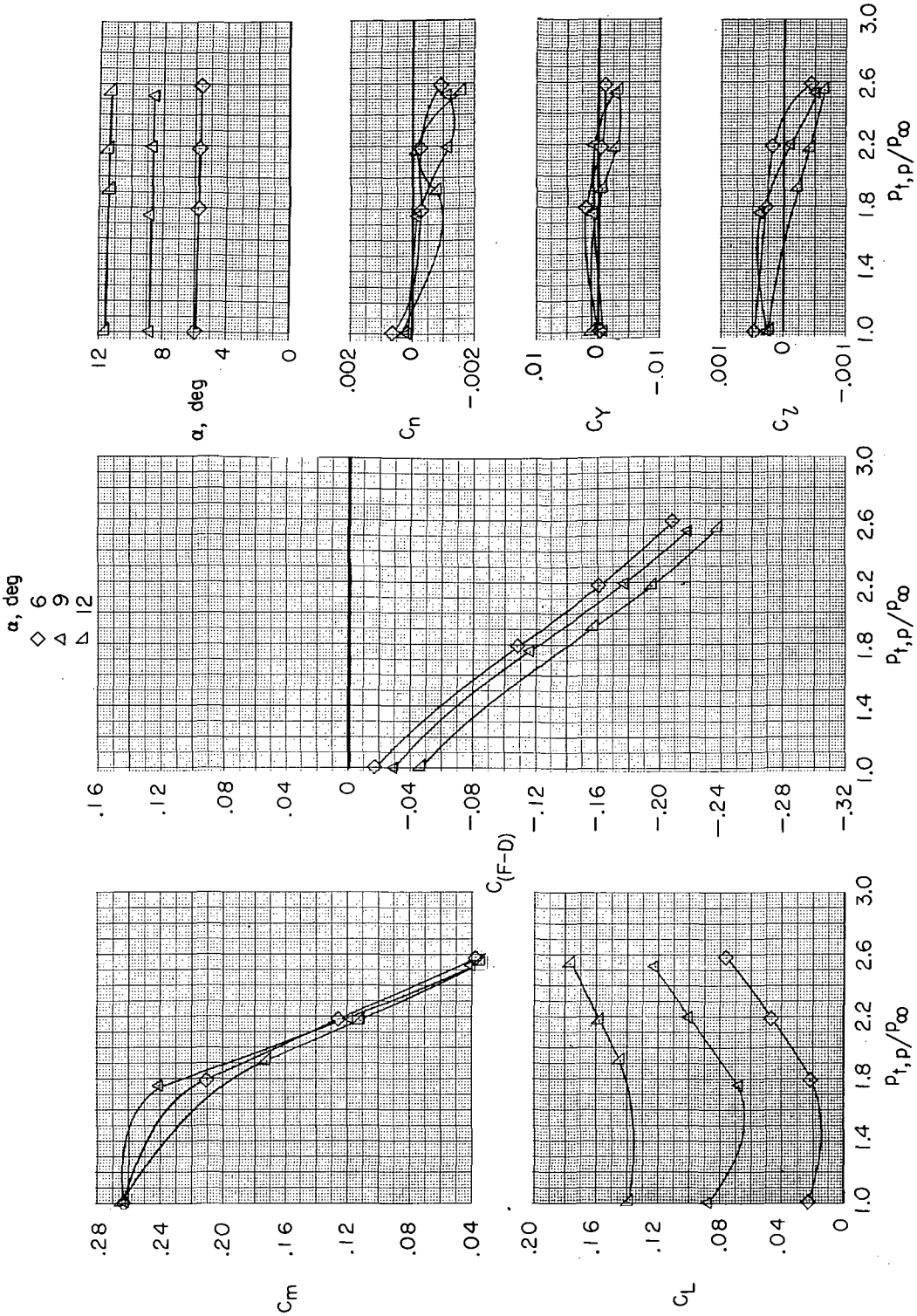

(s) $\beta = 0^o$; $\delta_b = 90$ percent; $\delta_h = -10^o$; $\delta_r = 0^o$.

Figure 16.- Concluded.

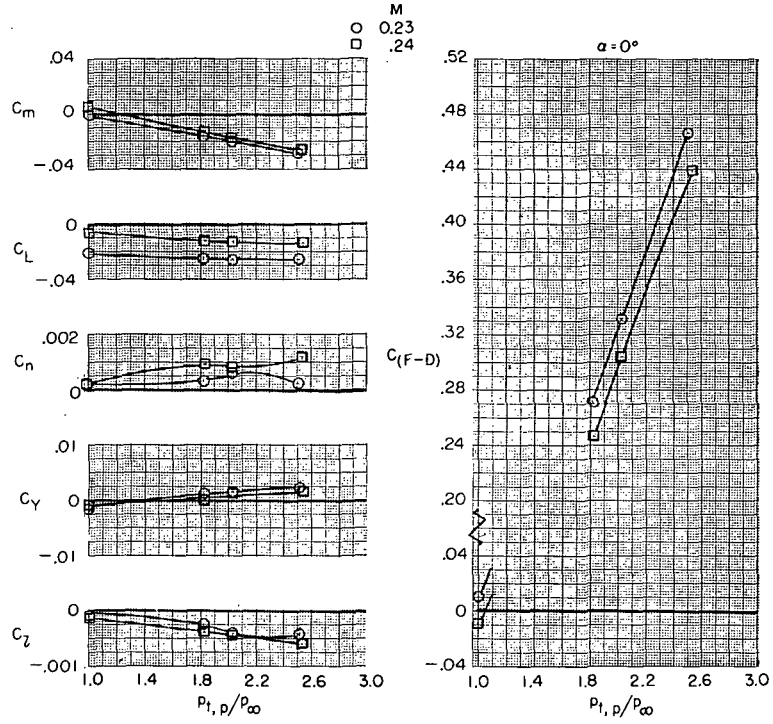

(a) M = 0.23 and 0.24; military power.

Figure 17.- Effect of jet-total-pressure ratio on aerodynamic characteristics of model with thrust control unit for several angles of attack and Mach numbers. $\beta = 0^o$; $\delta_f = 0^o$; $\delta_s = 0^o$; $\delta_h = -1.5^o$; $\delta_r = 0^o$; δ_{du} = Faired = 2^o; δ_{dl} = Faired = 2^o; and δ_b = 0 percent.

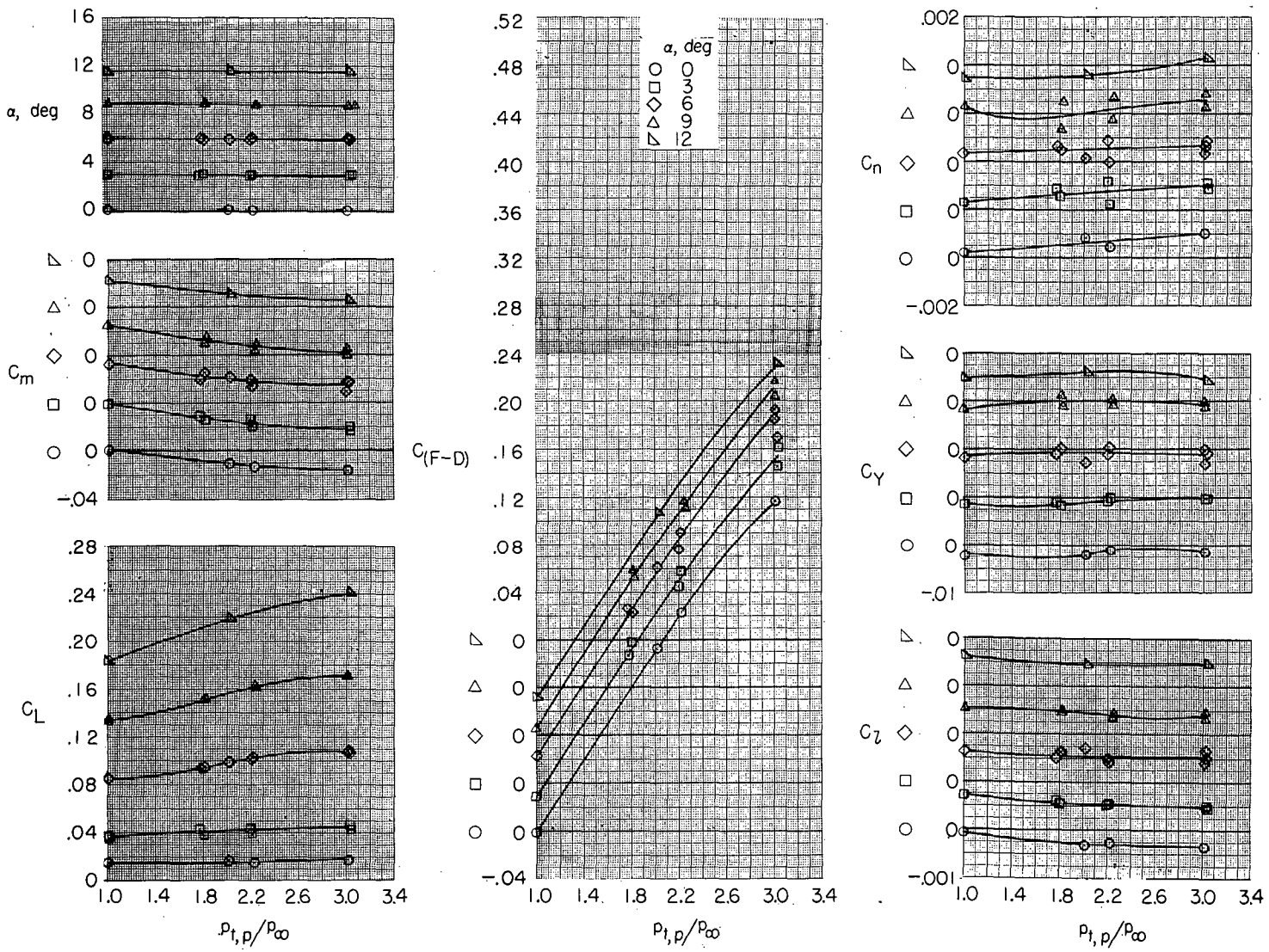

(b) M = 0.34; military power.

Figure 17.- Continued.

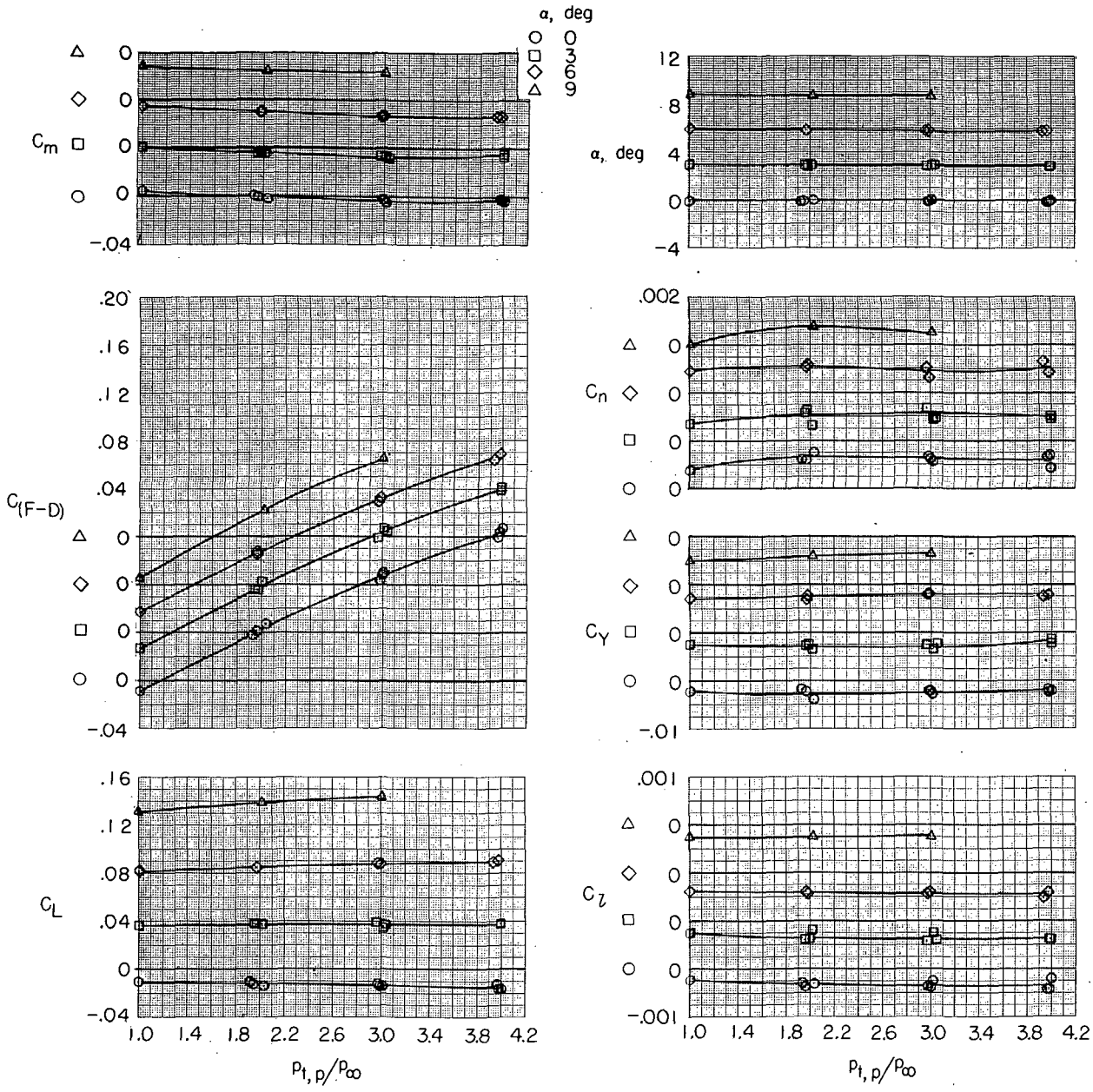

(c) M = 0.60; military power.

Figure 17.- Continued.

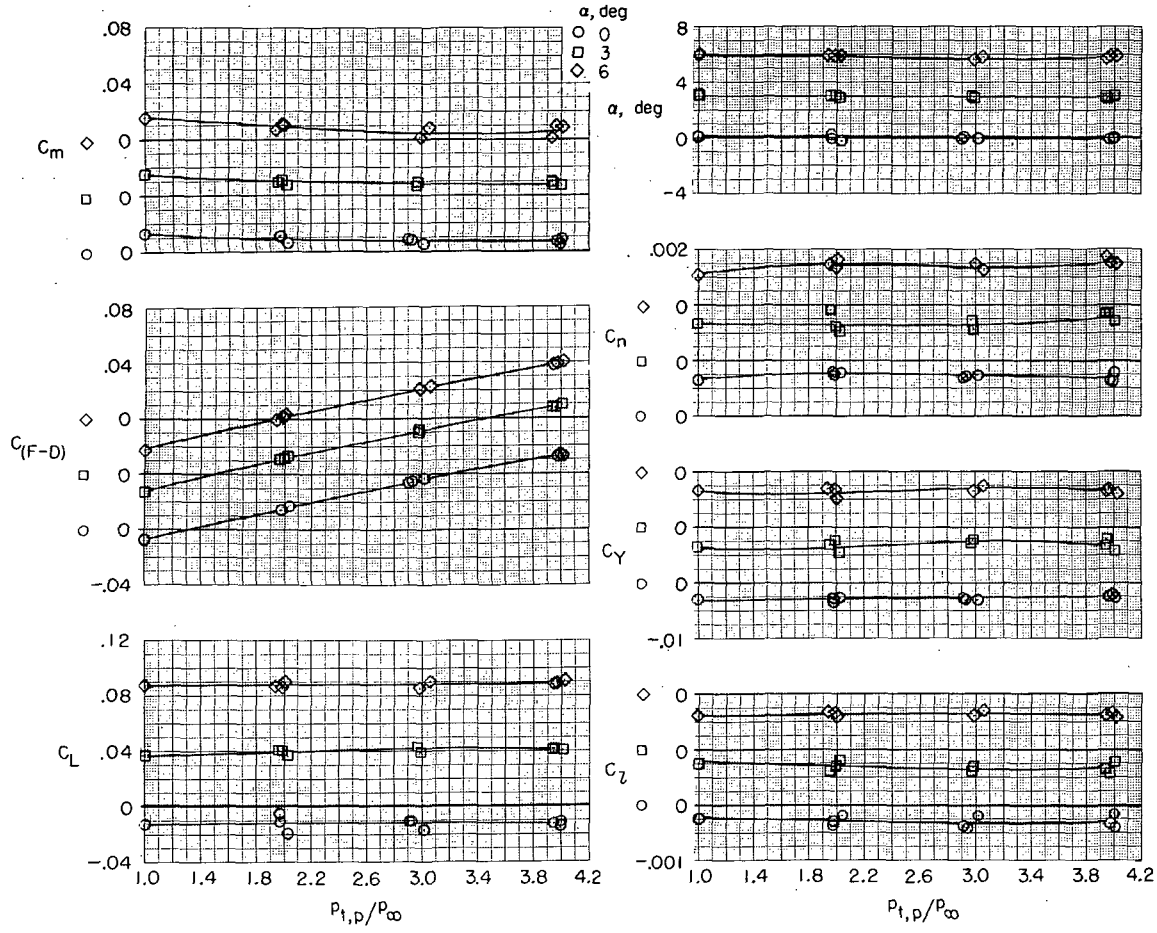

(d) M = 0.90; military power.

Figure 17.- Continued.

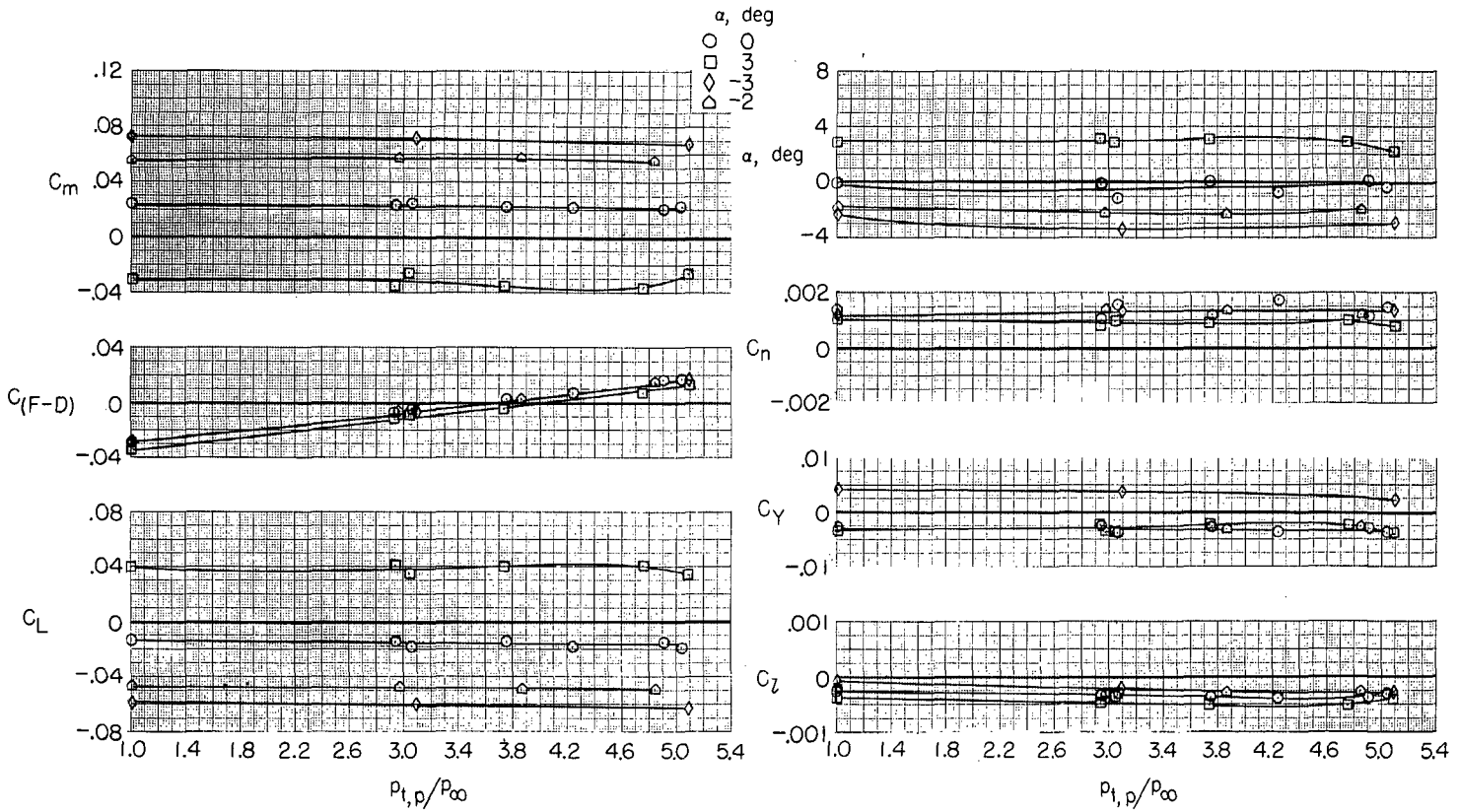

(e) M = 1.30; military power.

Figure 17.- Continued.

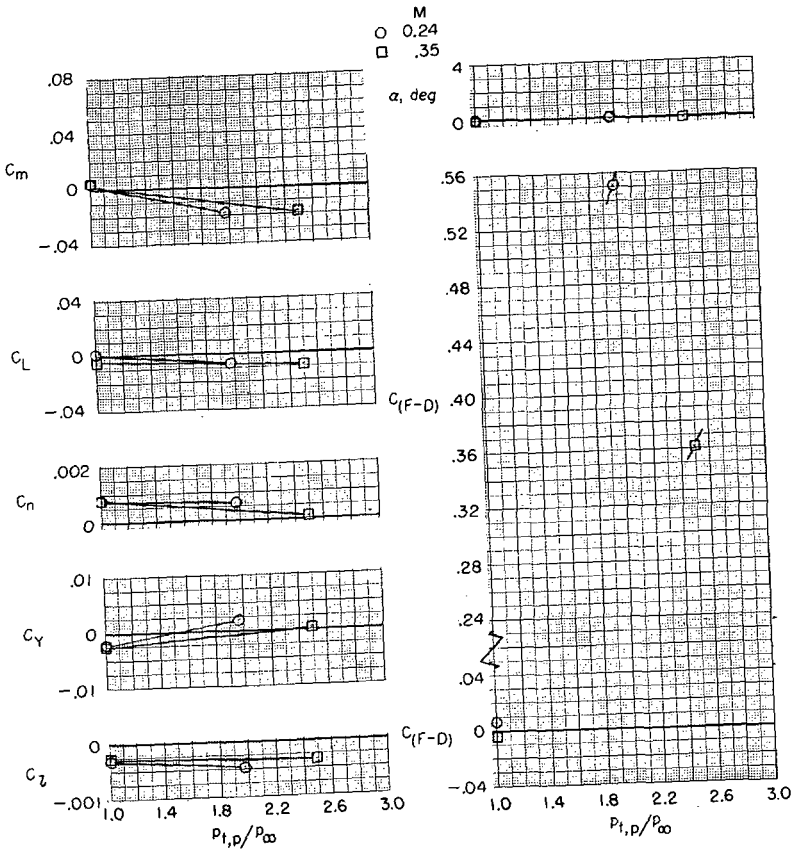

(f) M = 0.24 and 0.35; afterburning power.

Figure 17.- Continued.

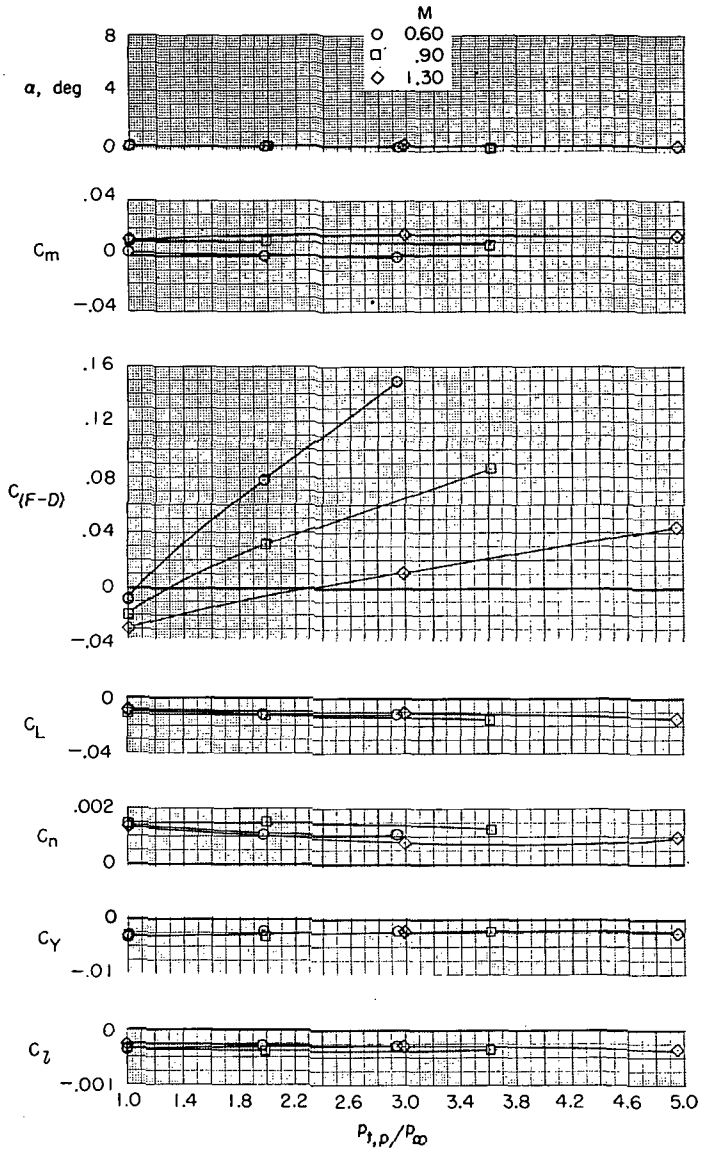

(g) M = 0.60, 0.90, and 1.30; afterburning power.

Figure 17.- Concluded.

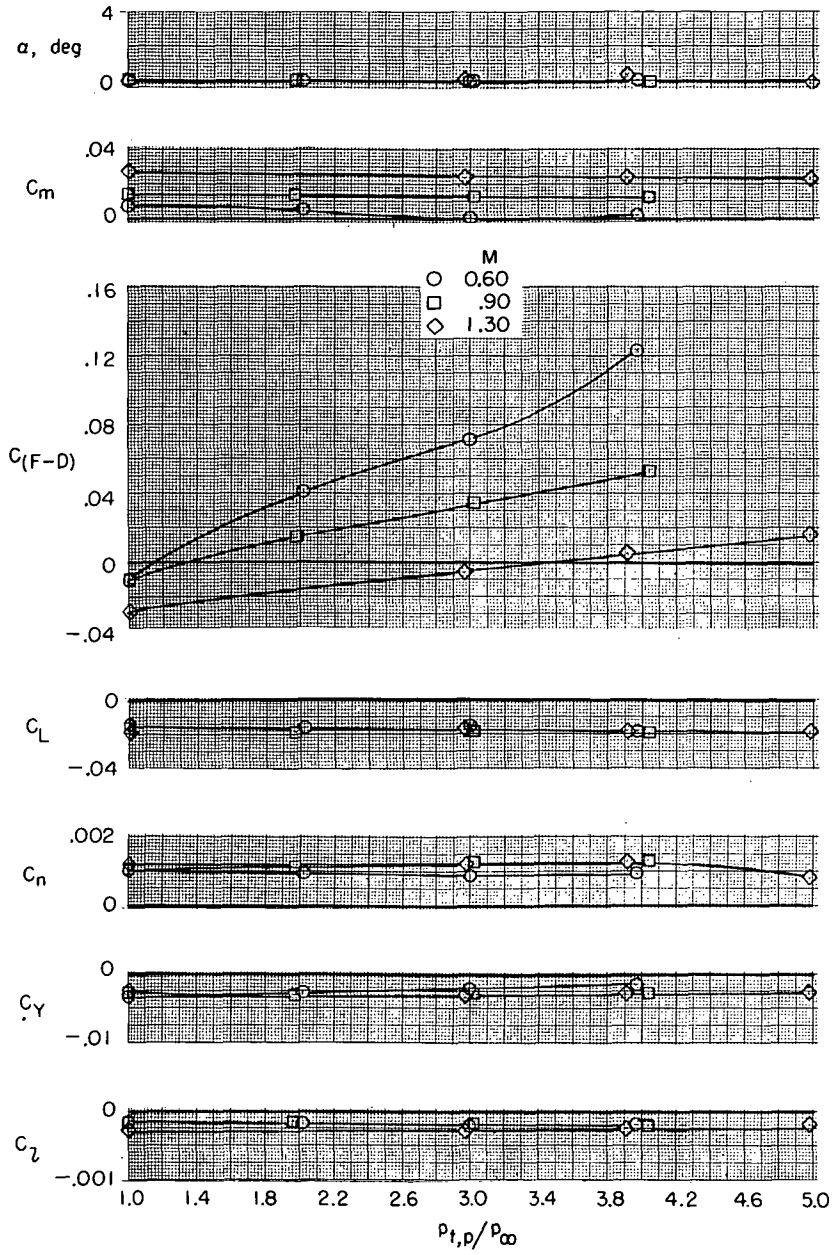

(a) Military power; δ_{du} = Closed; δ_{dl} = Closed.

Figure 18.- Effect of jet-total-pressure ratio on aerodynamic characteristics of model with thrust control unit for several Mach numbers. $\beta = 0^o$; $\delta_f = 0^o$; $\delta_s = 0^o$; $\delta_h = -1.5^o$; $\delta_r = 0^o$; and $\delta_b = 0$ percent.

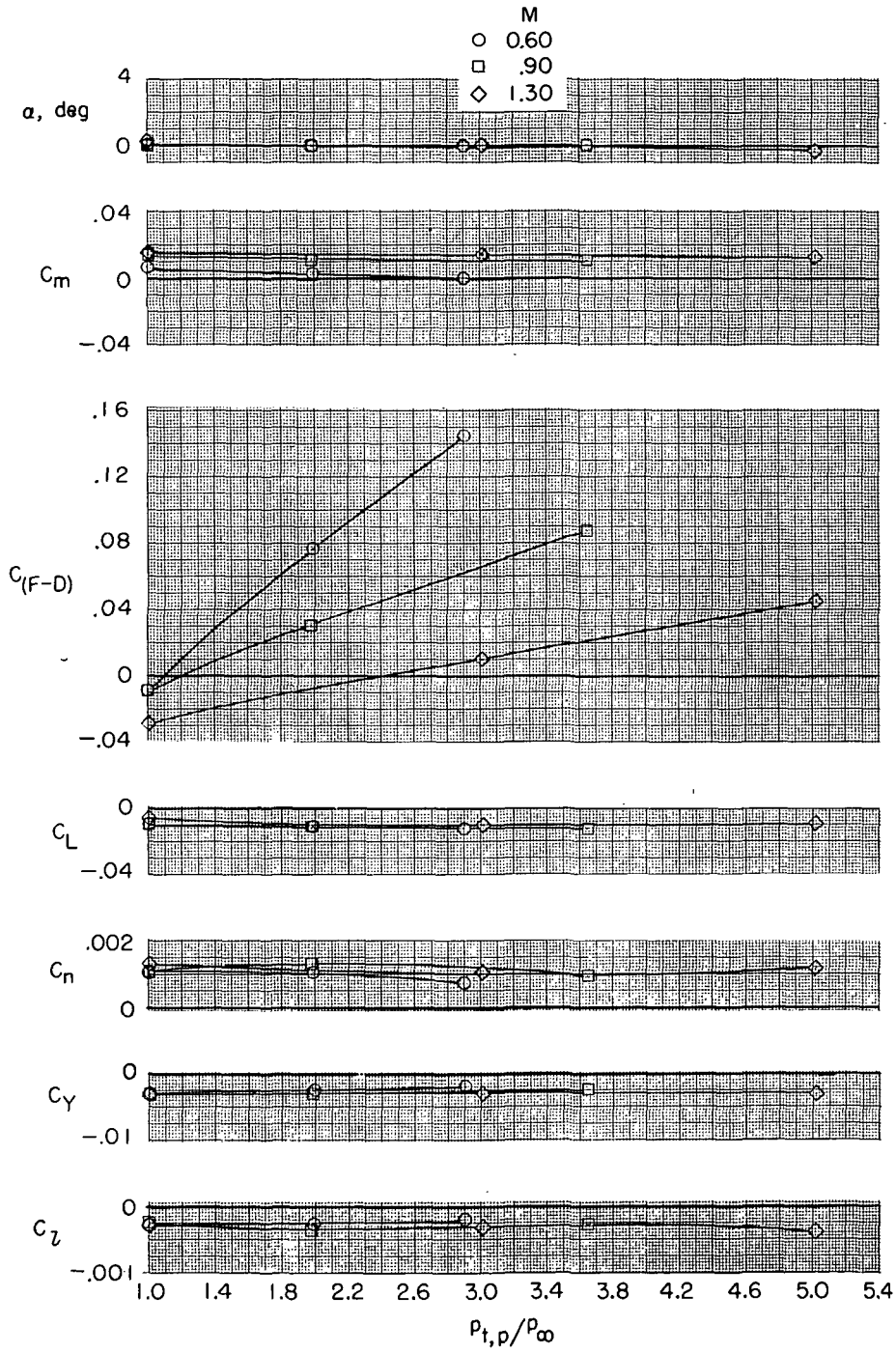

(b) Afterburning power; δ_{du} = Closed; δ_{dl} = Closed.

Figure 18.- Continued.

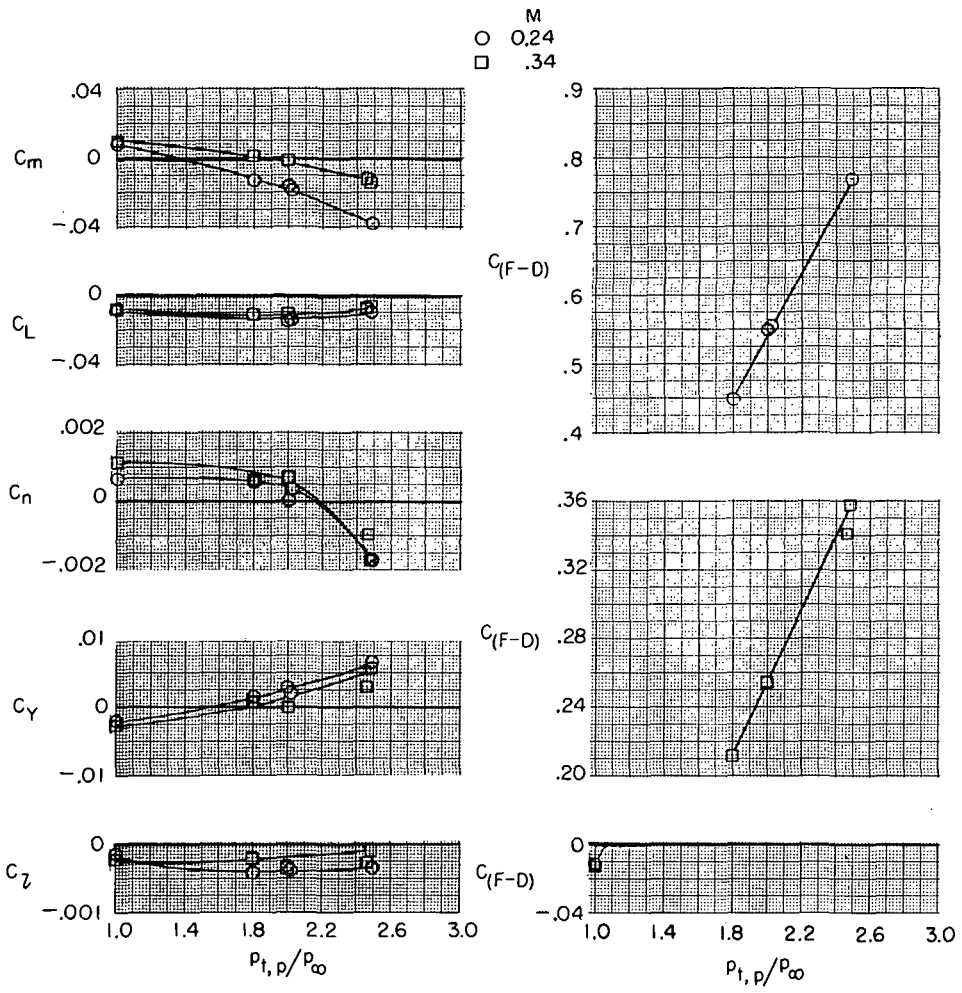

(c) Afterburning power; $\delta_{du} = 43.5^o$; $\delta_{dl} = 43.5^o$.

Figure 18.- Concluded.

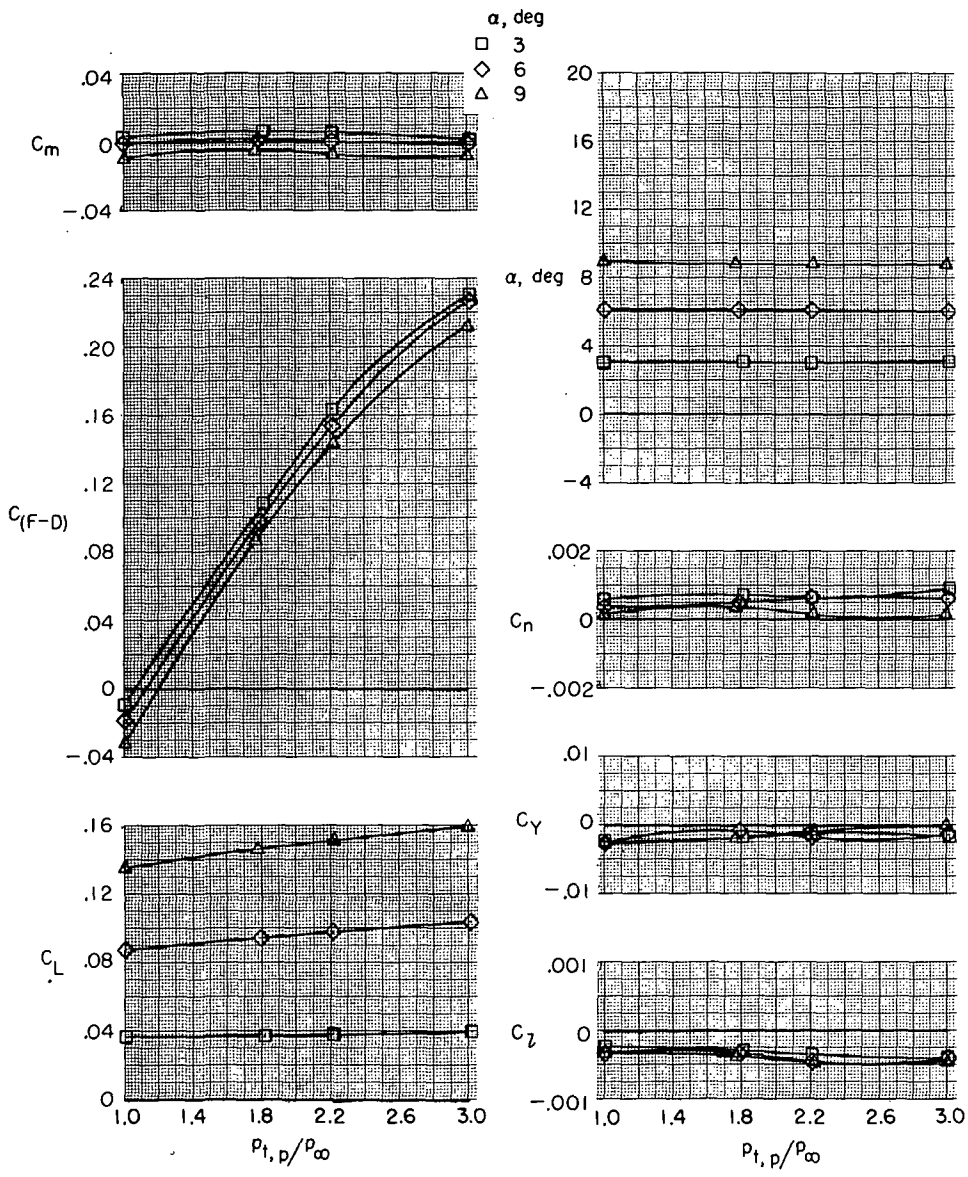

(a) M = 0.34.

Figure 19.- Effect of jet-total-pressure ratio on aerodynamic characteristics of model with thrust control unit for several angles of attack and Mach numbers. $\beta = 0^o$; $\delta_f = 0^o$; $\delta_s = 0^o$; $\delta_h = -1.5^o$; $\delta_r = 0^o$; δ_{du} = Closed; δ_{dl} = Faired = 2^o; δ_b = 0 percent; and military power.

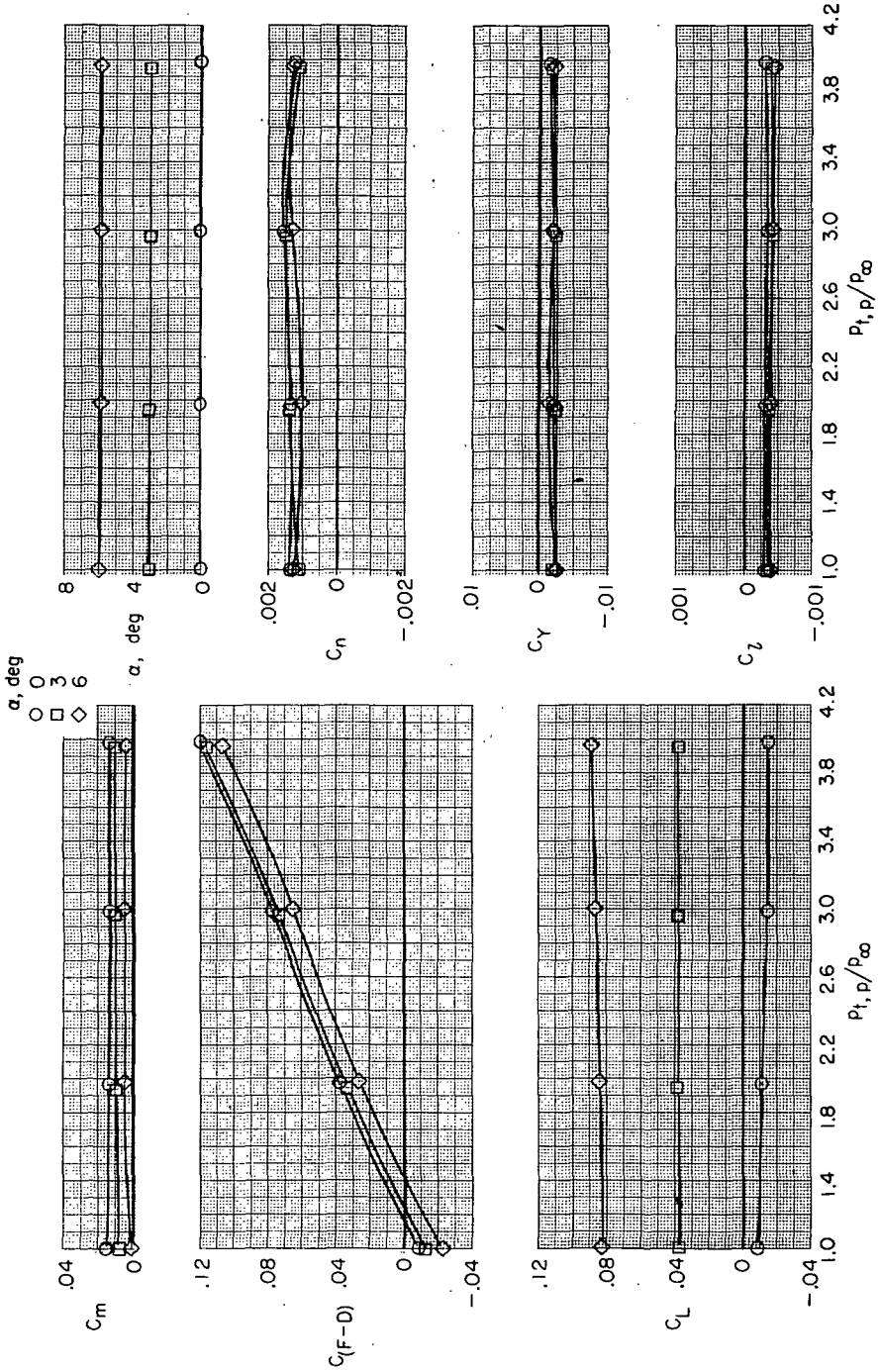

(b) $M = 0.60$.

Figure 19.- Continued.

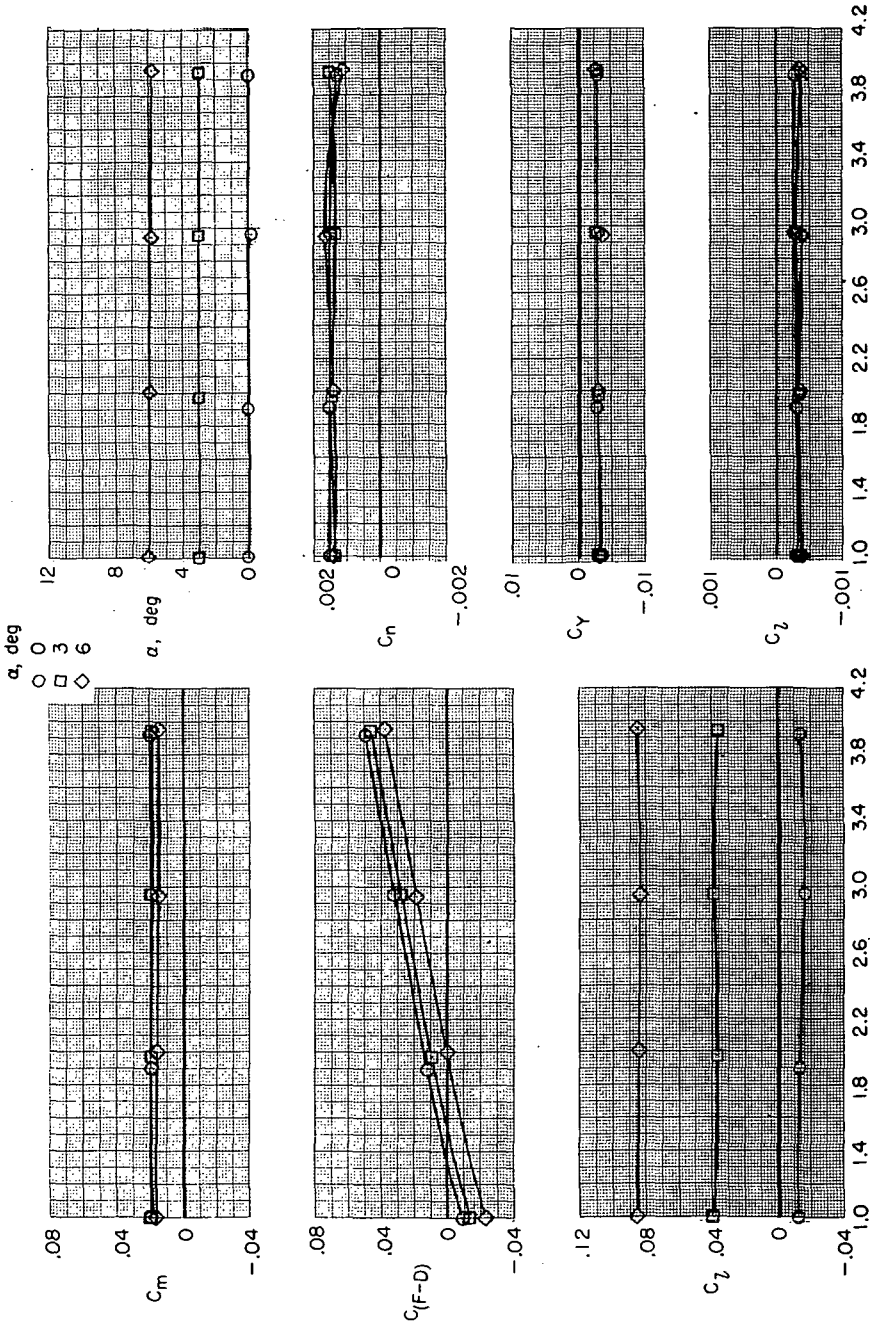

(c) M = 0.90.

Figure 19.- Continued.

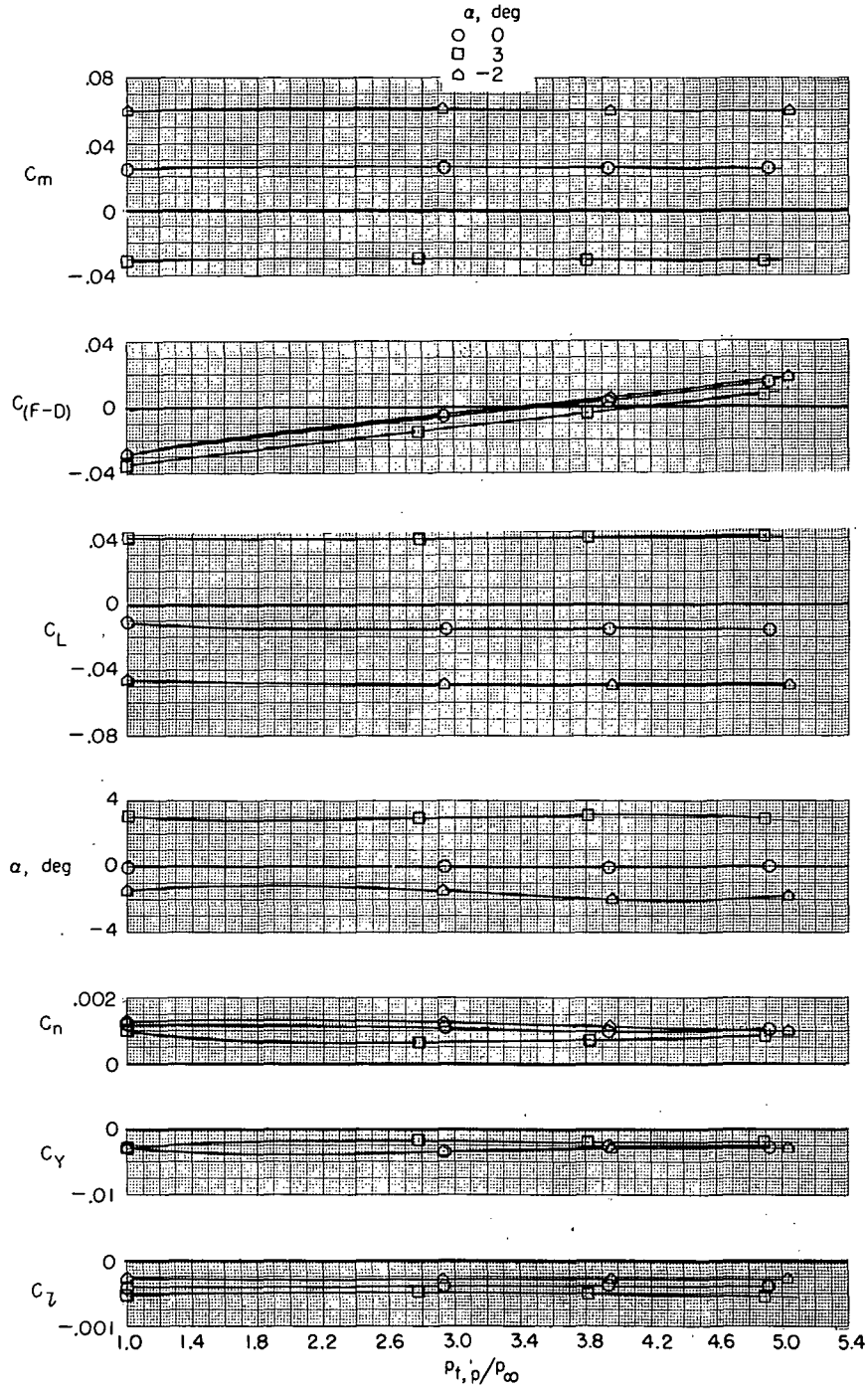

(d) M = 1.30.

Figure 19.- Concluded.

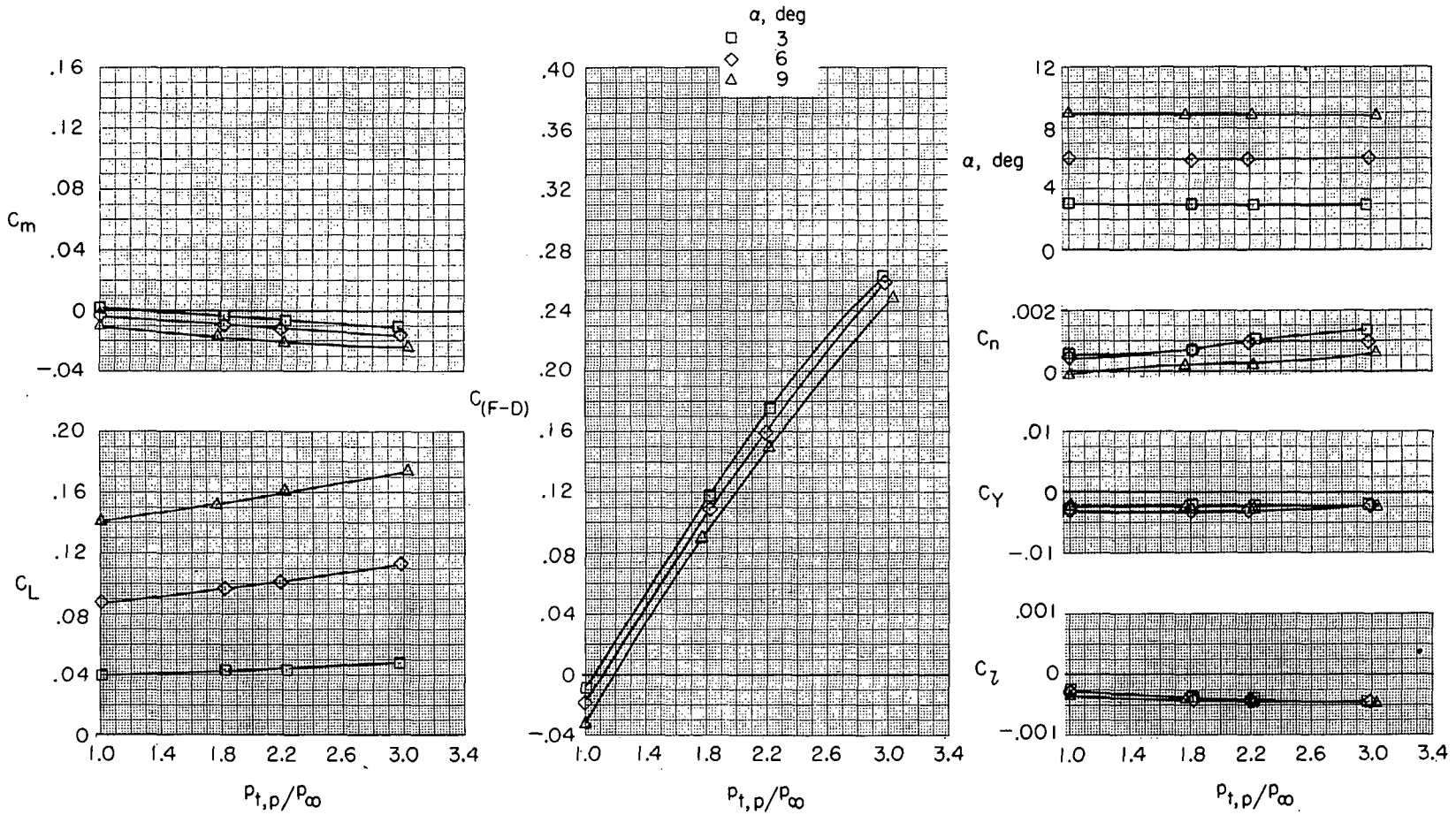

(a) M = 0.34.

Figure 20.- Effect of jet-total-pressure ratio on aerodynamic characteristics of model with thrust control unit for several angles of attack and Mach numbers. $\beta = 0^o$; $\delta_f = 0^o$; $\delta_s = 0^o$; $\delta_h = -1.5^o$; $\delta_r = 0^o$; δ_{du} = Faired = 2^o; $\delta_{dl} = 28.5^o$; $\delta_b = 0$ percent; and military power.

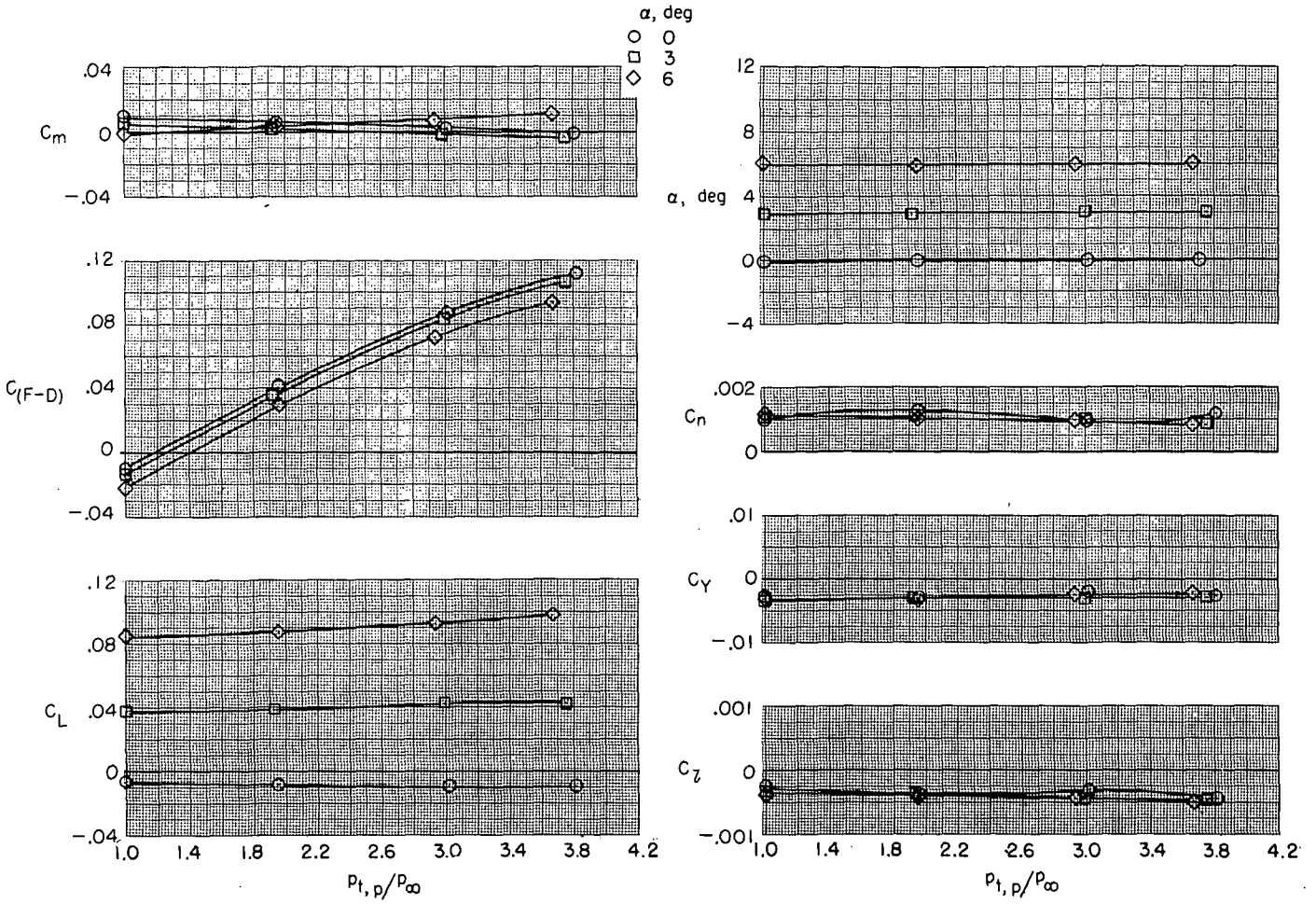

(b) M = 0.60.

Figure 20.- Continued.

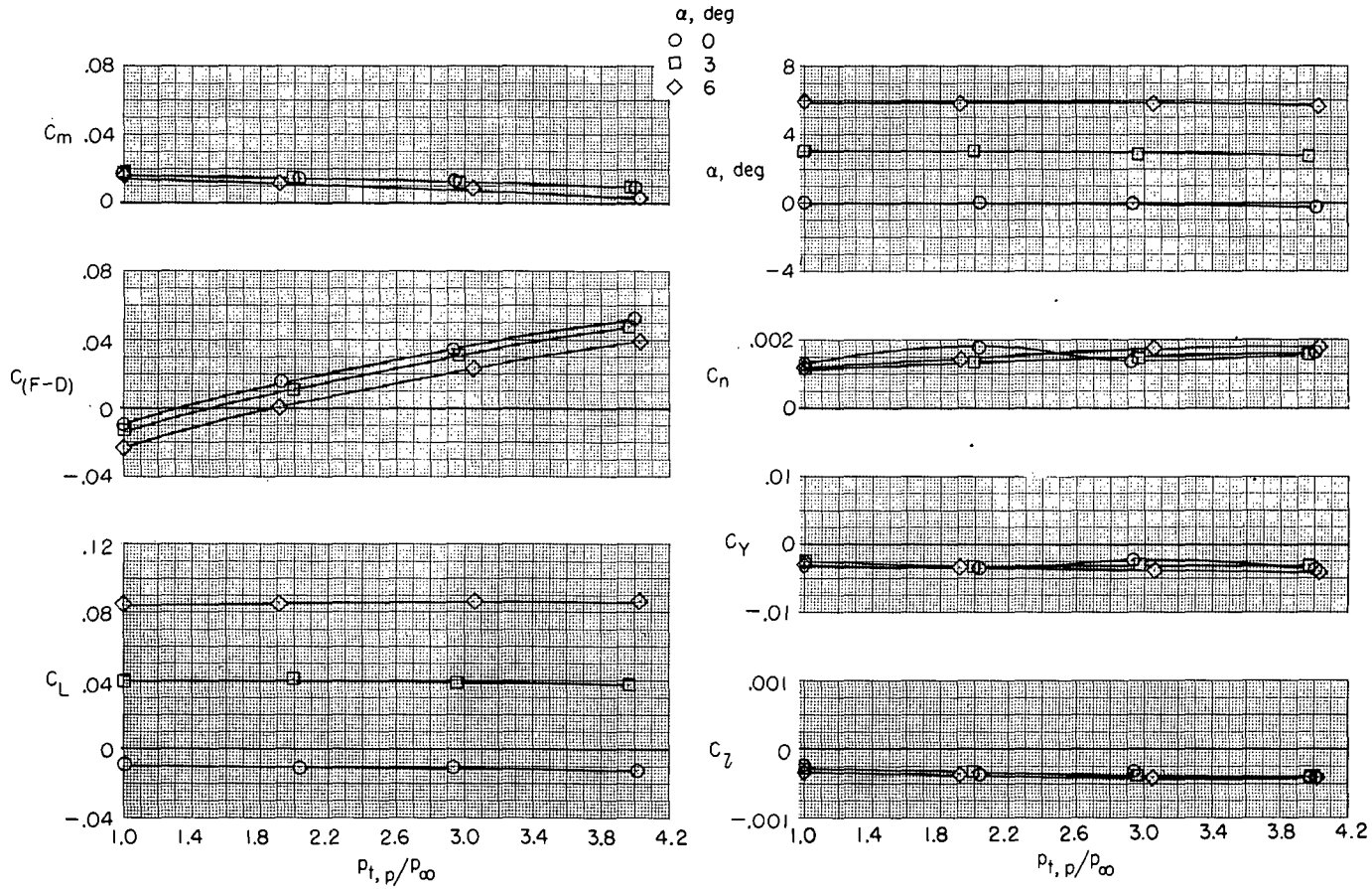

(c) M = 0.90.

Figure 20.- Concluded.

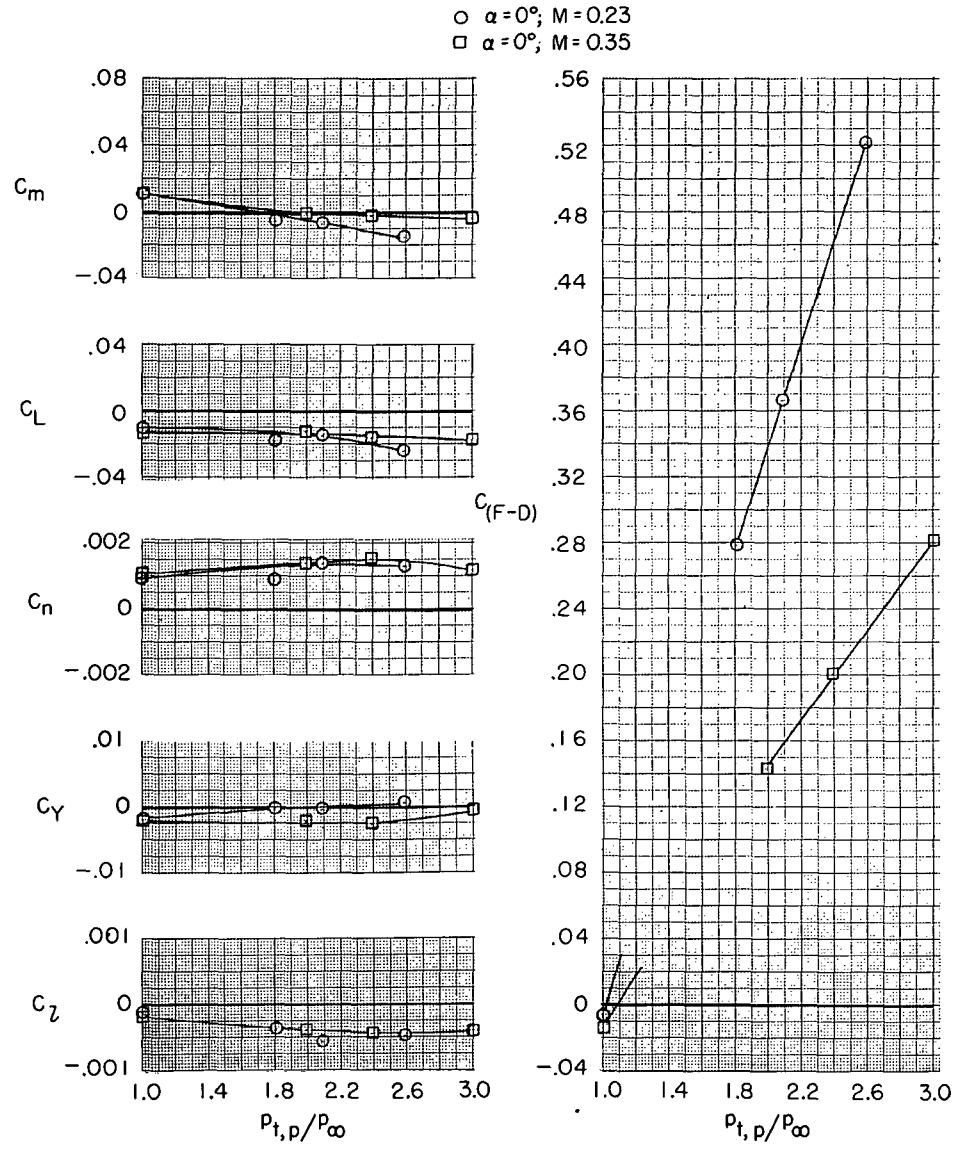

(a) M = 0.23 and 0.35; $\alpha = 0^o$.

Figure 21.- Effect of jet-total-pressure ratio on aerodynamic characteristics of model with thrust control unit for several angles of attack and Mach numbers. $\beta = 0^o$; $\delta_f = 0^o$; $\delta_s = 0^o$; $\delta_h = -1.5^o$; $\delta_r = 0^o$; $\delta_{du} = 32.5^o$; $\delta_{dl} = 52.5^o$; $\delta_b = 0$ percent; and military power.

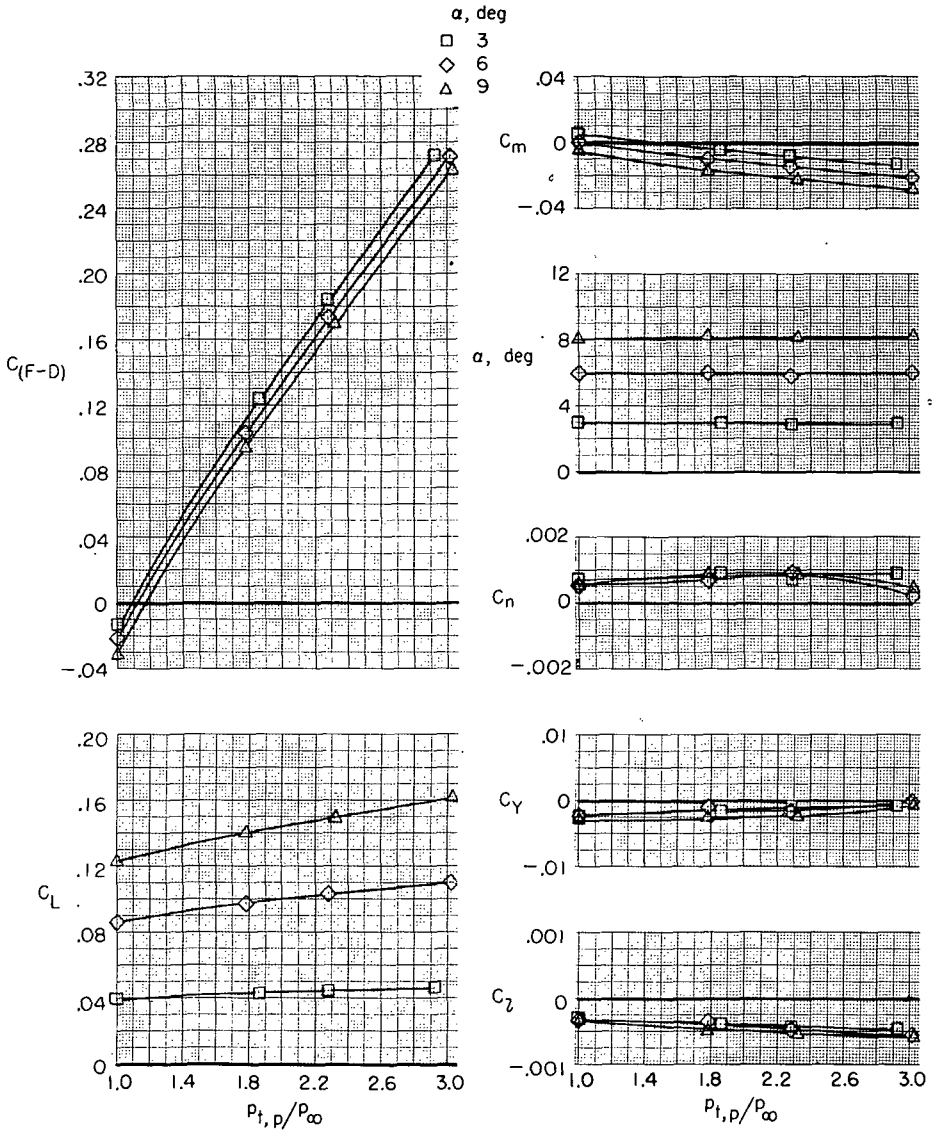

(b) M = 0.34.

Figure 21.- Continued.

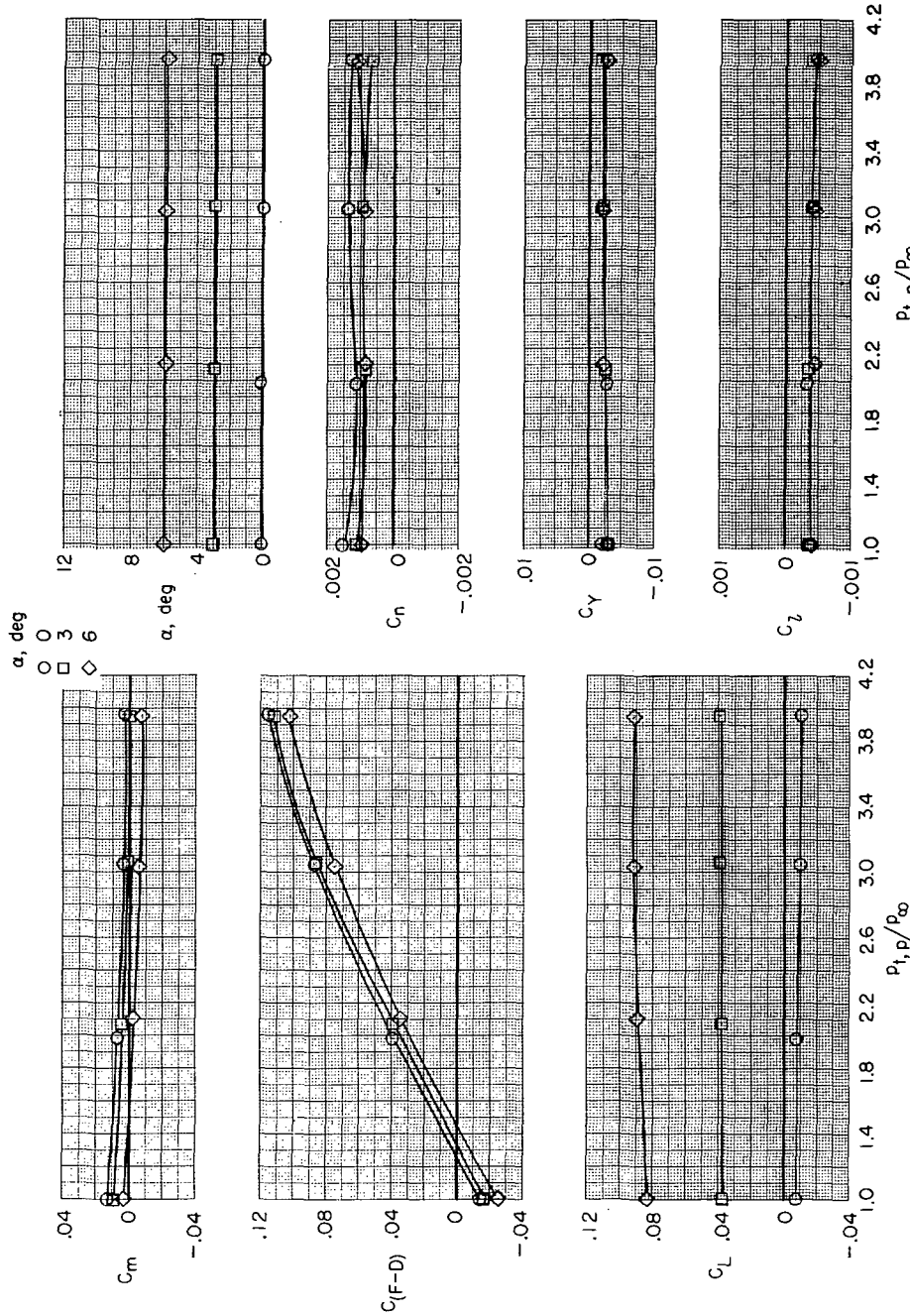

(c) M = 0.60.

Figure 21.- Continued.

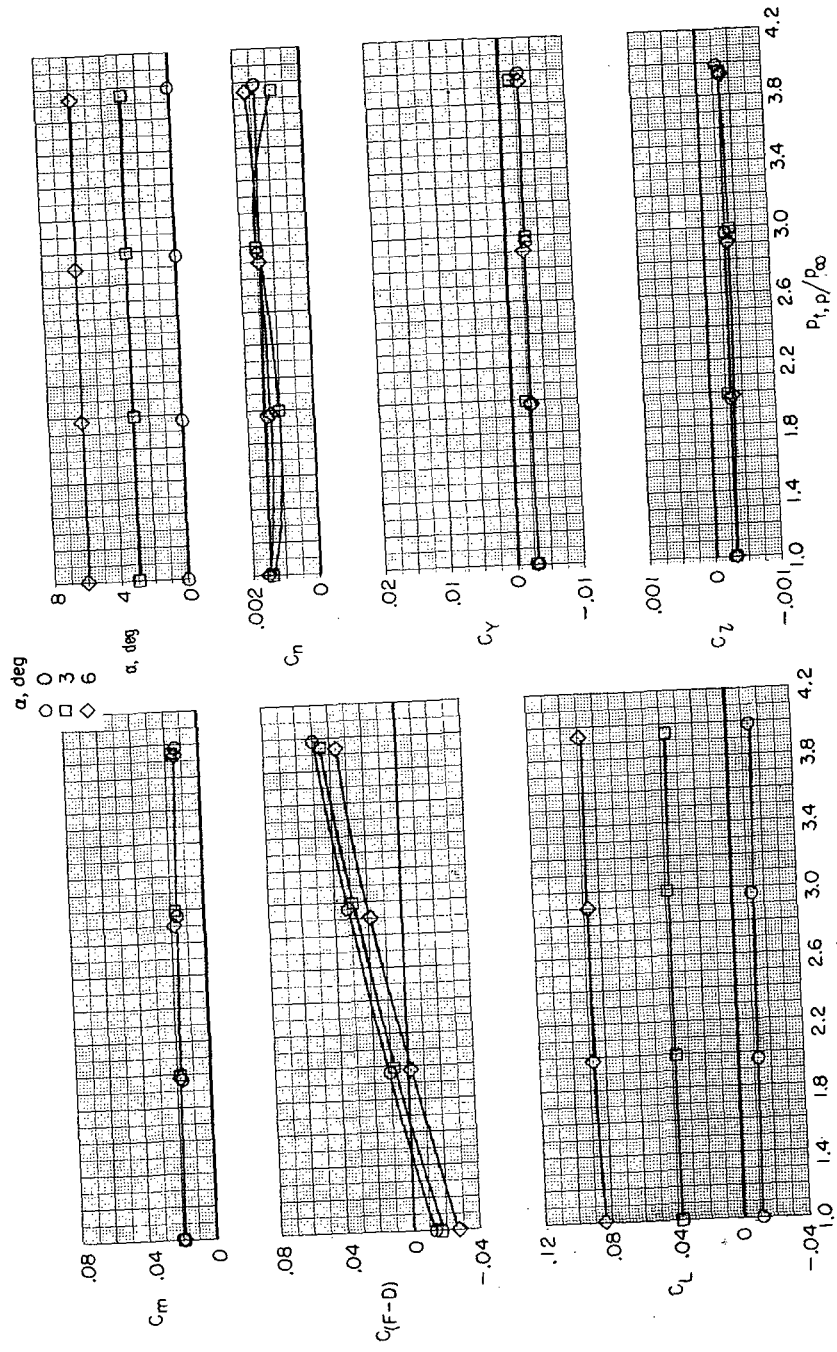

(d) M = 0.90.

Figure 21.- Continued.

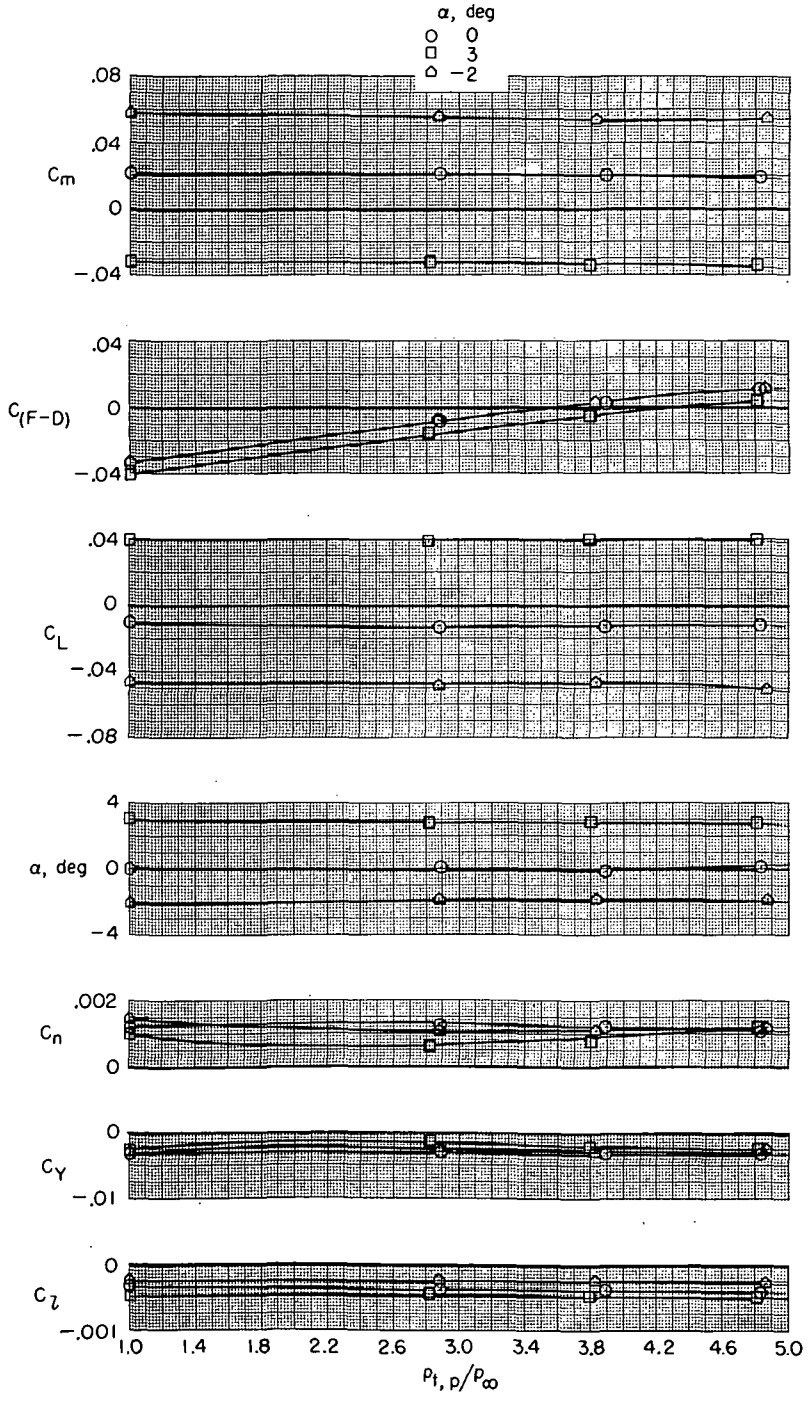

(e) M = 1.30.

Figure 21.- Concluded.

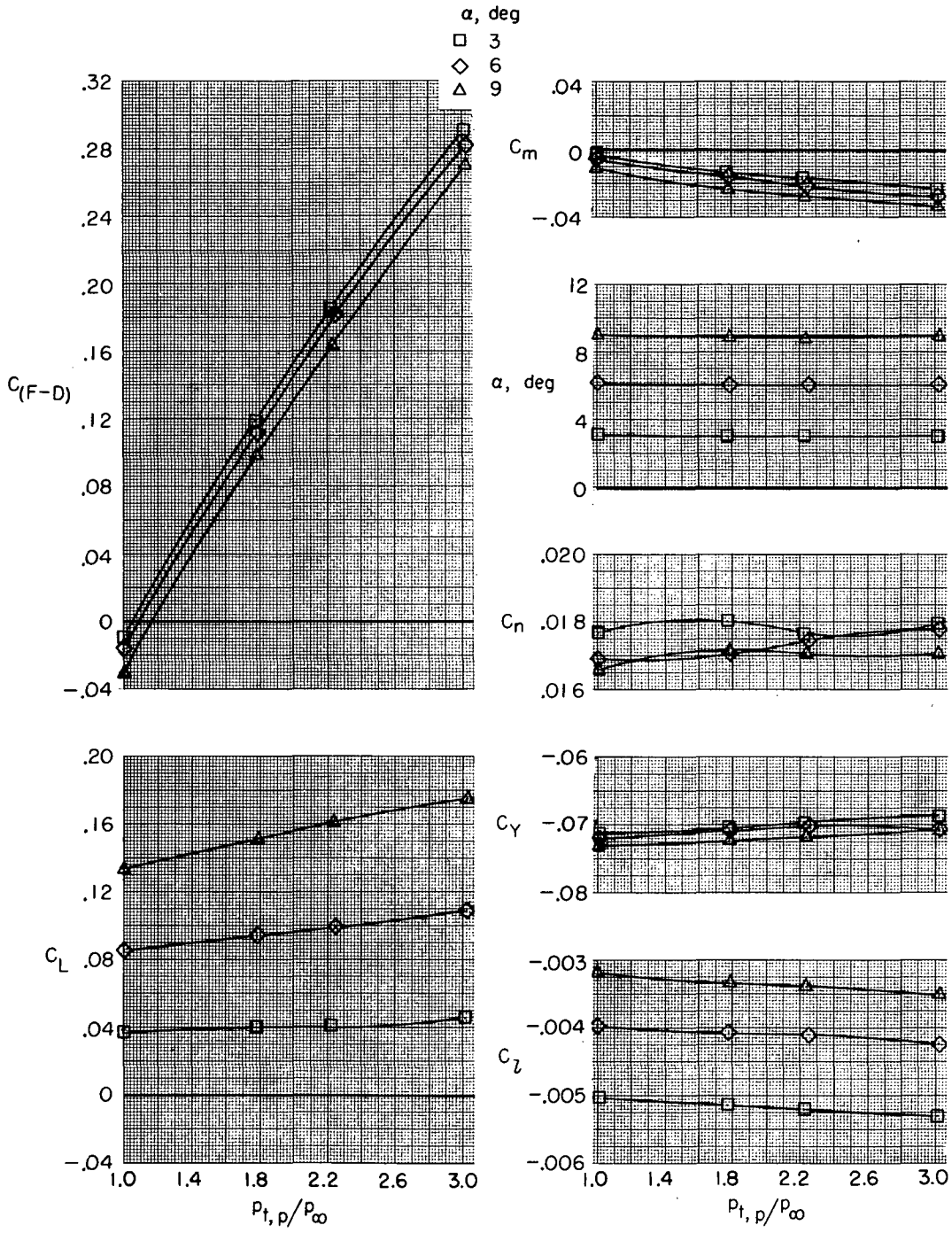

(a) M = 0.34.

Figure 22.- Effect of jet-total-pressure ratio on aerodynamic characteristics of model with thrust control unit for several angles of attack and Mach numbers. $\beta = 5^o$; $\delta_f = 0^o$; $\delta_s = 0^o$; $\delta_h = -1.5^o$; $\delta_r = 0^o$; $\delta_{du} = 32.5^o$; $\delta_{dl} = 52.5^o$; $\delta_b = 0$ percent; and military power.

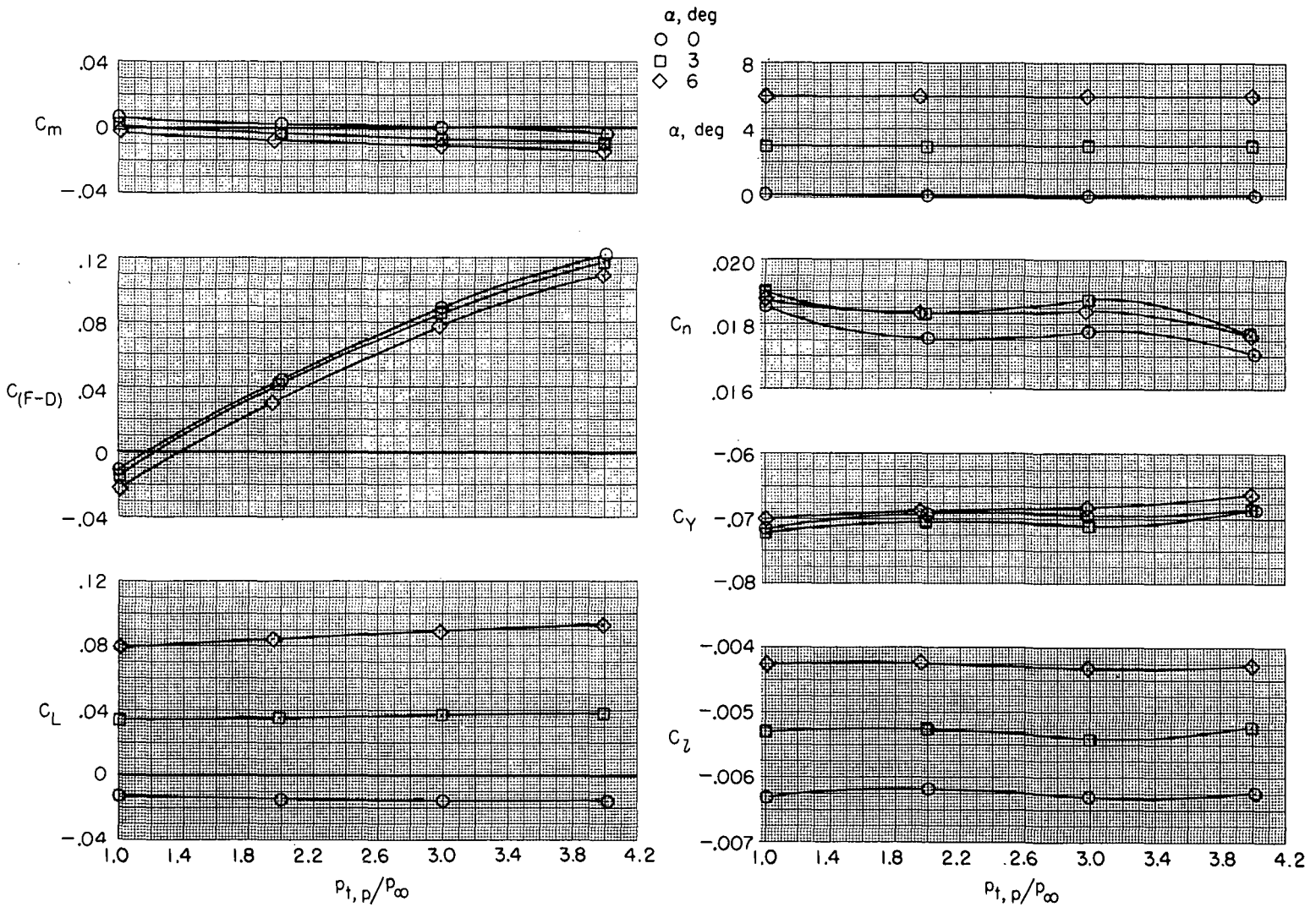

(b) M = 0.60.

Figure 22.- Continued.

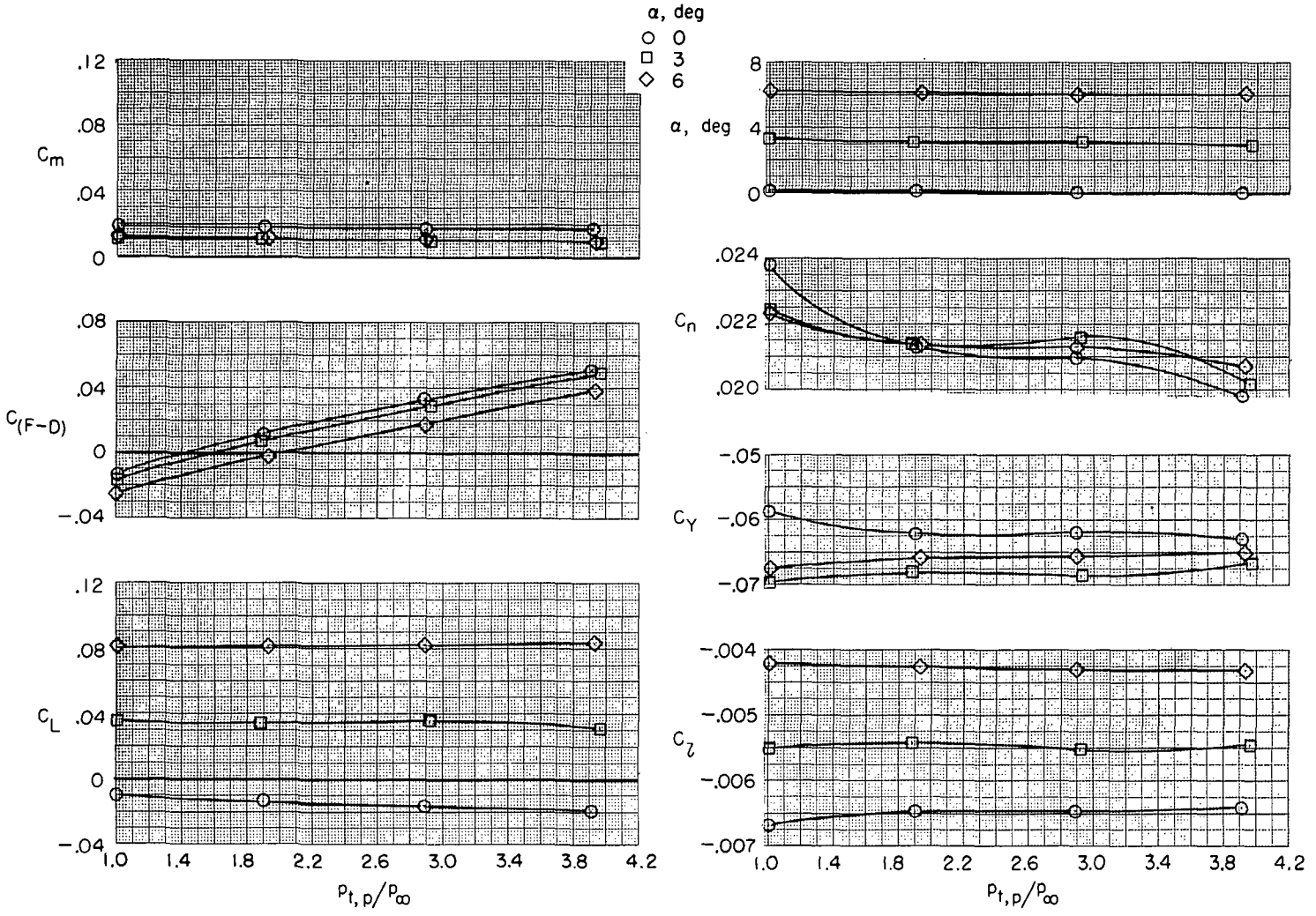

(c) M = 0.90.

Figure 22.- Concluded.

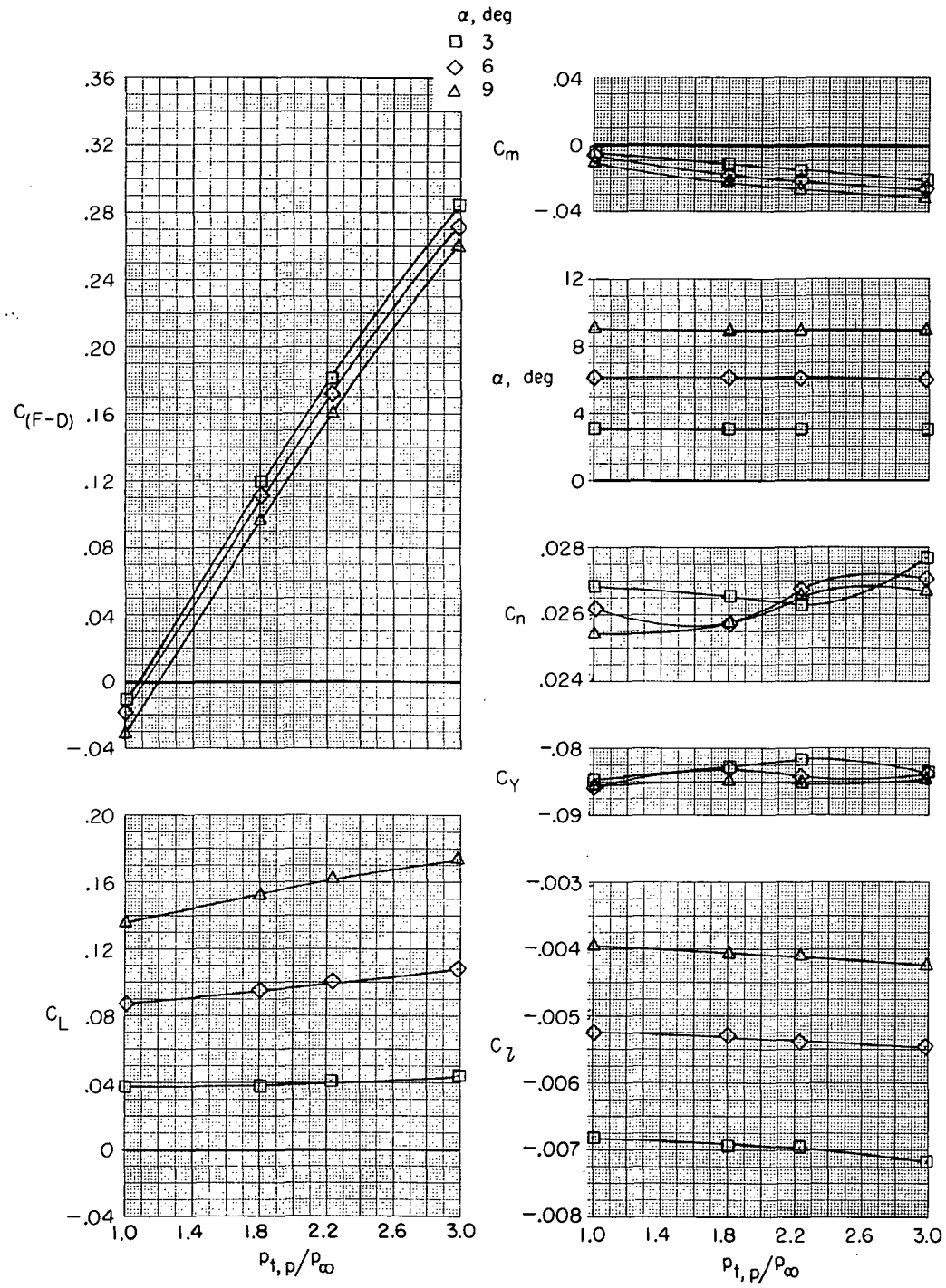

(a) M = 0.34.

Figure 23.- Effect of jet-total-pressure ratio on aerodynamic characteristics of model with thrust control unit for several angles of attack and Mach numbers. $\beta = 5^o$; $\delta_f = 0^o$; $\delta_s = 0^o$; $\delta_h = -1.5^o$; $\delta_r = -5^o$; $\delta_{du} = 32.5^o$; $\delta_{dl} = 52.5^o$; $\delta_b = 0$ percent; and military power.

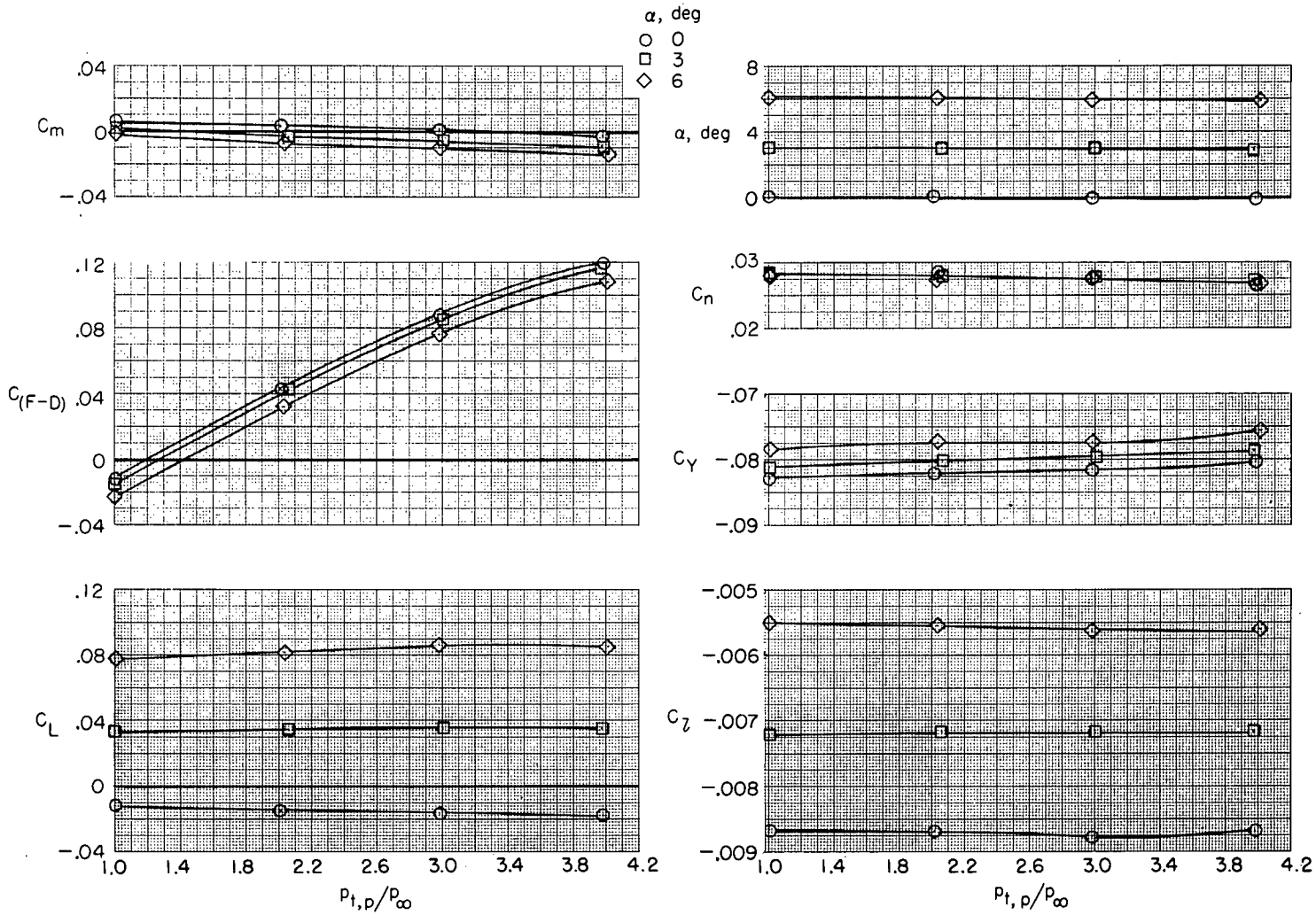

(b) M = 0.60.

Figure 23.- Concluded.

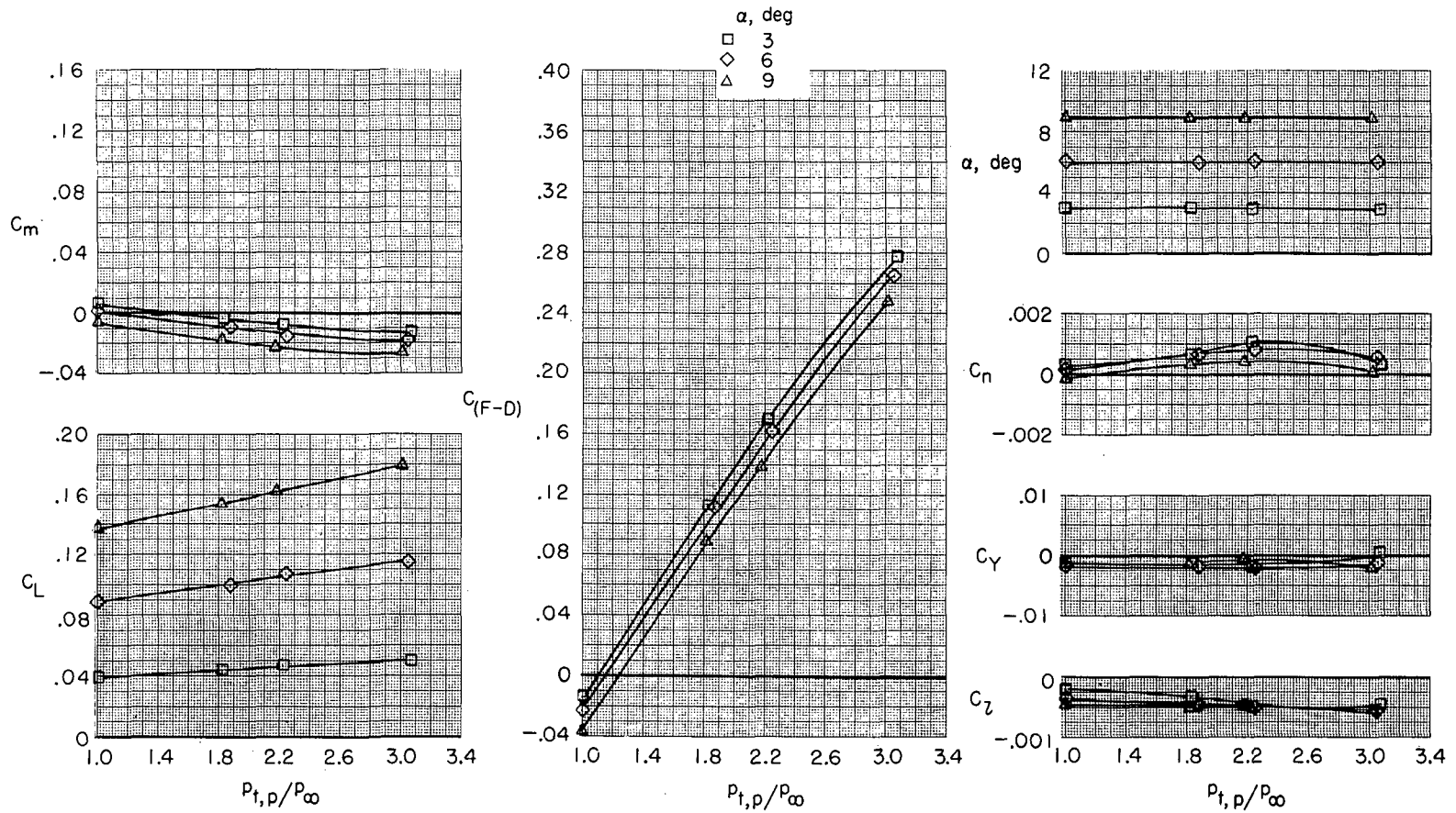

(a) M = 0.34.

Figure 24.- Effect of jet-total-pressure ratio on aerodynamic characteristics of model with thrust control unit for several angles of attack and Mach numbers. $\beta = 0^o$; $\delta_f = 0^o$; $\delta_s = 0^o$; $\delta_h = -1.5^o$; $\delta_r = 0^o$; $\delta_{du} = 32.5^o$; $\delta_{dl} = 52.5^o$; $\delta_b = 25$ percent; and military power.

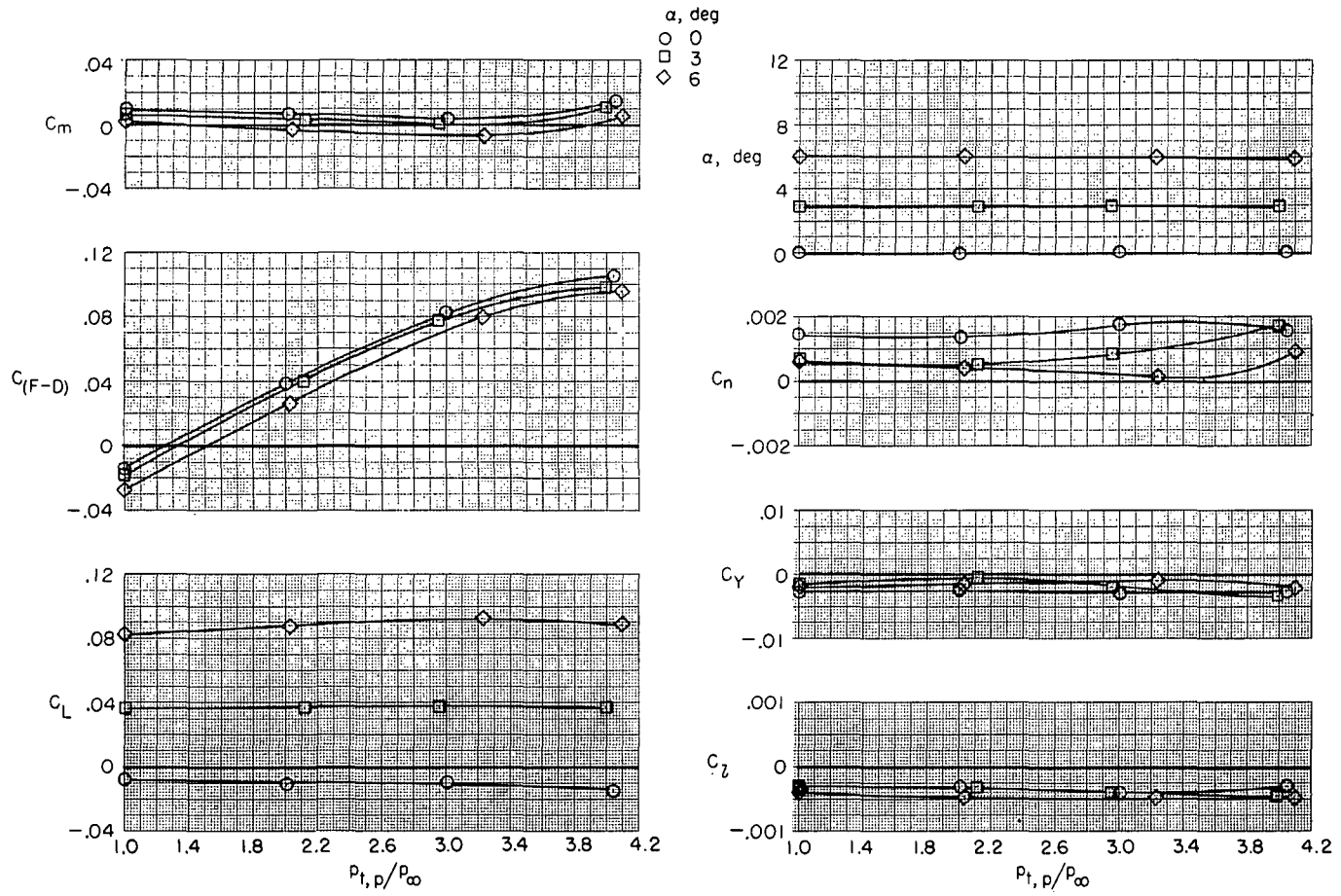

(b) M = 0.60.

Figure 24.- Continued.

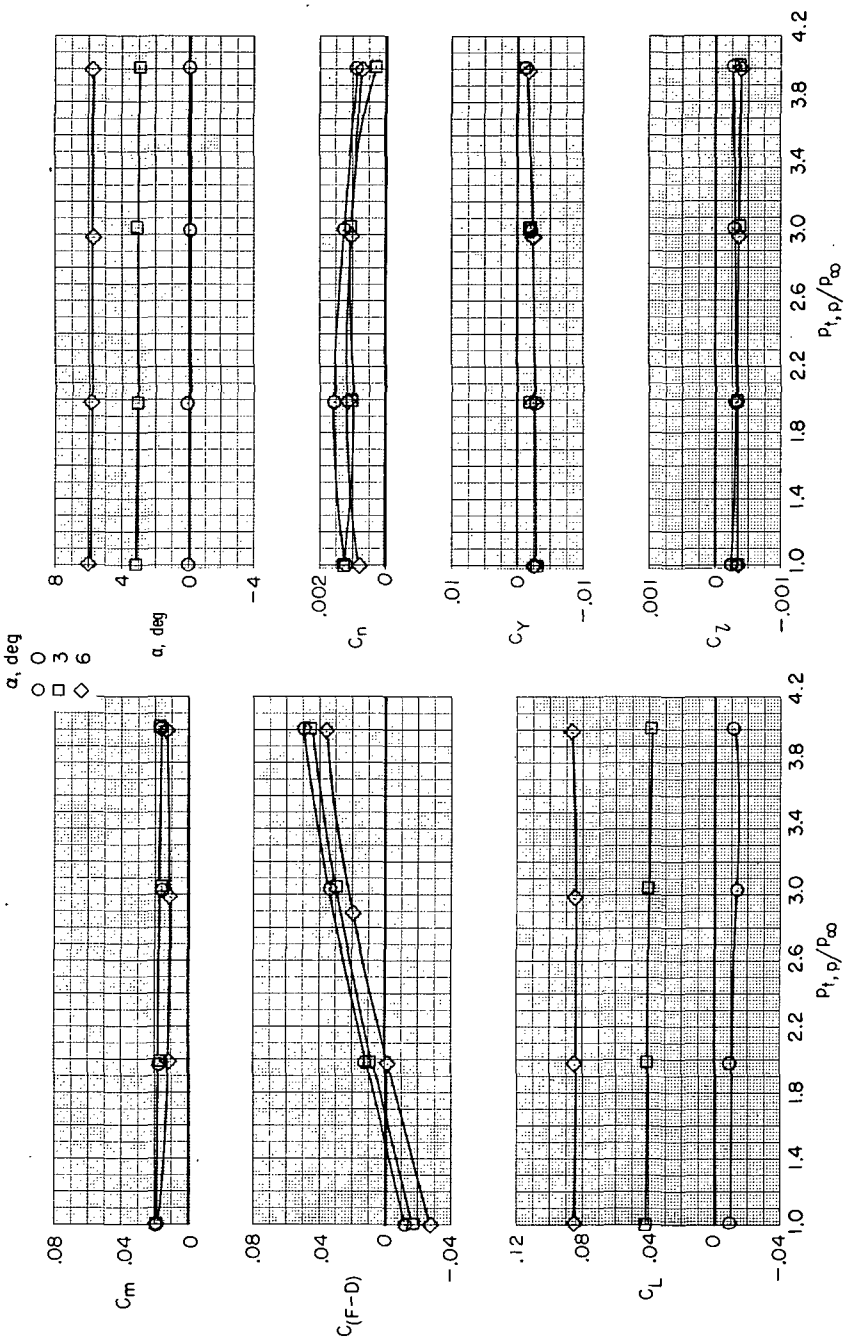

(c) M = 0.90.

Figure 24.- Continued.

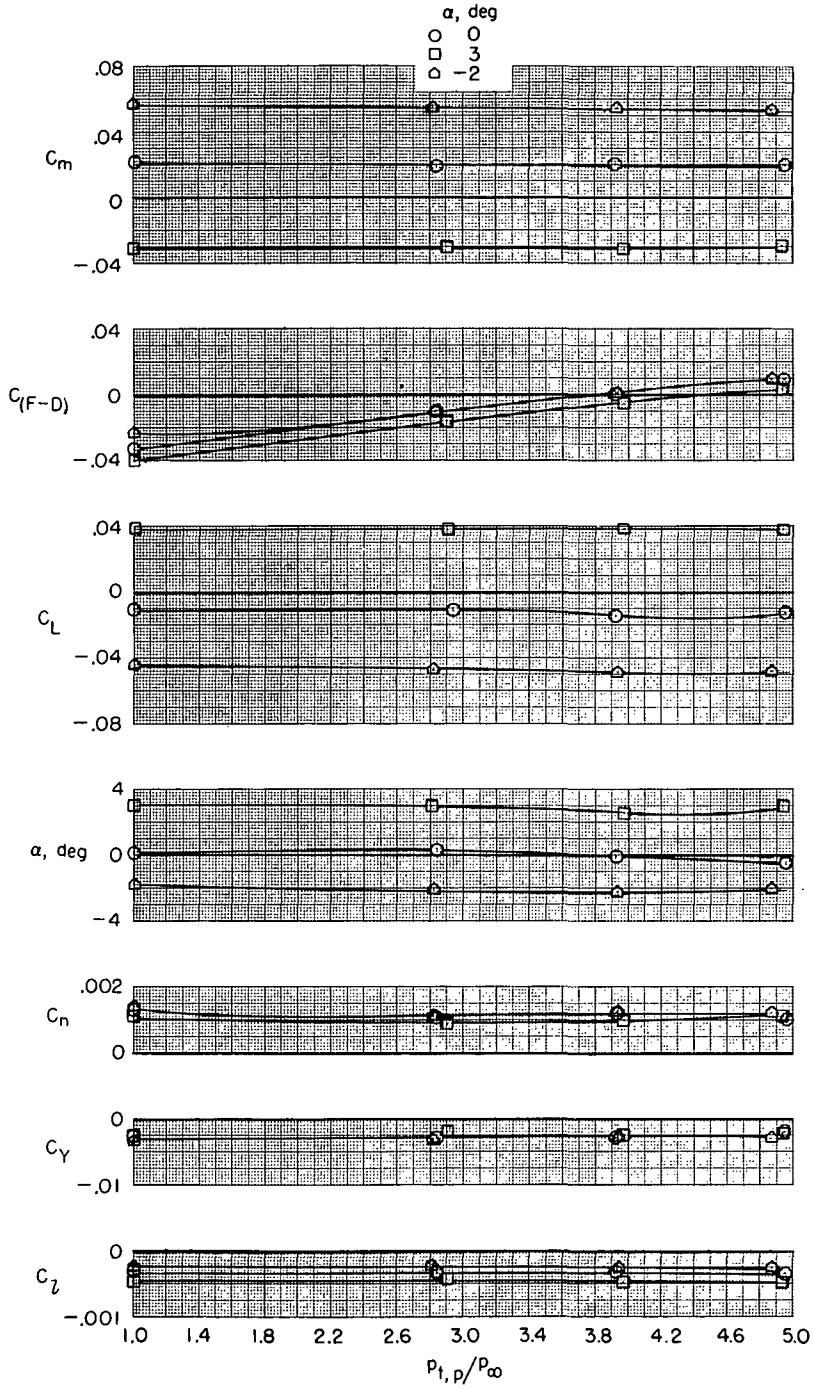

(d) M = 1.30.

Figure 24.- Concluded.

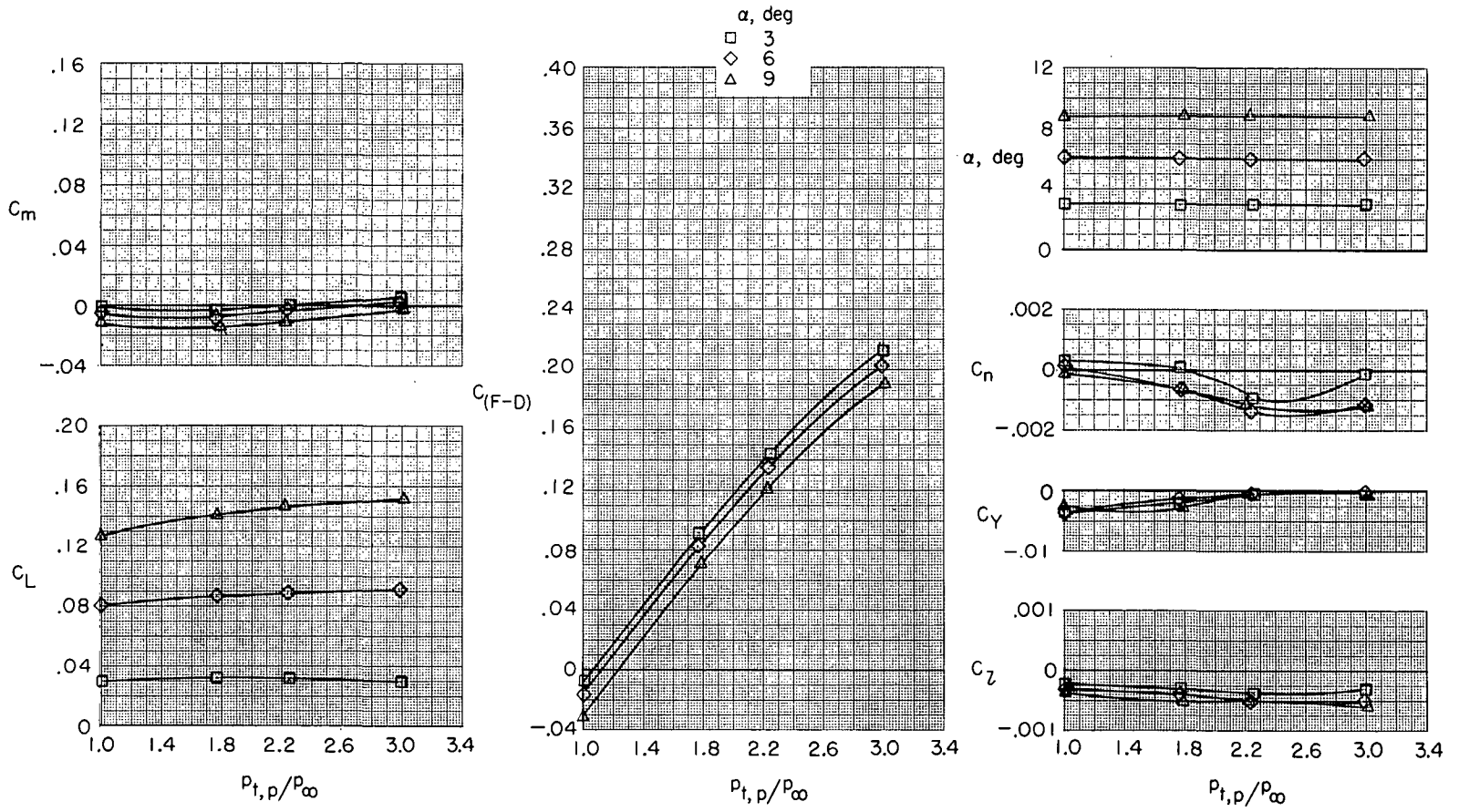

(a) M = 0.34.

Figure 25.- Effect of jet-total-pressure ratio on aerodynamic characteristics of model with thrust control unit for several angles of attack and Mach numbers. $\beta = 0^o$; $\delta_f = 0^o$; $\delta_s = 0^o$; $\delta_h = -1.5^o$; $\delta_r = 0^o$; $\delta_{du} = 32.5^o$; $\delta_{dl} = 52.5^o$; $\delta_b = 50$ percent; and military power.

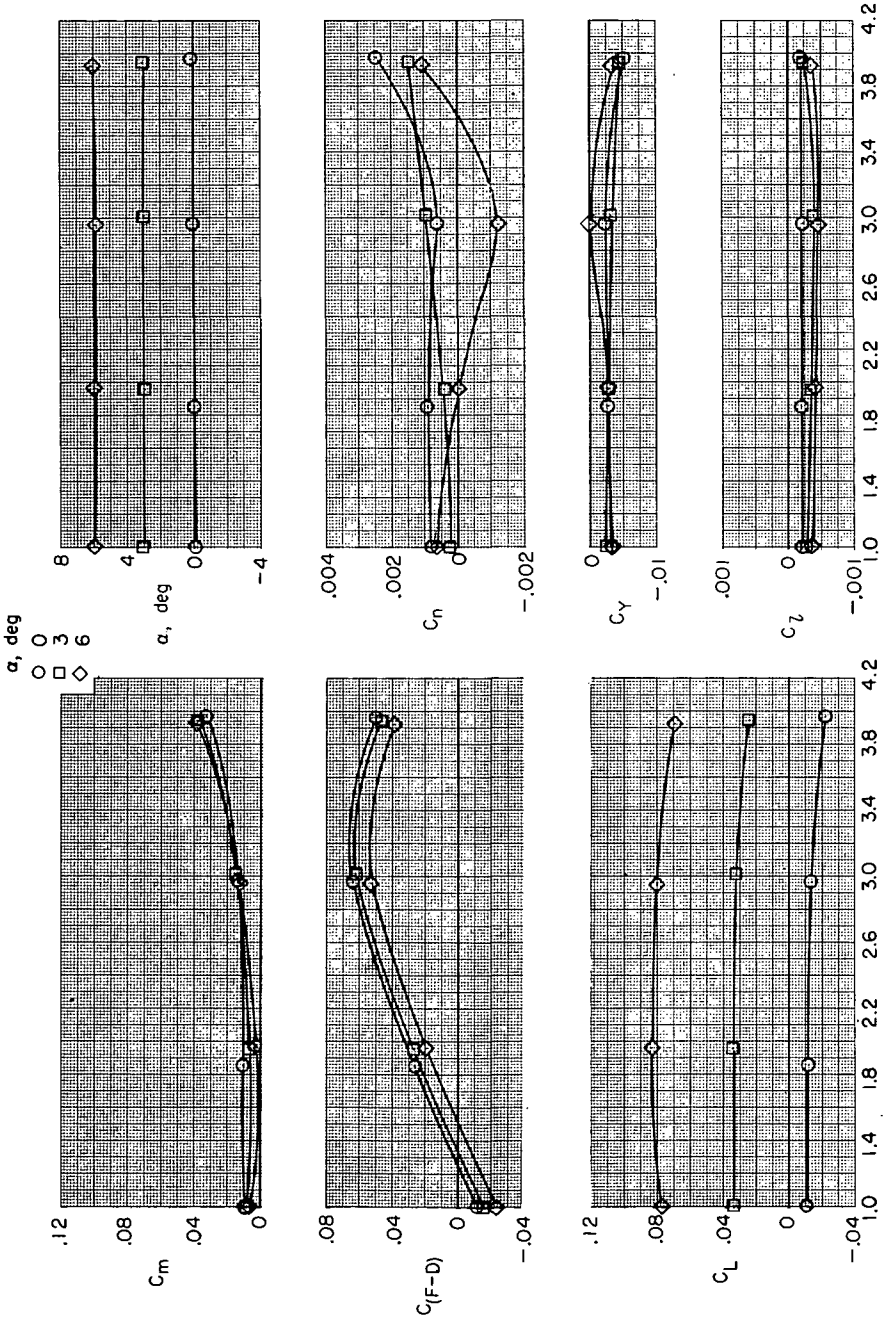

(b) M = 0.60.

Figure 25.- Continued.

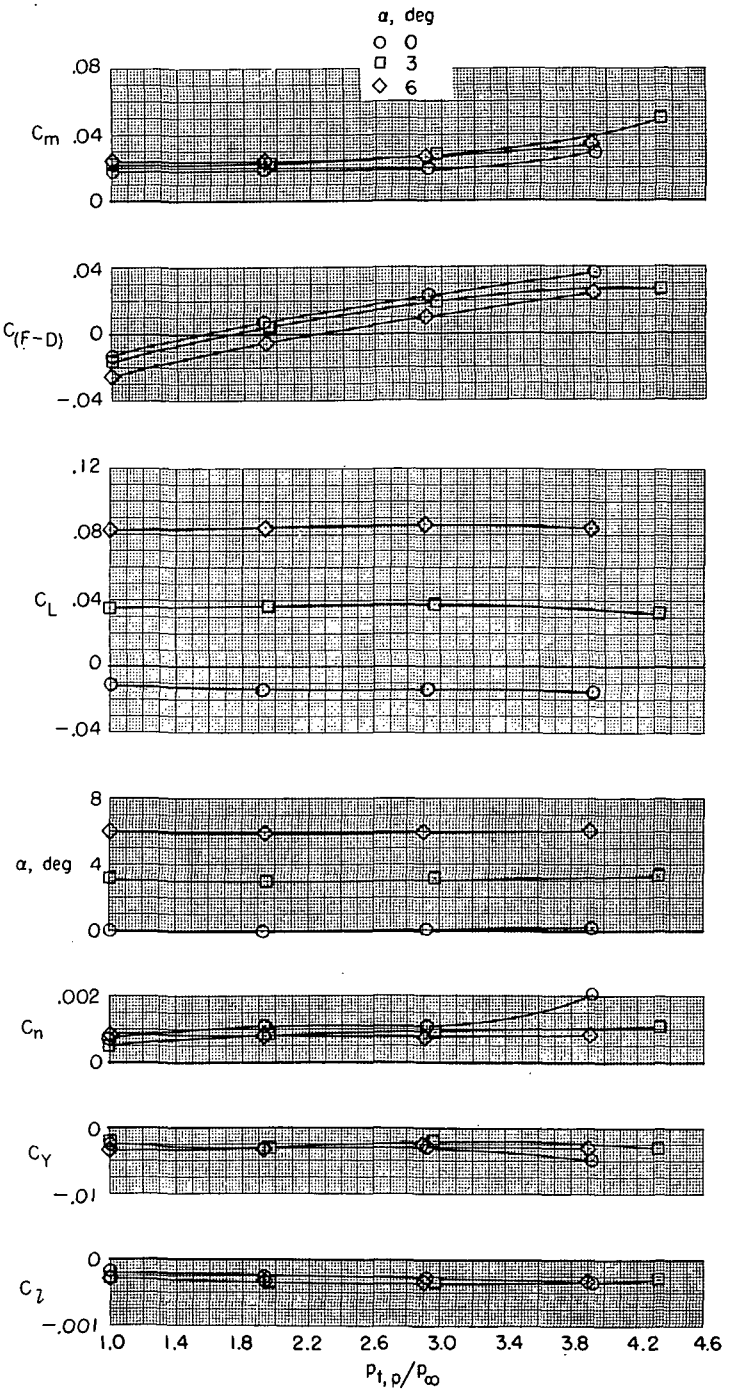

(c) M = 0.90.

Figure 25.- Continued.

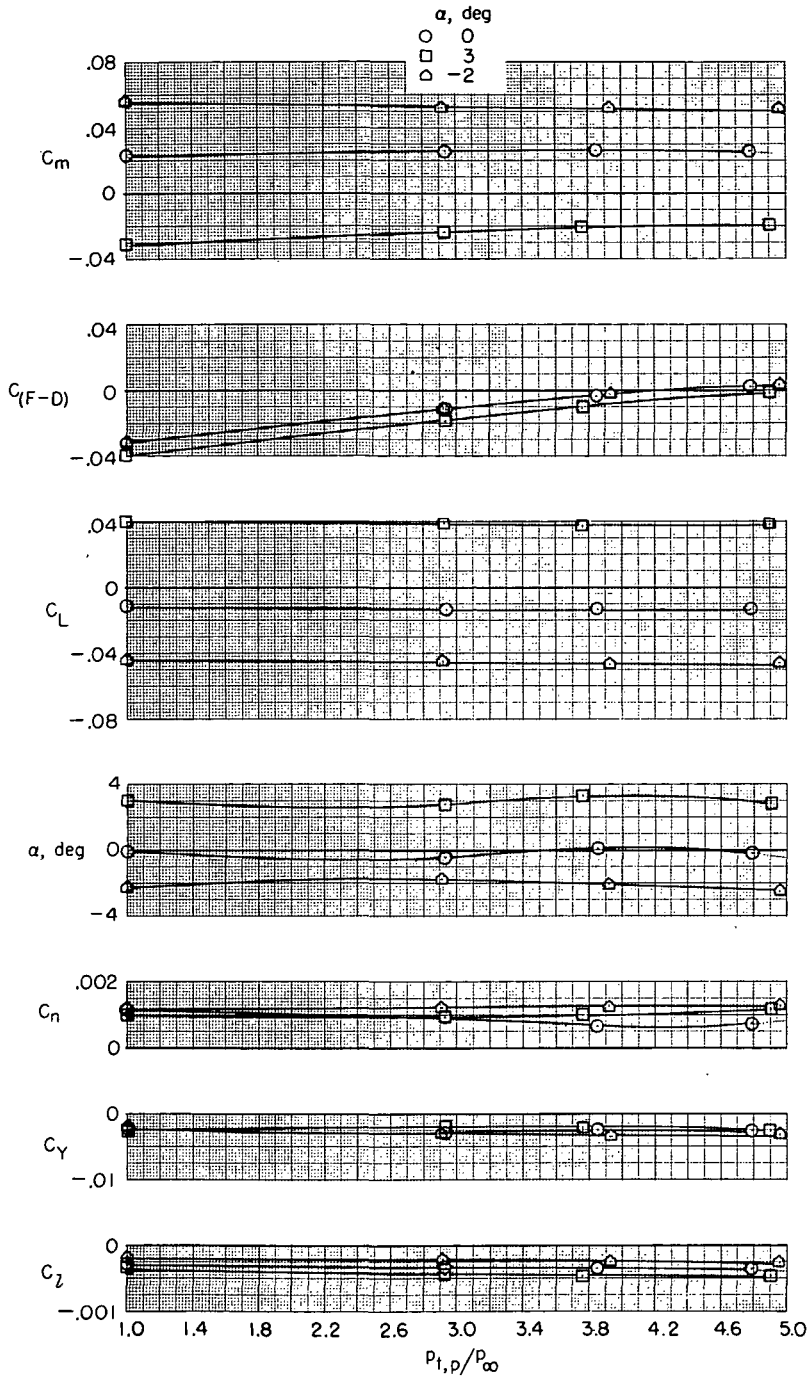

(d) M = 1.30.

Figure 25.- Concluded.

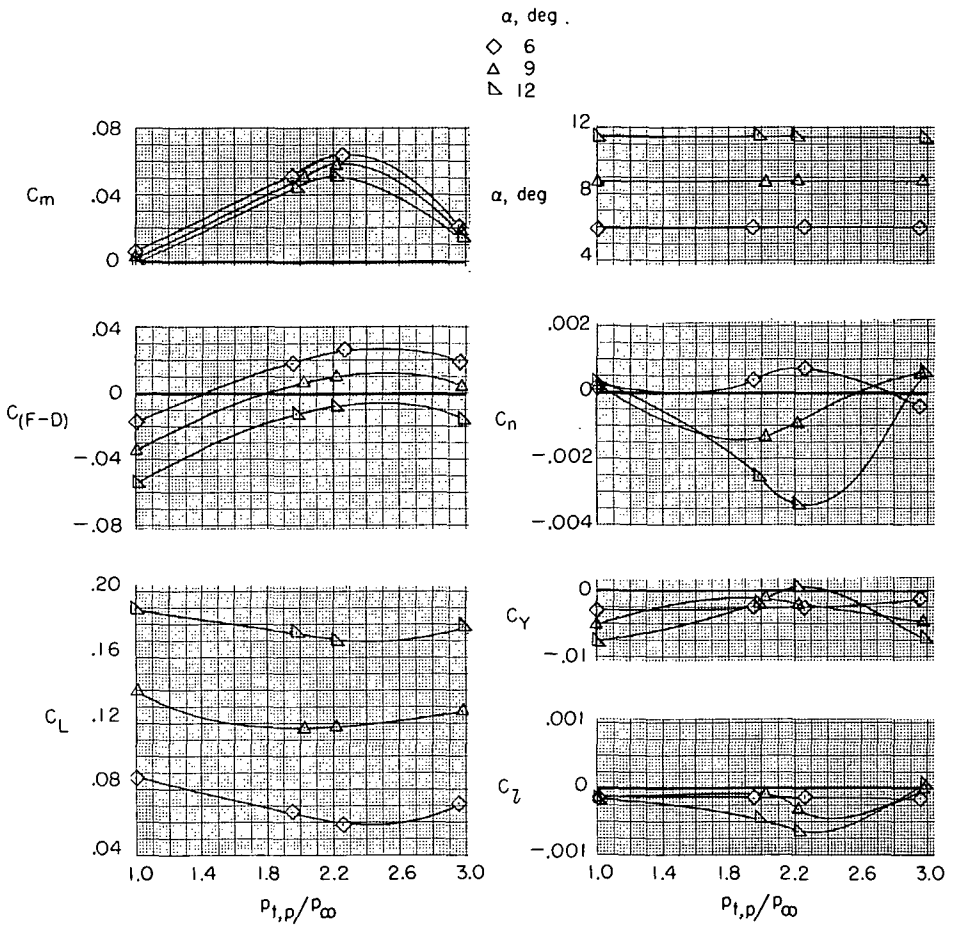

(a) M = 0.34.

Figure 26.- Effect of jet-total-pressure ratio on aerodynamic characteristics of model with thrust control unit for several Mach numbers and angles of attack. $\beta = 0^o$; $\delta_f = 0^o$; $\delta_s = 0^o$; $\delta_h = -1.5^o$; $\delta_r = 0^o$; $\delta_{du} = 32.5^o$; $\delta_{dl} = 52.5^o$; $\delta_b = 75$ percent; and military power.

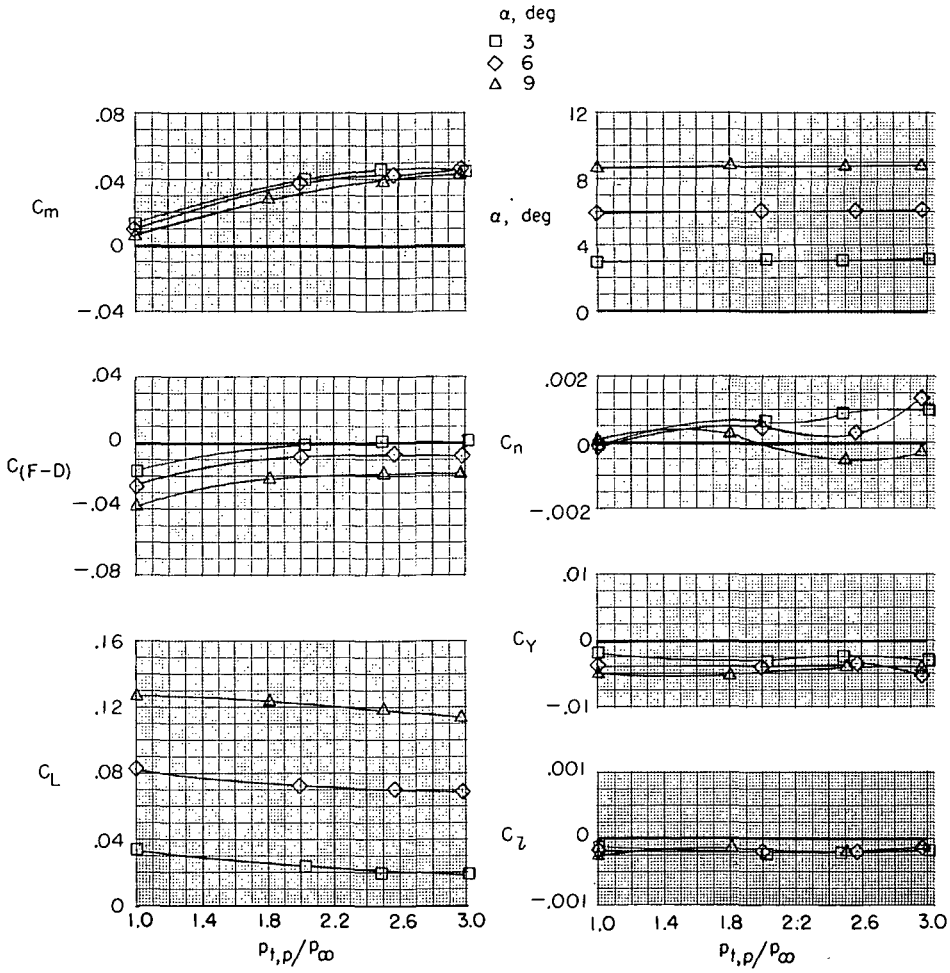

(b) M = 0.60.

Figure 26.- Continued.

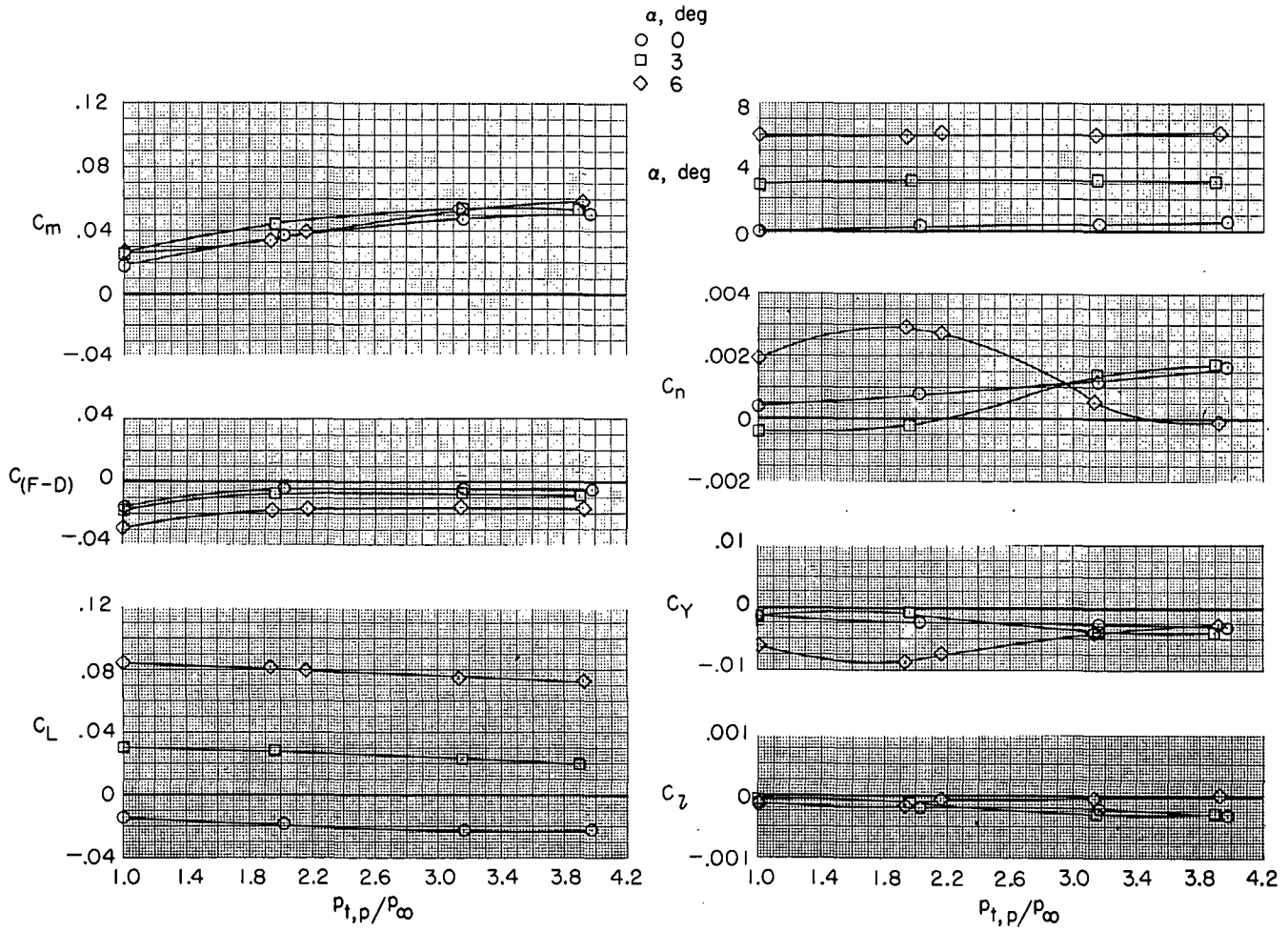

(c) M = 0.90.

Figure 26.- Continued.

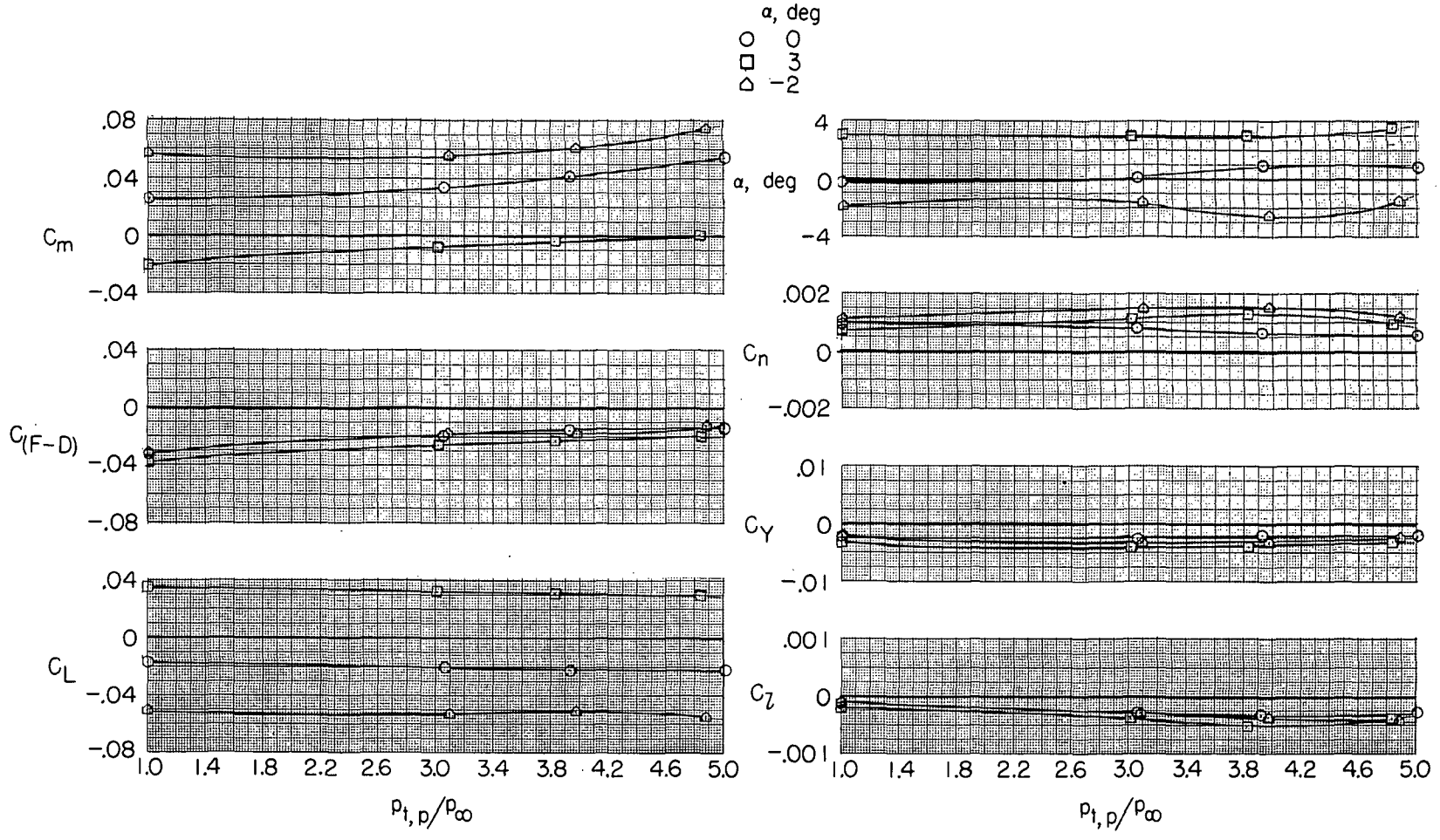

(d) M = 1.30.

Figure 26.- Concluded.

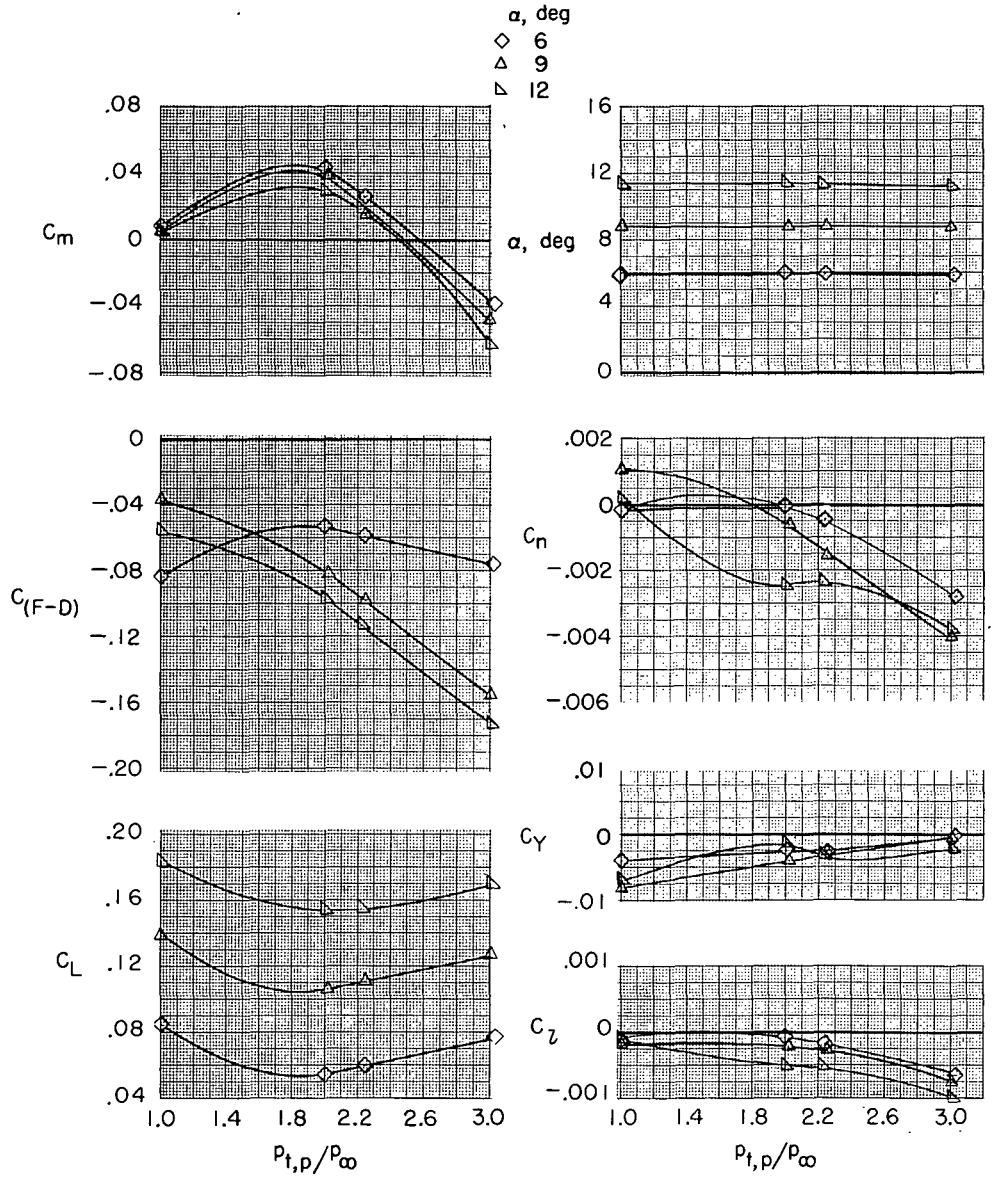

(a) M = 0.34.

Figure 27.- Effect of jet-total-pressure ratio on aerodynamic characteristics of model with thrust control unit for several angles of attack and Mach numbers. $\beta = 0^o$; $\delta_f = 0^o$; $\delta_s = 0^o$; $\delta_h = -1.5^o$; $\delta_r = 0^o$; $\delta_{du} = 32.5^o$; $\delta_{dl} = 52.5^o$; $\delta_b = 90$ percent; and military power.

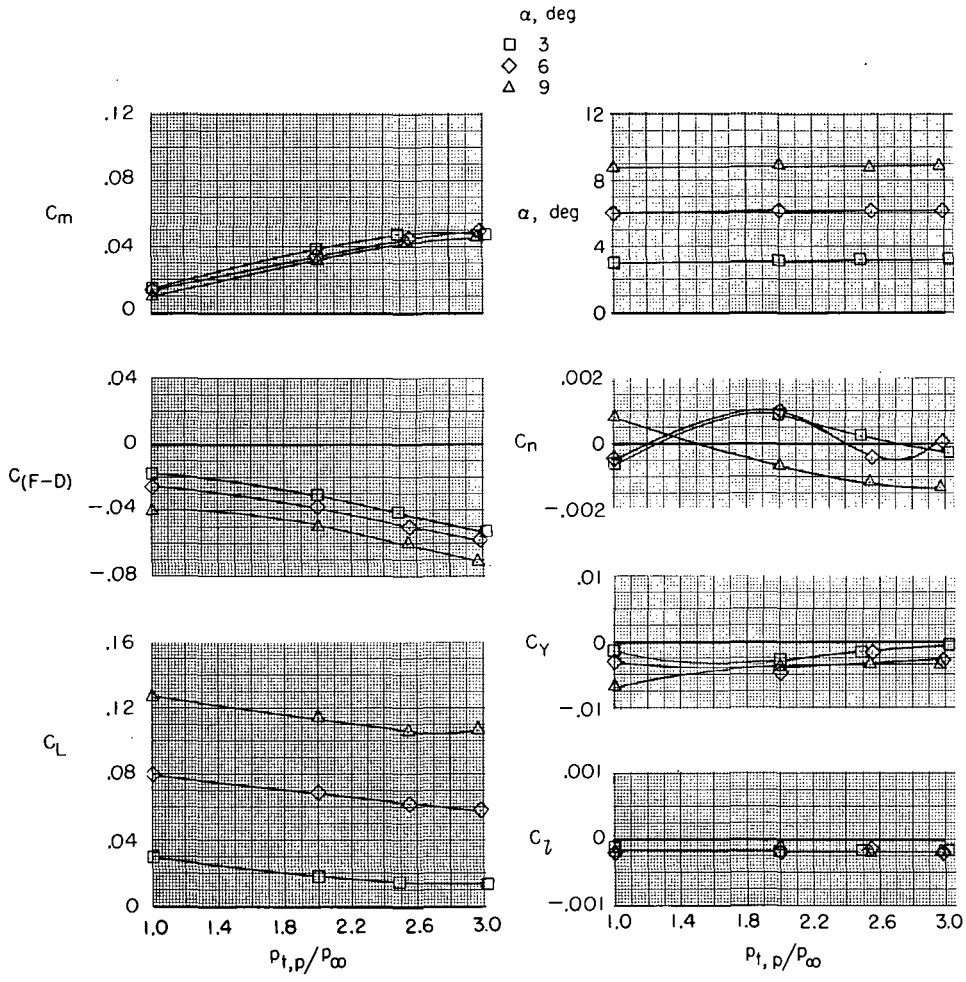

(b) M = 0.60.

Figure 27.- Continued.

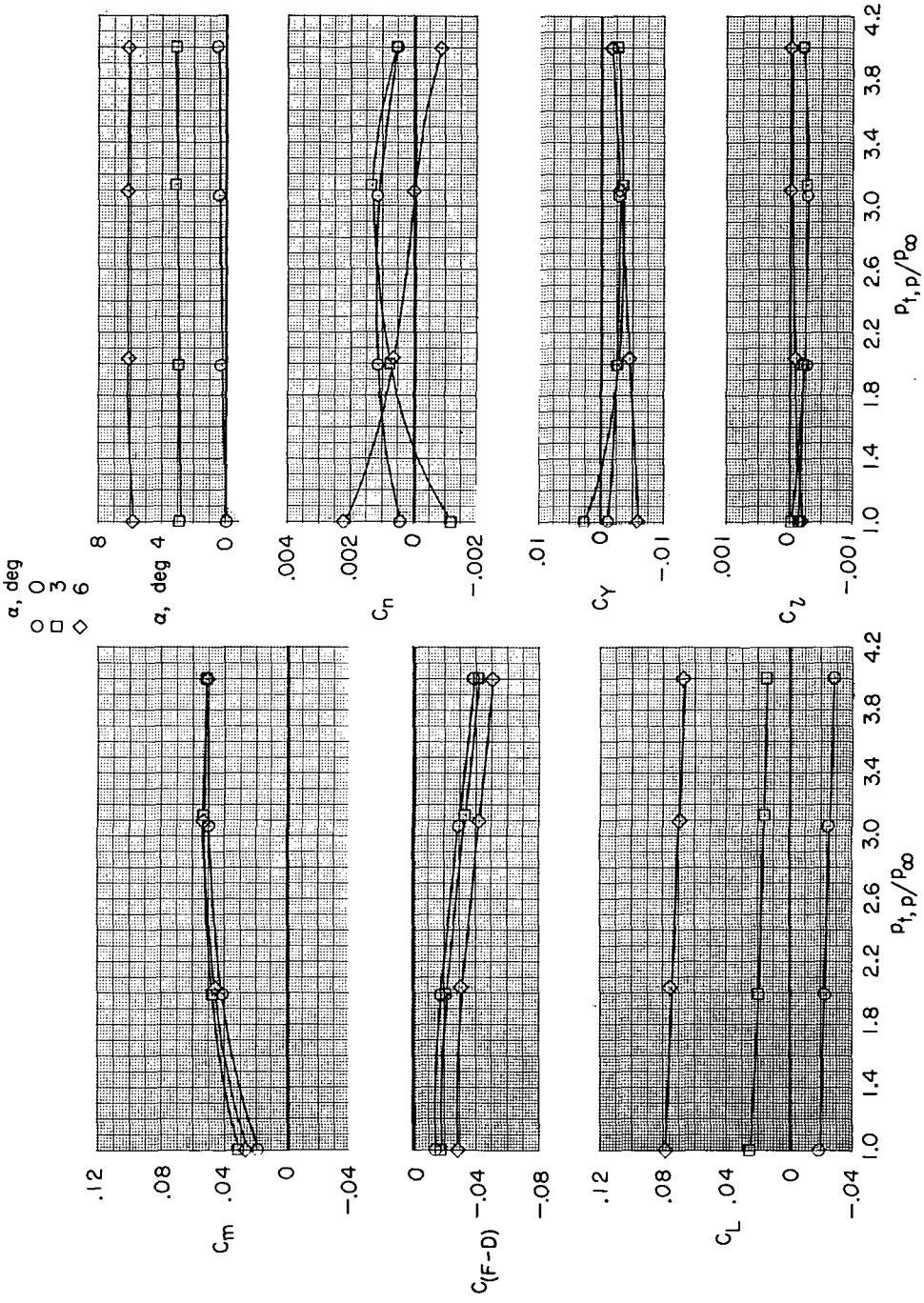

(c) M = 0.90.

Figure 27.- Continued.

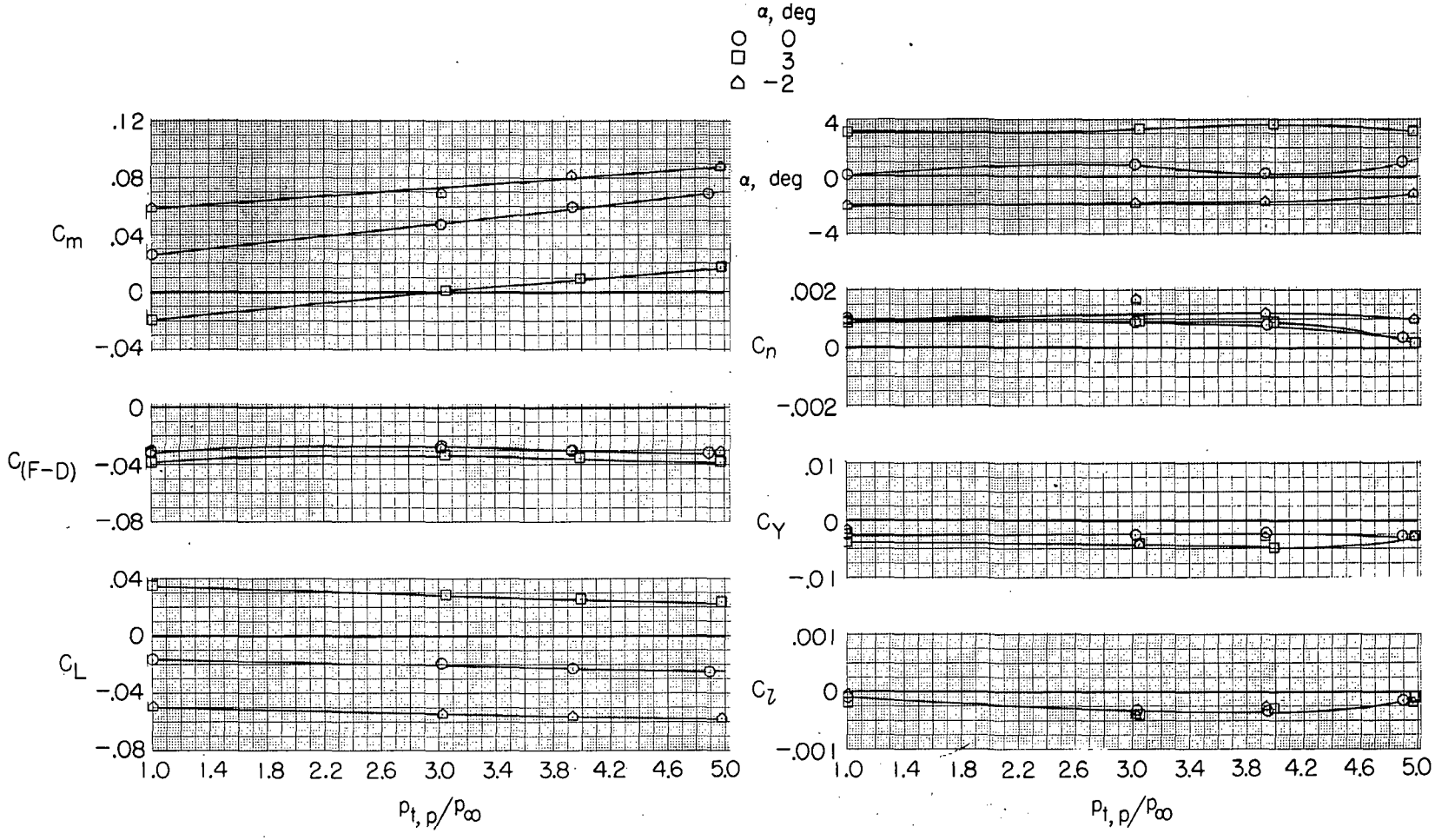

(d) M = 1.30.

Figure 27.- Concluded.

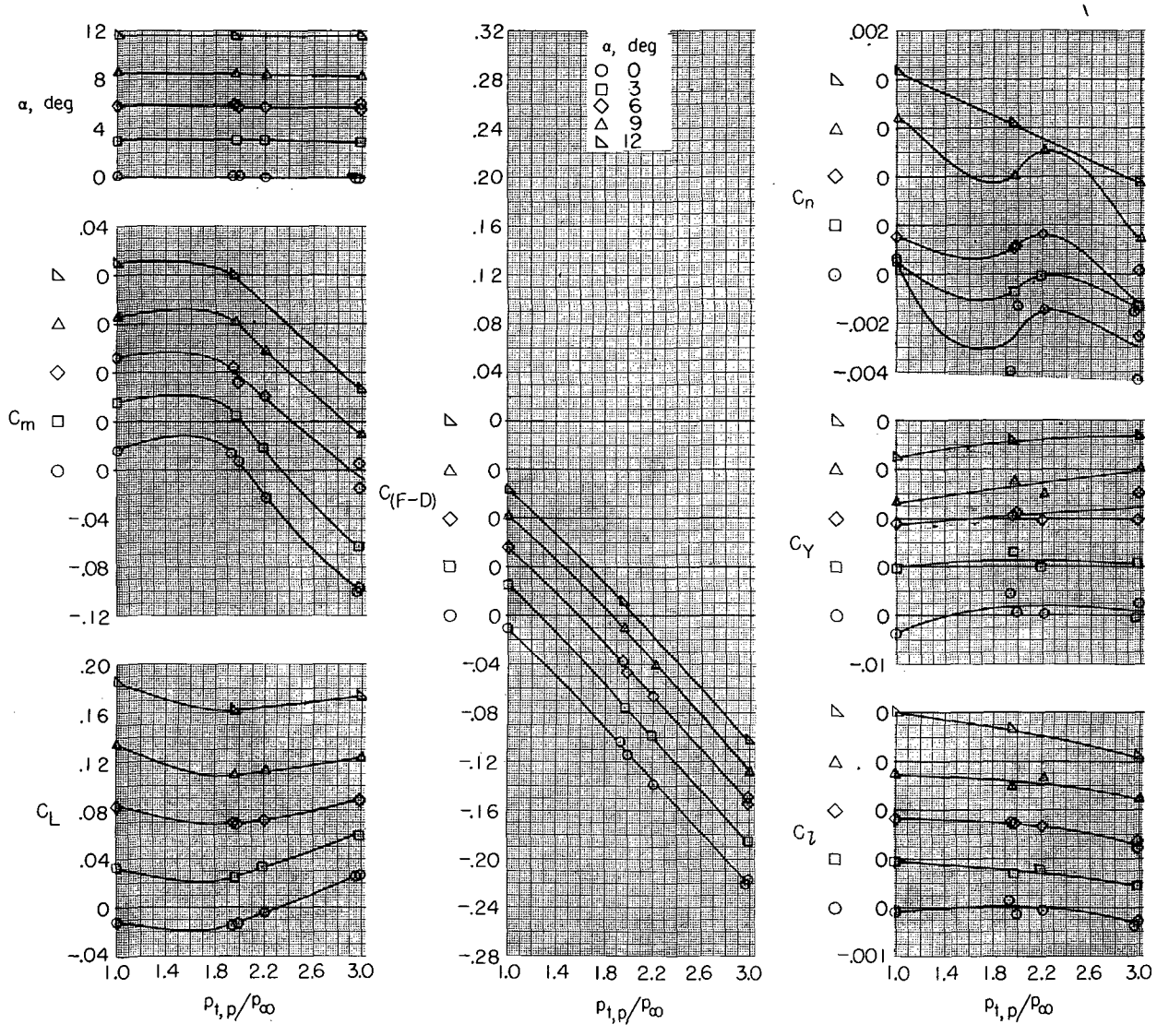

(a) M = 0.34.

Figure 28.- Effect of jet-total-pressure ratio on aerodynamic characteristics of model with thrust control unit for several angles of attack and Mach numbers. $\beta = 0^o$; $\delta_f = 0^o$; $\delta_s = 0^o$; $\delta_h = -1.5^o$; $\delta_r = 0^o$; $\delta_{du} = 32.5^o$; $\delta_{dl} = 52.5^o$; $\delta_b = 100$ percent; and military power.

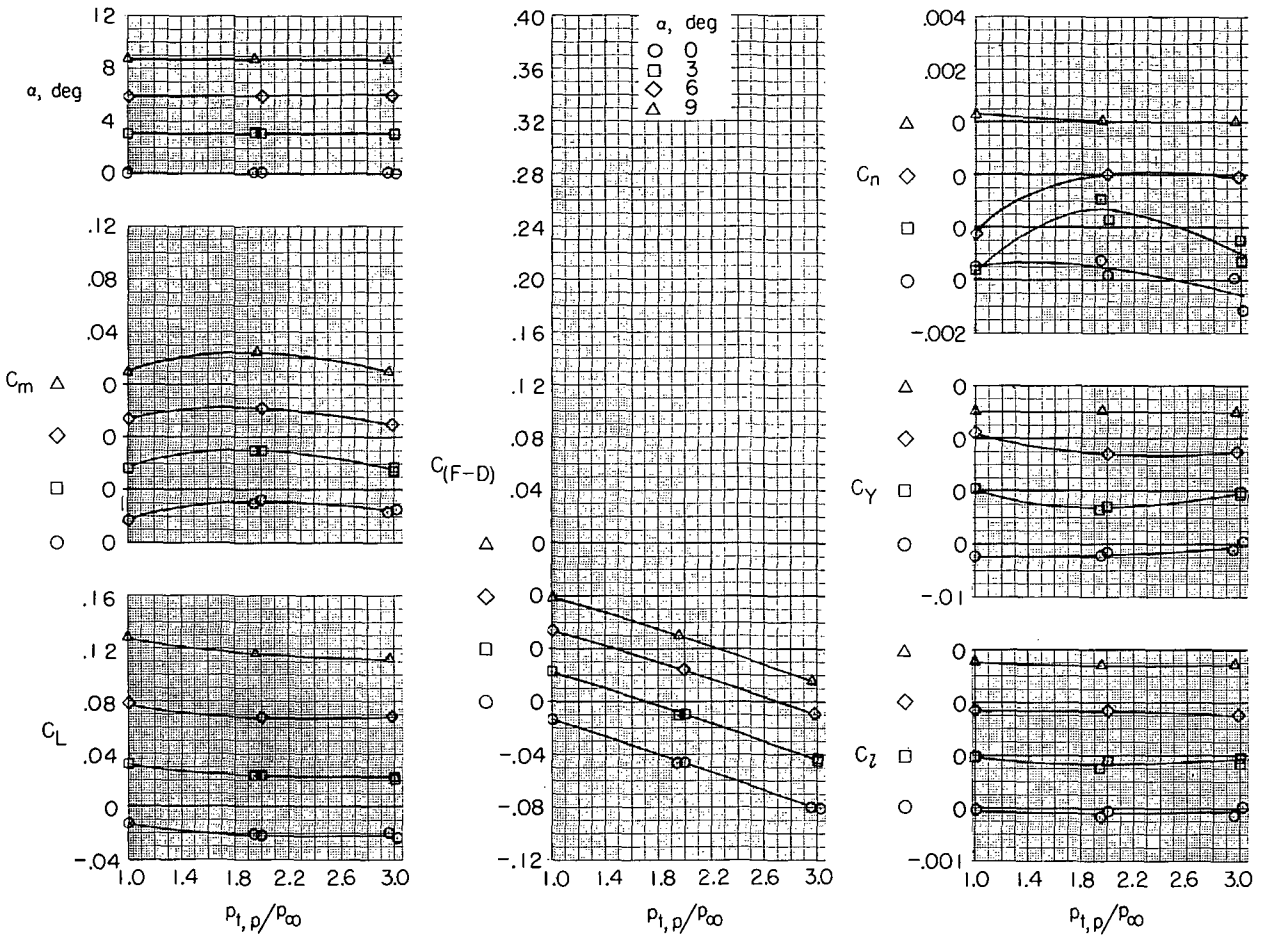

(b) M = 0.60.

Figure 28.- Continued.

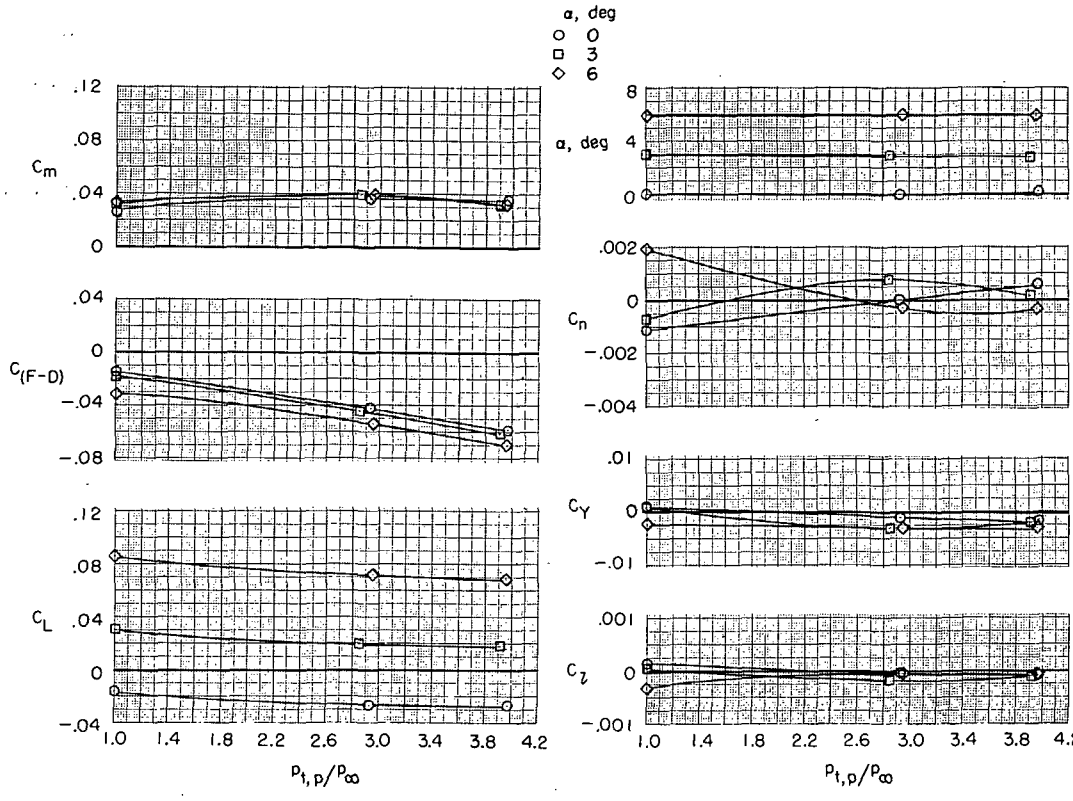

(c) M = 0.90.

Figure 28.- Continued.

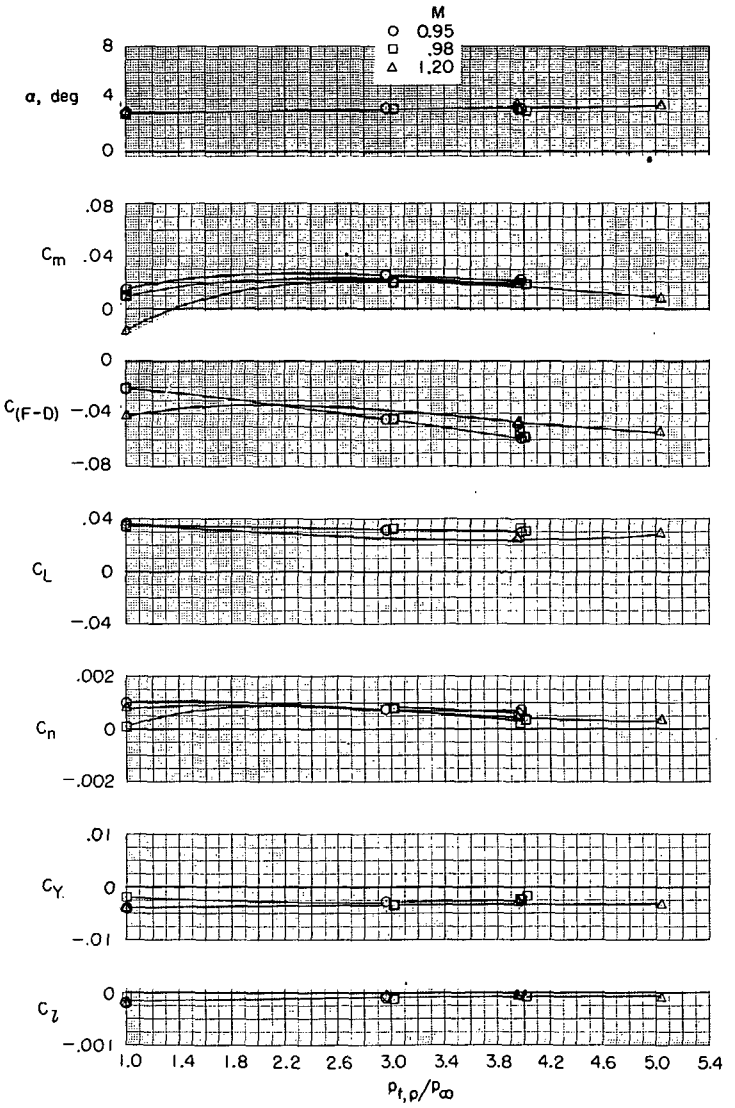

(d) M = 0.95 to 1.20.

Figure 28.- Continued.

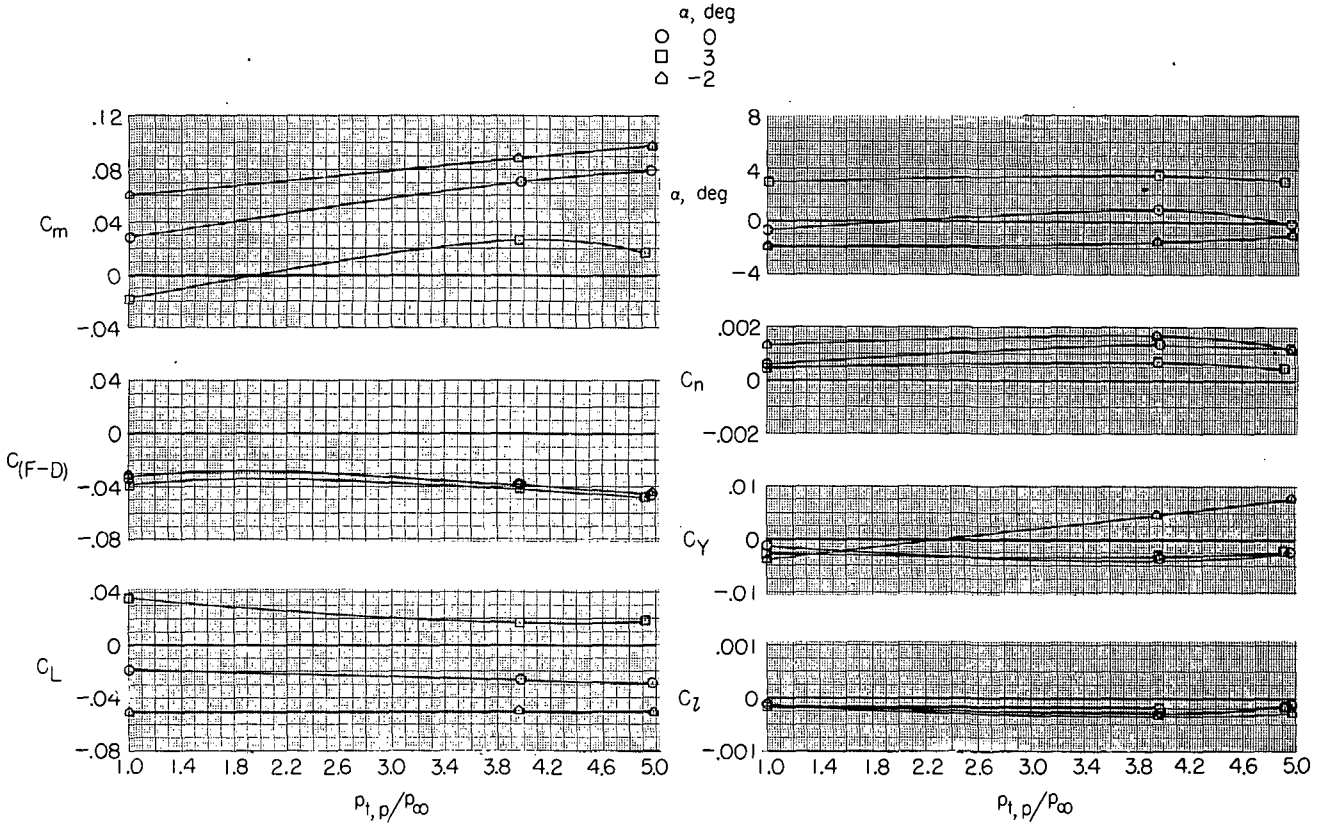

(e) M = 1.30.

Figure 28.- Concluded.

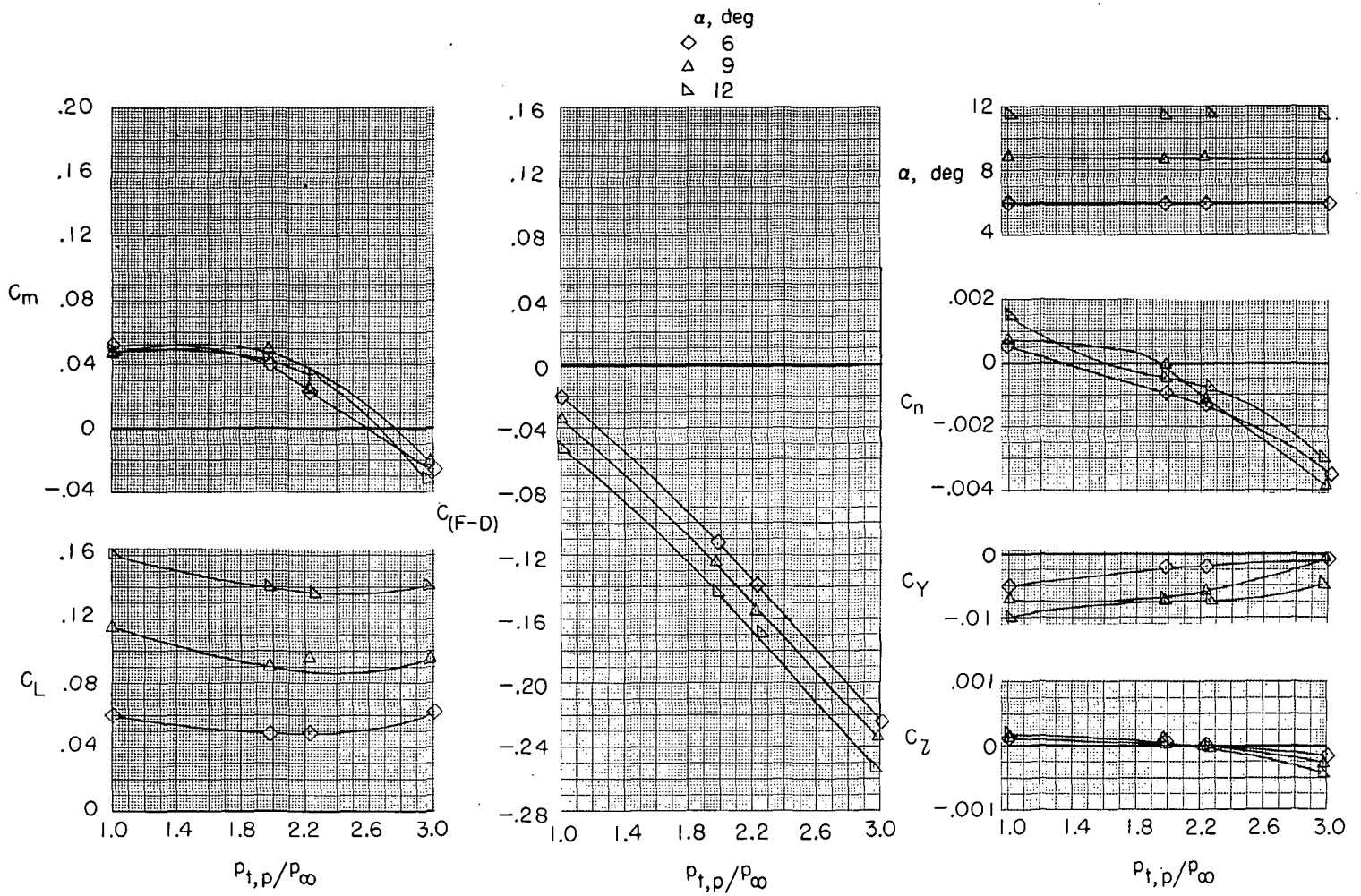

(a) $M = 0.35$; $\delta_h = -4^o$.

Figure 29.- Effect of jet-total-pressure ratio on aerodynamic characteristics of model with thrust control unit for several Mach numbers and angles of attack. $\beta = 0^o$; $\delta_f = 0^o$; $\delta_s = 0^o$; $\delta_r = 0^o$; $\delta_{du} = 32.5^o$; $\delta_{dl} = 52.5^o$; $\delta_b = 100$ percent; and military power.

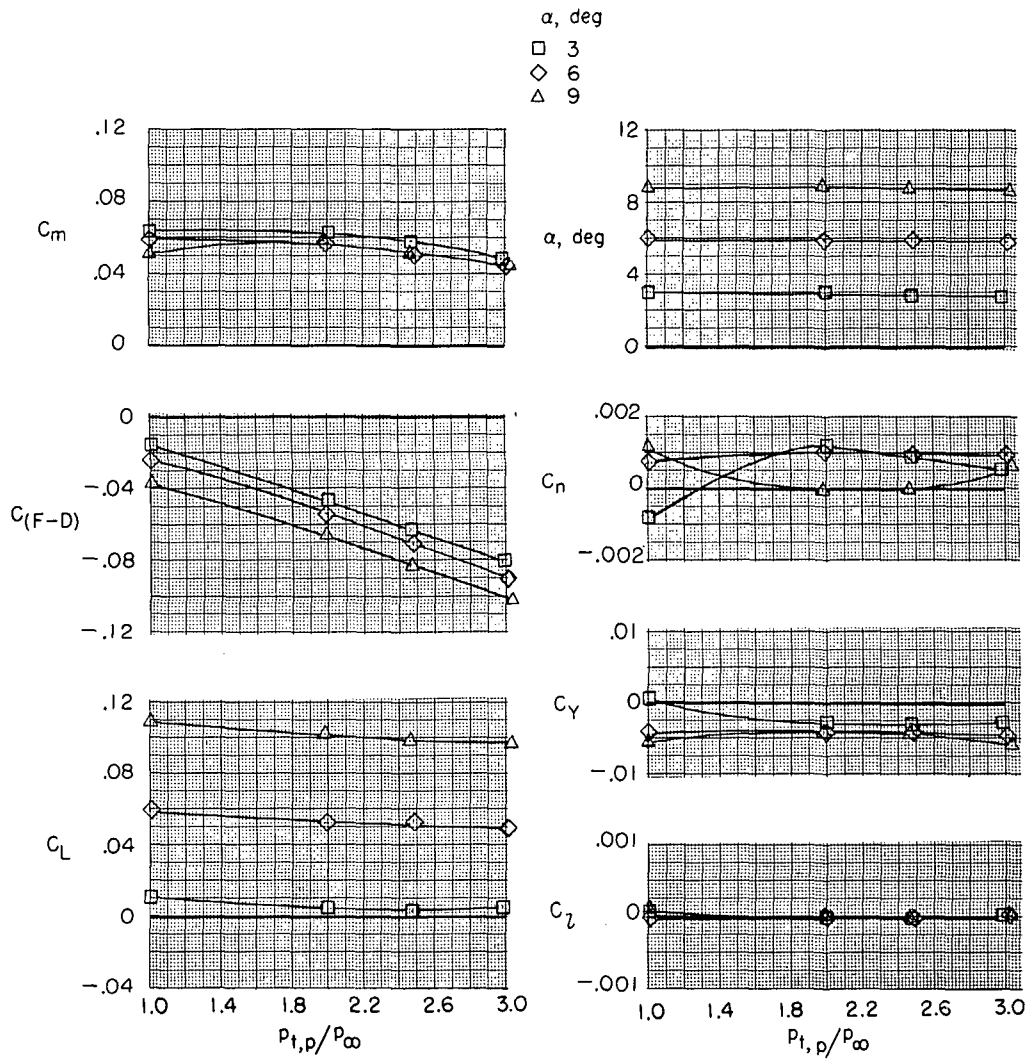

(b) $M = 0.60$; $\delta_h = -4^o$.

Figure 29.- Continued.

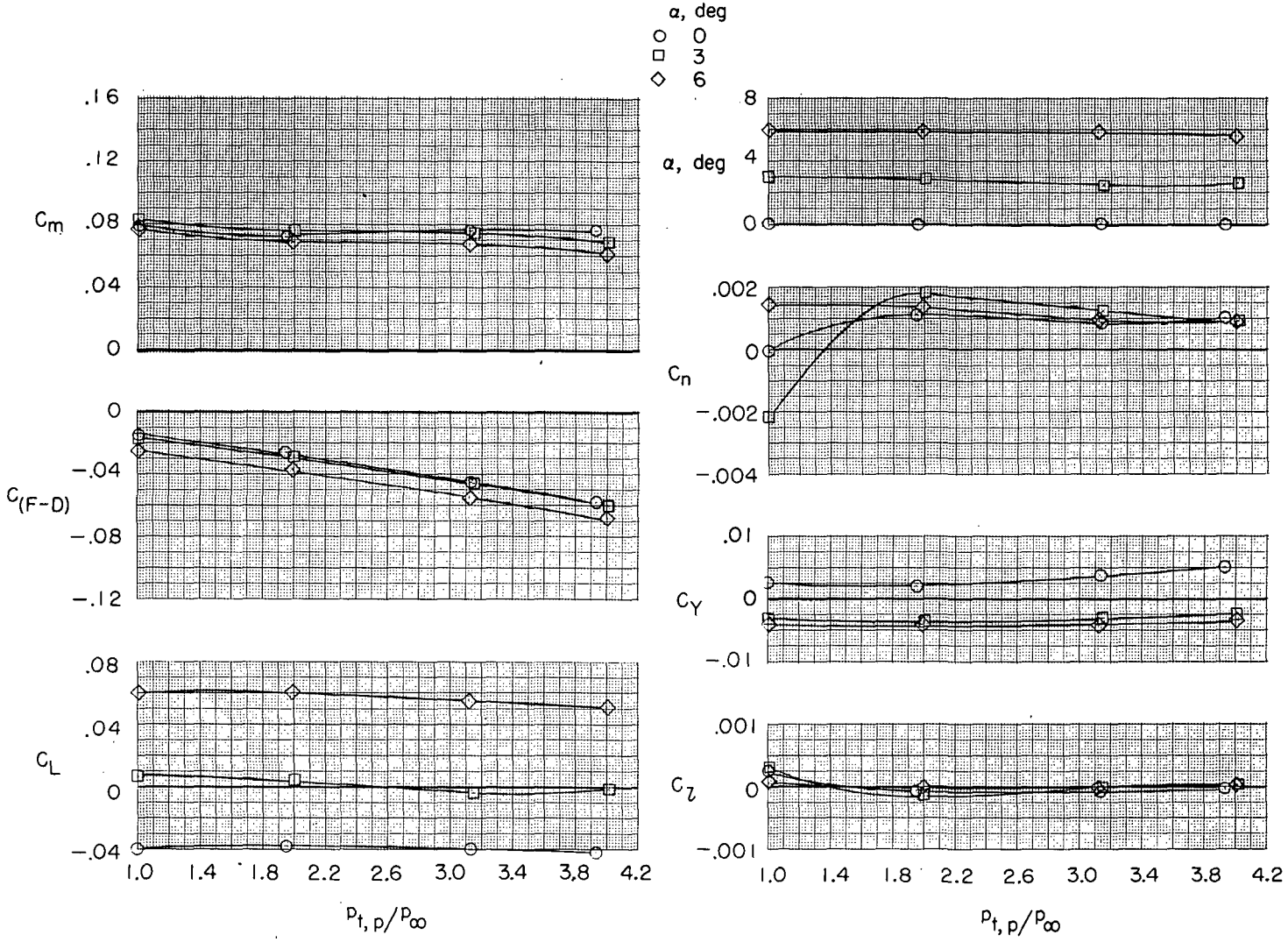

(c) M = 0.90; $\delta_{h1} = -4^o$.

Figure 29.- Continued.

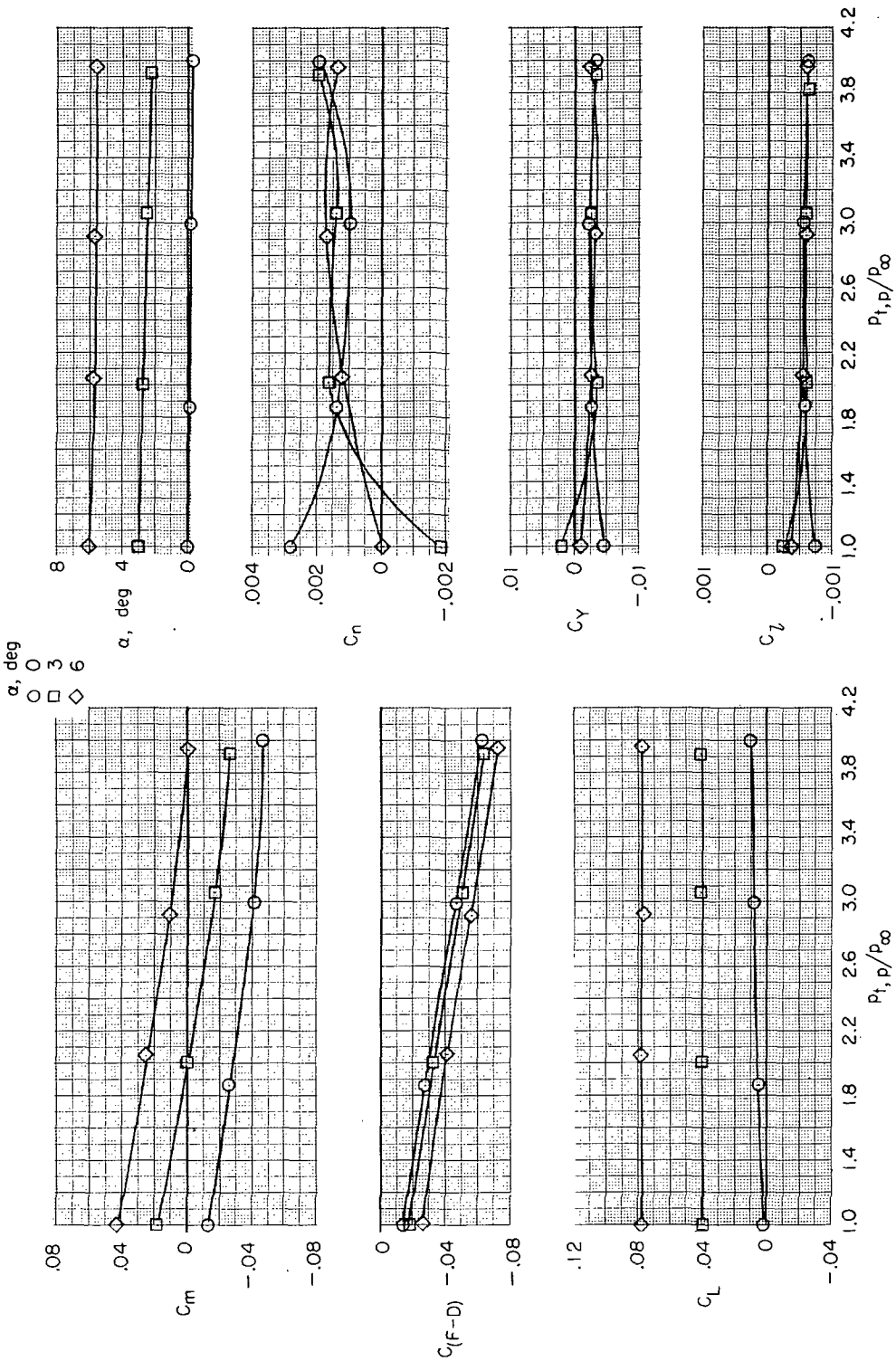

(d) M = 0.90; δ_h = Off.

Figure 29.- Concluded.

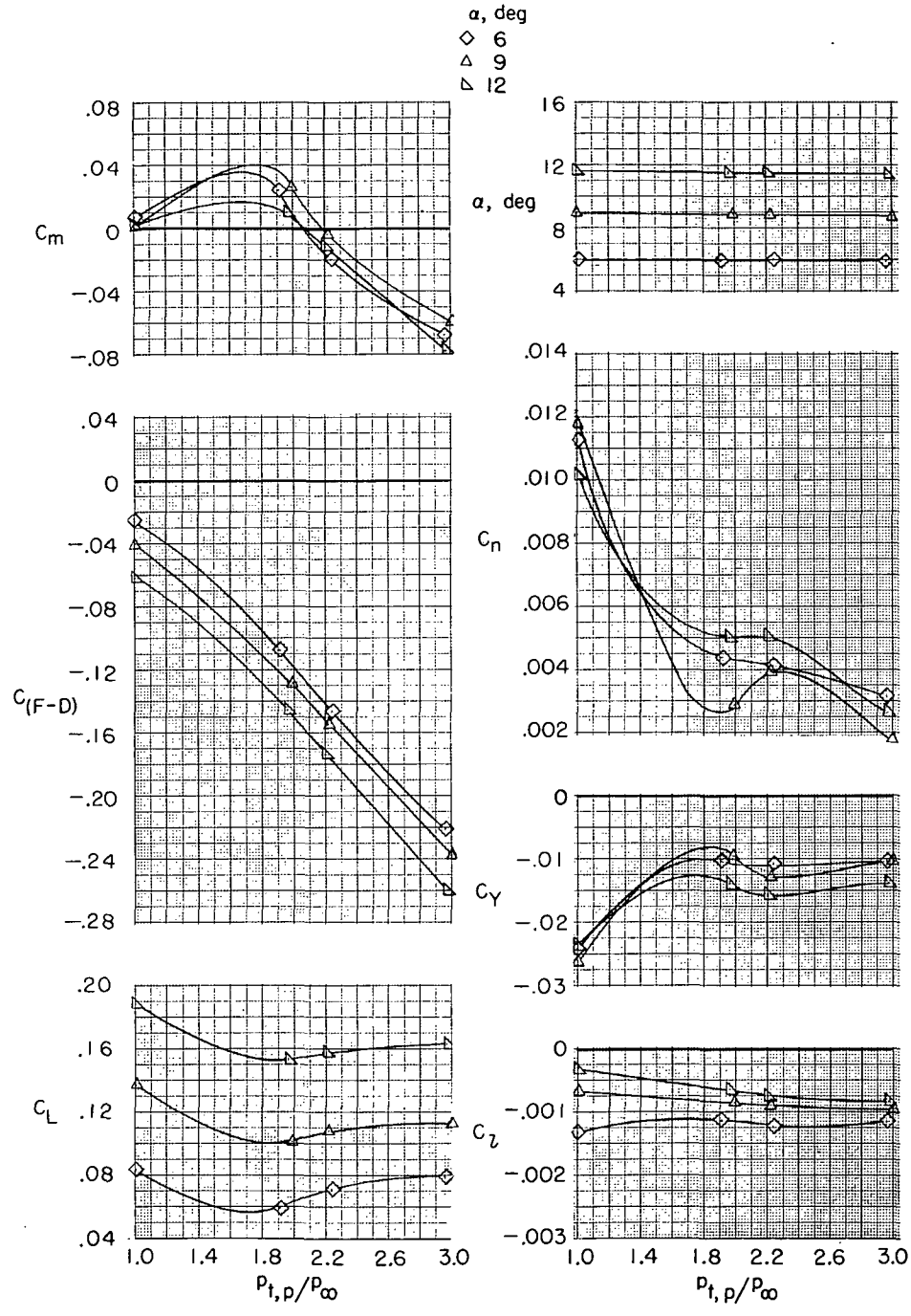

(a) M = 0.34.

Figure 30.- Effect of jet-total-pressure ratio on aerodynamic characteristics of model with thrust control unit for several angles of attack and Mach numbers. $\beta = 0^o$; $\delta_f = 0^o$; $\delta_s = 0^o$; $\delta_h = -1.5^o$; $\delta_r = -5^o$; $\delta_{du} = 32.5^o$; $\delta_{dl} = 52.5^o$; $\delta_b = 100$ percent; and military power.

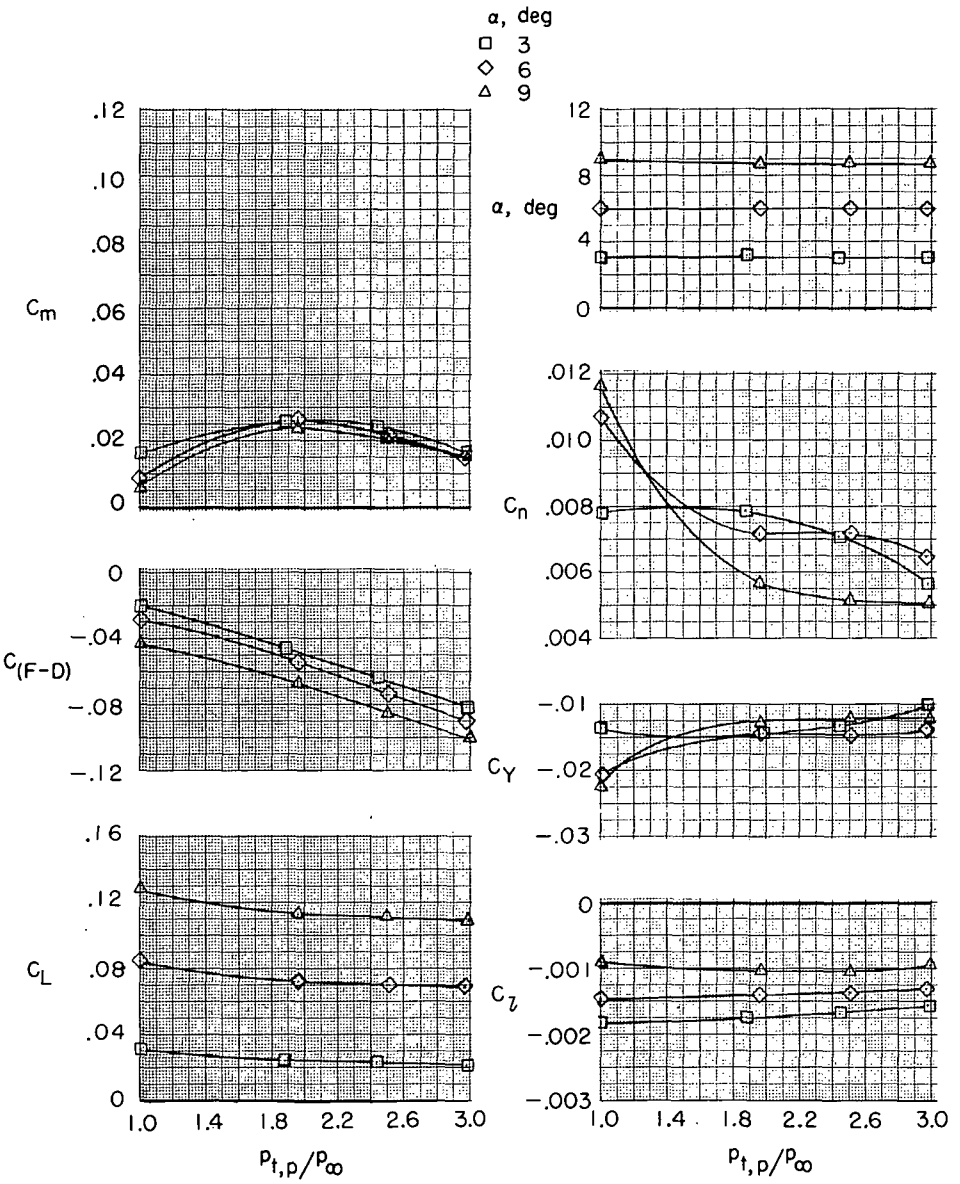

(b) M = 0.60.

Figure 30.- Continued.

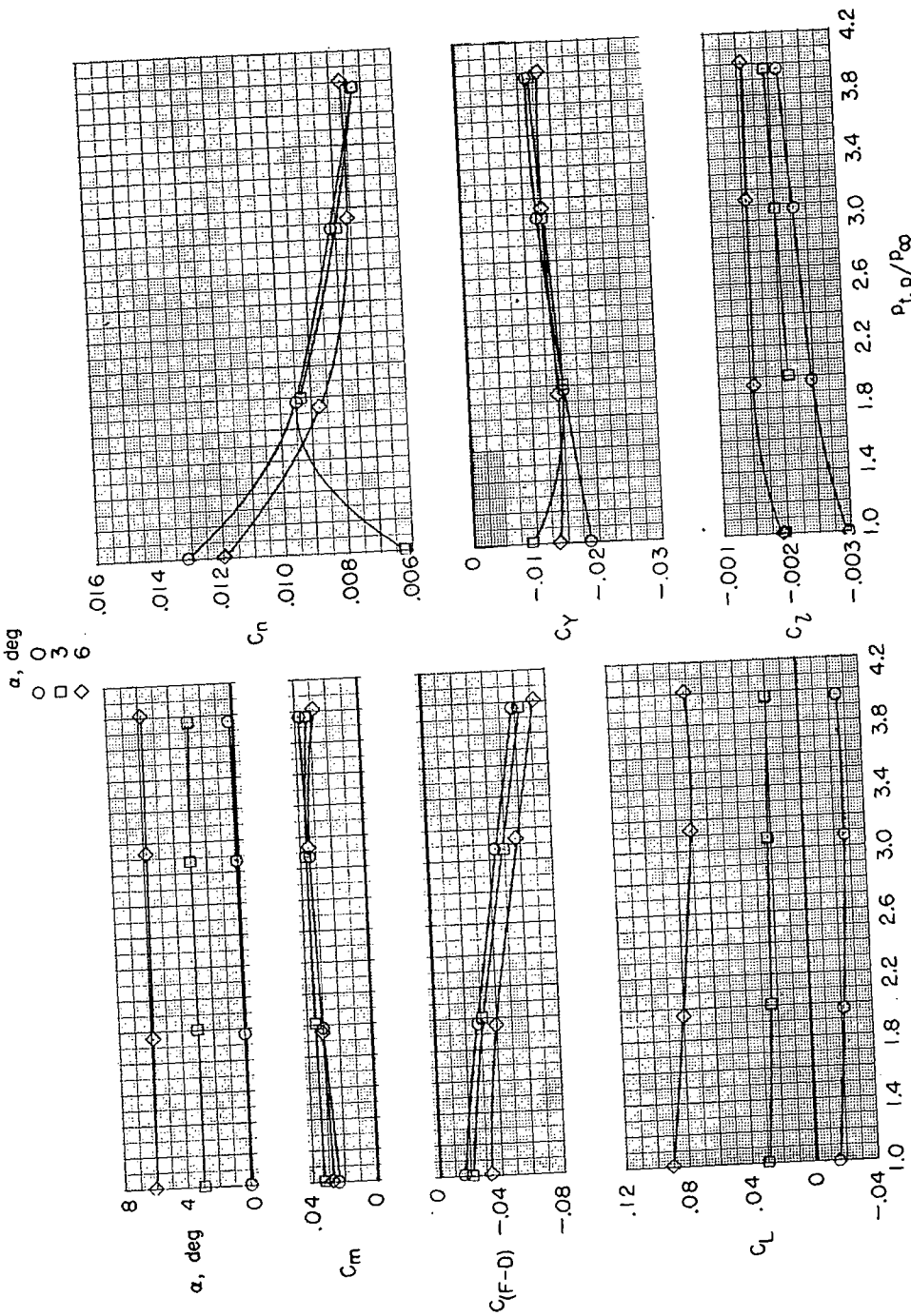

(c) M = 0.90.

Figure 30.- Continued.

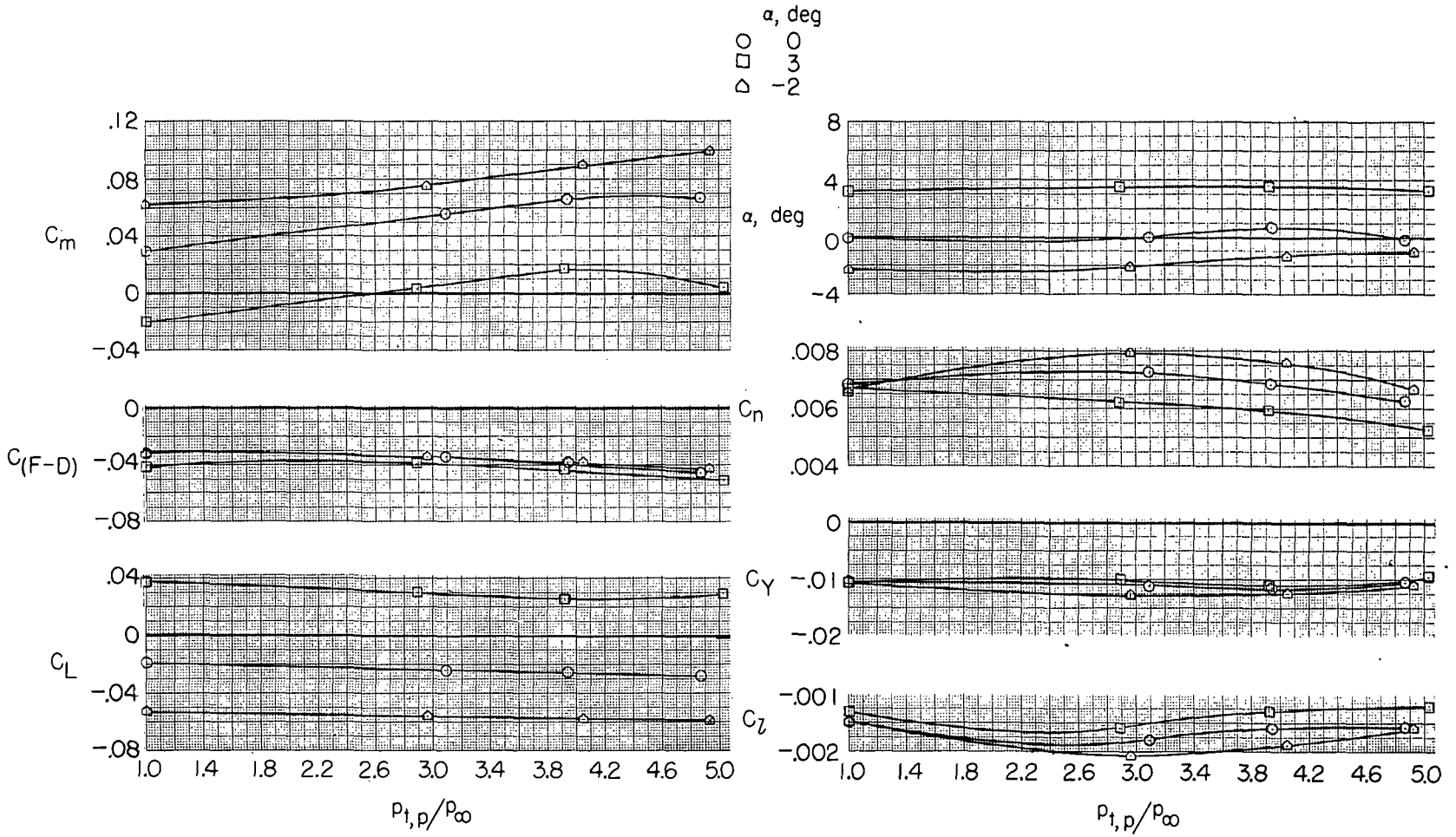

(d) M = 1.30.

Figure 30.- Concluded.

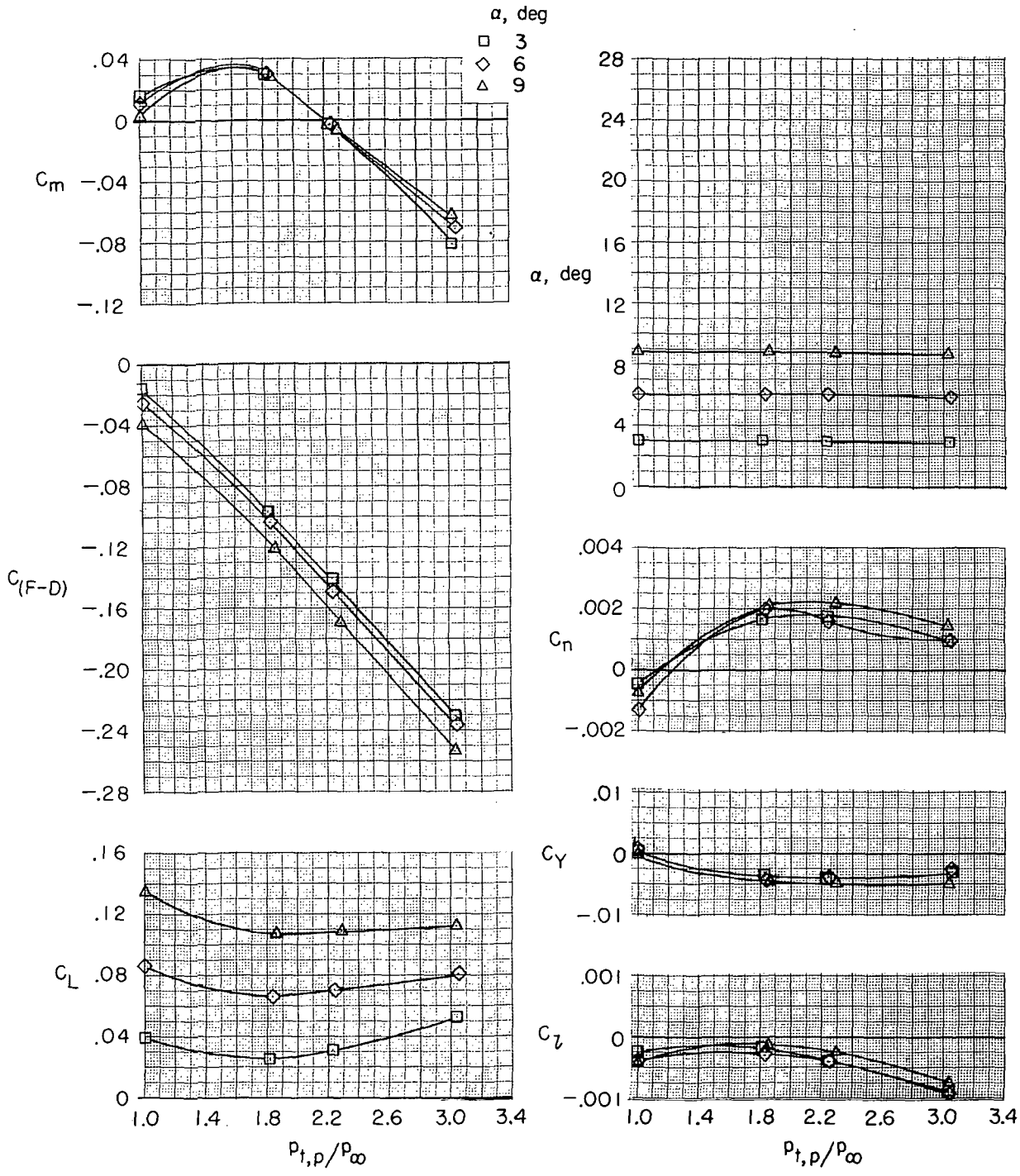

(a) M = 0.34.

Figure 31.- Effect of jet-total-pressure ratio on aerodynamic characteristics of model with thrust control unit for several angles of attack and Mach numbers. $\beta = 0^o$; $\delta_f = 0^o$; $\delta_s = 0^o$; $\delta_h = -1.5^o$; $\delta_r = 0^o$; $\delta_{du} = 32.5^o$ with side plates; $\delta_{dl} = 52.5^o$; $\delta_b = 100$ percent; and military power.

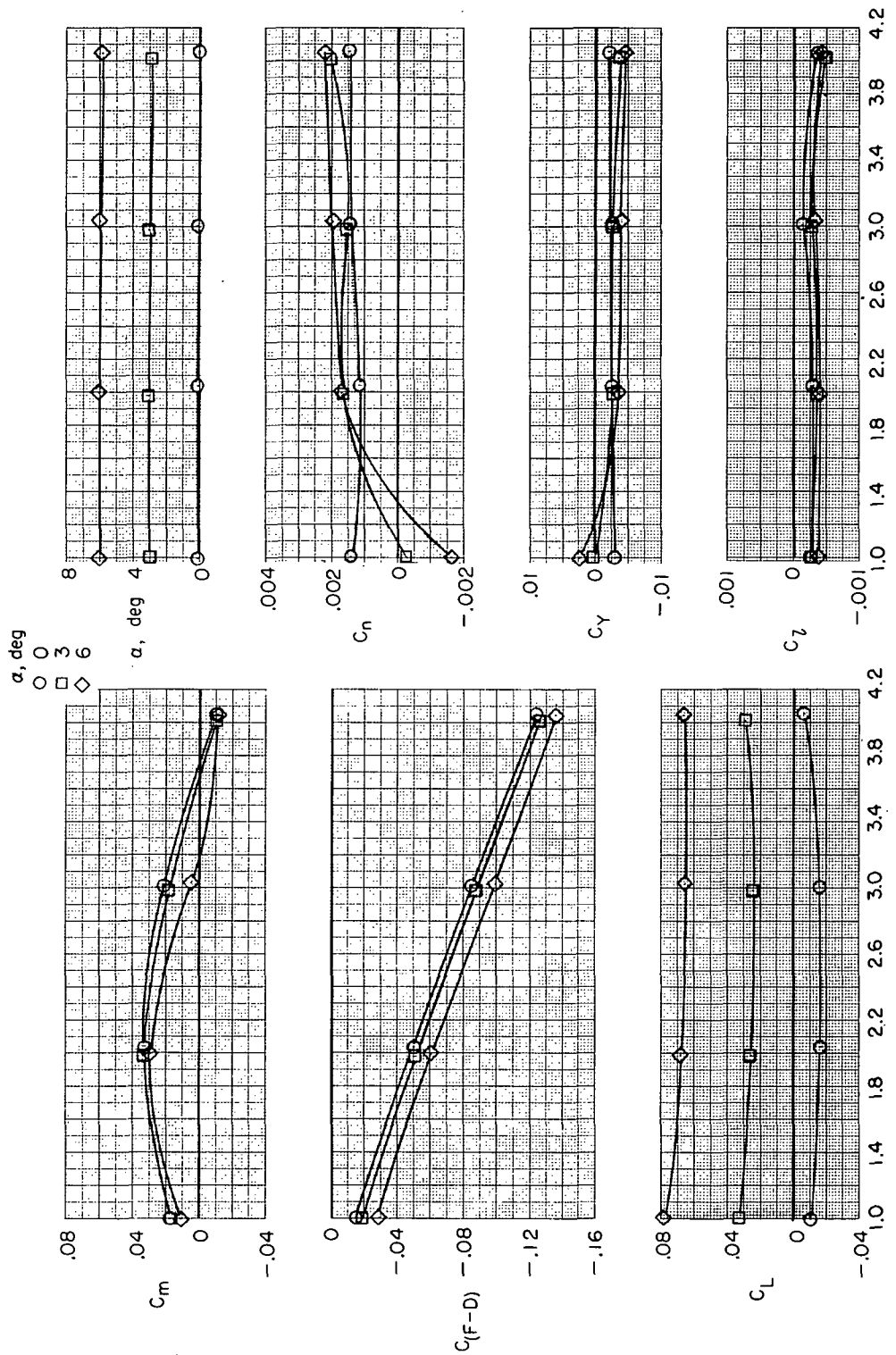

(b) M = 0.60.

Figure 31.- Continued.

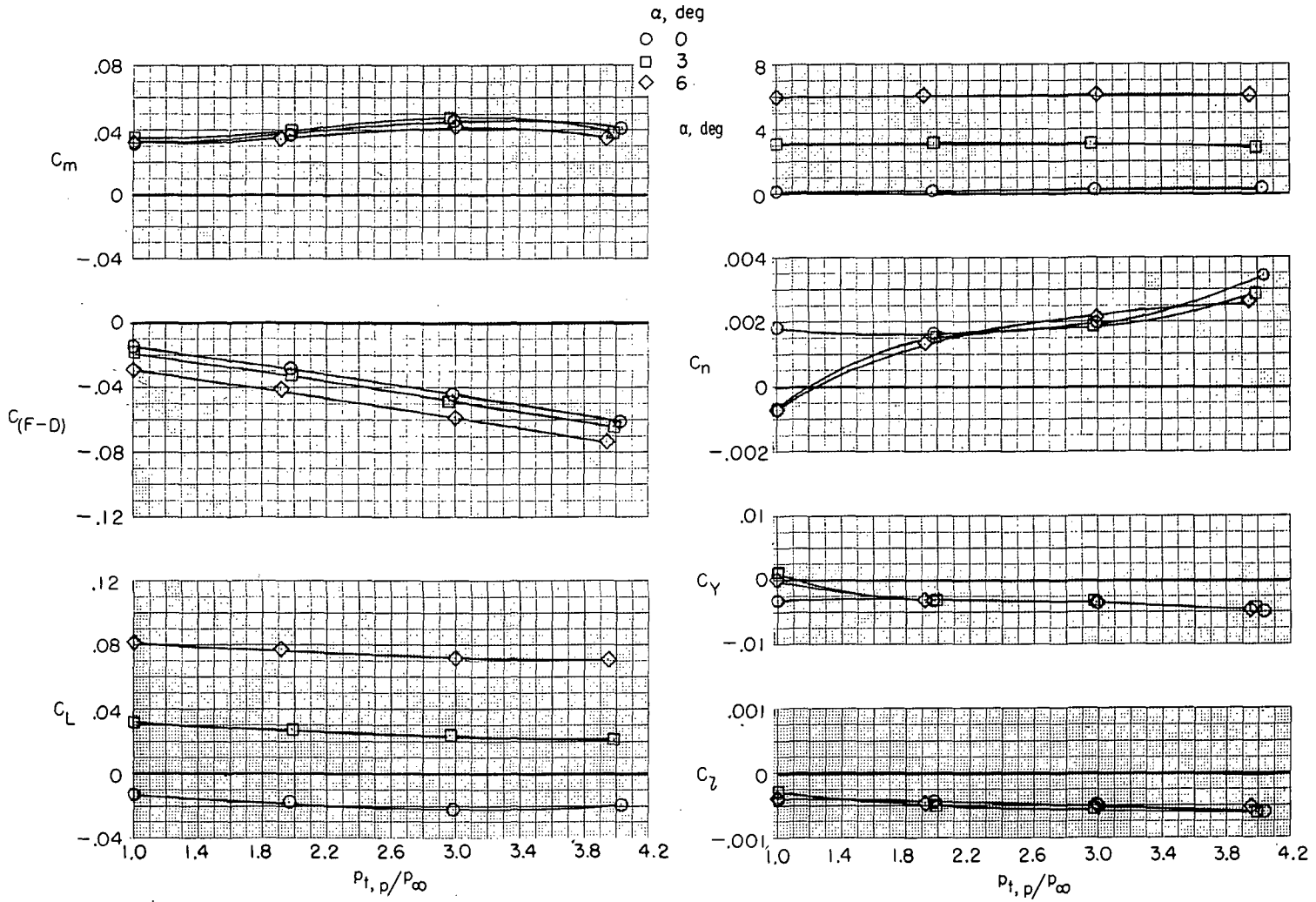

(c) M = 0.90.

Figure 31.- Concluded.

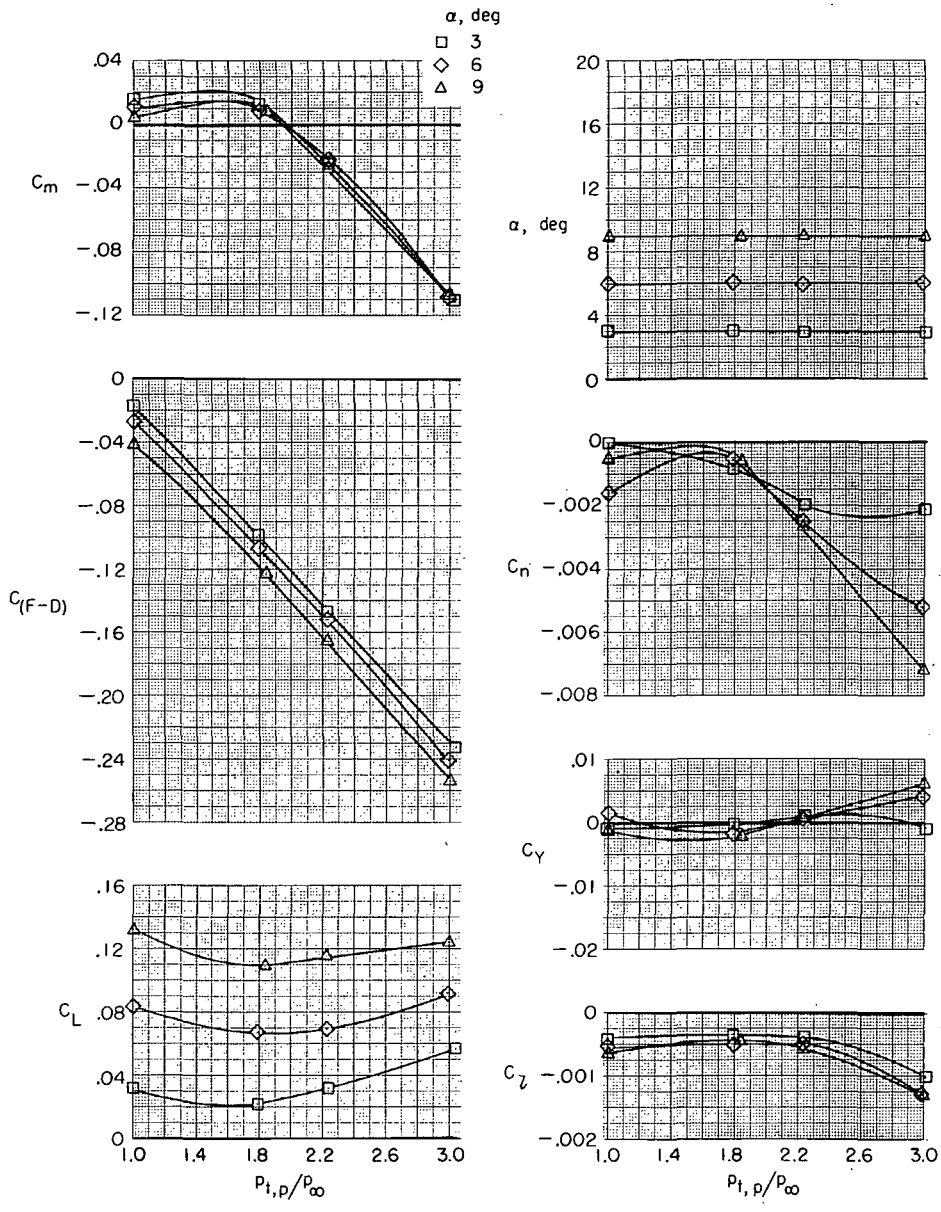

(a) M = 0.34.

Figure 32.- Effect of jet-total-pressure ratio on aerodynamic characteristics of model with thrust control unit for several angles of attack and Mach numbers. $\beta = 0^o$; $\delta_f = 0^o$; $\delta_s = 0^o$; $\delta_h = -1.5^o$; $\delta_r = 0^o$; $\delta_{du} = 32.5^o$; $\delta_{dl} = 52.5^o$; $\delta_b = 100$ percent; A_u decreased 14 percent; and military power.

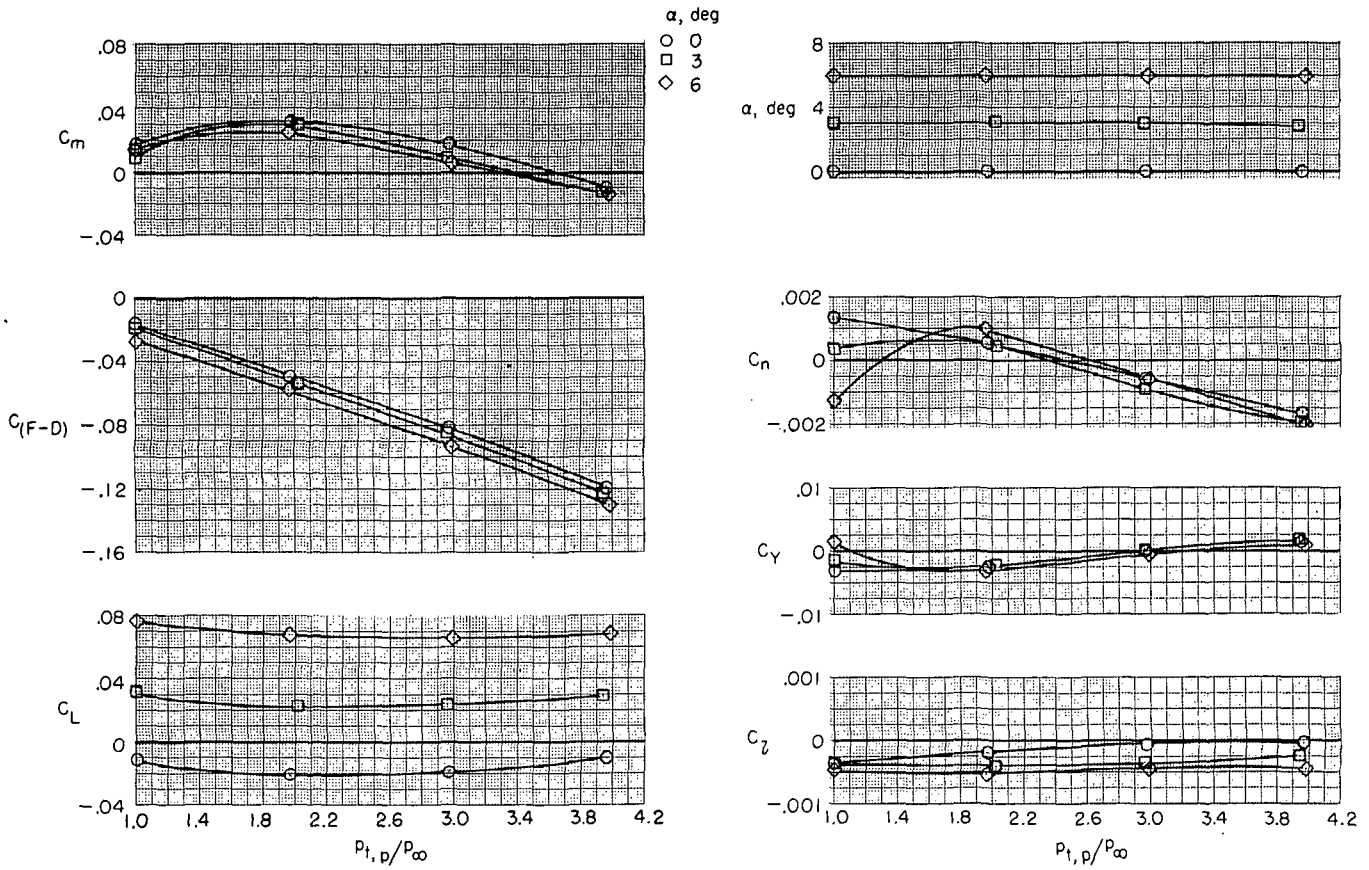

(b) M = 0.60.

Figure 32.- Continued.

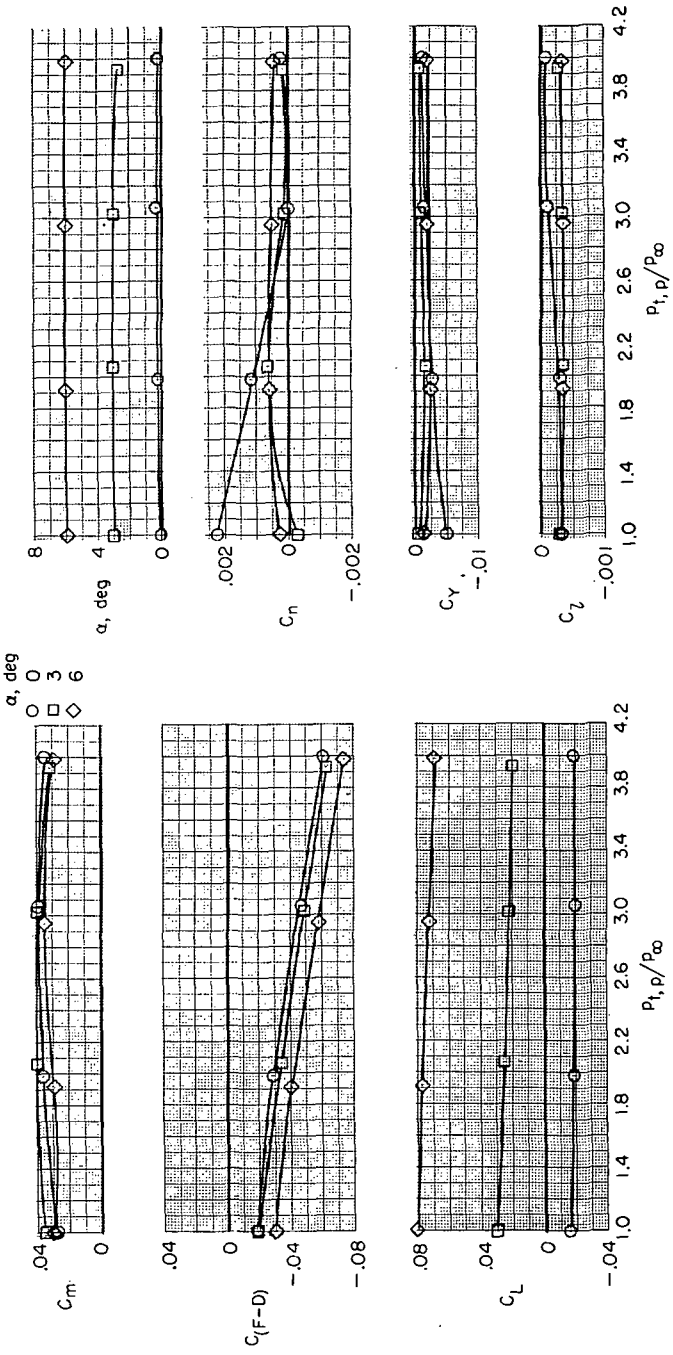

(c) M = 0.90.

Figure 32.- Continued.

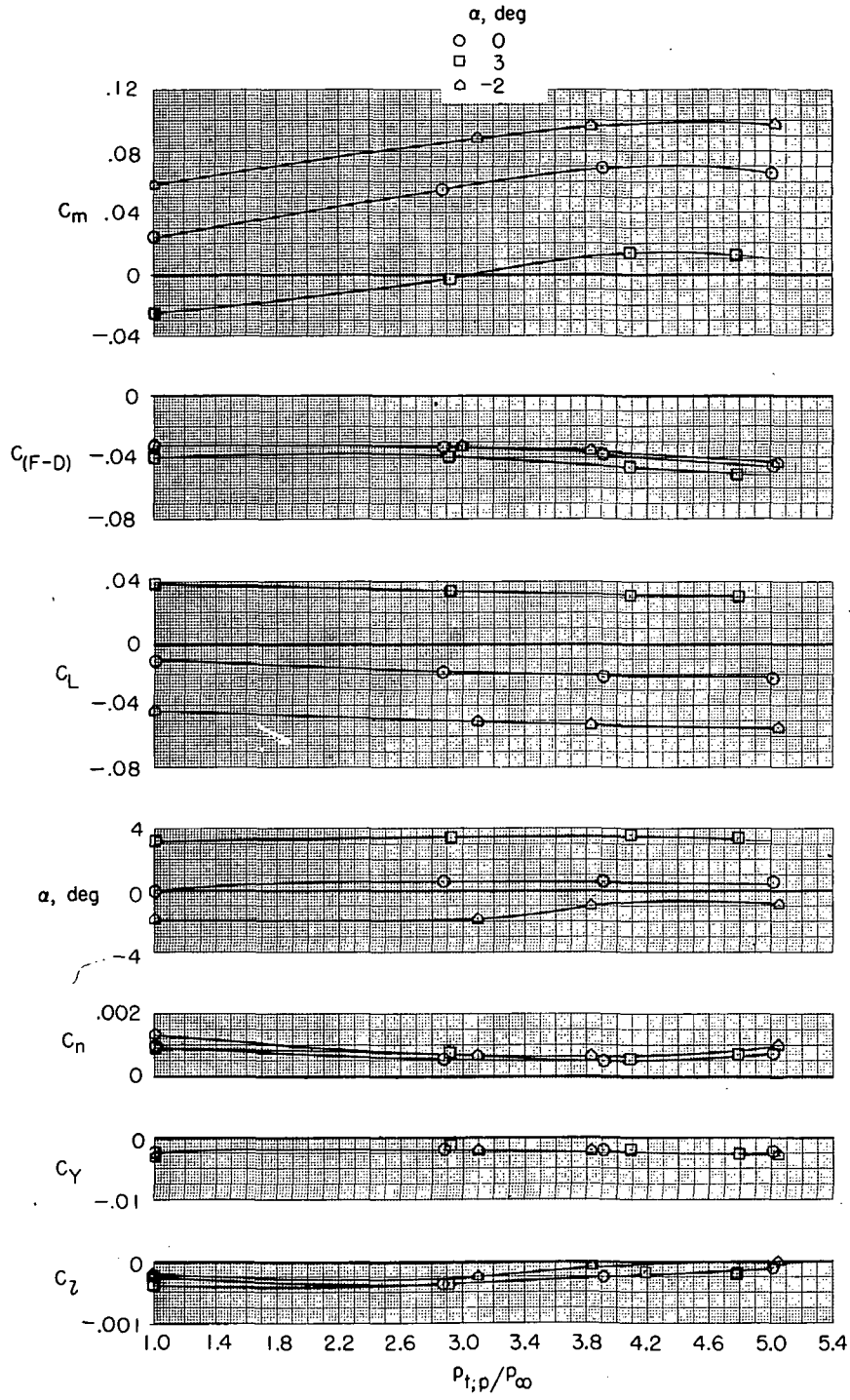

(d) M = 1.30.

Figure 32.- Concluded.

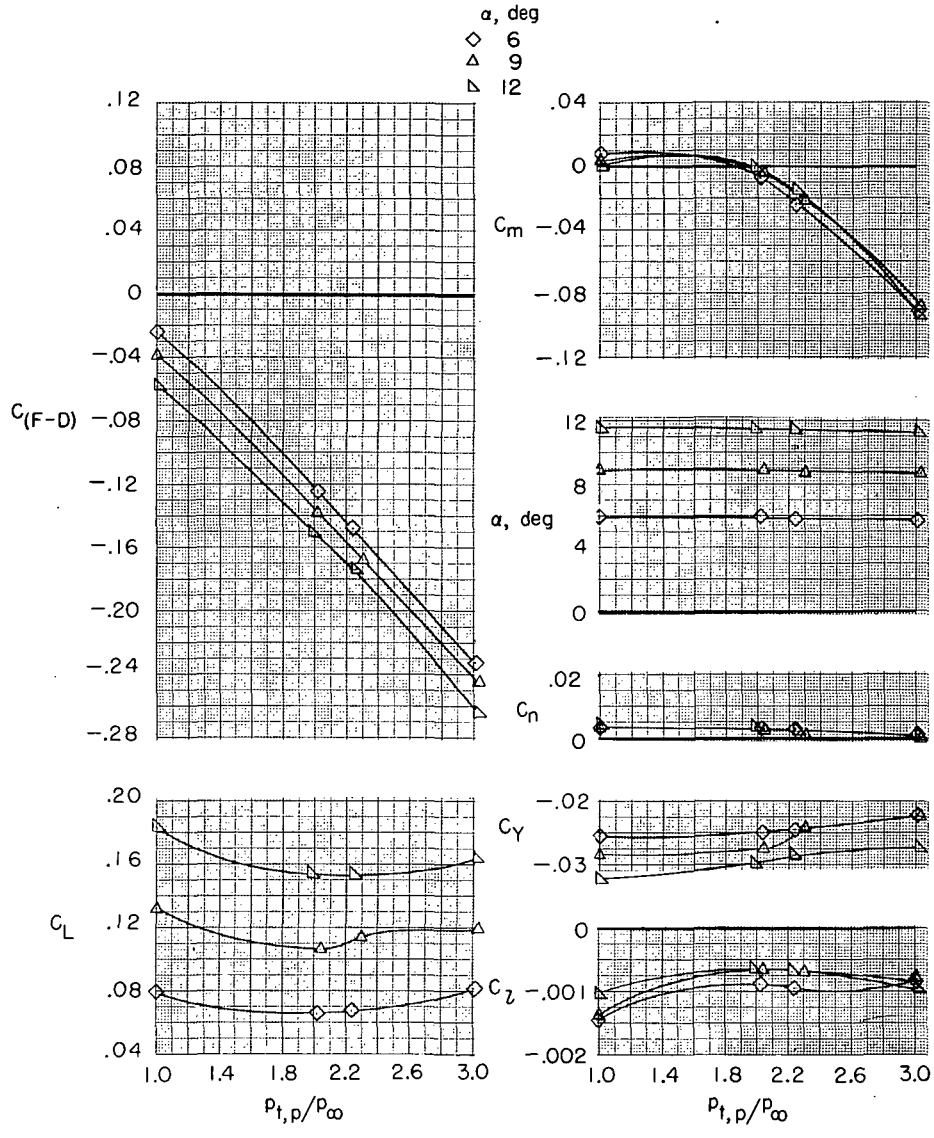

(a) M = 0.34.

Figure 33.- Effect of jet-total-pressure ratio on aerodynamic characteristics of model with thrust control unit for several angles of attack and Mach numbers. $\beta = 2^o$; $\delta_f = 0^o$; $\delta_s = 0^o$; $\delta_h = -1.5^o$; $\delta_r = 0^o$; $\delta_{du} = 32.5^o$; $\delta_{dl} = 52.5^o$; $\delta_b = 100$ percent; and military power.

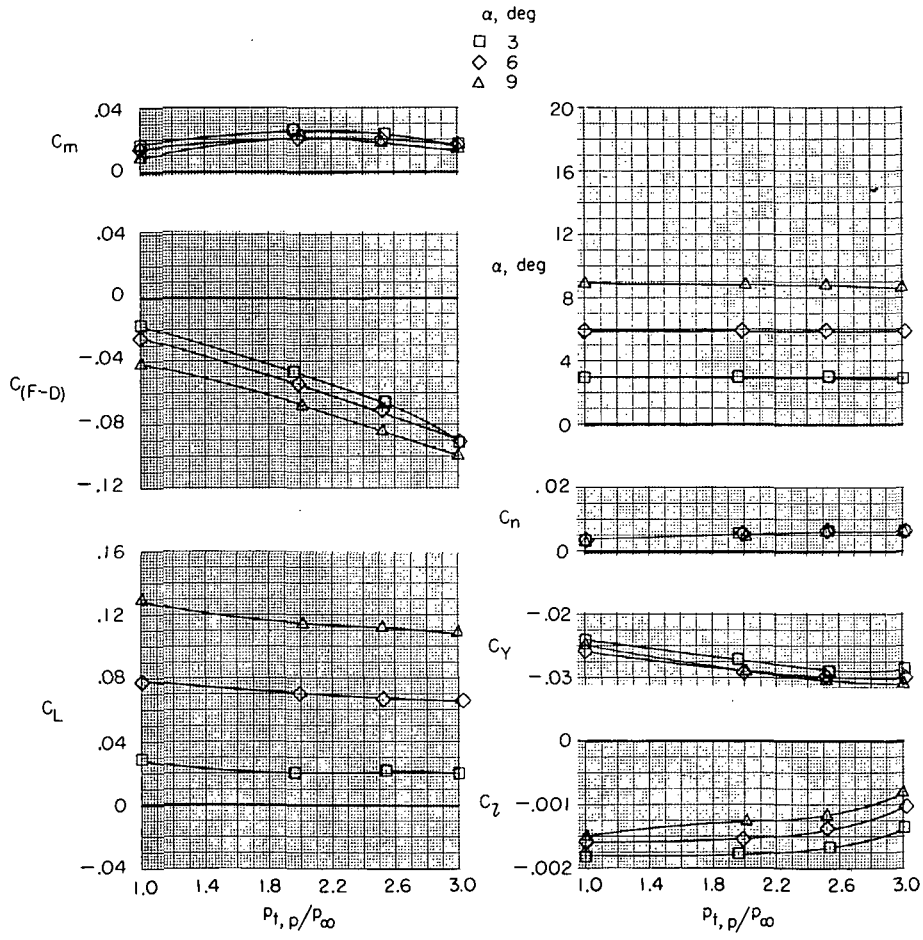

(b) M = 0.60.

Figure 33.- Continued.

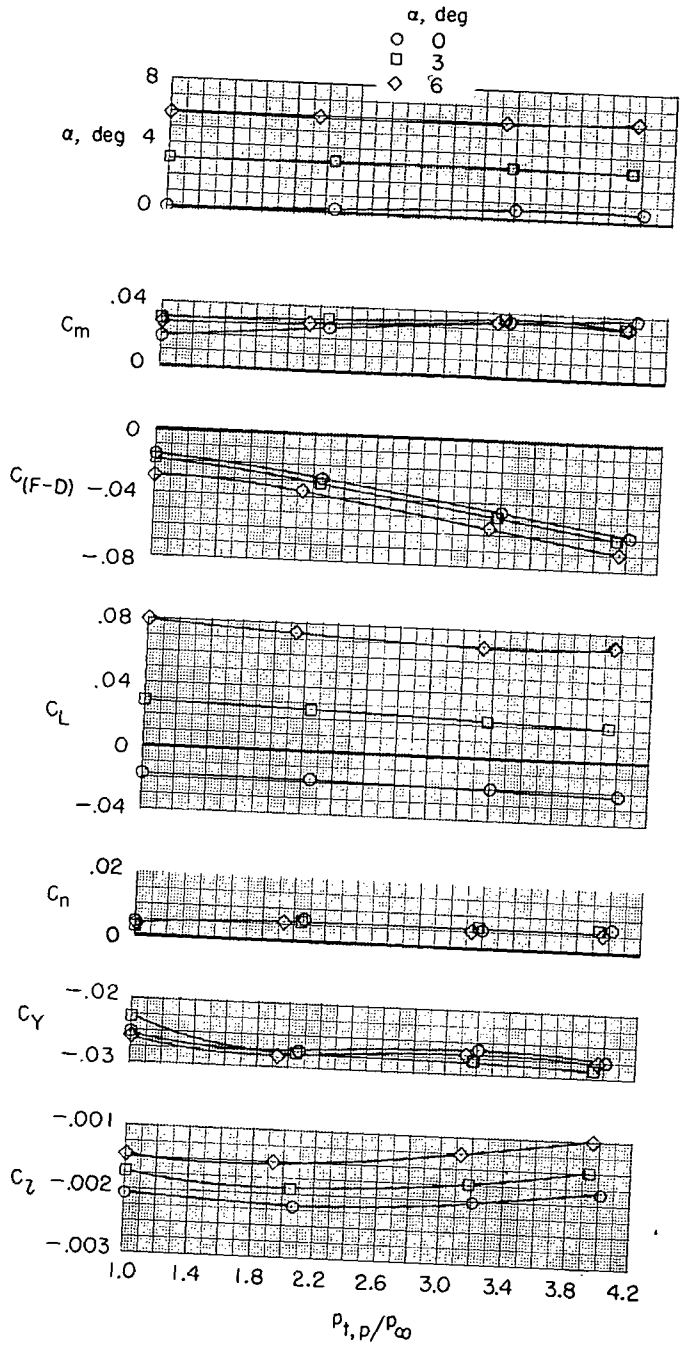

(c) M = 0.90.

Figure 33.- Continued.

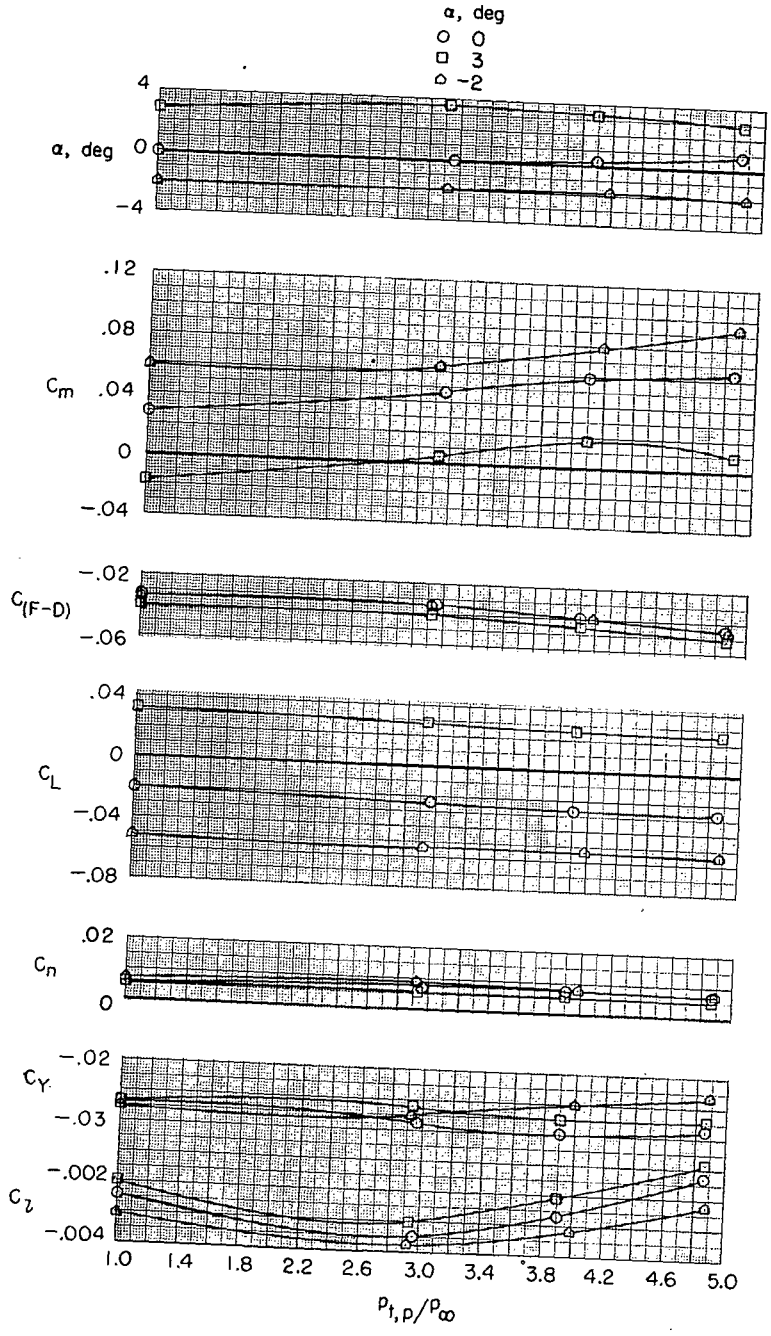

(d) M = 1.30.

Figure 33.- Concluded.

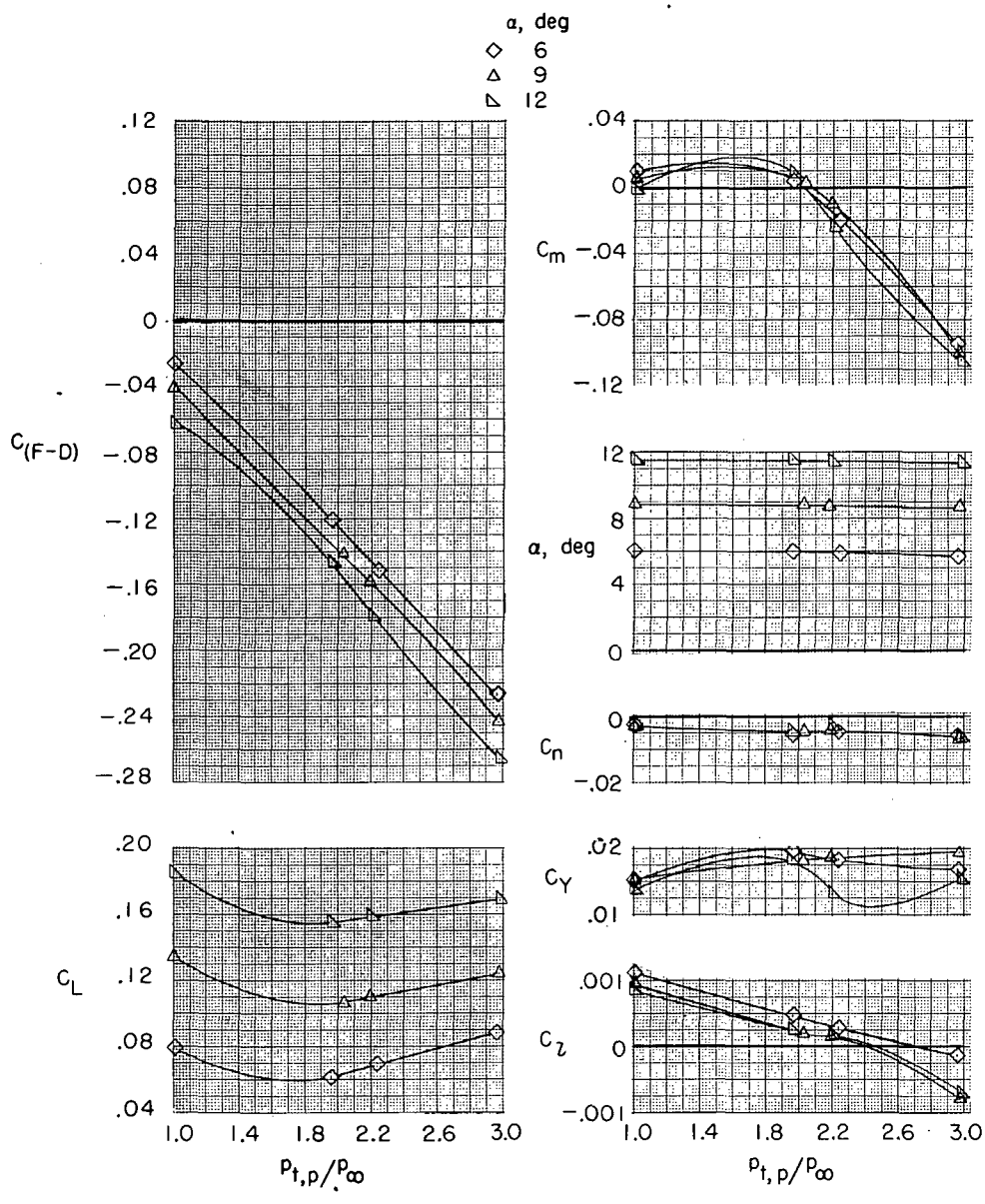

(a) $M = 0.34$.

Figure 34.- Effect of jet-total-pressure ratio on aerodynamic characteristics of model with thrust control unit for several angles of attack and Mach numbers. $\beta = -2^{o}$; $\delta_f = 0^{o}$; $\delta_s = 0^{o}$; $\delta_h = -1.5^{o}$; $\delta_r = 0^{o}$; $\delta_{du} = 32.5^{o}$; $\delta_{dl} = 52.5^{o}$; $\delta_b = 100$ percent; and military power.

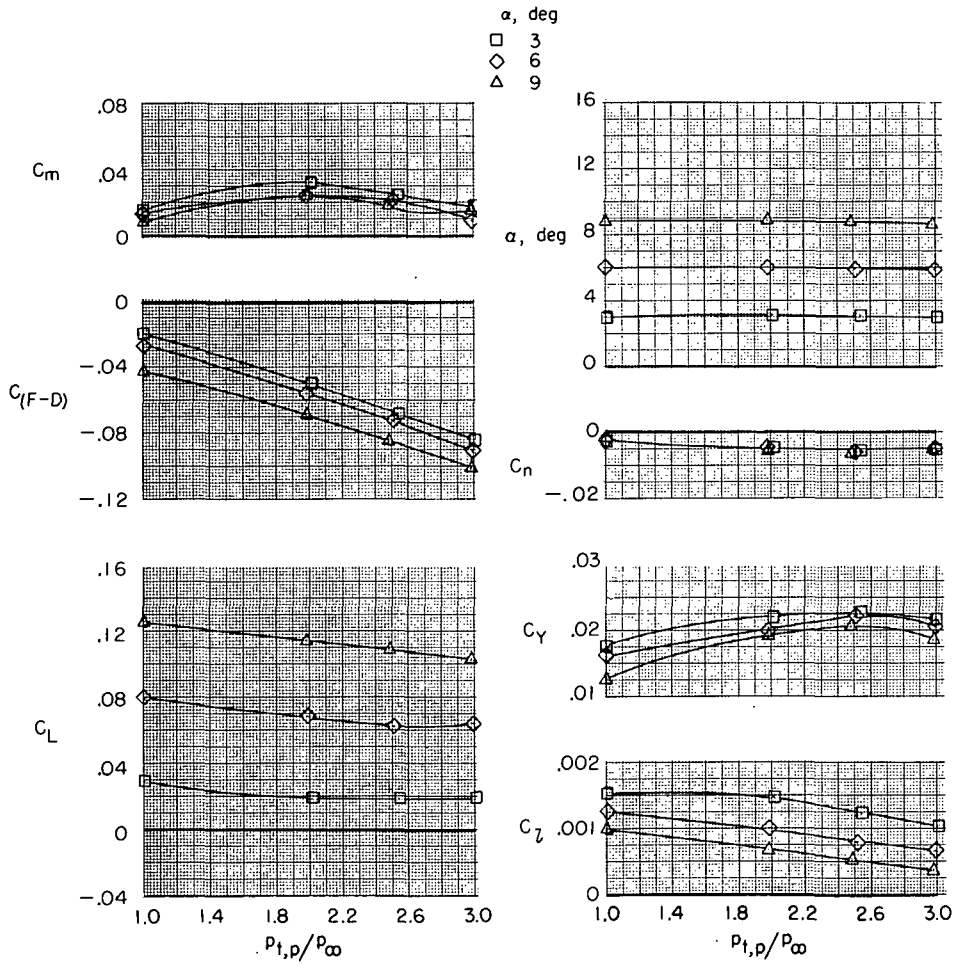

(b) M = 0.60.

Figure 34.- Continued.

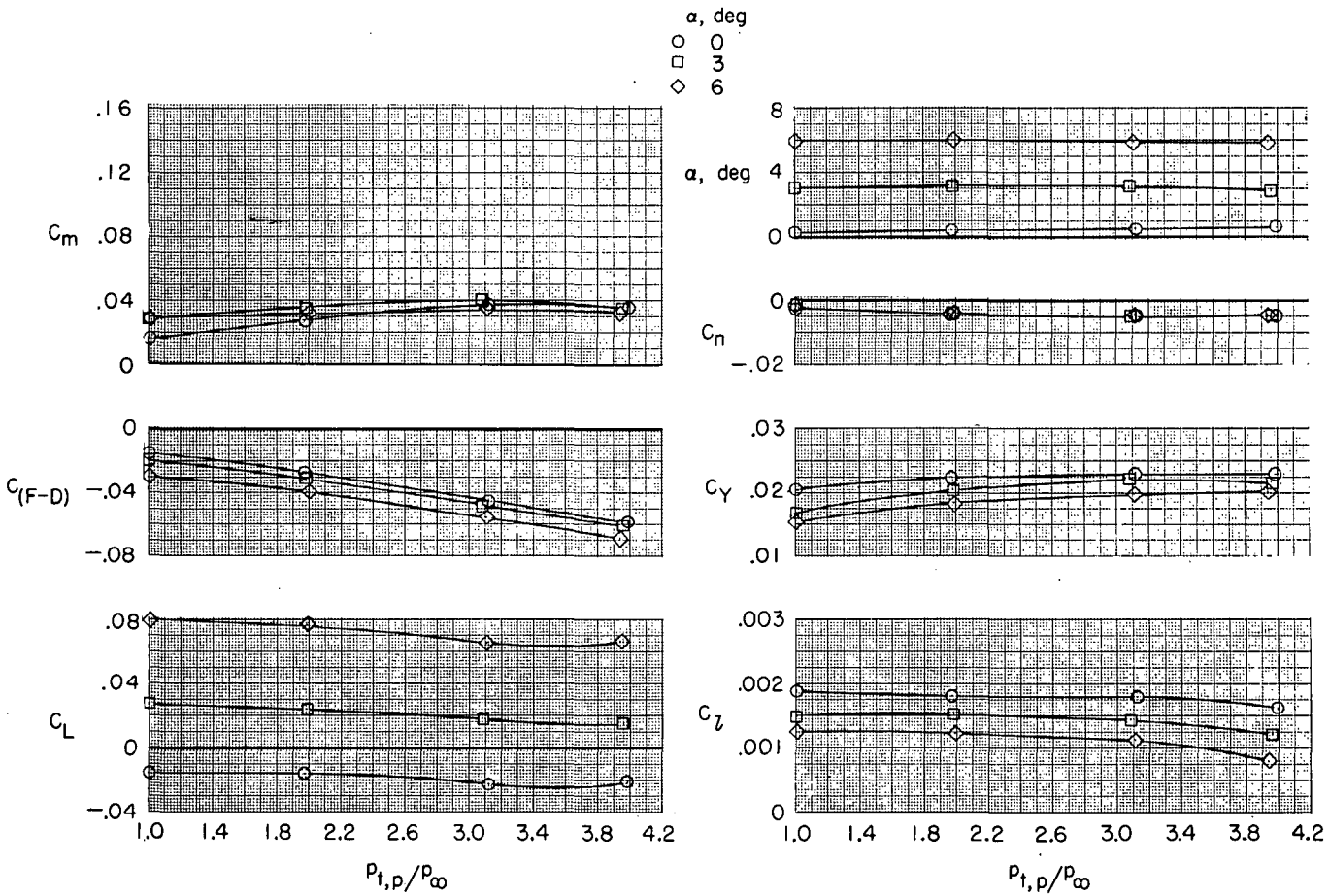

(c) M = 0.90.

Figure 34.- Continued.

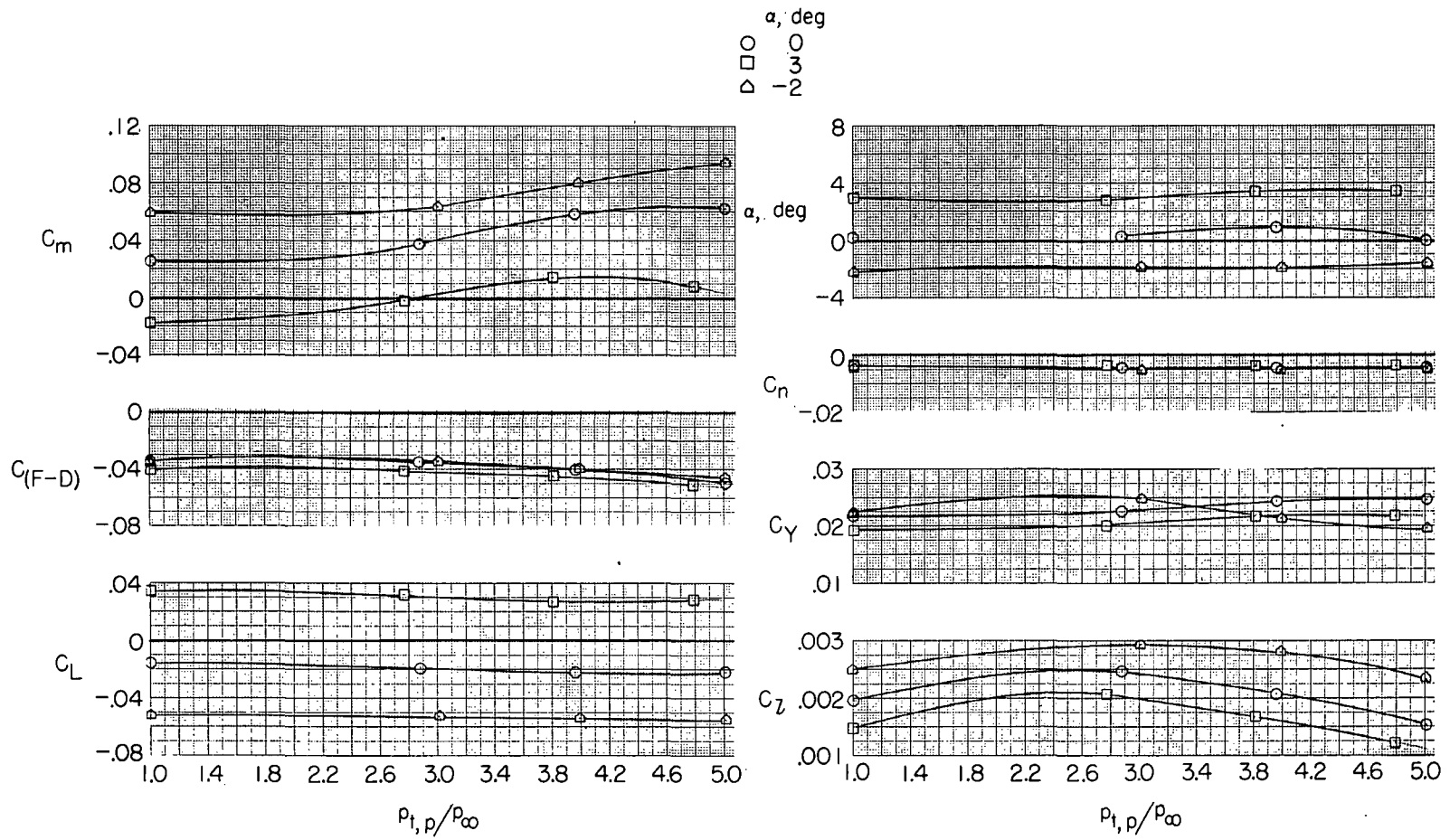

(d) M = 1.30.

Figure 34.- Concluded.

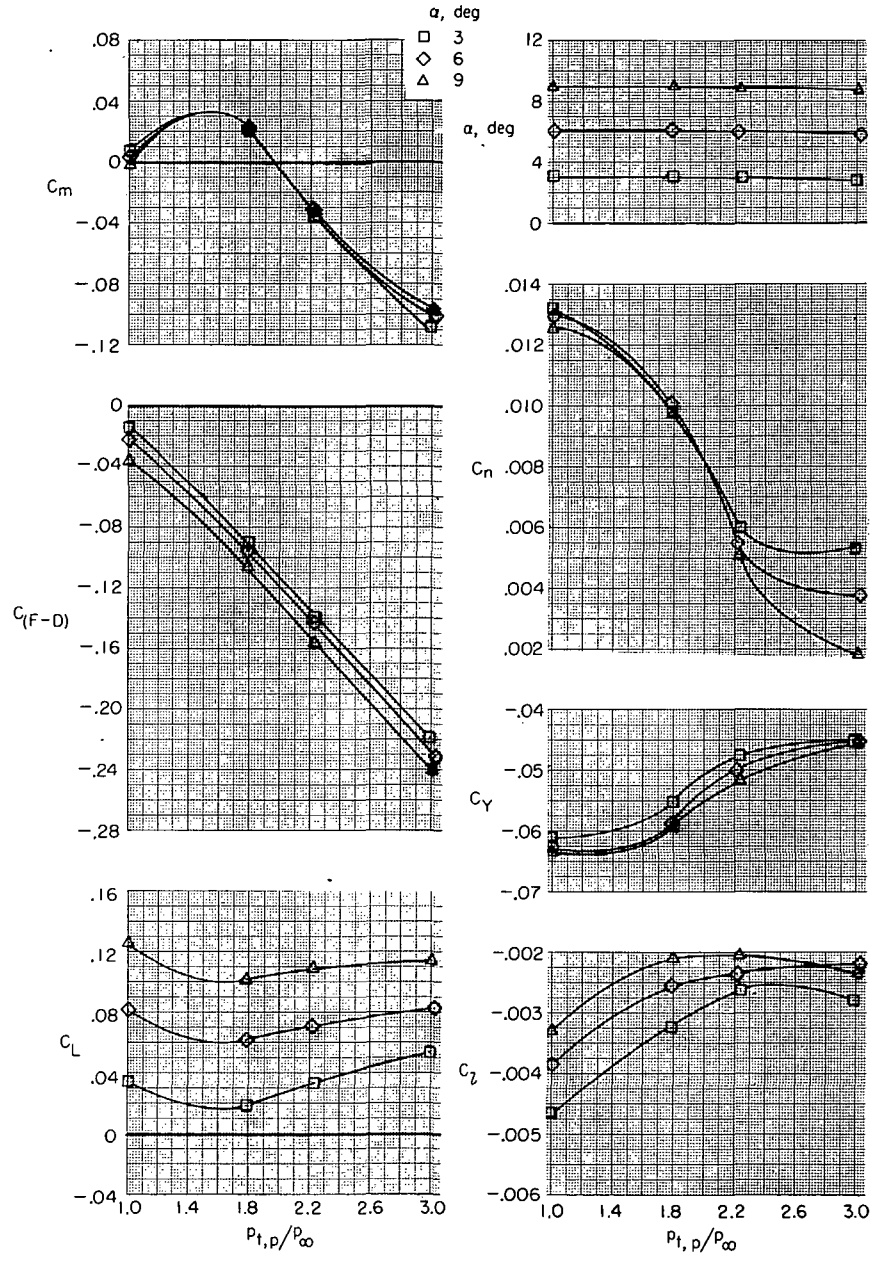

(a) M = 0.34.

Figure 35.- Effect of jet-total-pressure ratio on aerodynamic characteristics of model with thrust control unit for several angles of attack and Mach numbers. $\beta = 5^o$; $\delta_f = 0^o$; $\delta_s = 0^o$; $\delta_h = -1.5^o$; $\delta_r = 0^o$; $\delta_{du} = 32.5^o$; $\delta_{dl} = 52.5^o$; $\delta_b = 100$ percent; and military power.

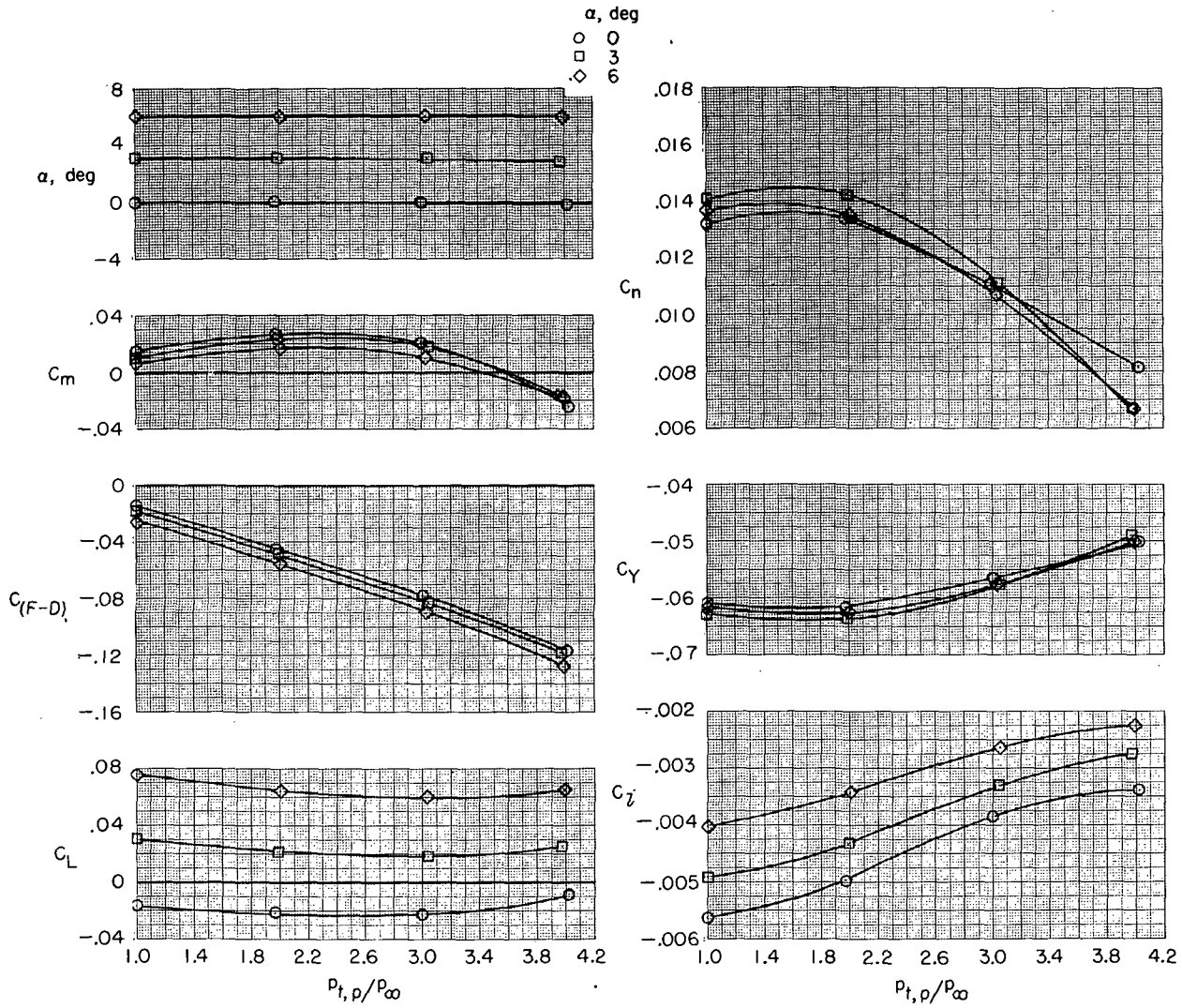

(b) M = 0.60.

Figure 35.- Continued.

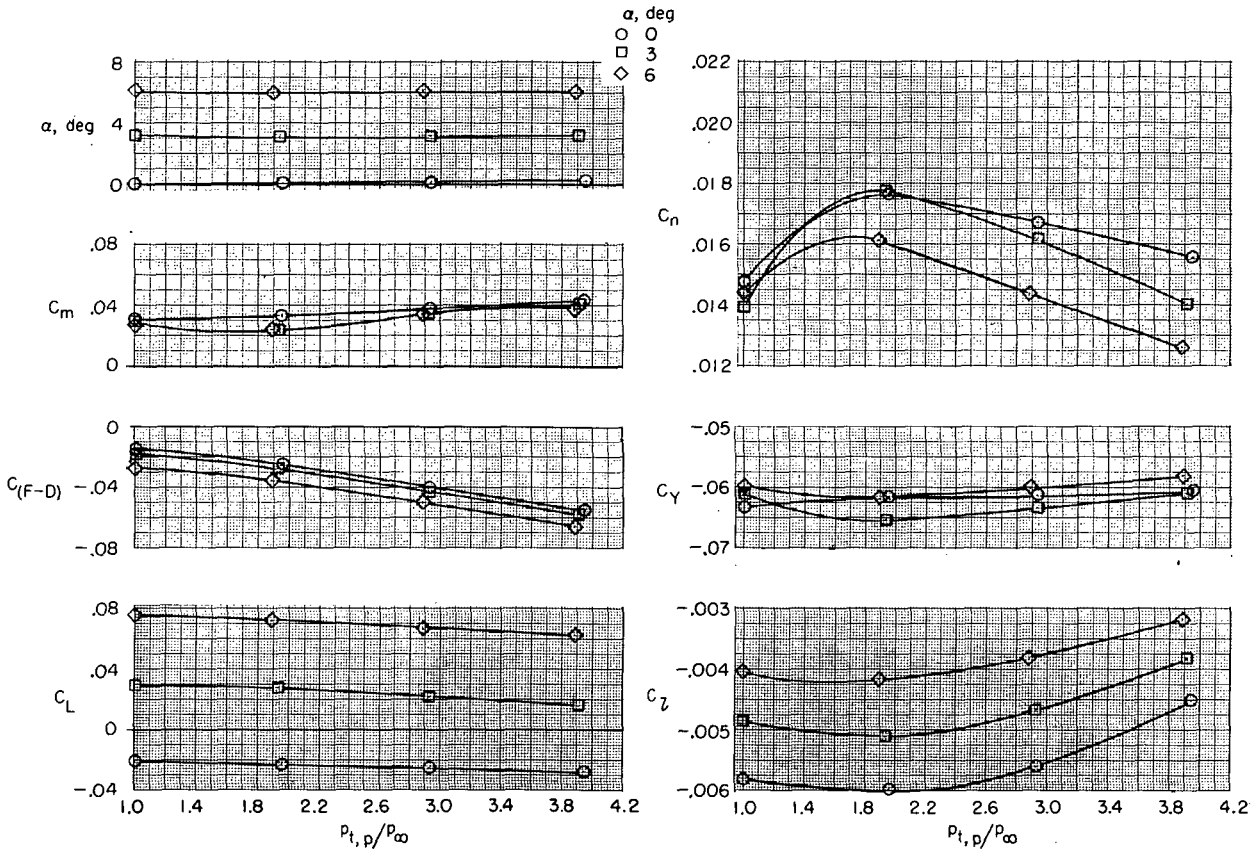

(c) M = 0.90.

Figure 35.- Concluded.

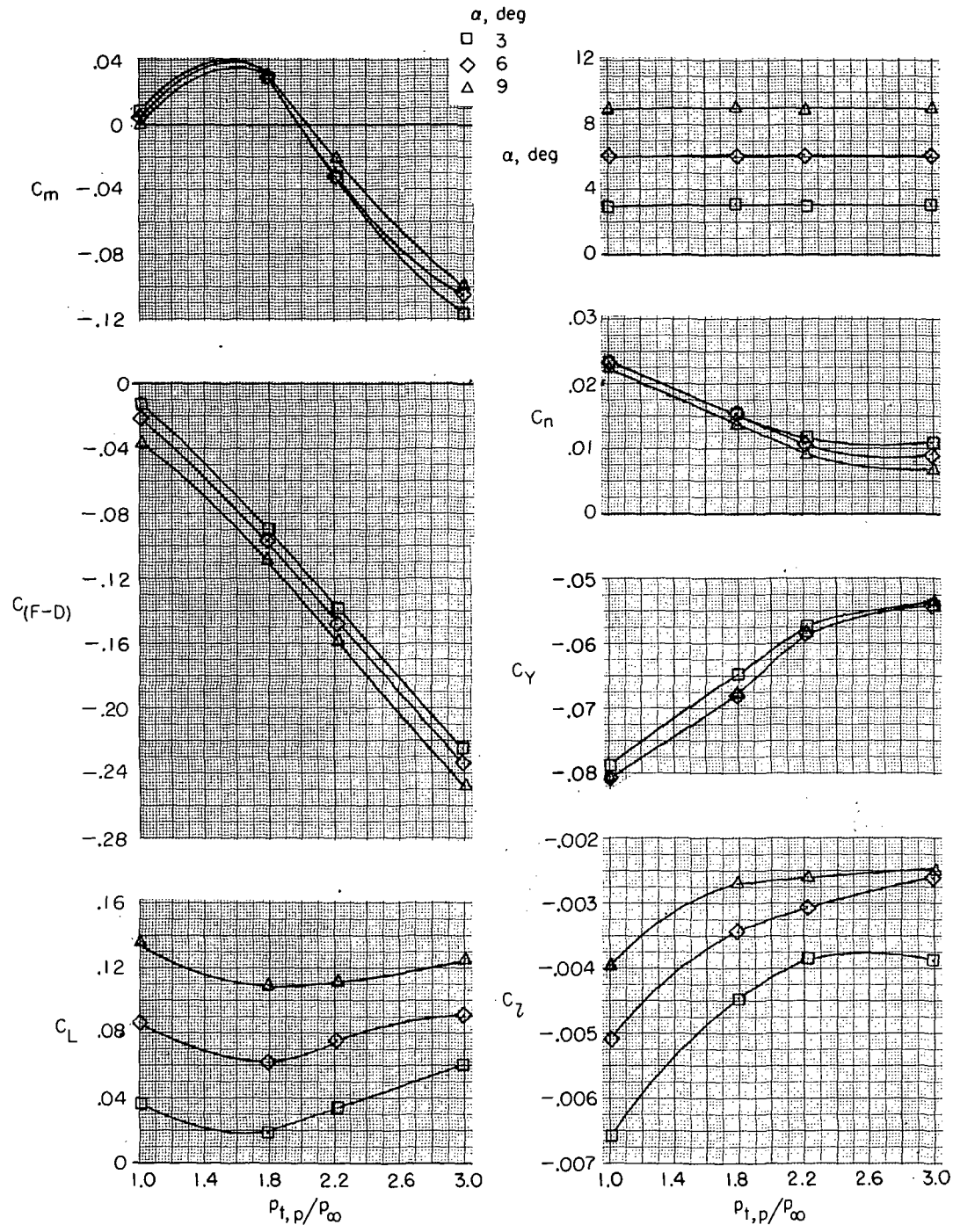

(a) M = 0.34.

Figure 36.- Effect of jet-total-pressure ratio on aerodynamic characteristics of model with thrust control unit for several angles of attack and Mach numbers. $\beta = 5^o$; $\delta_f = 0^o$; $\delta_s = 0^o$; $\delta_h = -1.5^o$; $\delta_r = -5^o$; $\delta_{du} = 32.5^o$; $\delta_{dl} = 52.5^o$; $\delta_b = 100$ percent; and military power.

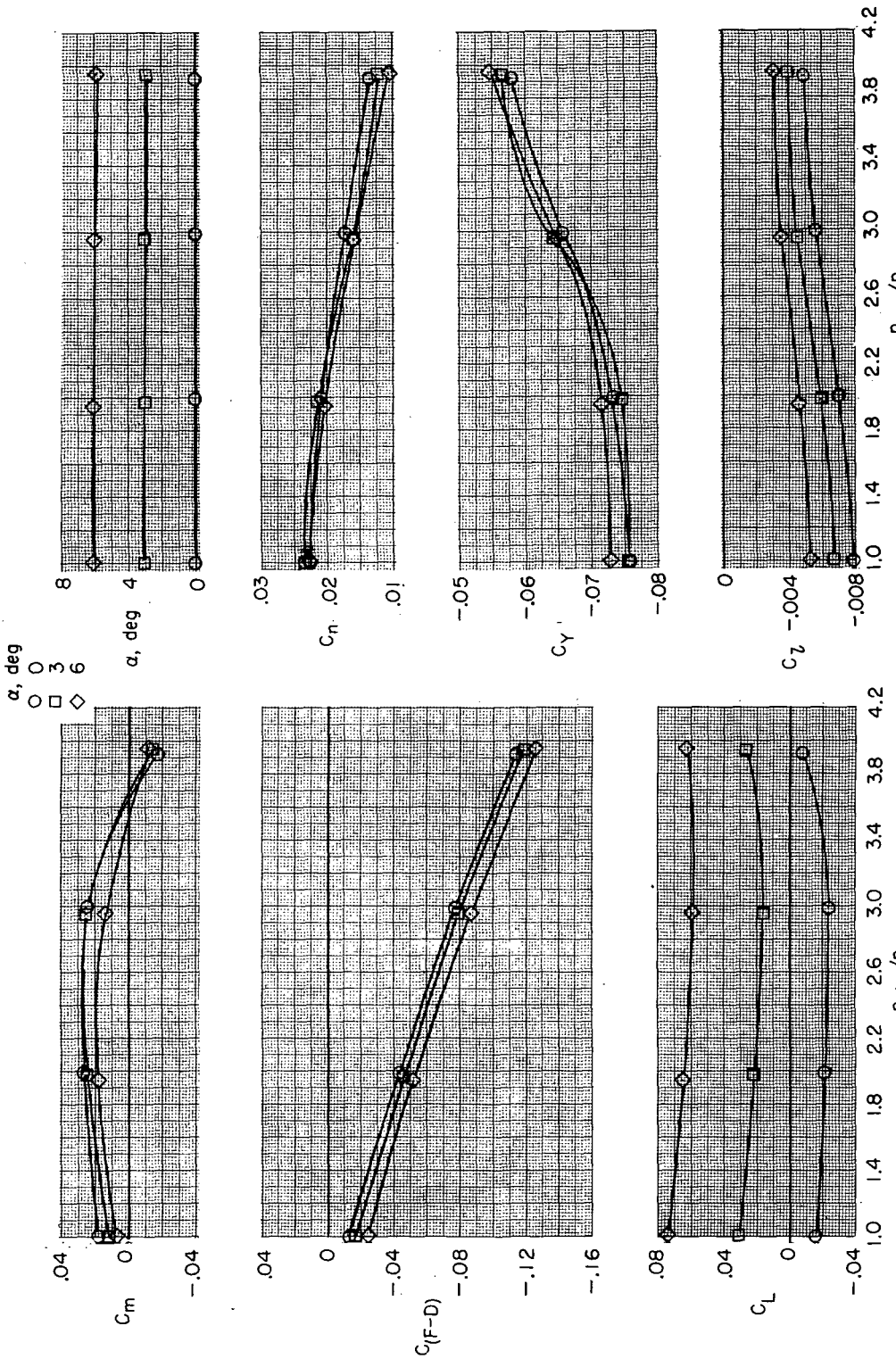

(b) M = 0.60.

Figure 36.- Continued.

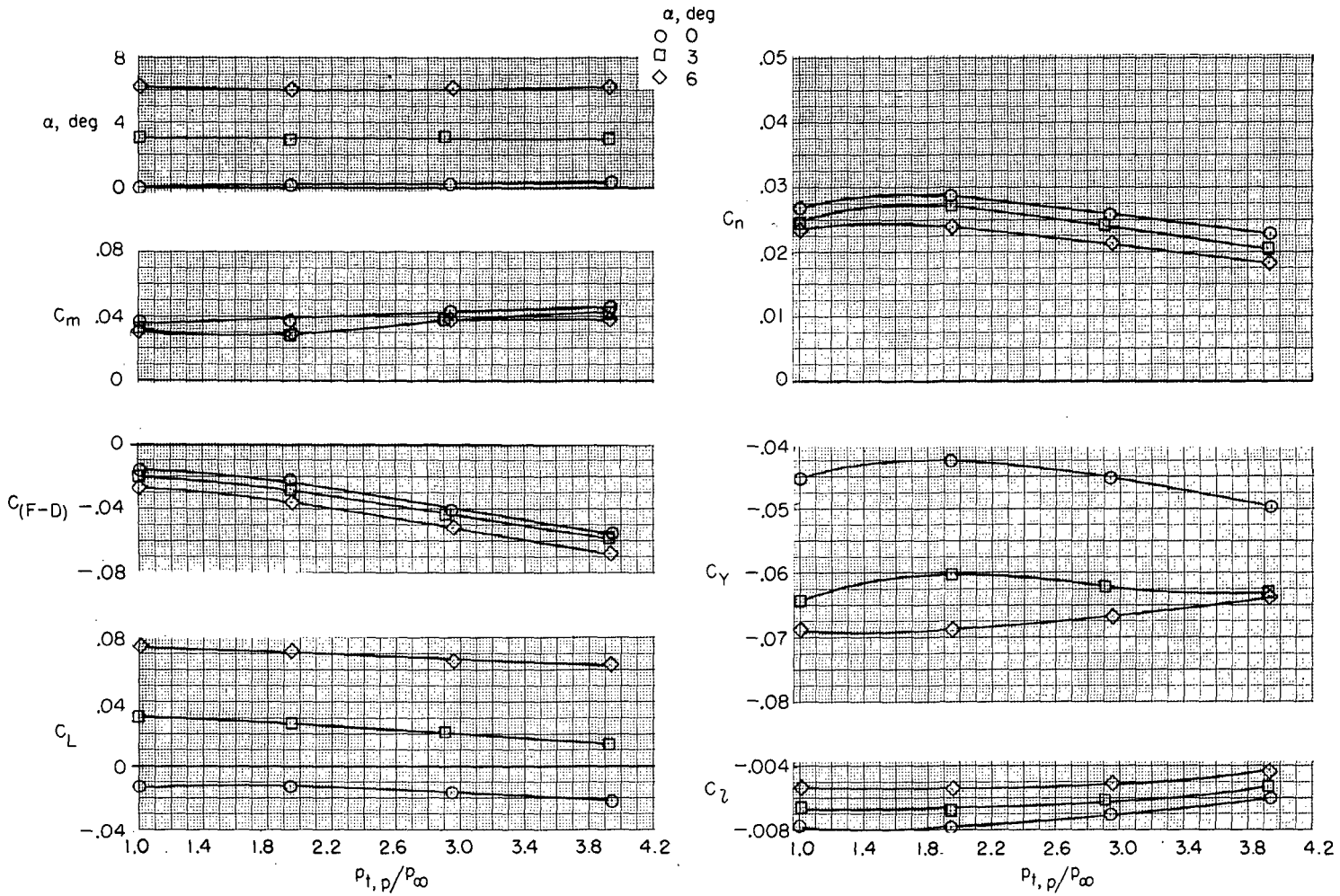

(c) M = 0.90.

Figure 36.- Concluded.

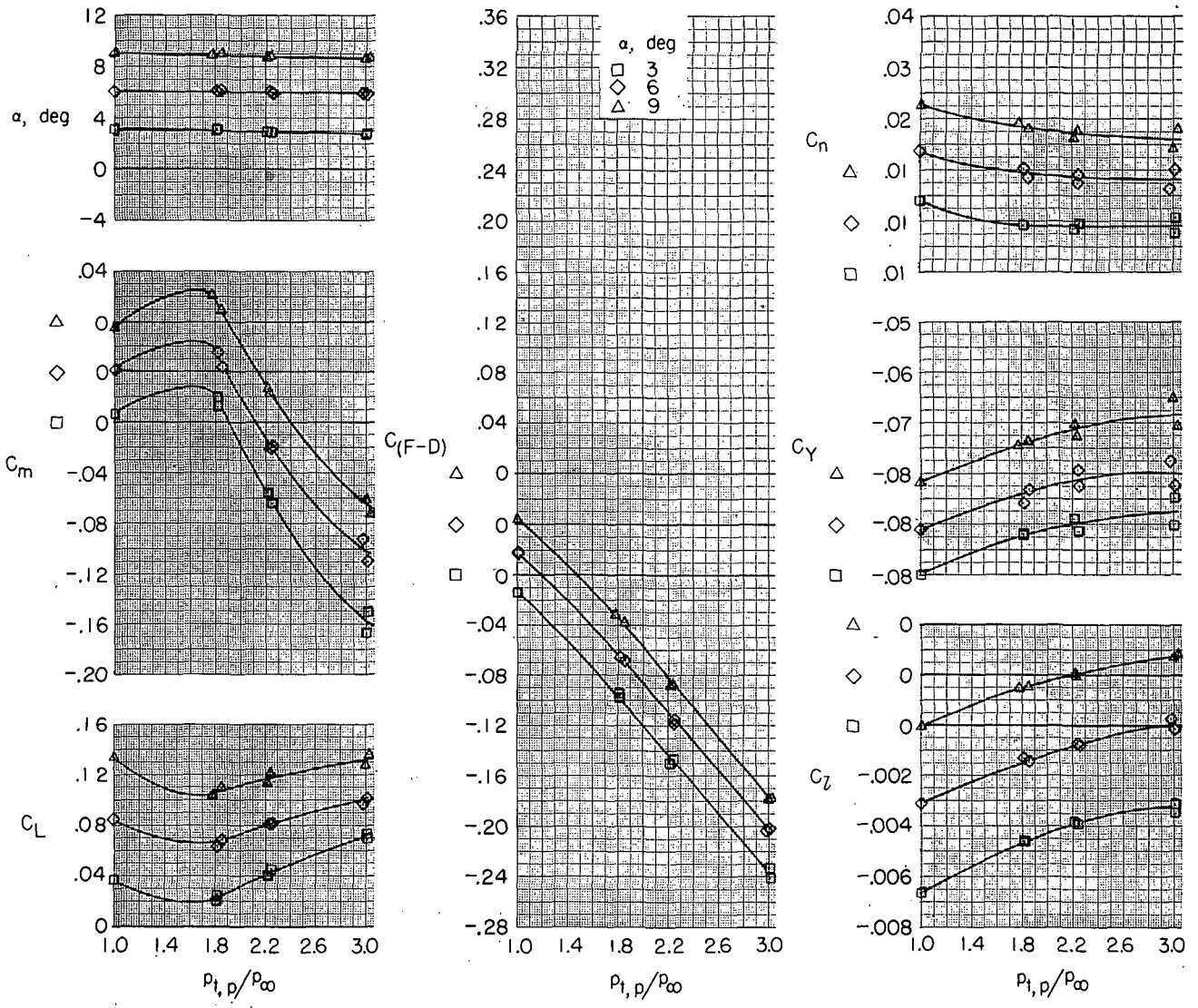

(a) M = 0.34.

Figure 37.- Effect of jet-total-pressure ratio on aerodynamic characteristics of model with thrust control unit for several angles of attack and Mach numbers. $\beta = 5^o$; $\delta_f = 0^o$; $\delta_s = 0^o$; $\delta_h = -1.5^o$; $\delta_r = -5^o$; $\delta_{du} = 32.5^o$ with side plates; $\delta_{dl} = 52.5^o$; $\delta_b = 100$ percent; and military power.

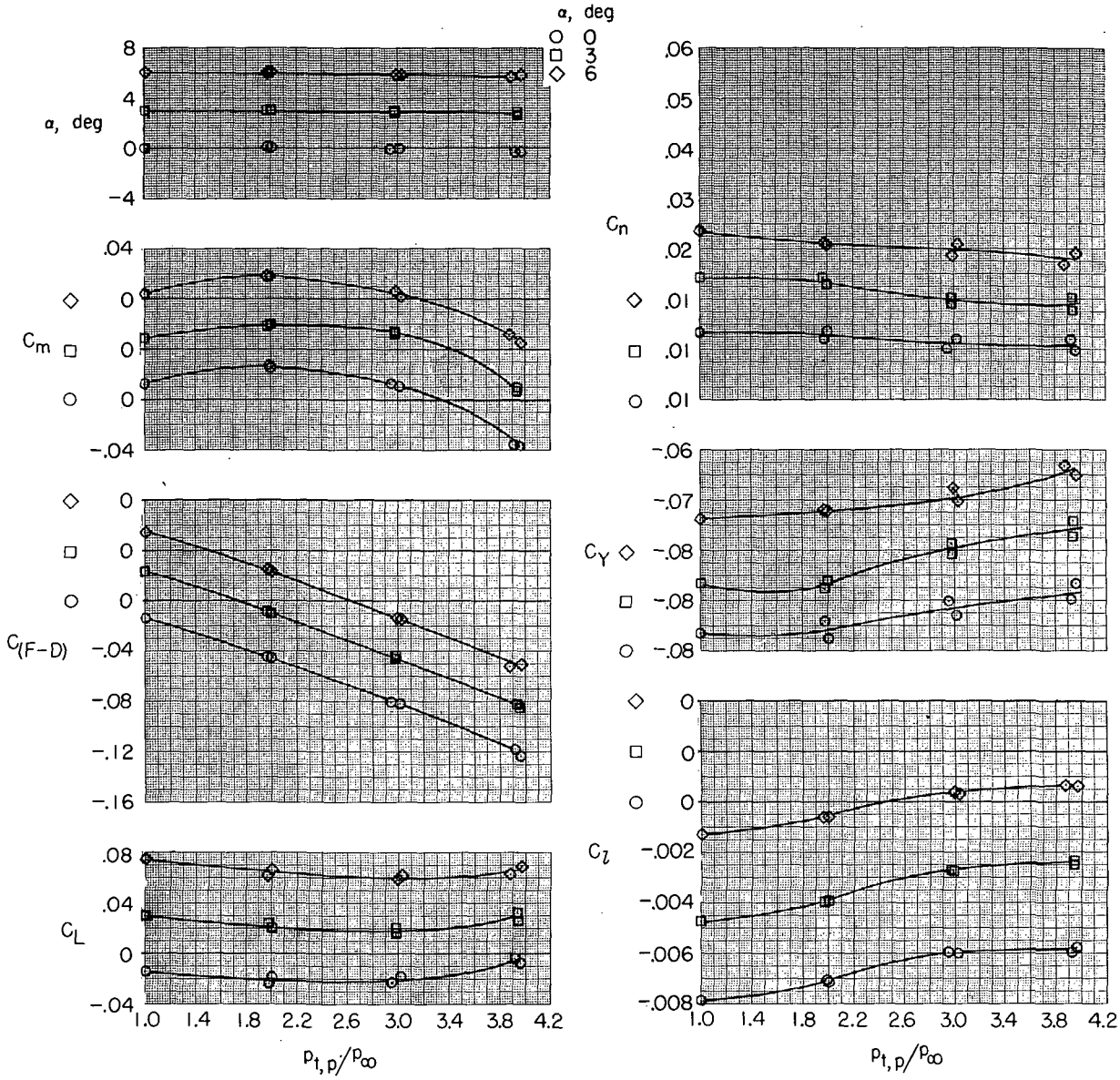

(b) M = 0.60.

Figure 37.- Continued.

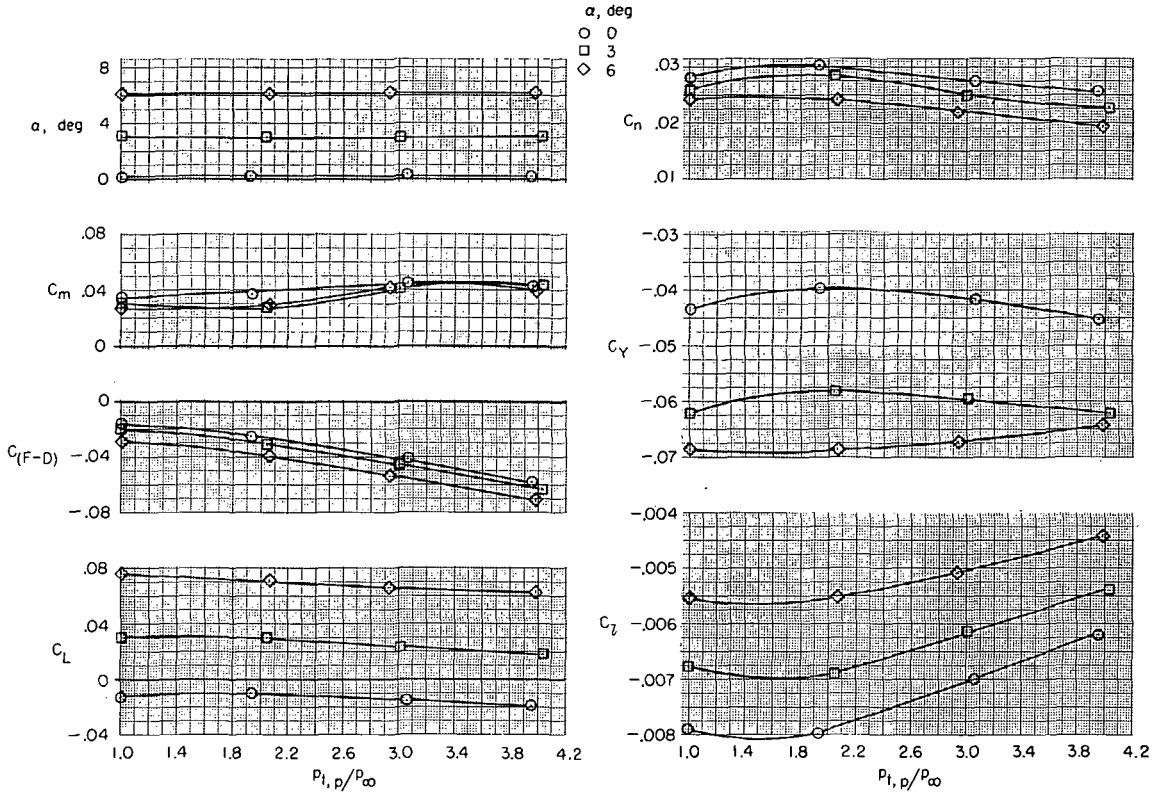

(c) M = 0.90.

Figure 37.- Concluded.

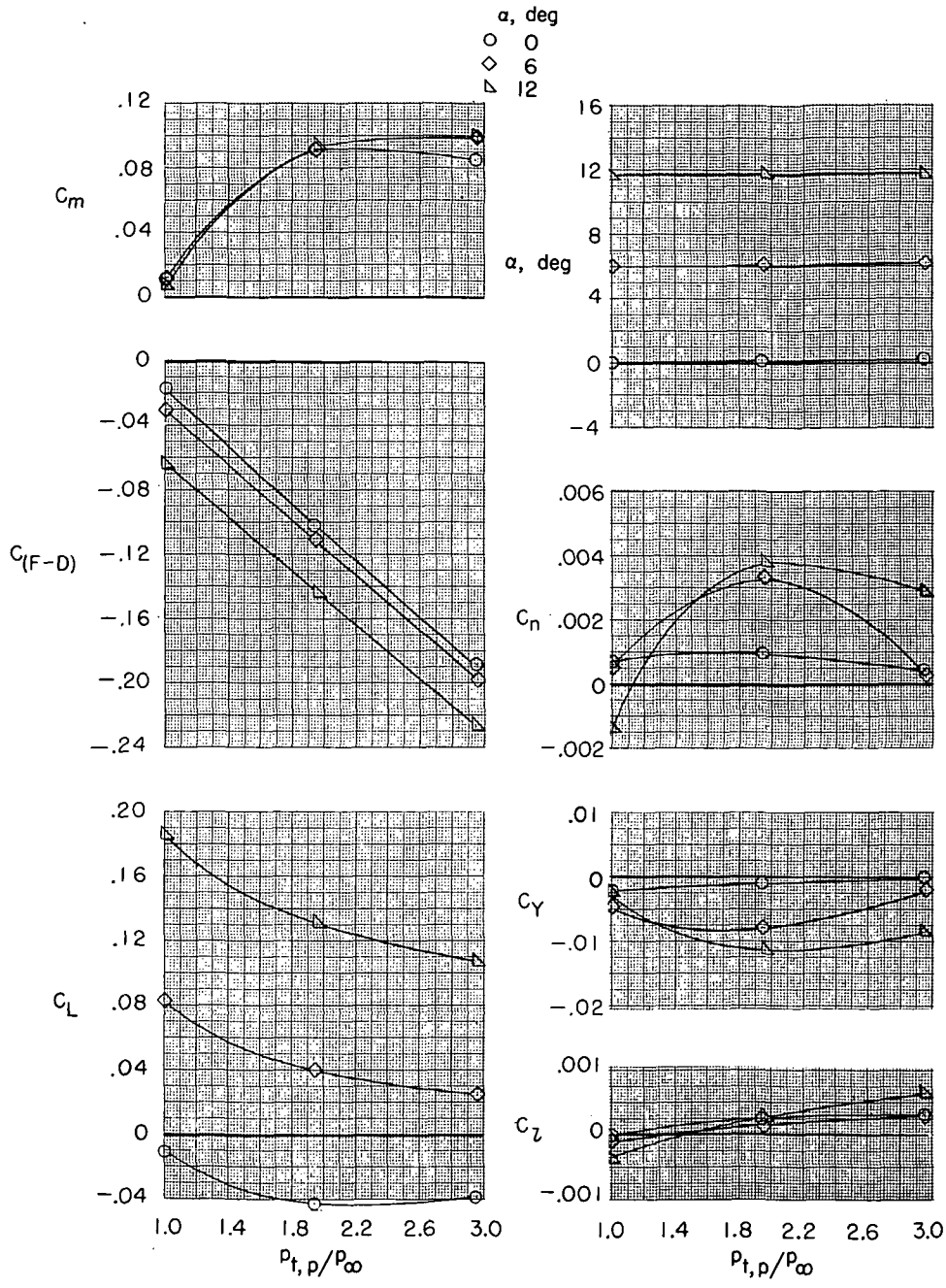

(a) M = 0.35.

Figure 38.- Effect of jet-total-pressure ratio on aerodynamic characteristics of model with thrust control unit for several angles of attack and Mach numbers. $\beta = 0^o$; $\delta_f = 0^o$; $\delta_s = 0^o$; $\delta_h = -1.5^o$; $\delta_r = 0^o$; $\delta_{du} = 43.5^o$; $\delta_{dl} = 43.5^o$; $\delta_b = 100$ percent; and military power.

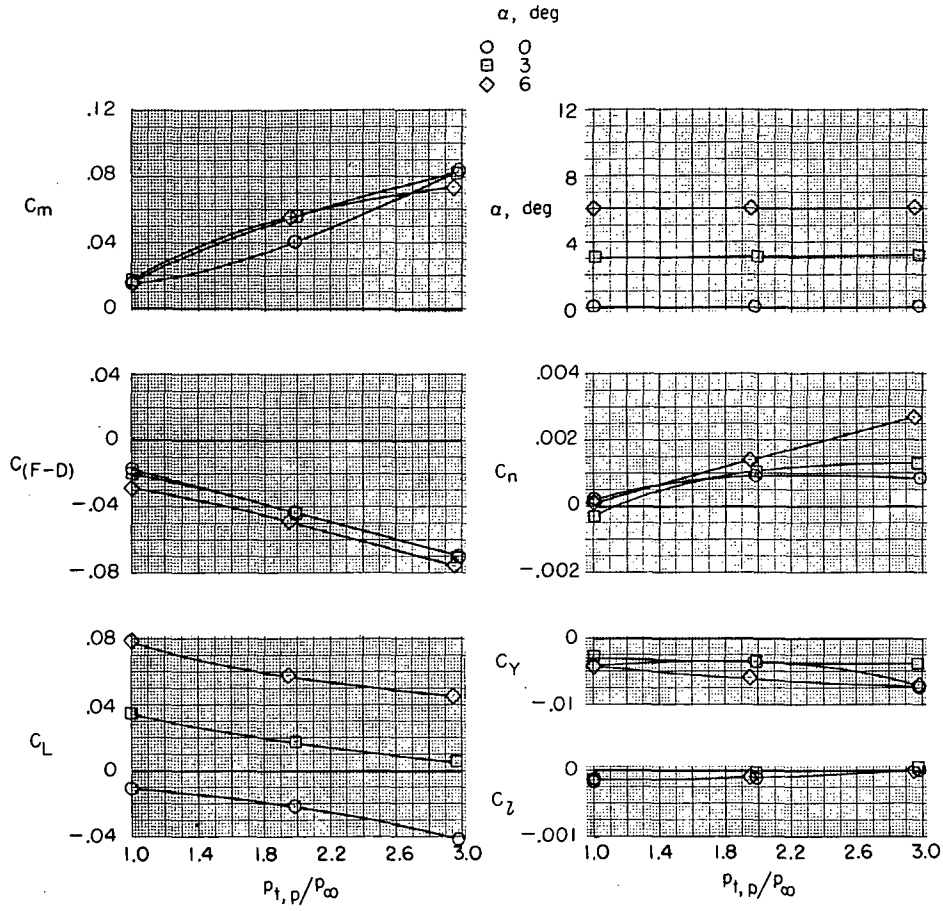

(b) M = 0.60.

Figure 38.- Continued.

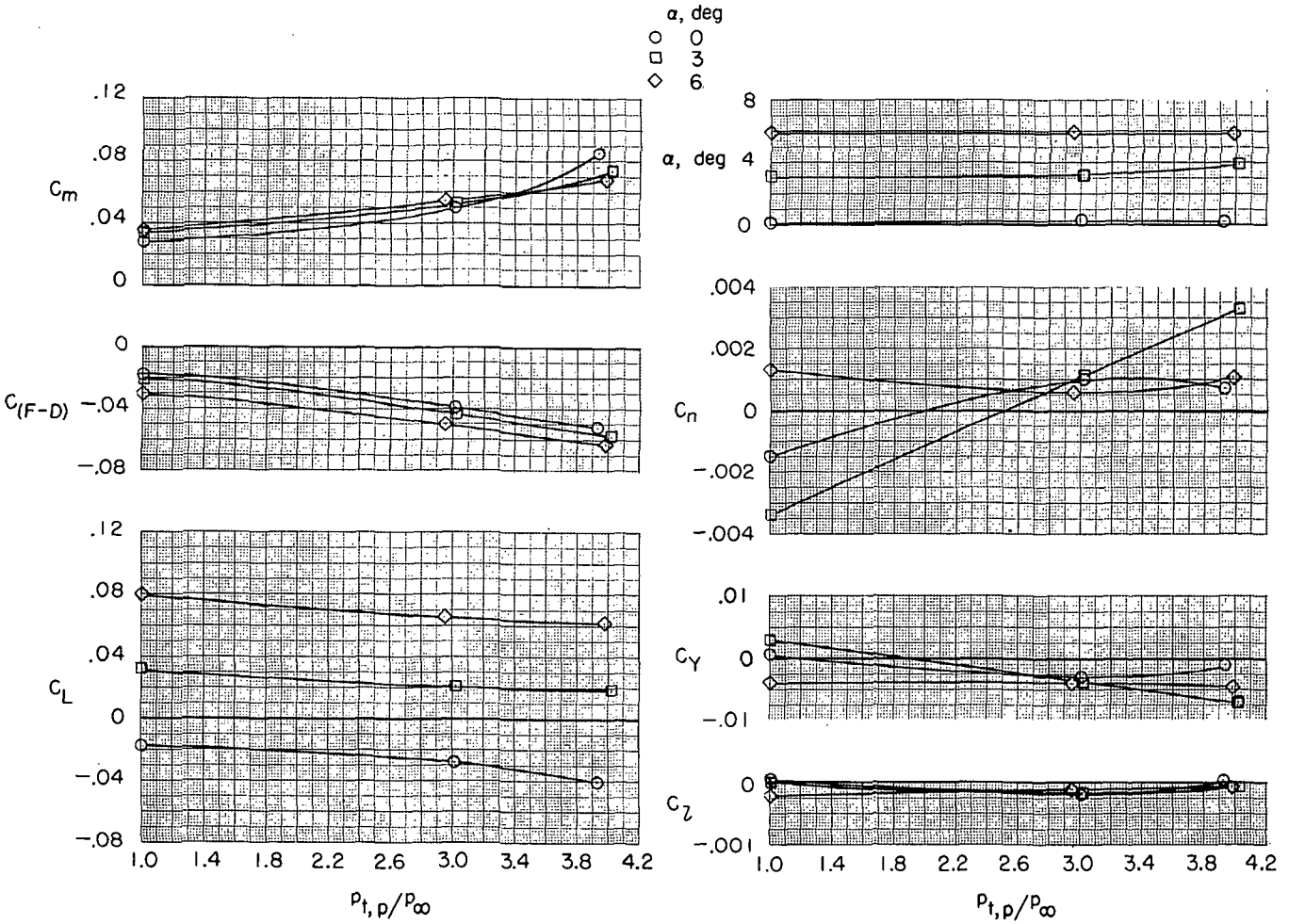

(c) M = 0.90.

Figure 38.- Continued.

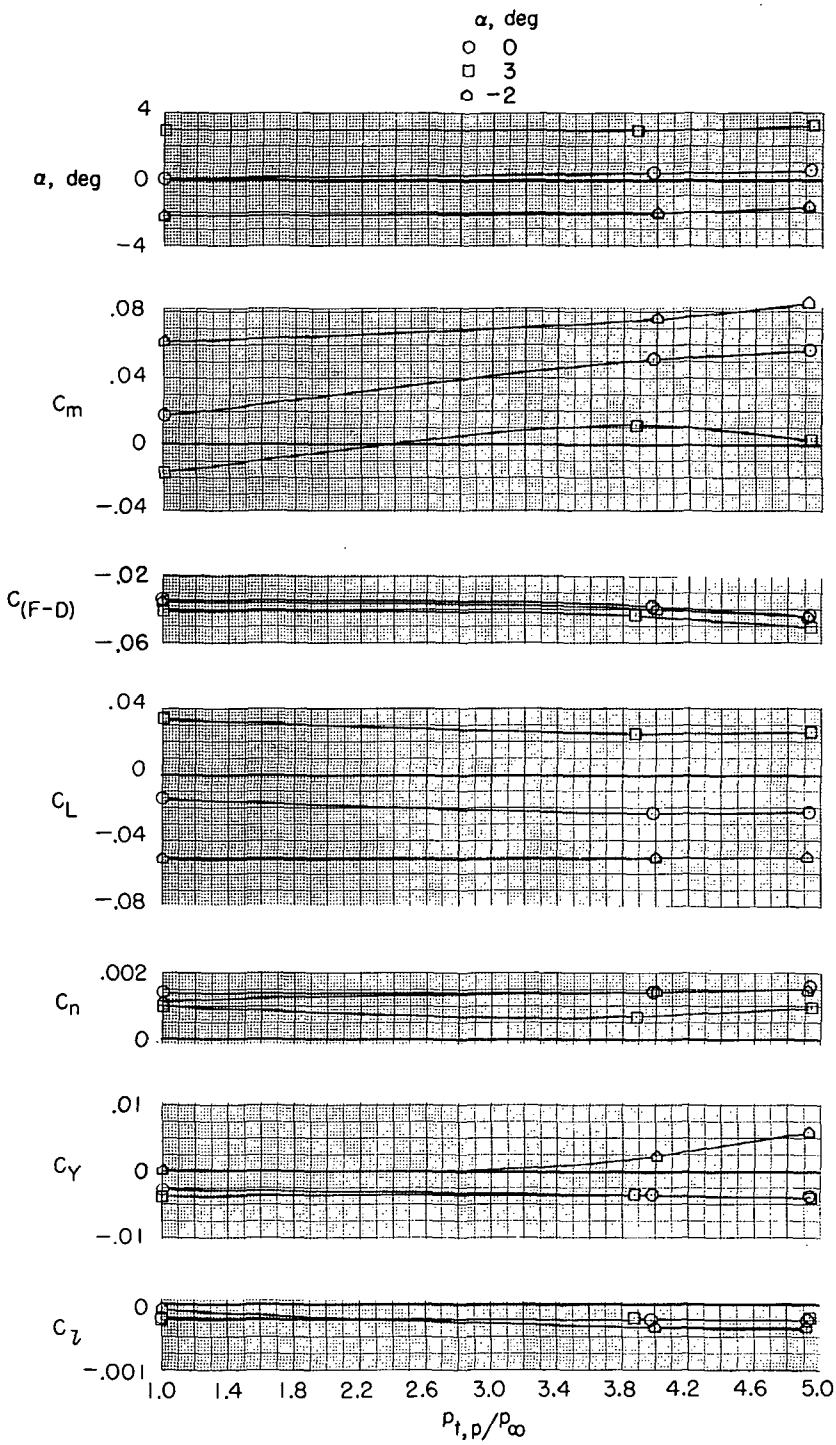

(d) M = 1.30.

Figure 38.- Concluded.

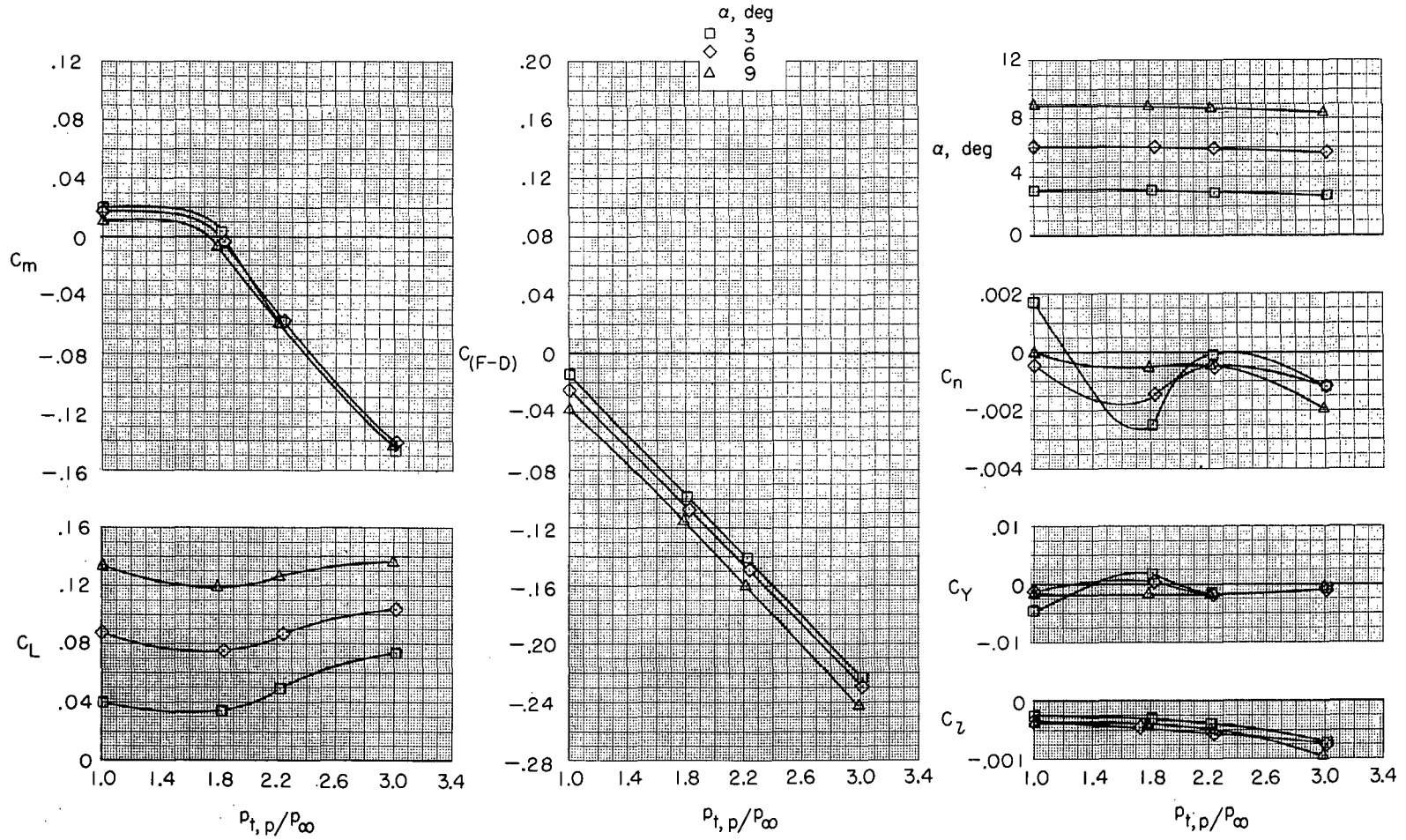

(a) M = 0.34.

Figure 39.- Effect of jet-total-pressure ratio on aerodynamic characteristics of model with thrust control unit for several angles of attack and Mach numbers. $\beta = 0^o$; $\delta_f = 0^o$; $\delta_s = 0^o$; $\delta_h = -1.5^o$; $\delta_r = 0^o$; $\delta_{du} = 28^o$; $\delta_{dl} = 60^o$; $\delta_b = 100$ percent; and military power.

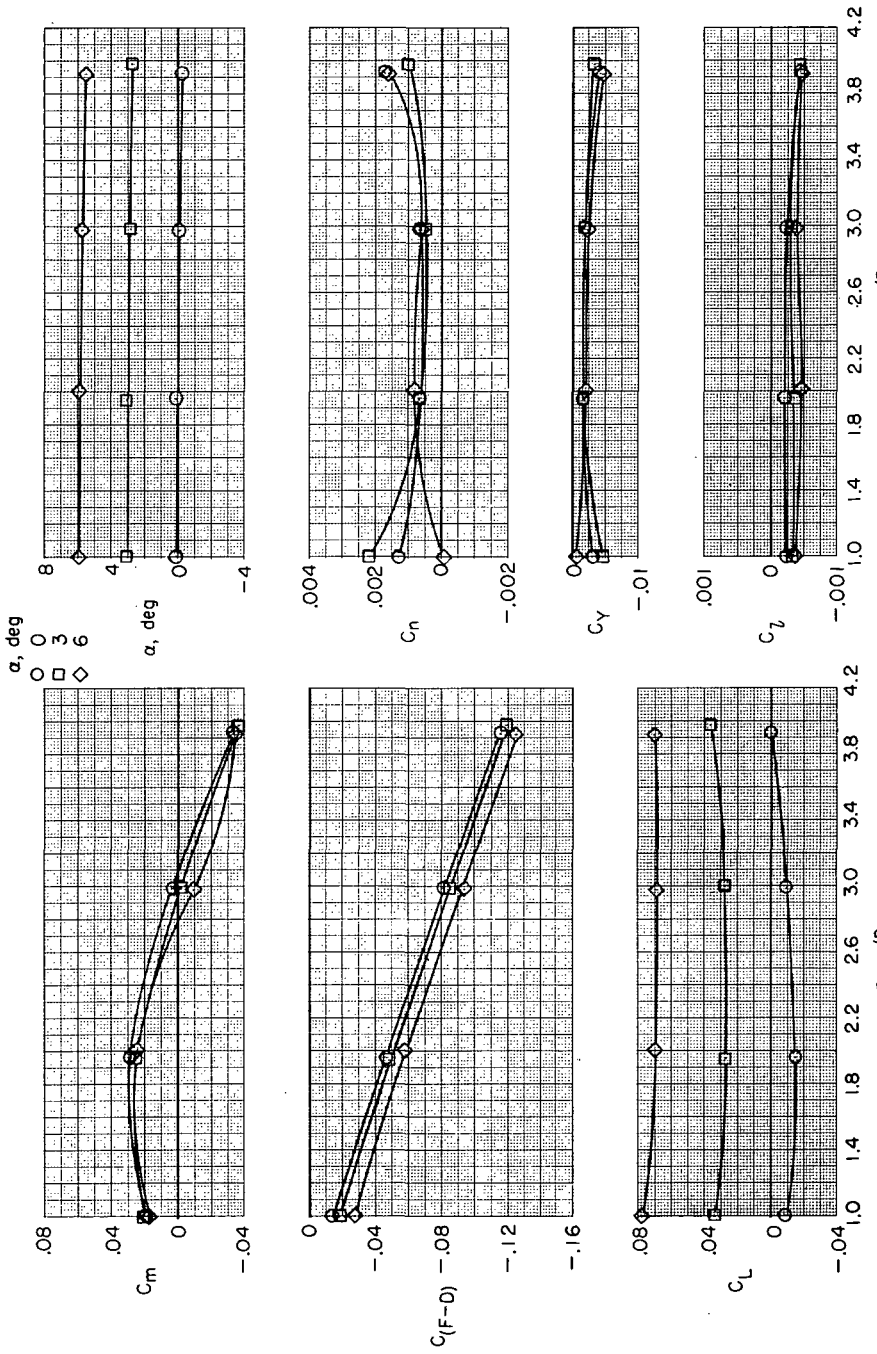

(b) M = 0.60.

Figure 39.- Continued.

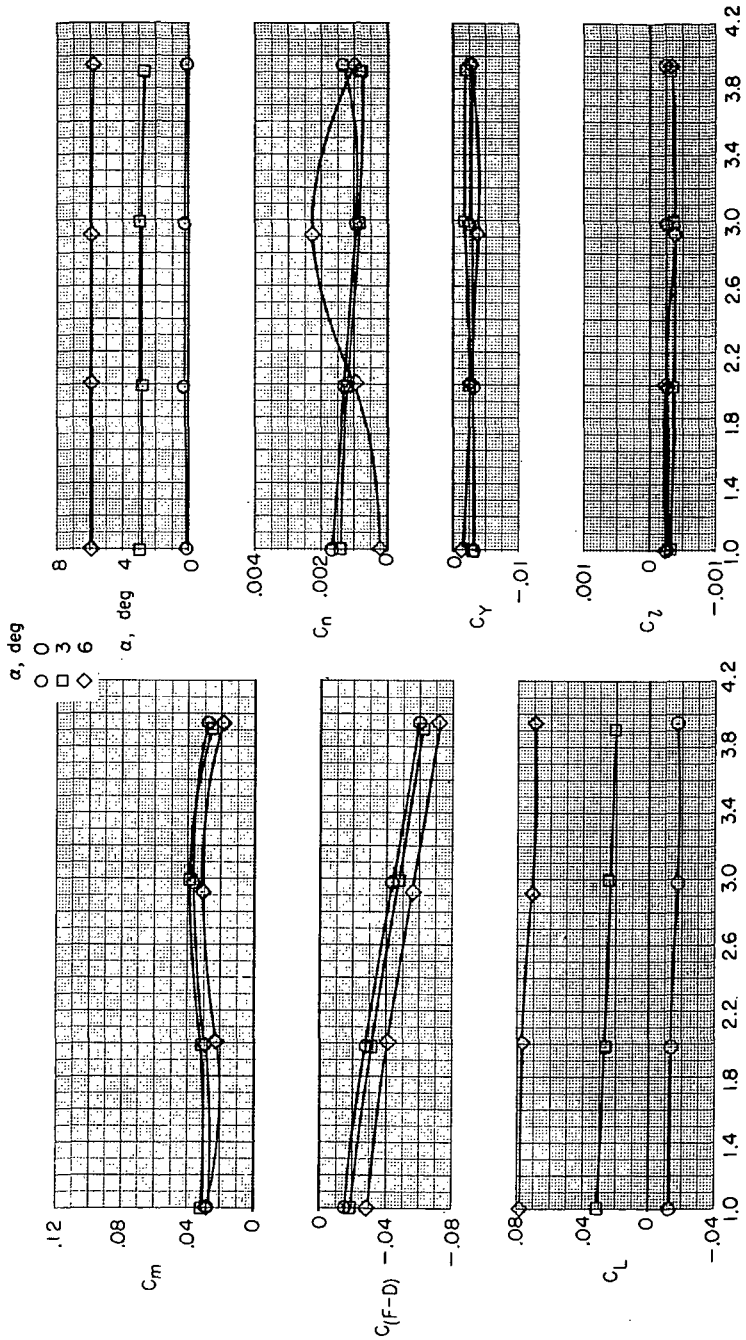

(c) M = 0.90.

Figure 39.- Concluded.

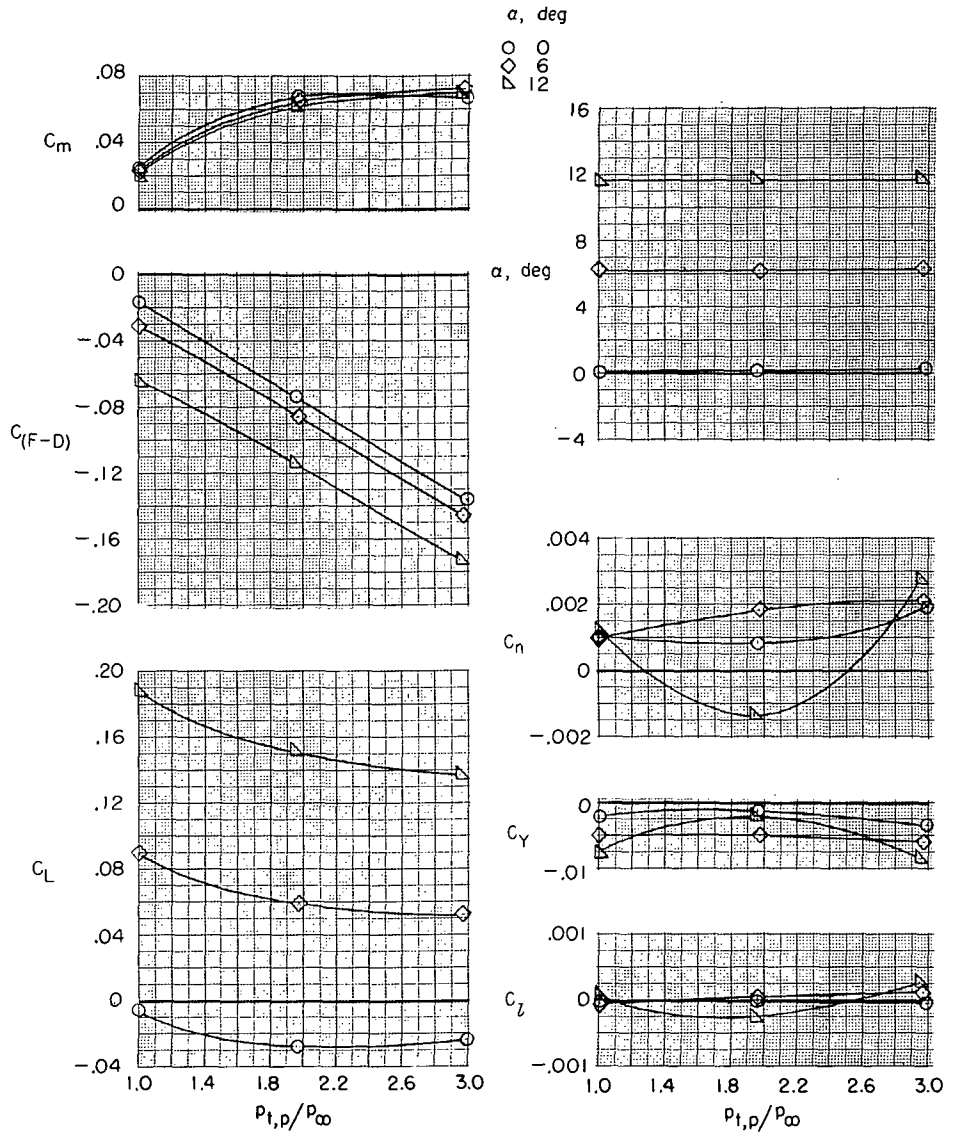

(a) M = 0.34.

Figure 40.- Effect of jet-total-pressure ratio on aerodynamic characteristics of model with thrust control unit for several angles of attack and Mach numbers. $\beta = 0^o$; $\delta_f = 0^o$; $\delta_s = 0^o$; $\delta_h = -1.5^o$; $\delta_r = 0^o$; $\delta_{du} = 60^o$; $\delta_{dl} = 60^o$; $\delta_b = 100$ percent; and military power.

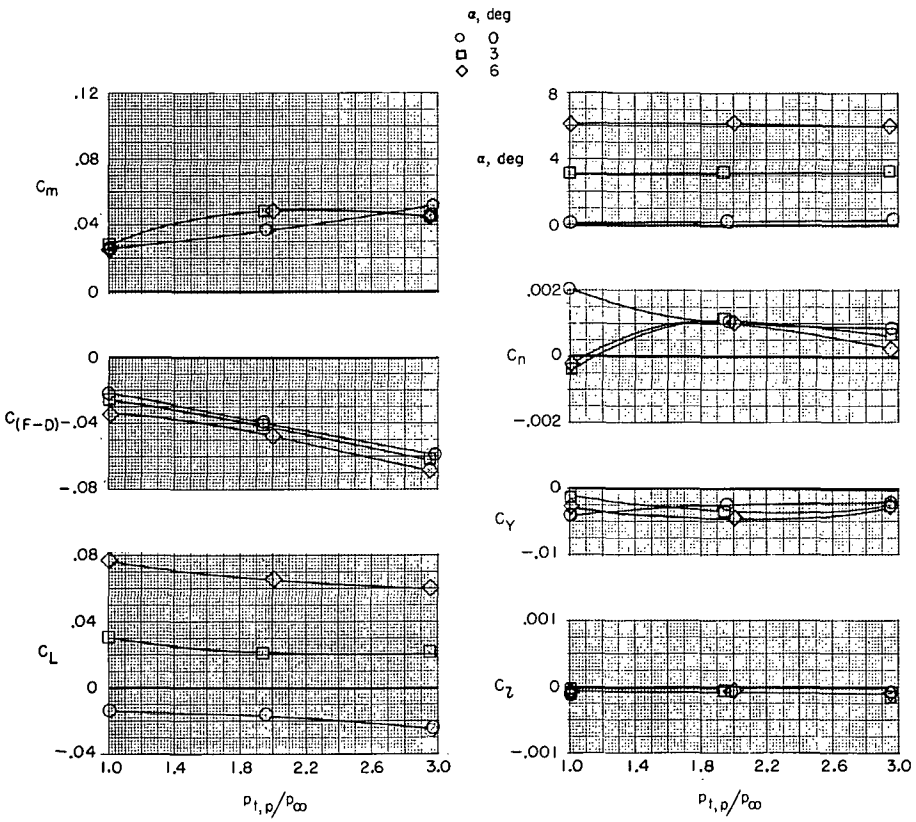

(b) M = 0.60.

Figure 40.- Continued.

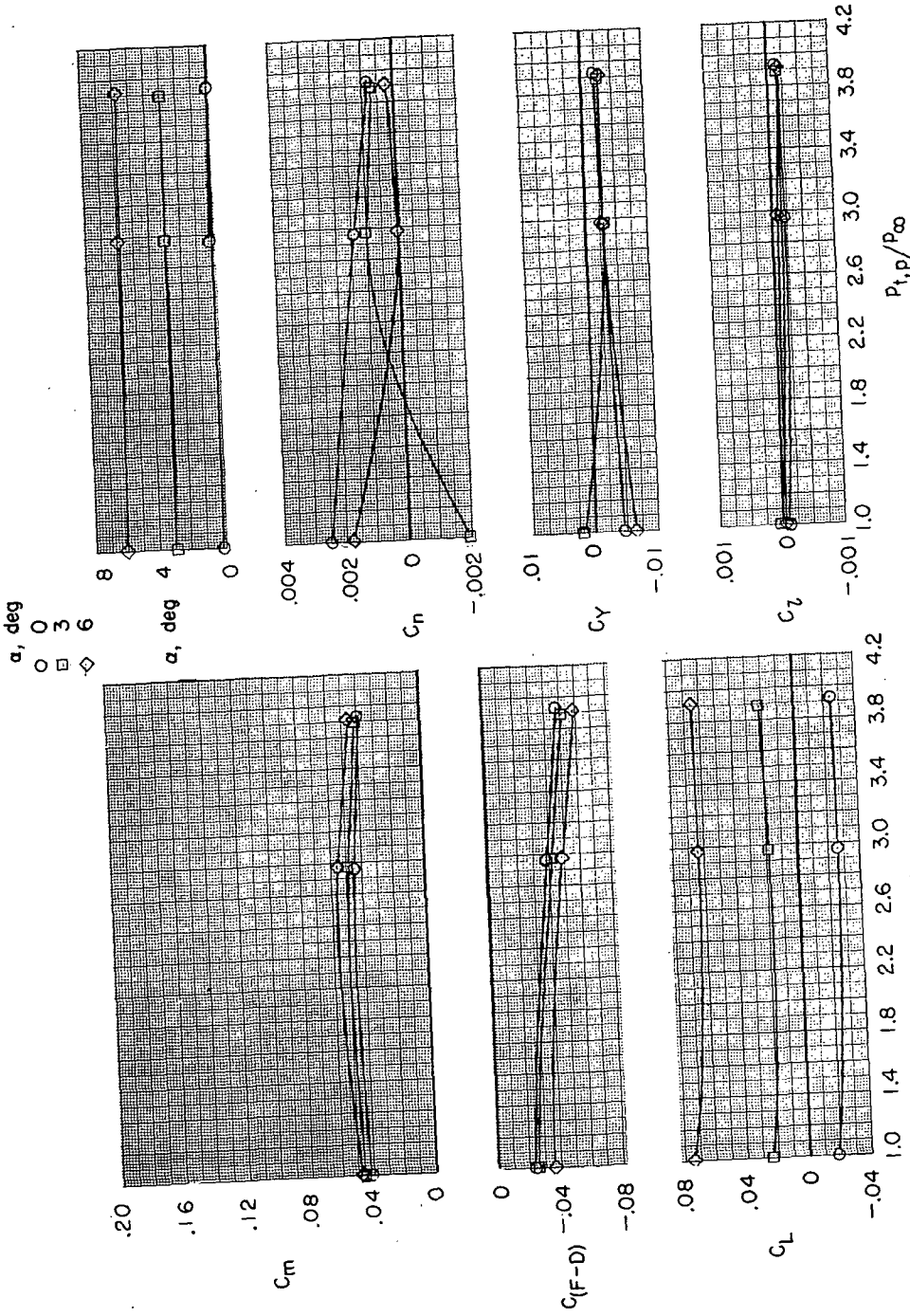

(c) M = 0.90.

Figure 40.- Continued.

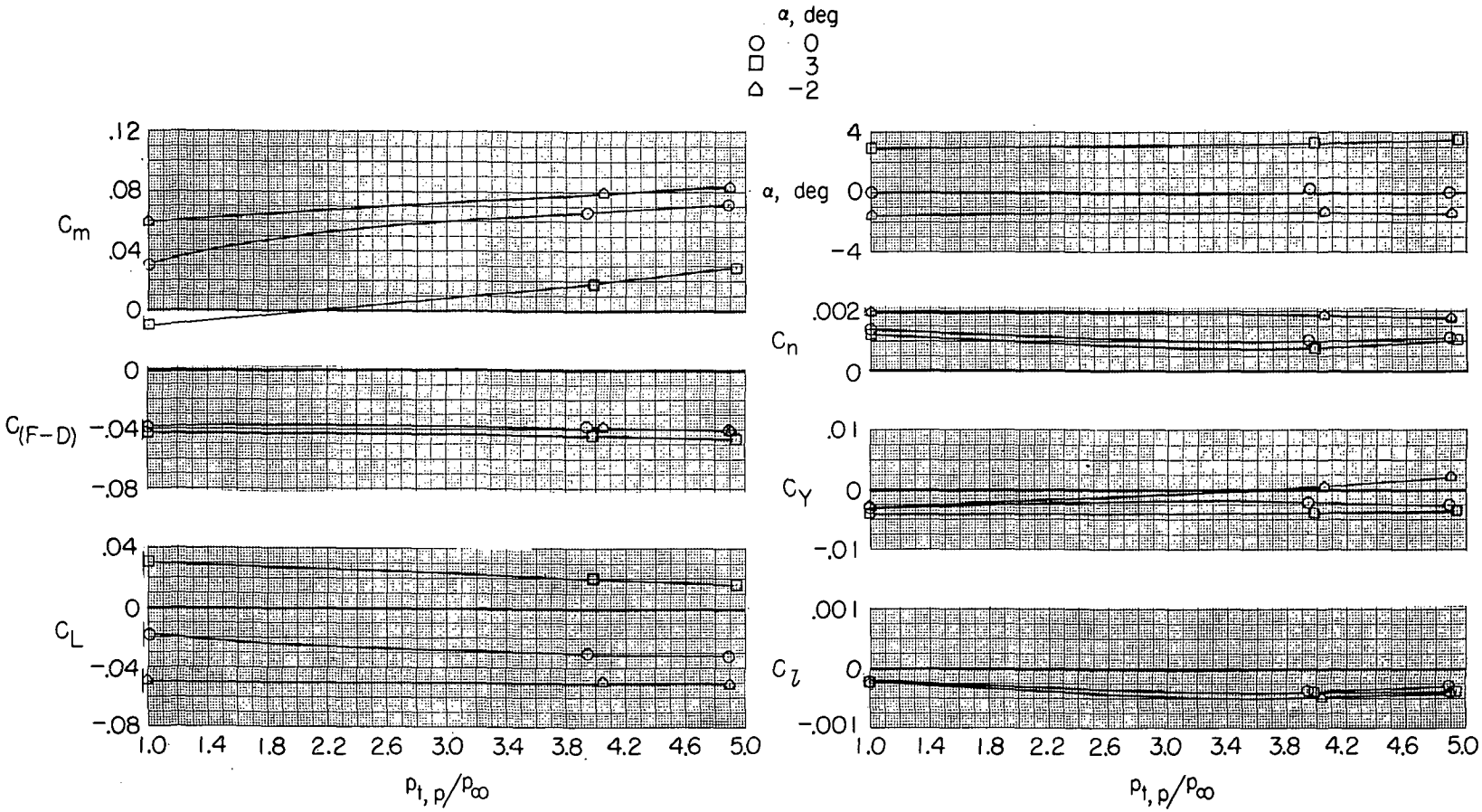

(d) M = 1.30.

Figure 40.- Concluded.

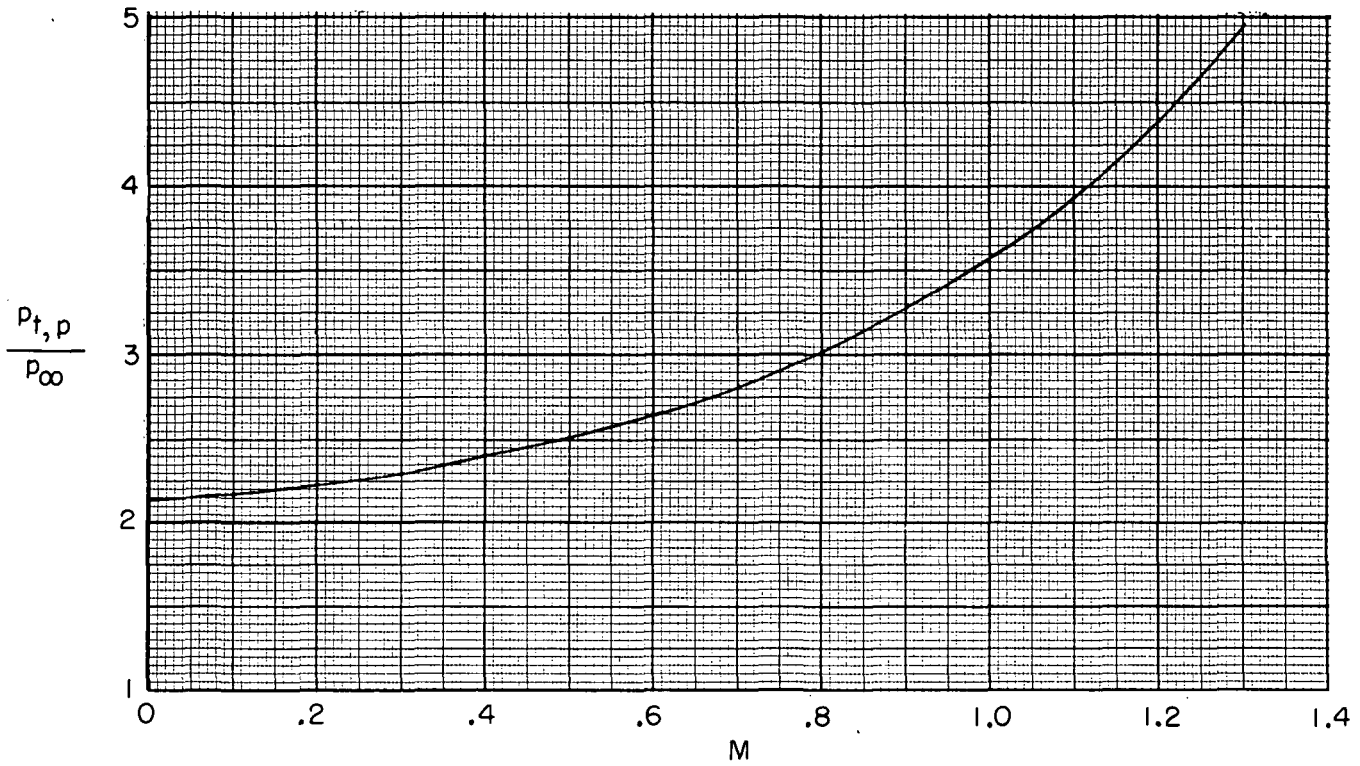

Figure 41.- Assumed engine operating-pressure ratio schedule with Mach number for a turbojet engine for military and afterburner power settings.

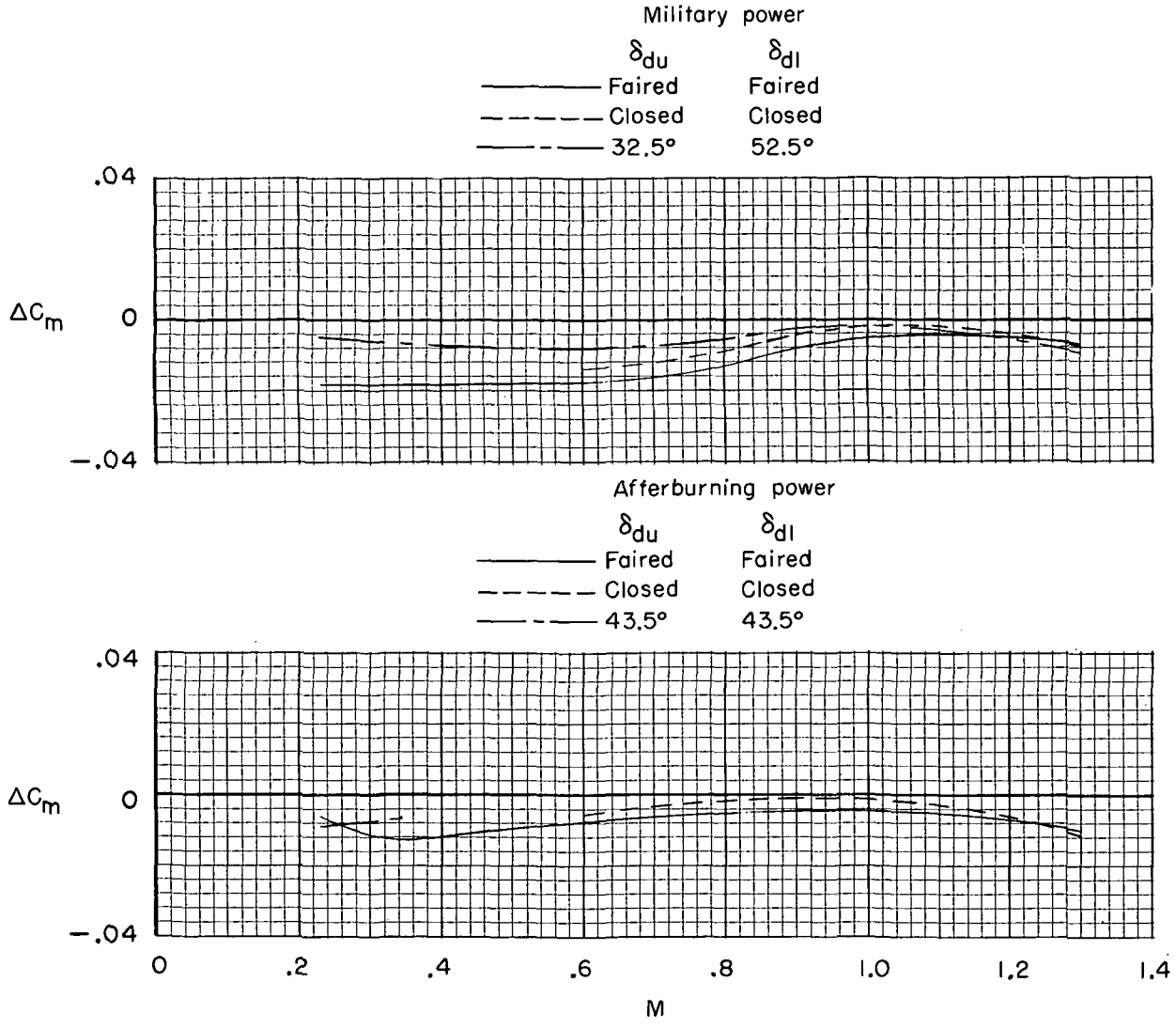

Figure 42.- Effect of TCU (forward-thrust mode) on pitching-moment increment for Mach number range at scheduled jet-total-pressure ratios. $\beta = 0^o$; $\alpha = 0^o$; $\delta_f = 0^o$; $\delta_s = 0^o$; $\delta_h = -1.5^o$; and $\delta_r = 0^o$.

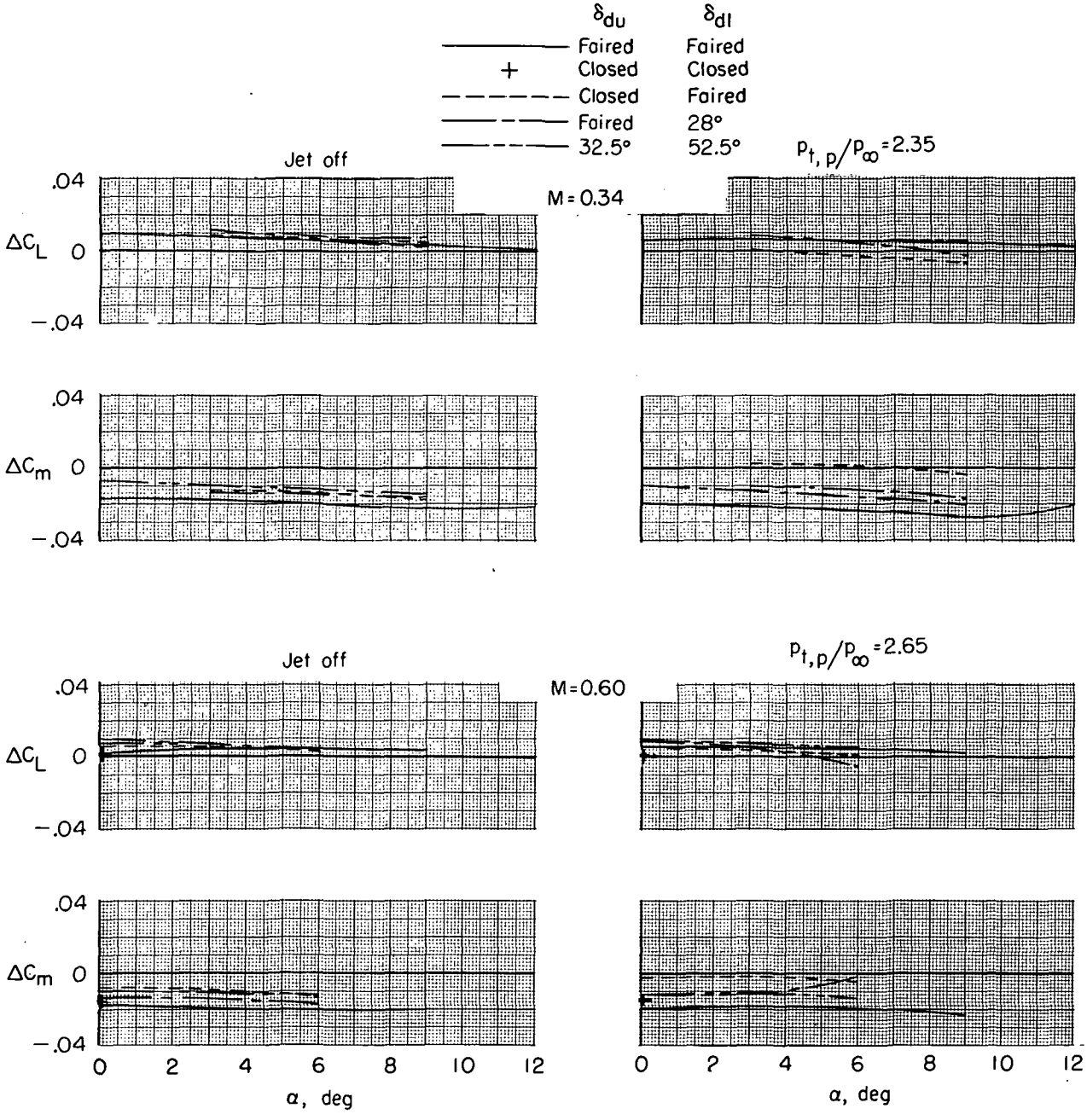

Figure 43.- Effect of deflector-door position on lift and pitching-moment increments for model with TCU in forward-thrust mode (δ_b = 0 percent). $\beta = 0^o$; $\delta_f = 0^o$; $\delta_s = 0^o$; $\delta_h = -1.5^o$; $\delta_r = 0^o$; and military power.

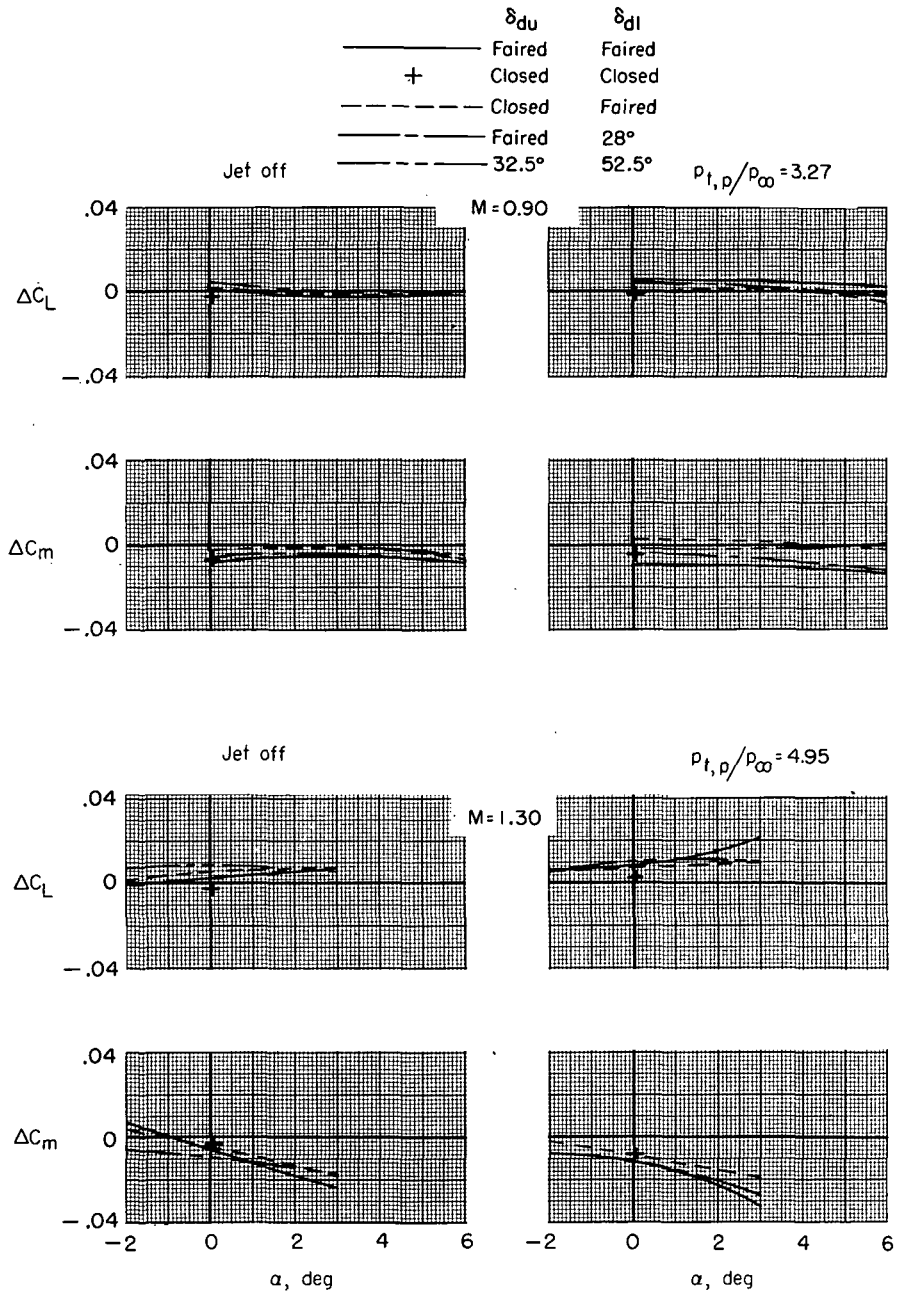

Figure 43.- Concluded.

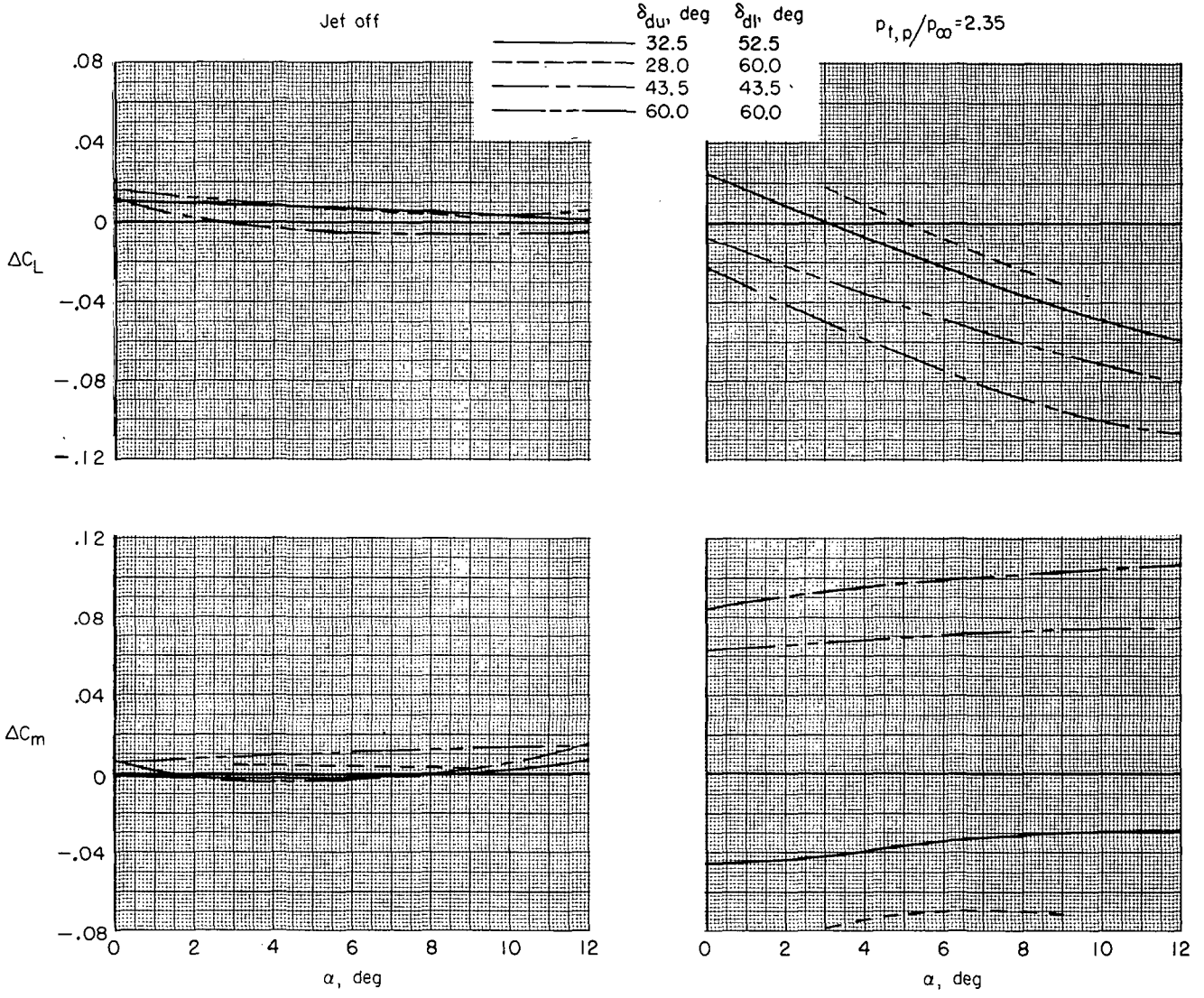

(a) M = 0.34.

Figure 44.- Effect of deflector-door position on lift and pitching-moment increments for TCU in reverse-thrust mode (δ_b = 100 percent). $\beta = 0^o$; $\delta_f = 0^o$; $\delta_s = 0^o$; $\delta_h = -1.5^o$; $\delta_r = 0^o$; and military power.

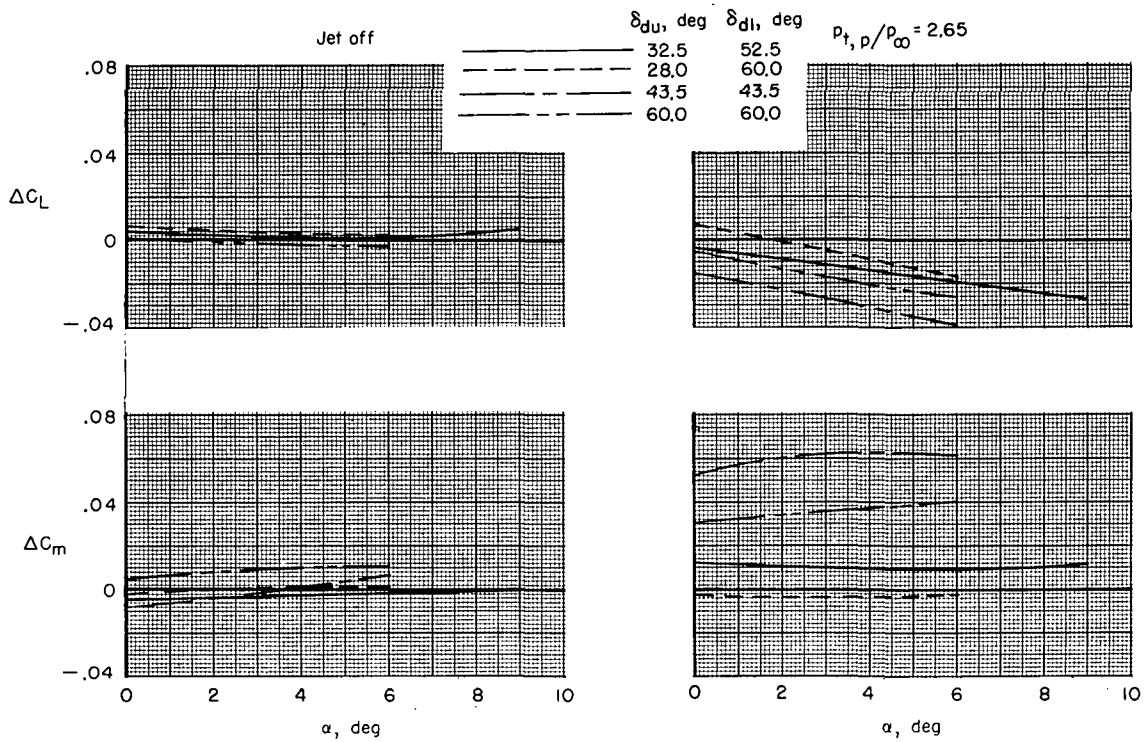

(b) M = 0.60.

Figure 44.- Continued.

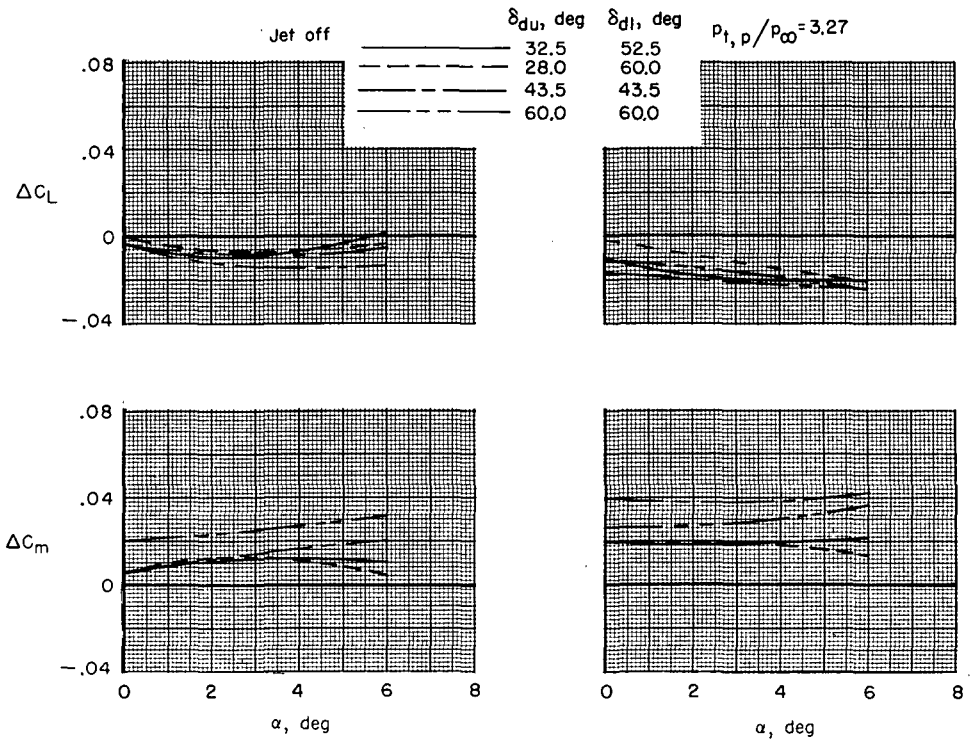

(c) M = 0.90.

Figure 44.- Continued.

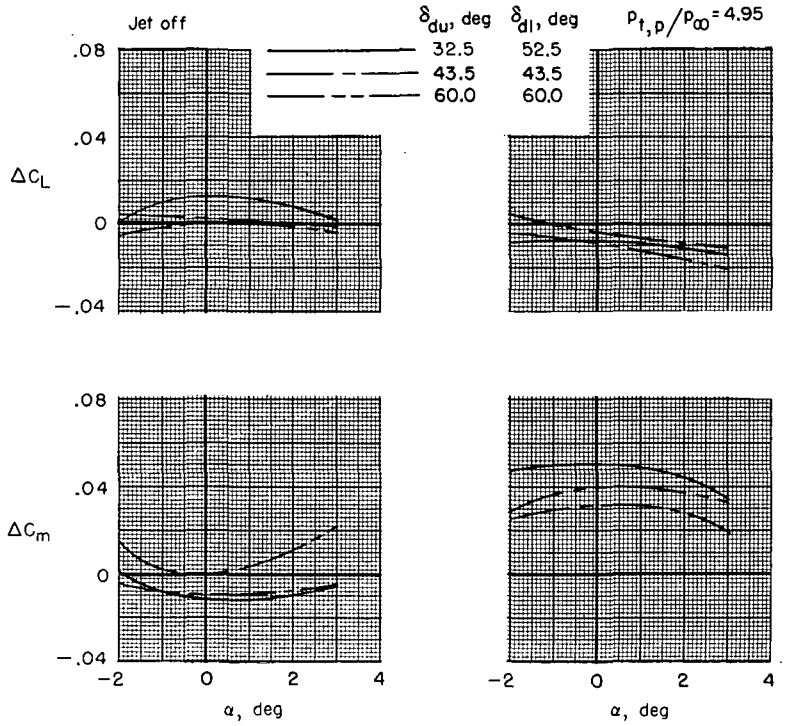

(d) M = 1.30.

Figure 44.- Concluded.

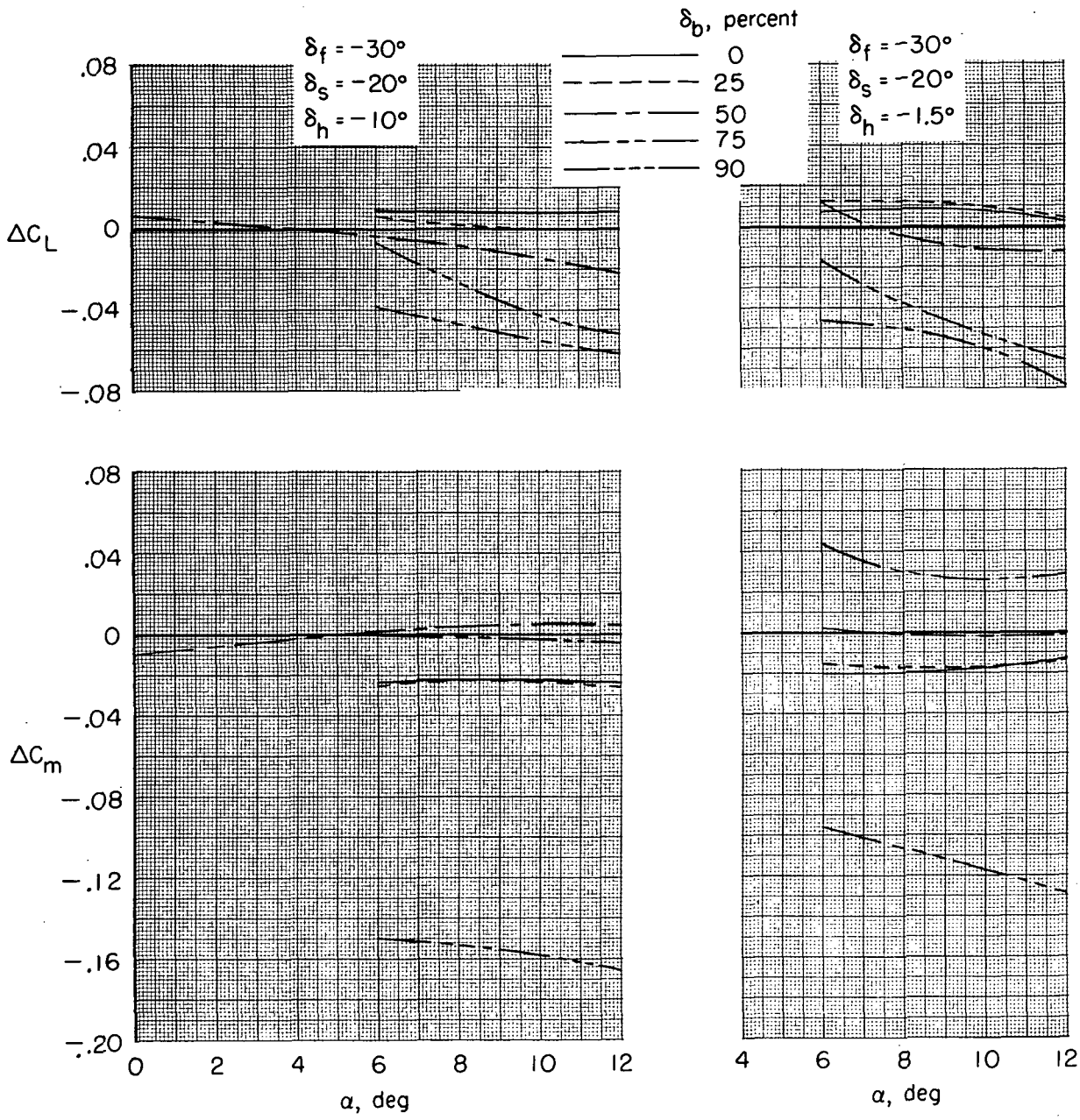

(a) M = 0.23.

Figure 45.- Effect of blocker-door closure on lift and pitching-moment increments for TCU ($\delta_{du} = 32.5^o$; $\delta_{dl} = 52.5^o$) at scheduled jet-total-pressure ratio. $\beta = 0^o$; $\delta_r = 0^o$; and military power.

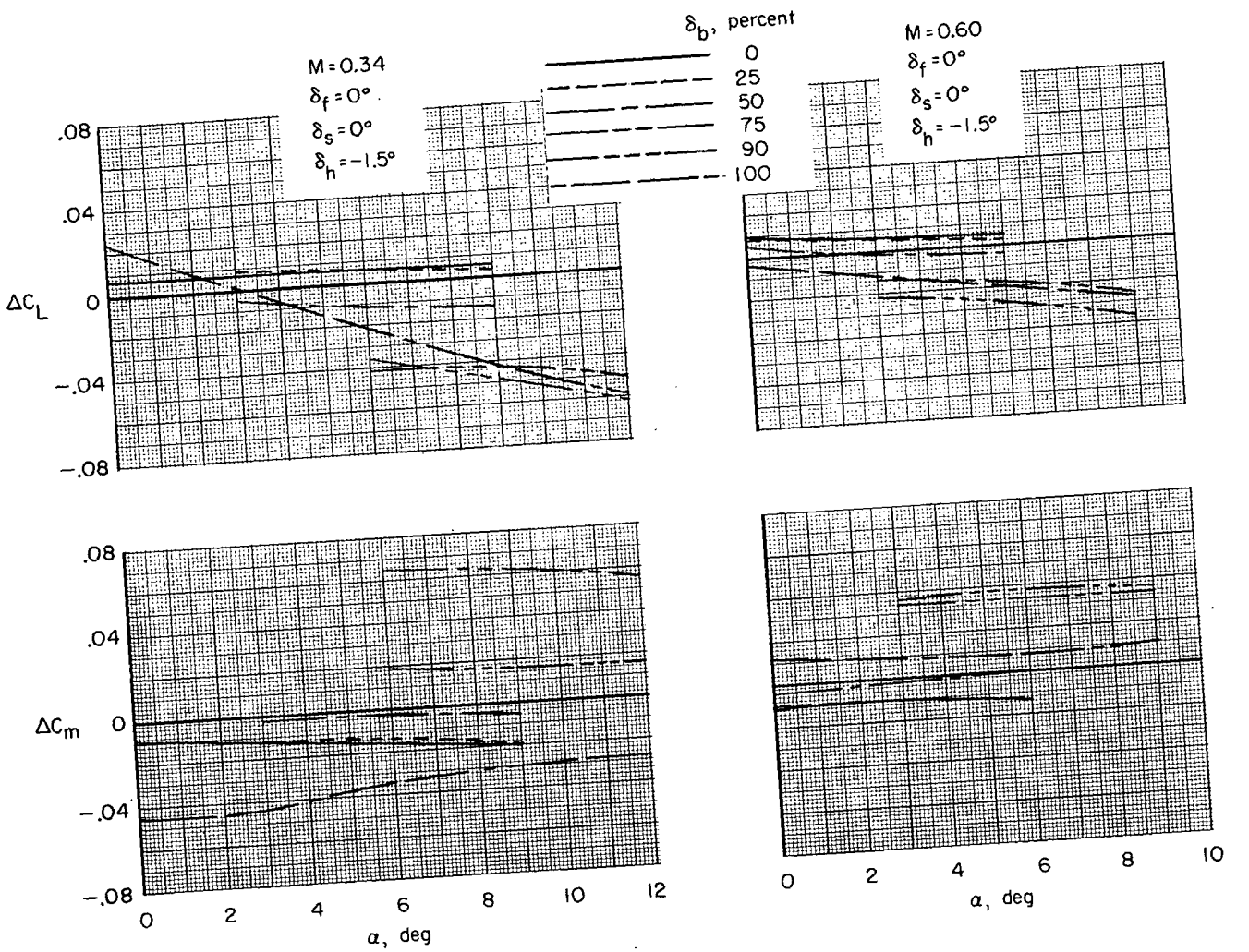

(b) M = 0.34 and 0.60.

Figure 45.- Continued.

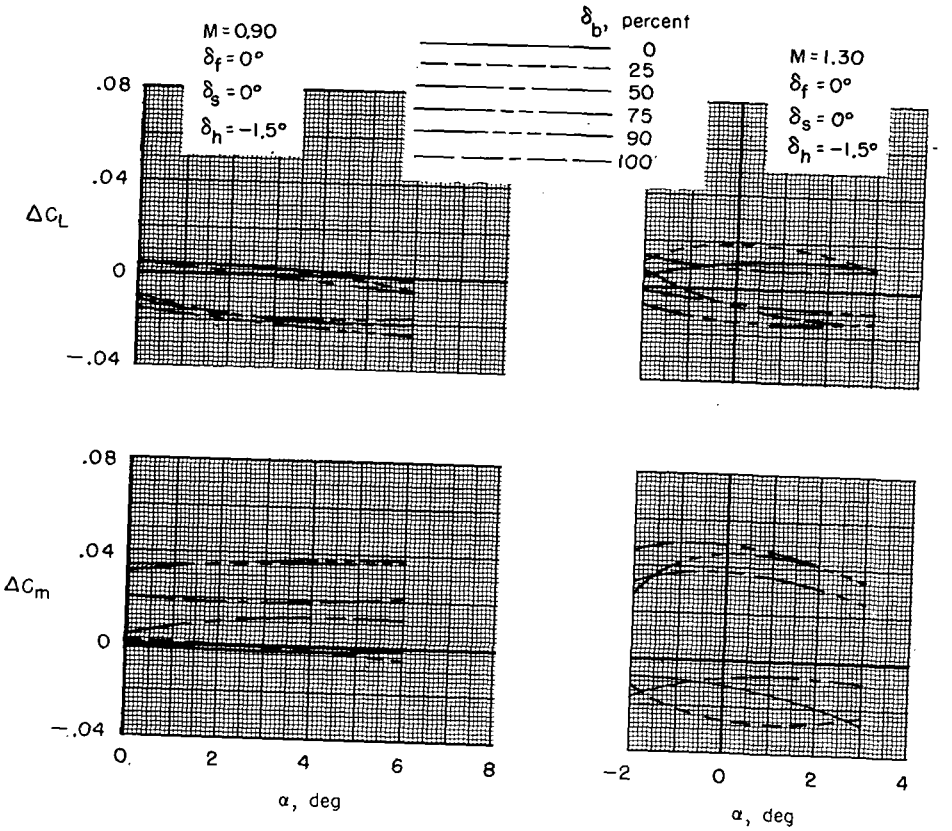

(c) M = 0.90 and 1.30.

Figure 45.- Concluded.

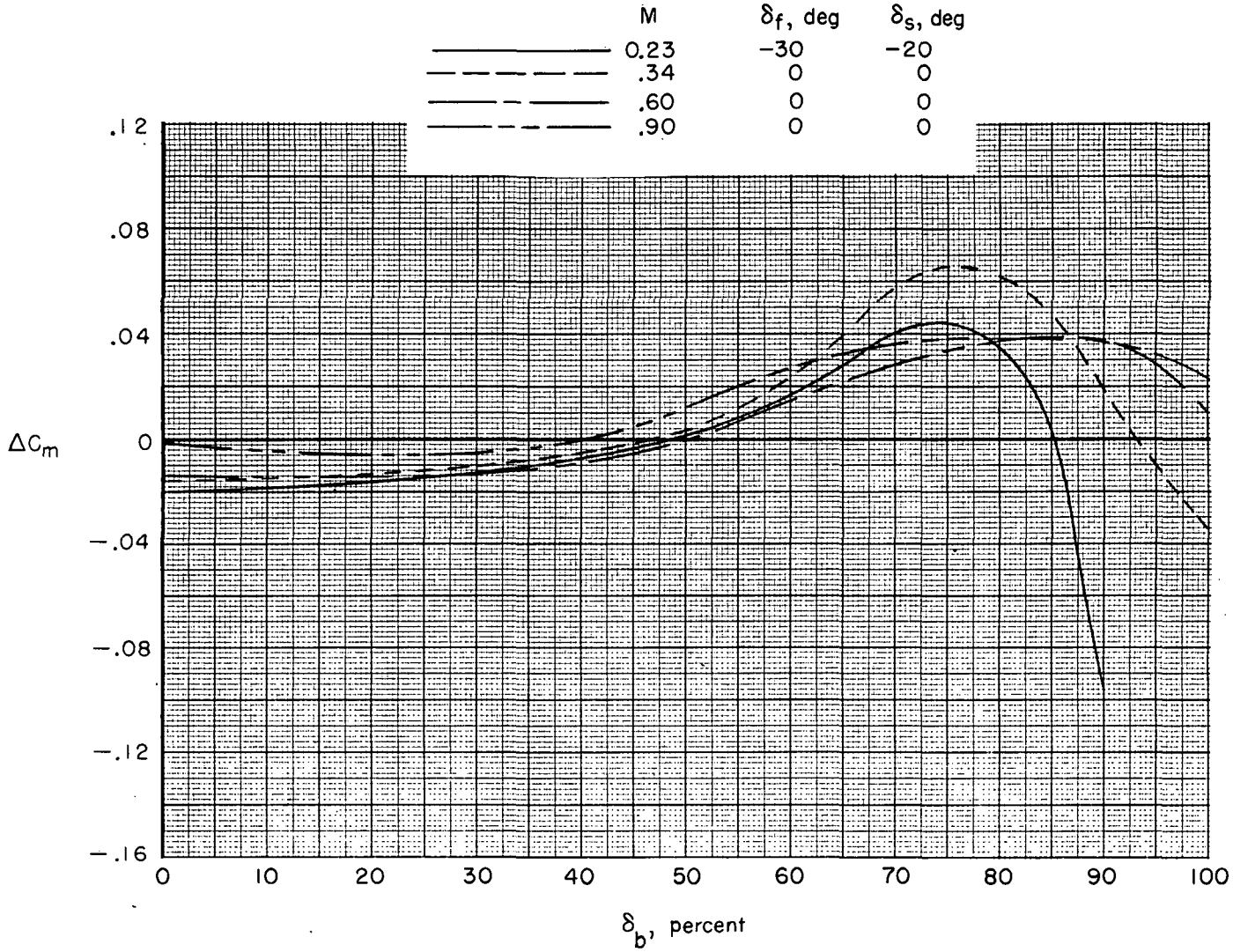

(a) $\alpha = 6^o$.

Figure 46.- Summary of effects of blocker-door deployment on pitching-moment increment for several Mach numbers. $\beta = 0^o$; $\delta_t = -1.5^o$; $\delta_r = 0^o$; $\delta_{du} = 32.5^o$; $\delta_{dl} = 52.5^o$; and military power.

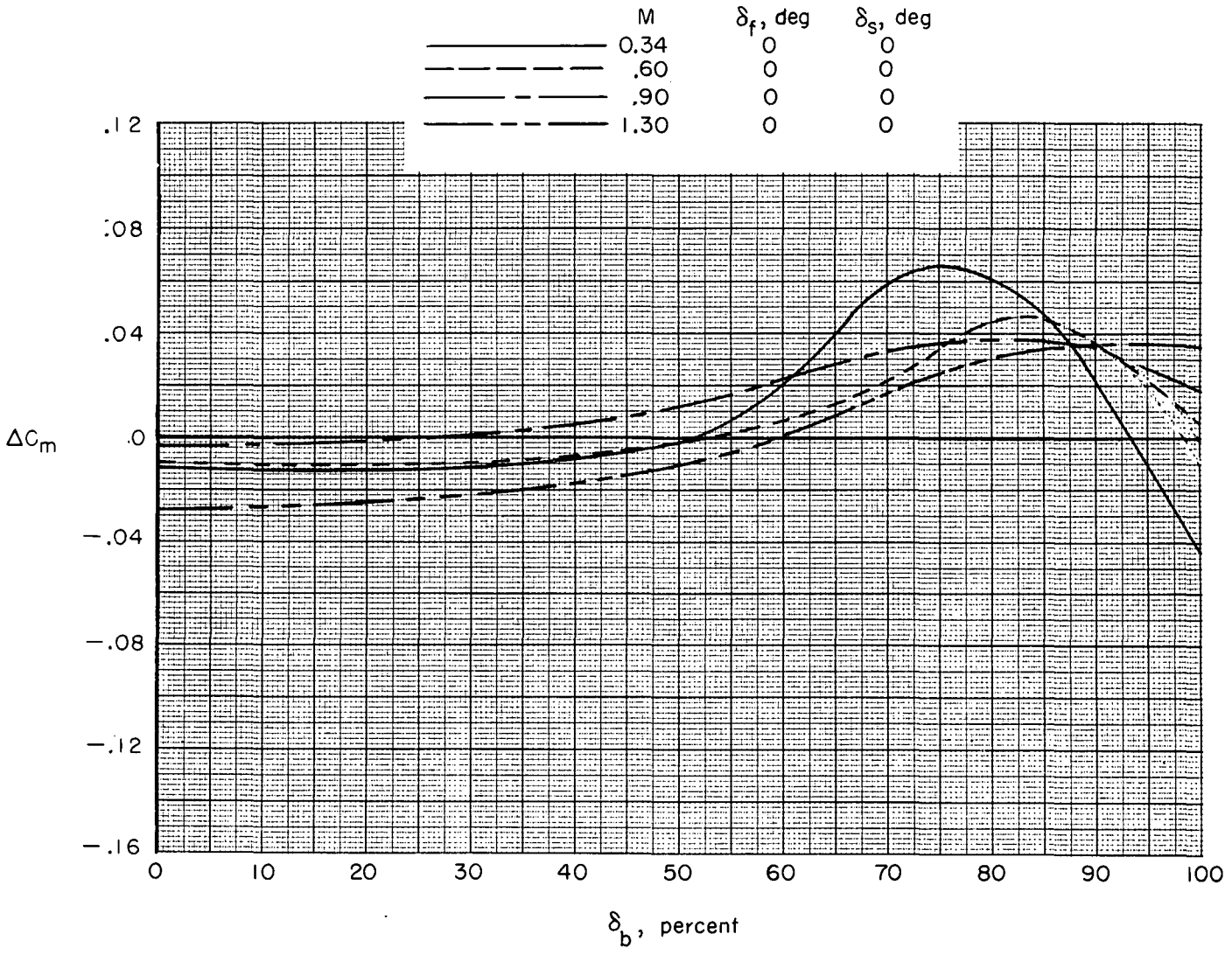

(b) $\alpha = 3^o$.

Figure 46.- Concluded.

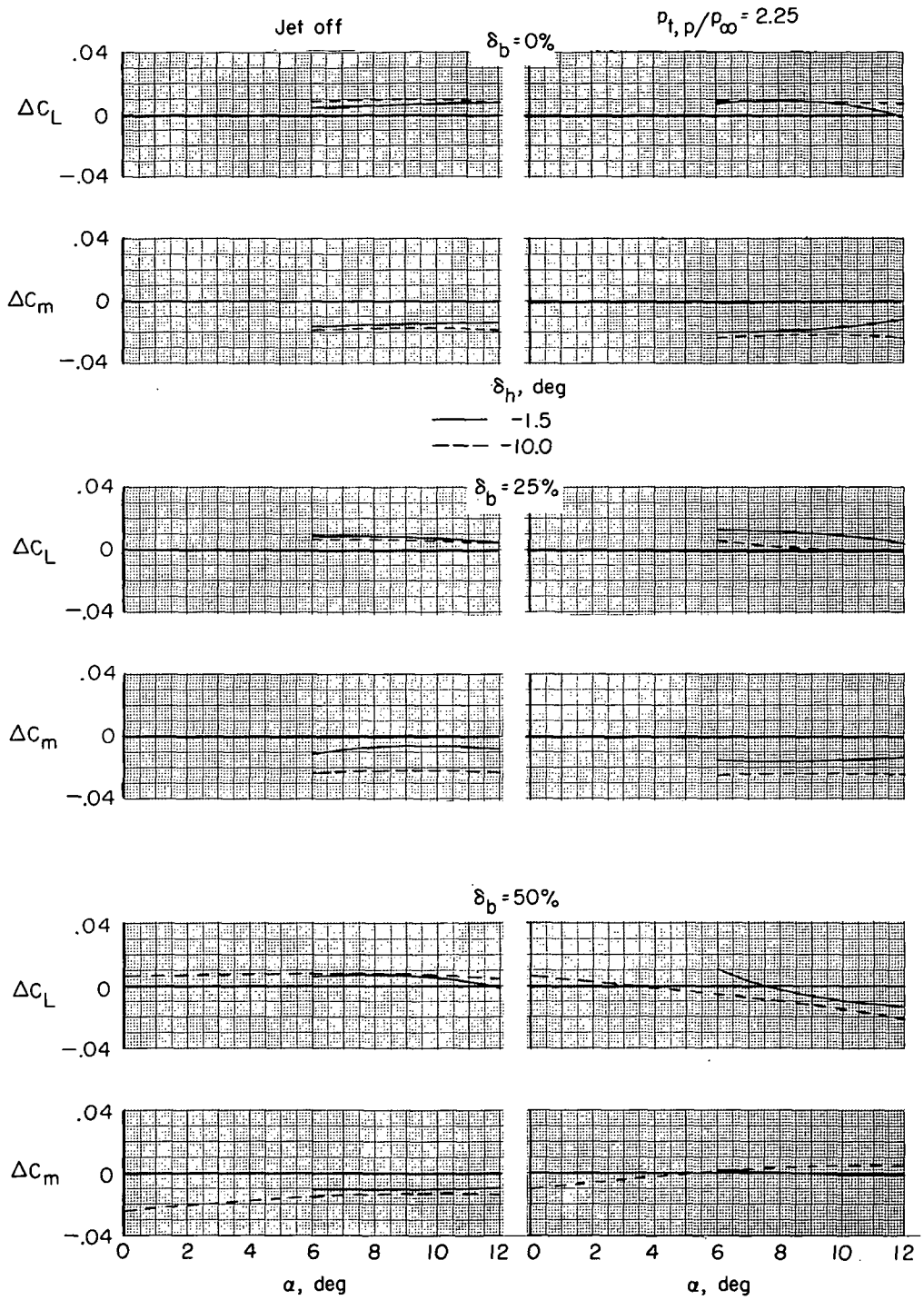

(a) M = 0.23; $\delta_f = -30^o$; $\delta_s = -20^o$.

Figure 47.- Effect of horizontal-tail deployment on incremental lift and pitching-moment coefficients of model with TCU (reverse-thrust mode) for various angles of attack. $\beta = 0^o$; $\delta_{du} = 32.5^o$; $\delta_{dl} = 52.5^o$; $\delta_r = 0^o$; and military power.

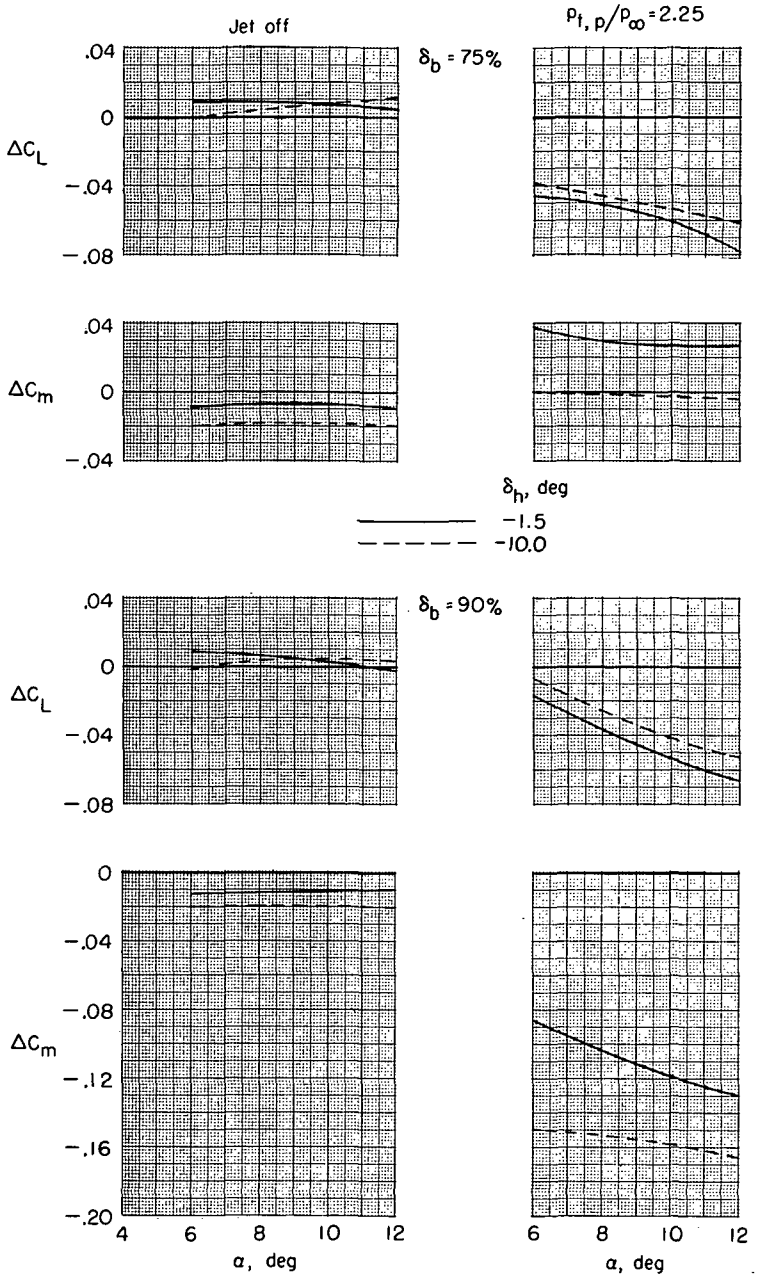

(b) M = 0.23; $\delta_f = -30^o$; $\delta_S = -20^o$.

Figure 47.- Continued.

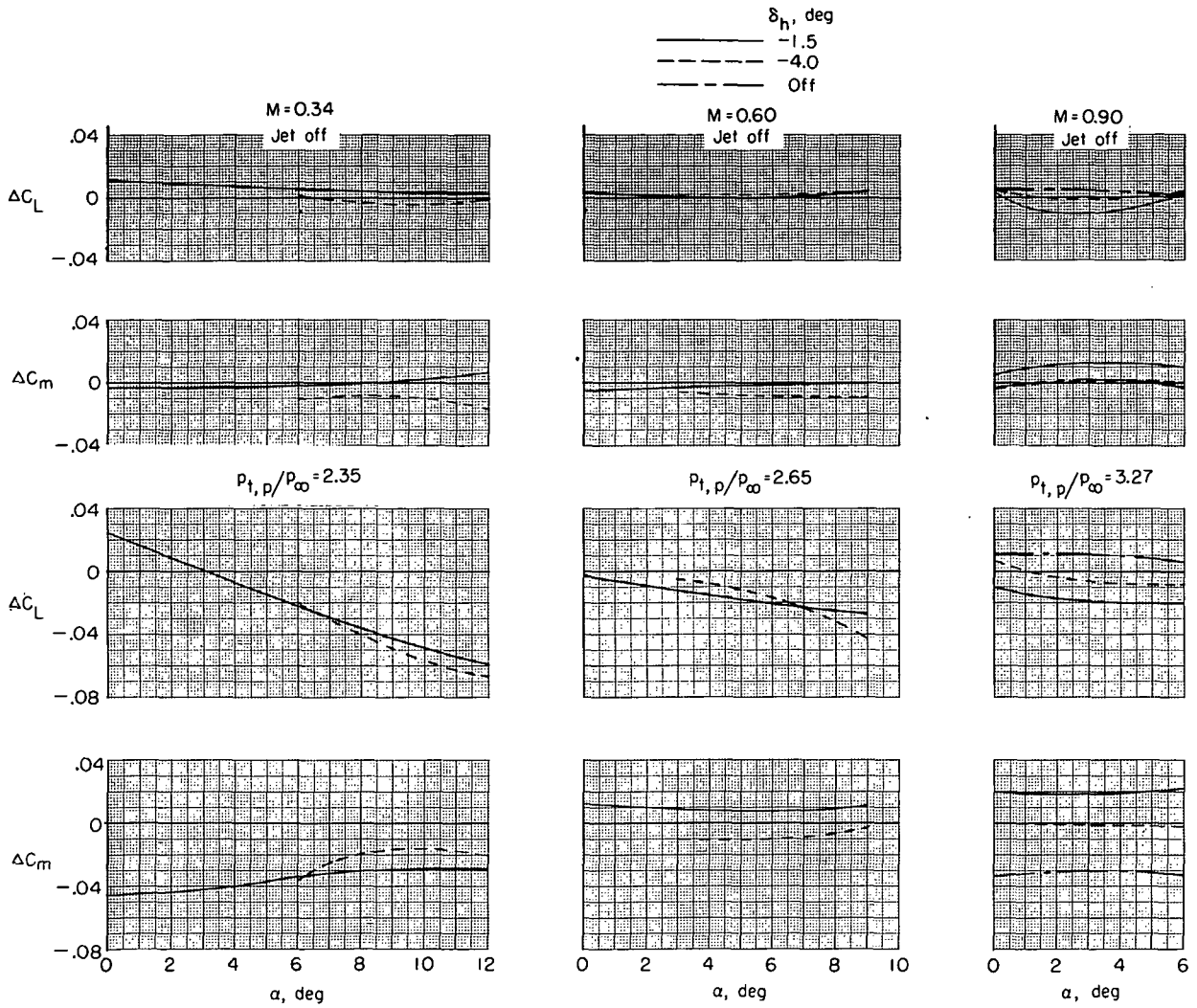

(c) M = 0.34 to 0.90; $\delta_f = 0^o$; $\delta_s = 0^o$.

Figure 47.- Concluded.

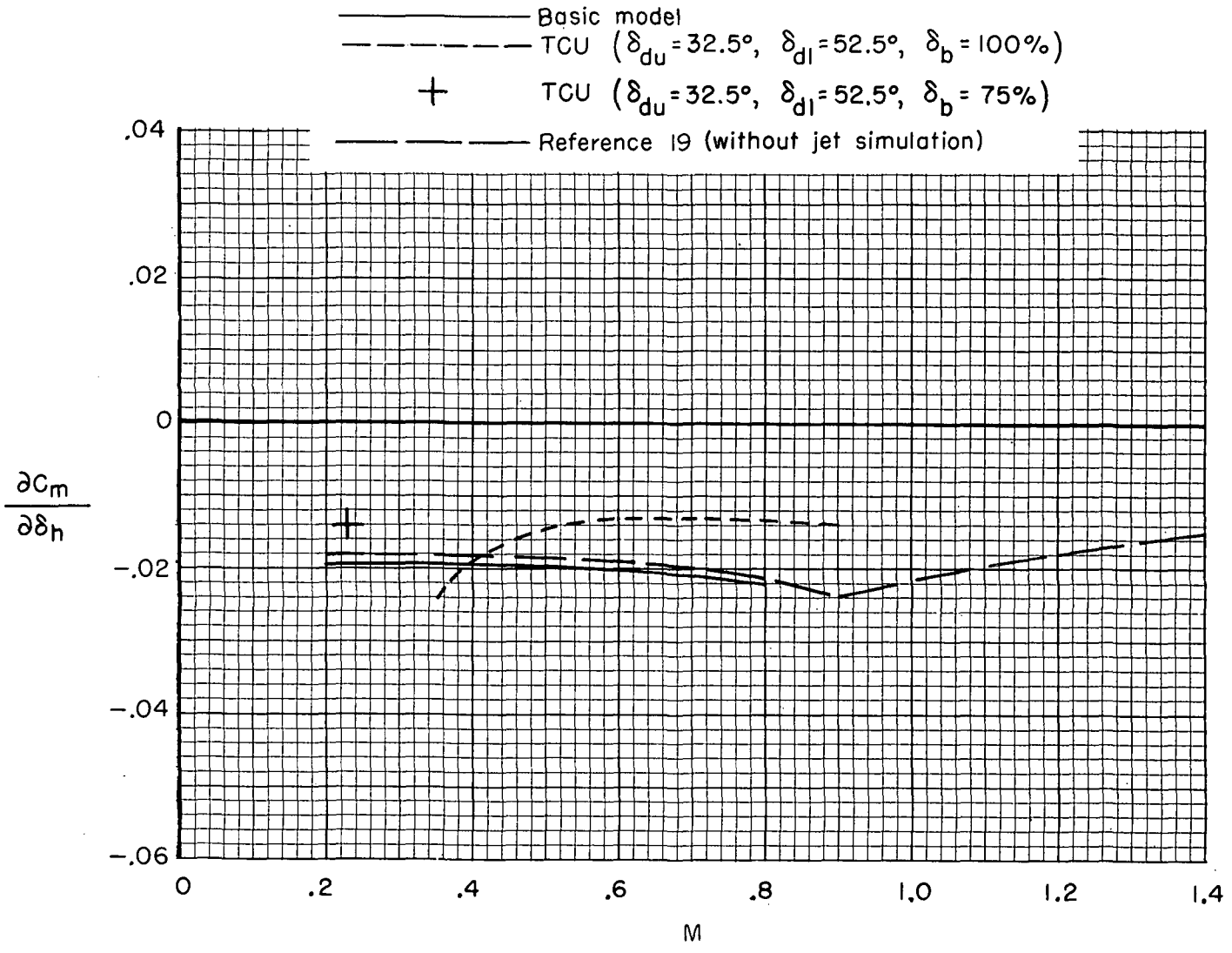

Figure 48.- Stabilizer effectiveness of basic model and TCU (reverse-thrust mode) for Mach range and at scheduled jet-total-pressure ratios. Military power.

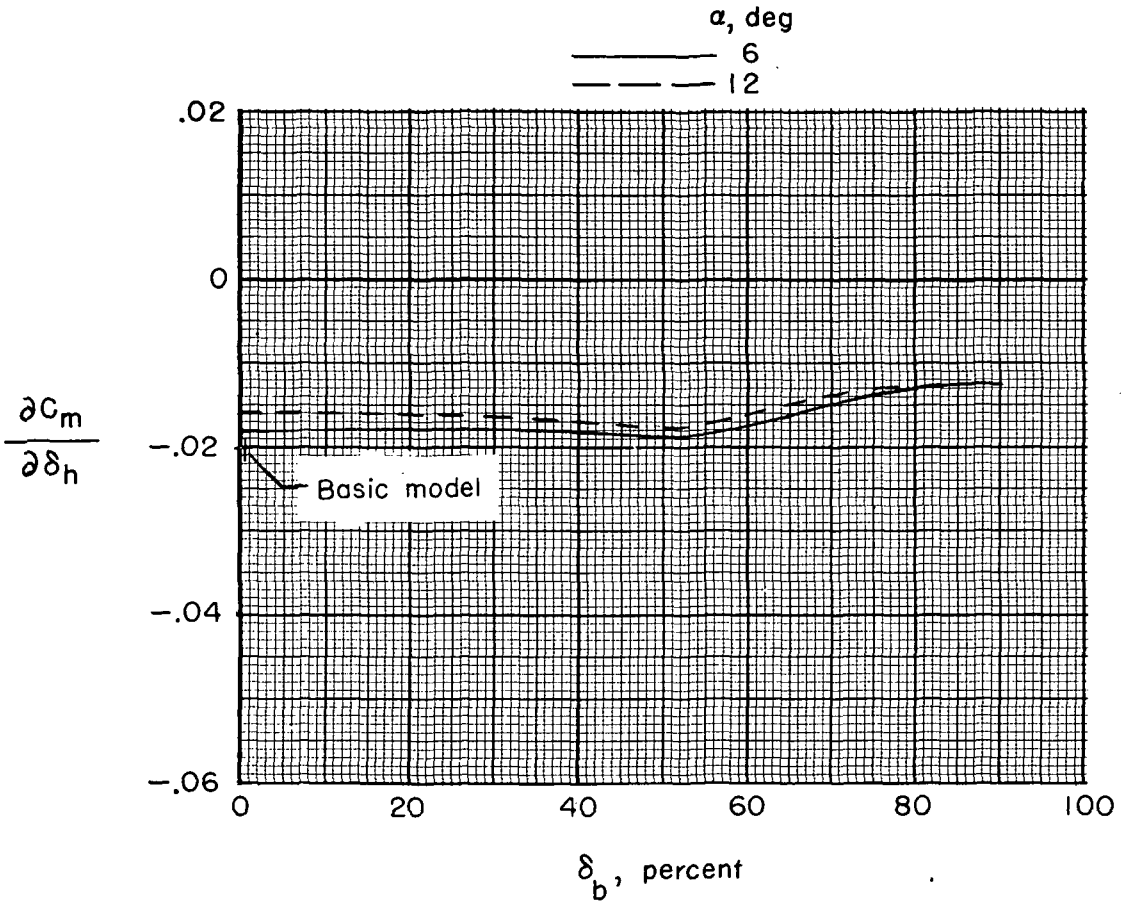

Figure 49.- Effect of blocker-door closure on stabilizer effectiveness. $M = 0.23$; $\beta = 0^{o}$; $\delta_f = -30^{o}$; $\delta_s = -20^{o}$; $\delta_r = 0^{o}$; $\delta_{du} = 32.5^{o}$; $\delta_{dl} = 52.5^{o}$; and military power.

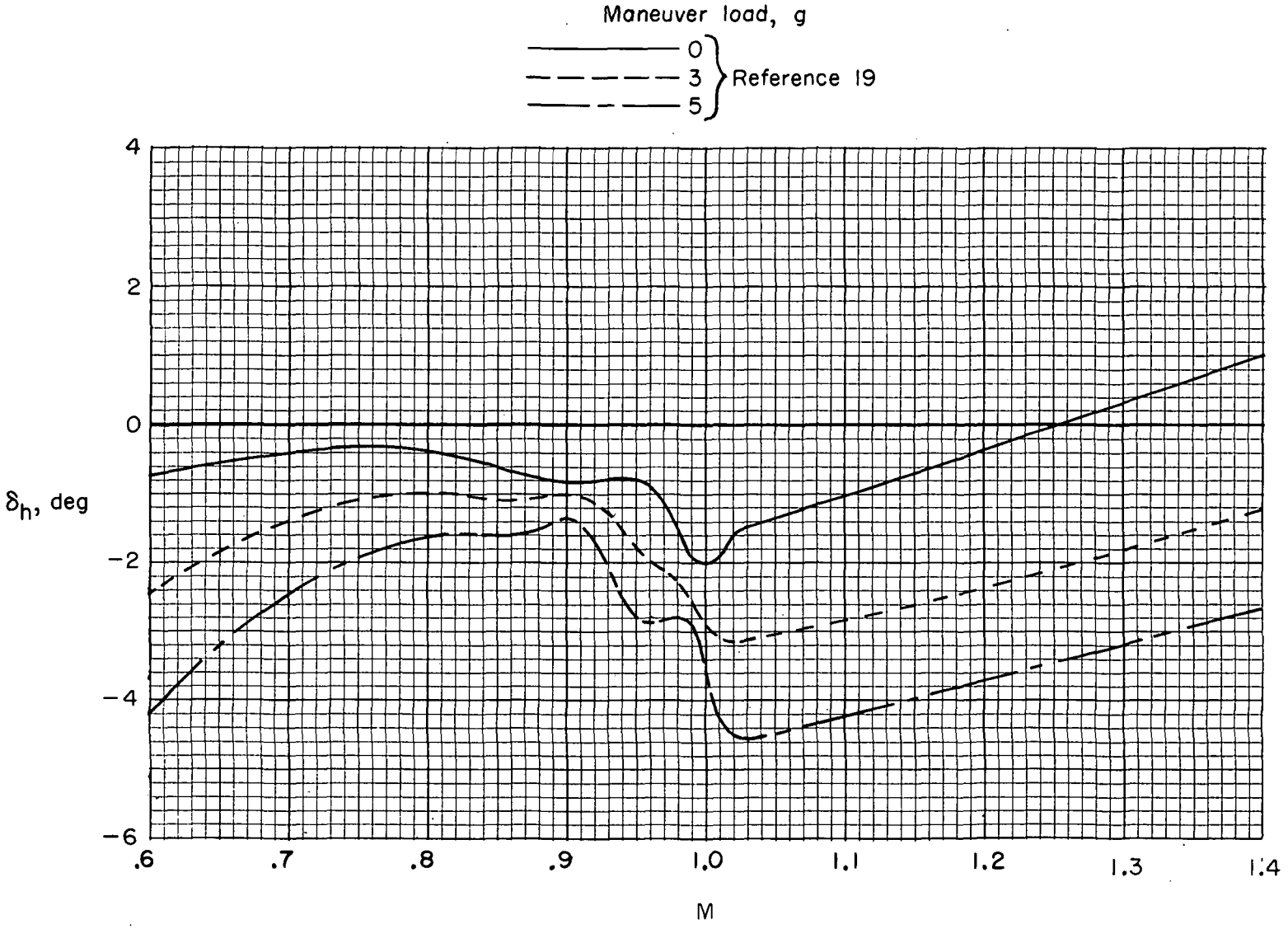

Figure 50.- Schedule of acceleration forces due to horizontal-tail deflection for basic airplane from reference 19.

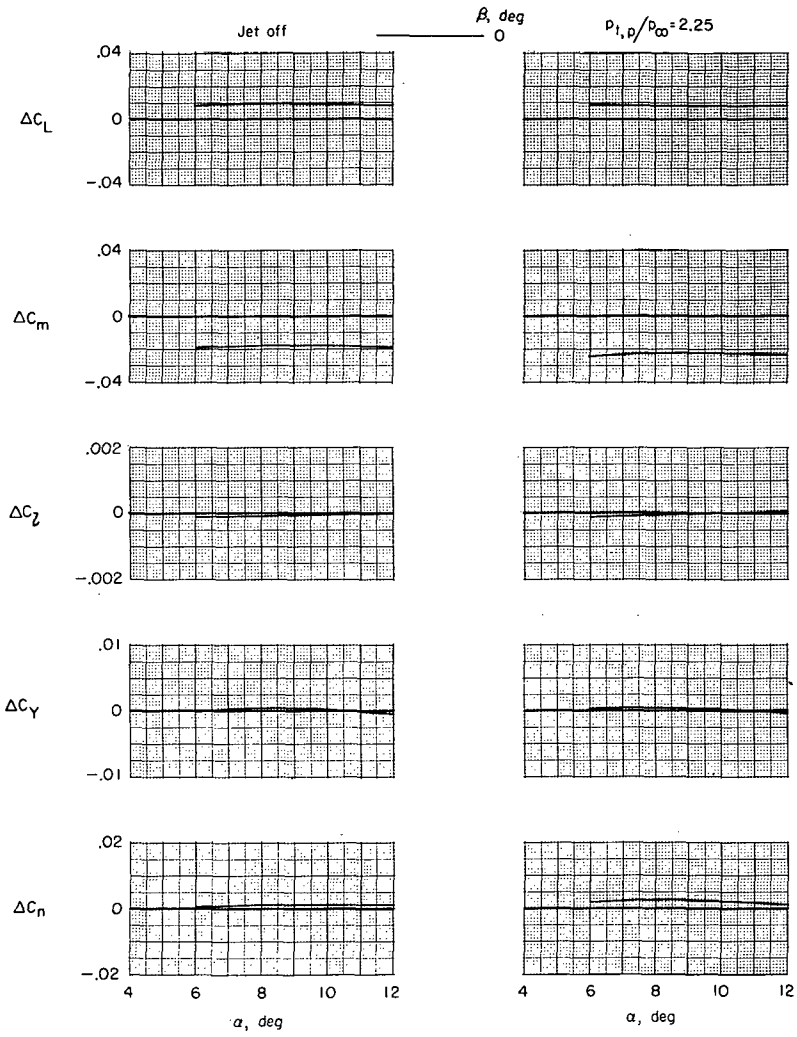

(a) M = 0.23; $\delta_f = -30^o$; $\delta_s = -20^o$; $\delta_h = -10^o$; $\delta_b = 0$ percent.

Figure 51.- Effect of angle of attack on incremental aerodynamic characteristics of model with TCU for several angles of sideslip. $\delta_r = 0^o$; $\delta_{du} = 32.5^o$; $\delta_{dl} = 52.5^o$; and military power.

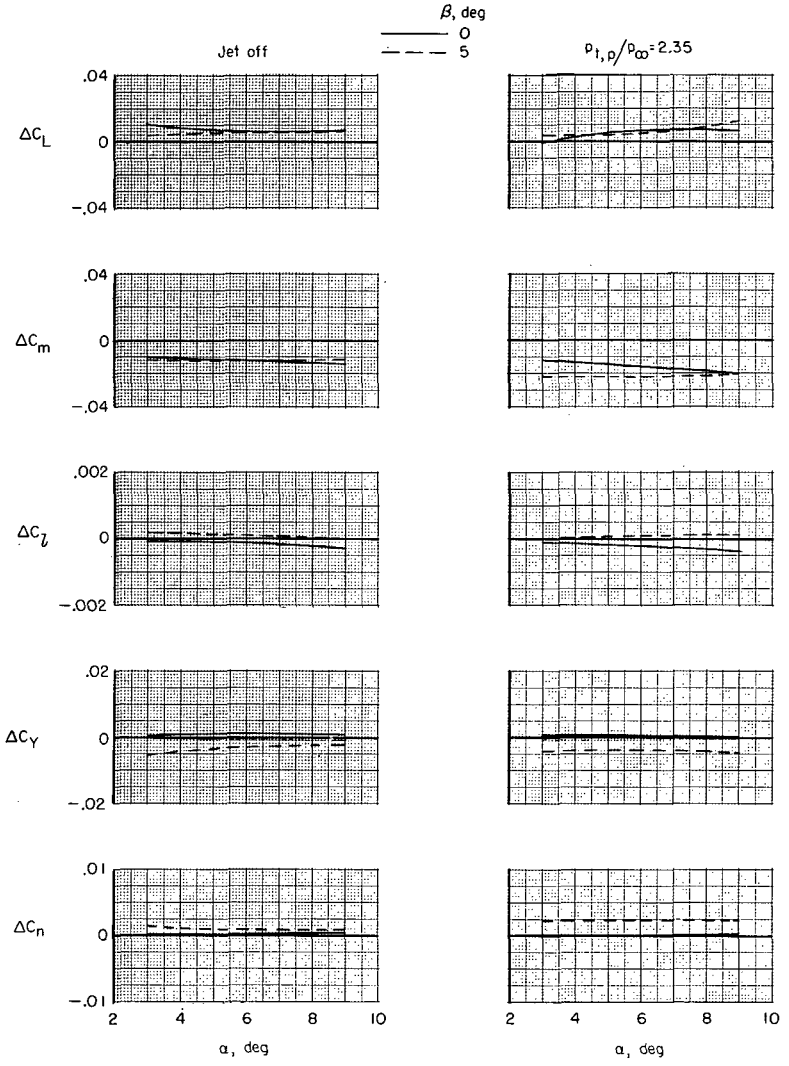

(b) M = 0.34; $\delta_f = 0^o$; $\delta_s = 0^o$; $\delta_h = -1.5^o$; δ_b = 0 percent.

Figure 51.- Continued.

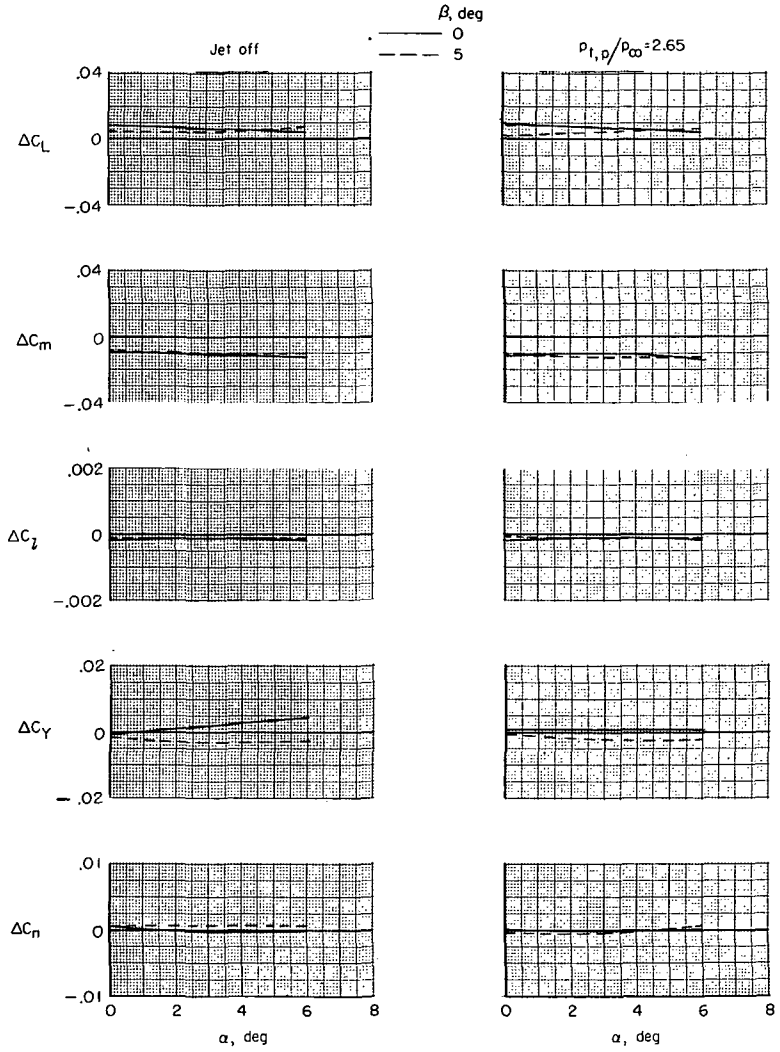

(c) M = 0.60; $\delta_f = 0^o$; $\delta_s = 0^o$; $\delta_h = -1.5^o$; $\delta_b = 0$ percent.

Figure 51.- Continued.

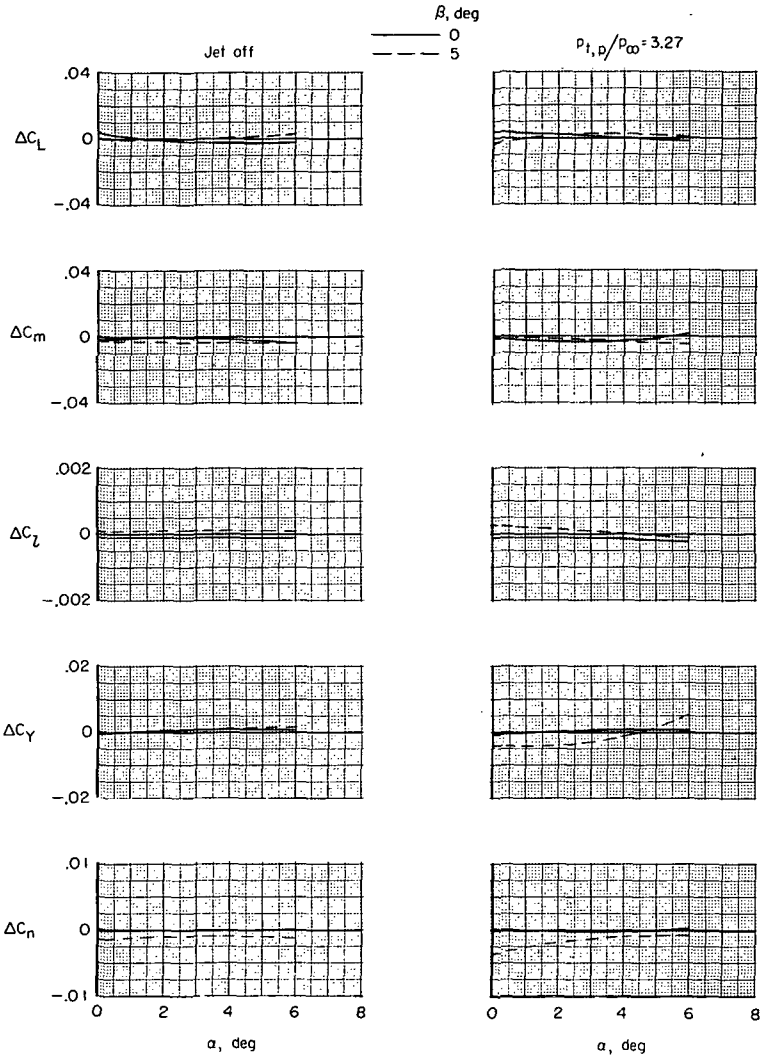

(d) M = 0.90; $\delta_f = 0^o$; $\delta_s = 0^o$; $\delta_h = -1.5^o$; $\delta_b = 0$ percent.

Figure 51.- Continued.

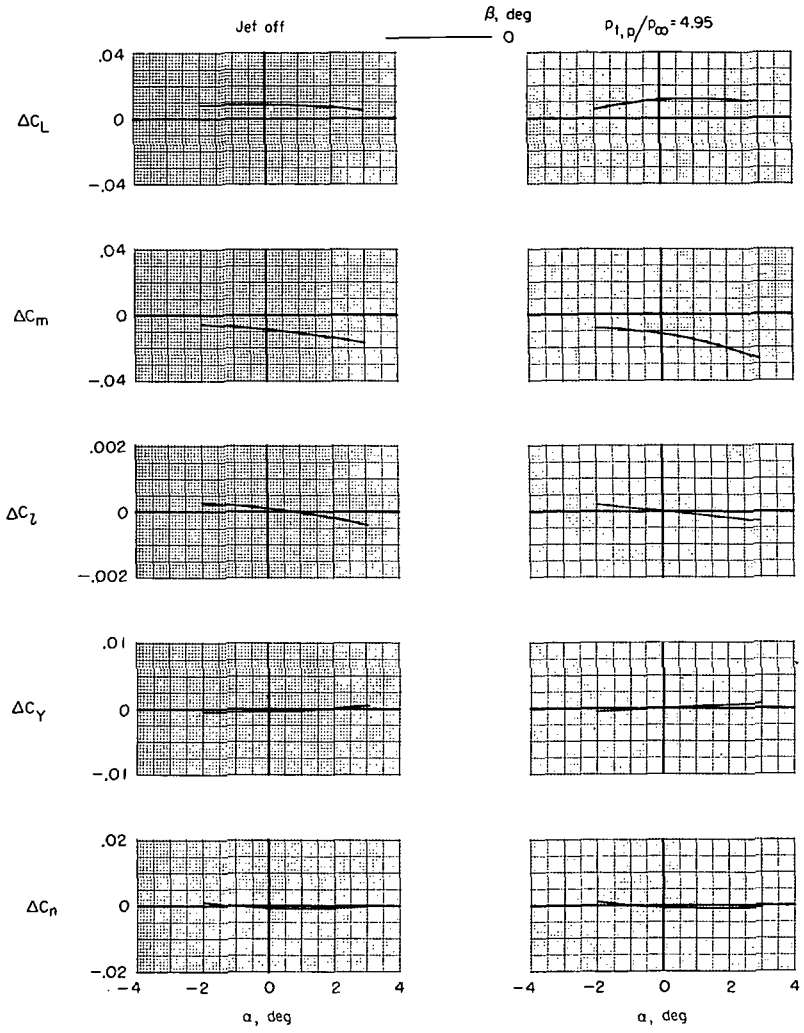

(e) M = 1.30; $\delta_f = 0^o$; $\delta_s = 0^o$; $\delta_h = -1.5^o$; $\delta_b = 0$ percent.

Figure 51.- Continued.

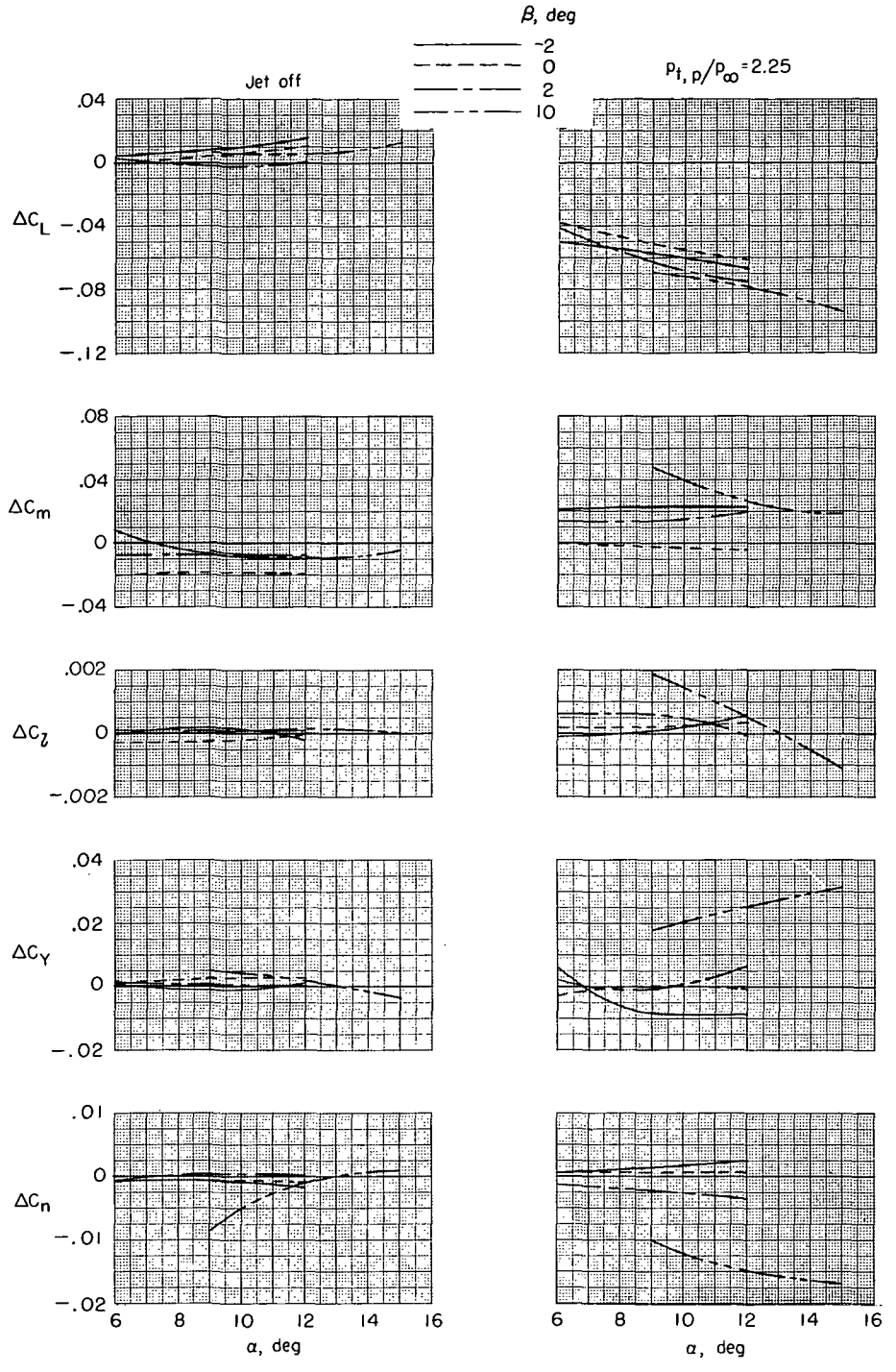

(f) M = 0.23; $\delta_f = -30^o$; $\delta_s = -20^o$; $\delta_h = -10^o$; δ_b = 75 percent.

Figure 51.- Continued.

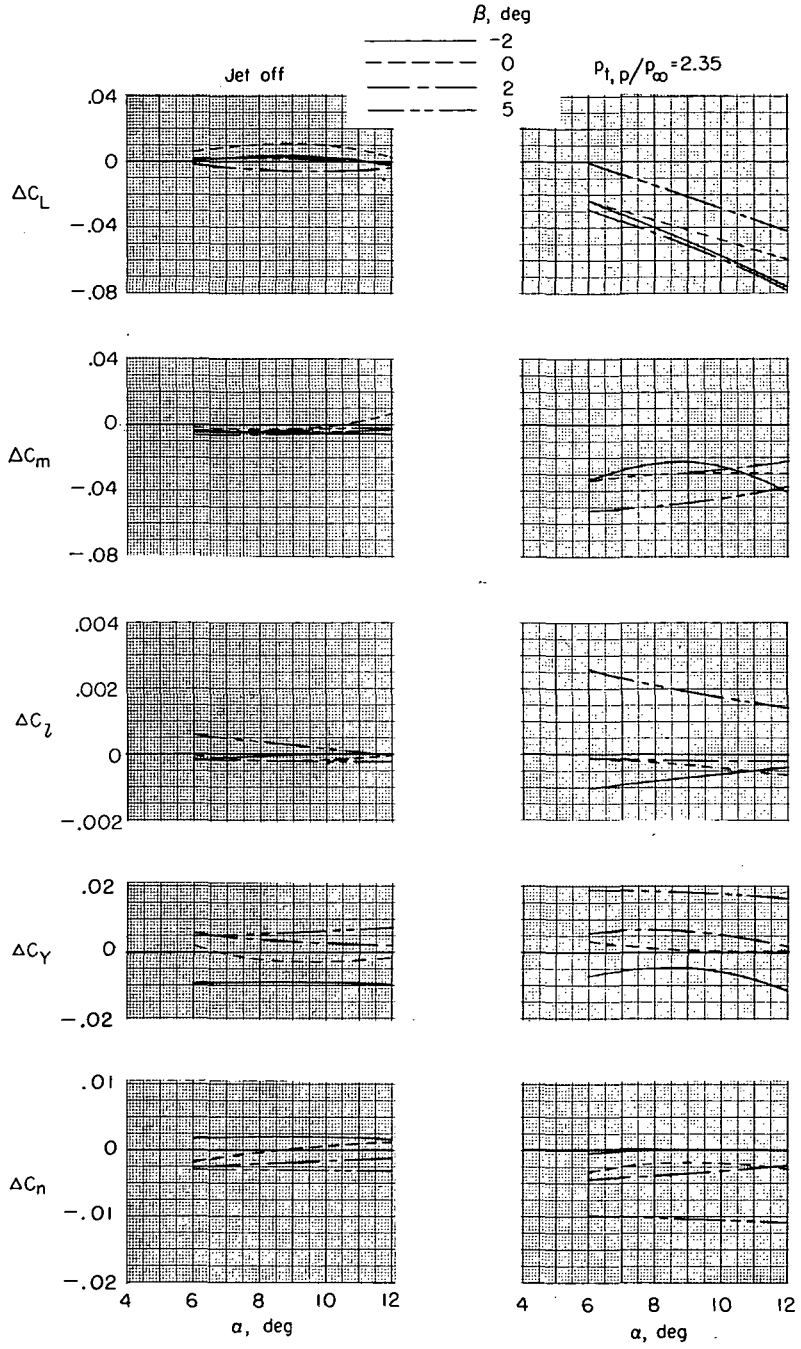

(g) M = 0.34; $\delta_f = 0^o$; $\delta_s = 0^o$; $\delta_h = -1.5^o$; δ_b = 100 percent.

Figure 51.- Continued.

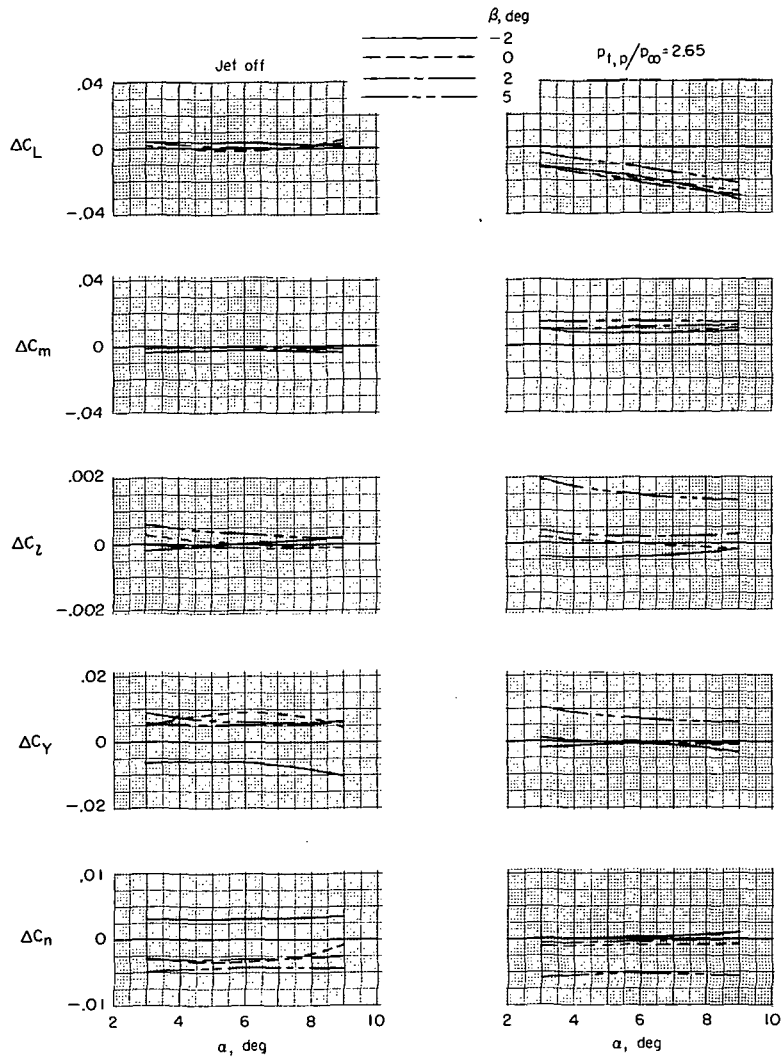

(h) M = 0.60; $\delta_f = 0^o$; $\delta_s = 0^o$; $\delta_h = -1.5^o$; δ_b = 100 percent.

Figure 51.- Continued.

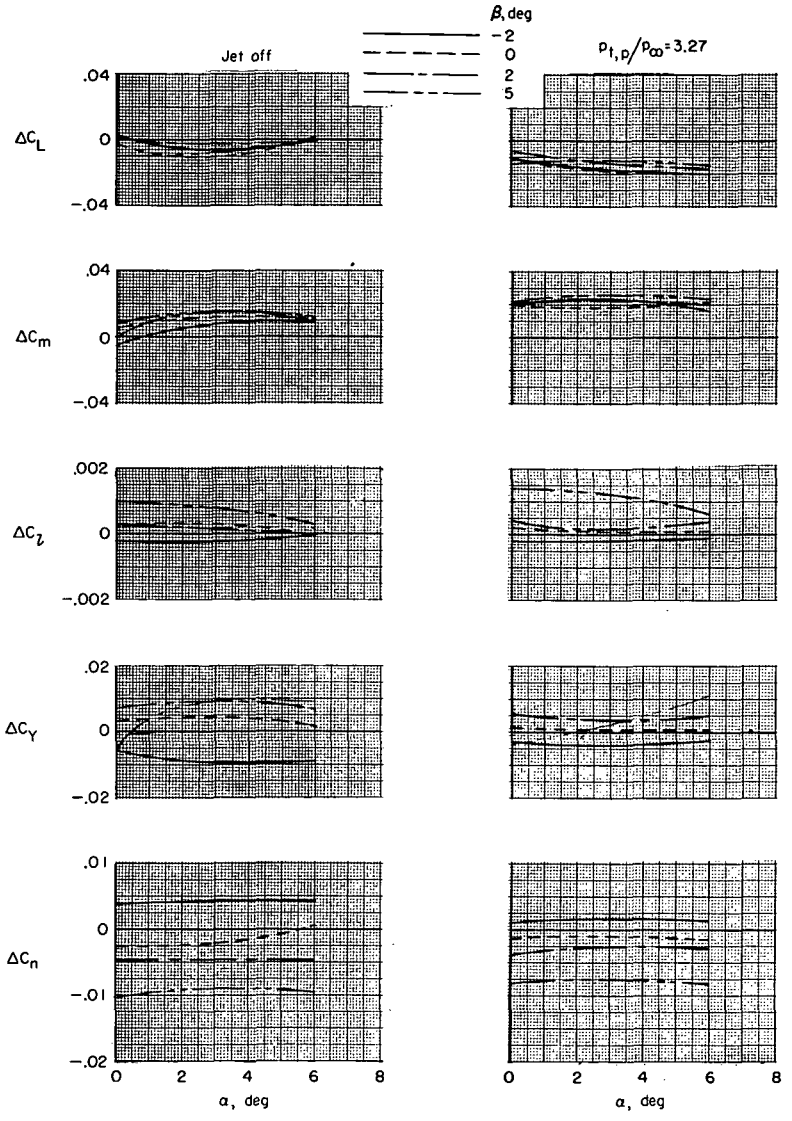

(i) M = 0.90; $\delta_f = 0^o$; $\delta_s = 0^o$; $\delta_h = -1.5^o$; δ_b = 100 percent.

Figure 51.- Continued.

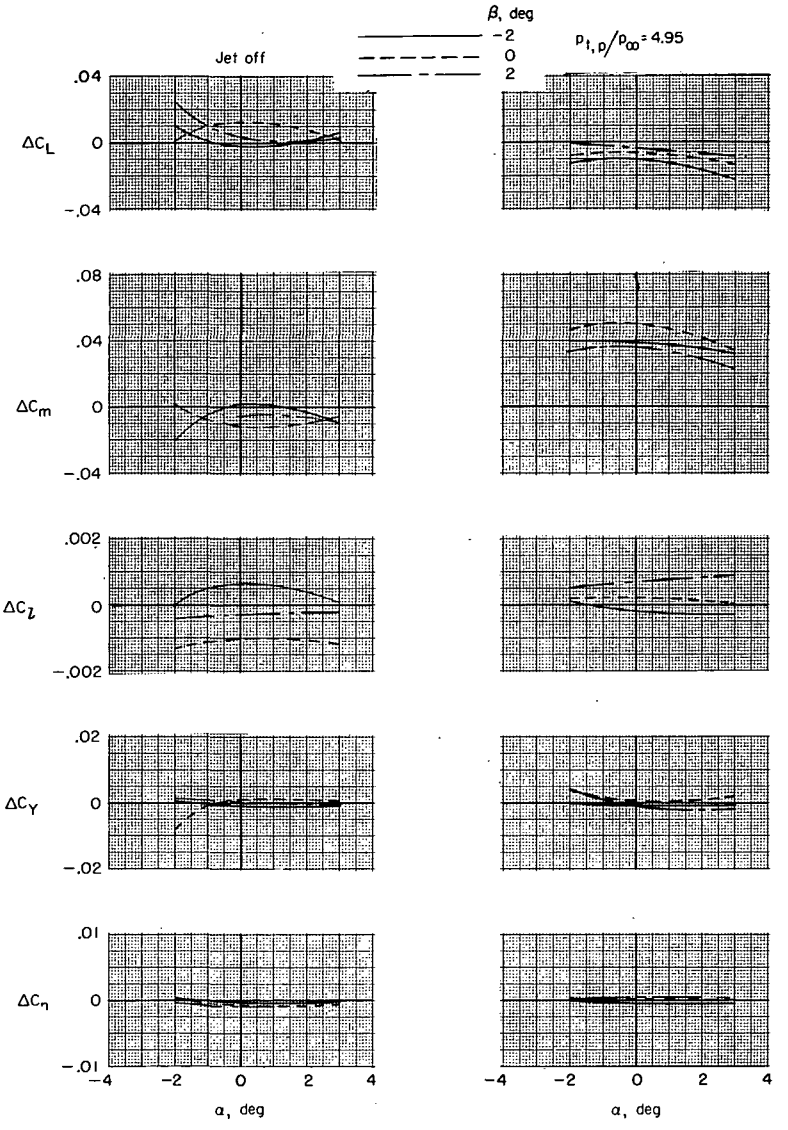

(j) M = 1.30; $\delta_f = 0^o$; $\delta_s = 0^o$; $\delta_h = -1.5^o$; δ_b = 100 percent.

Figure 51.- Concluded.

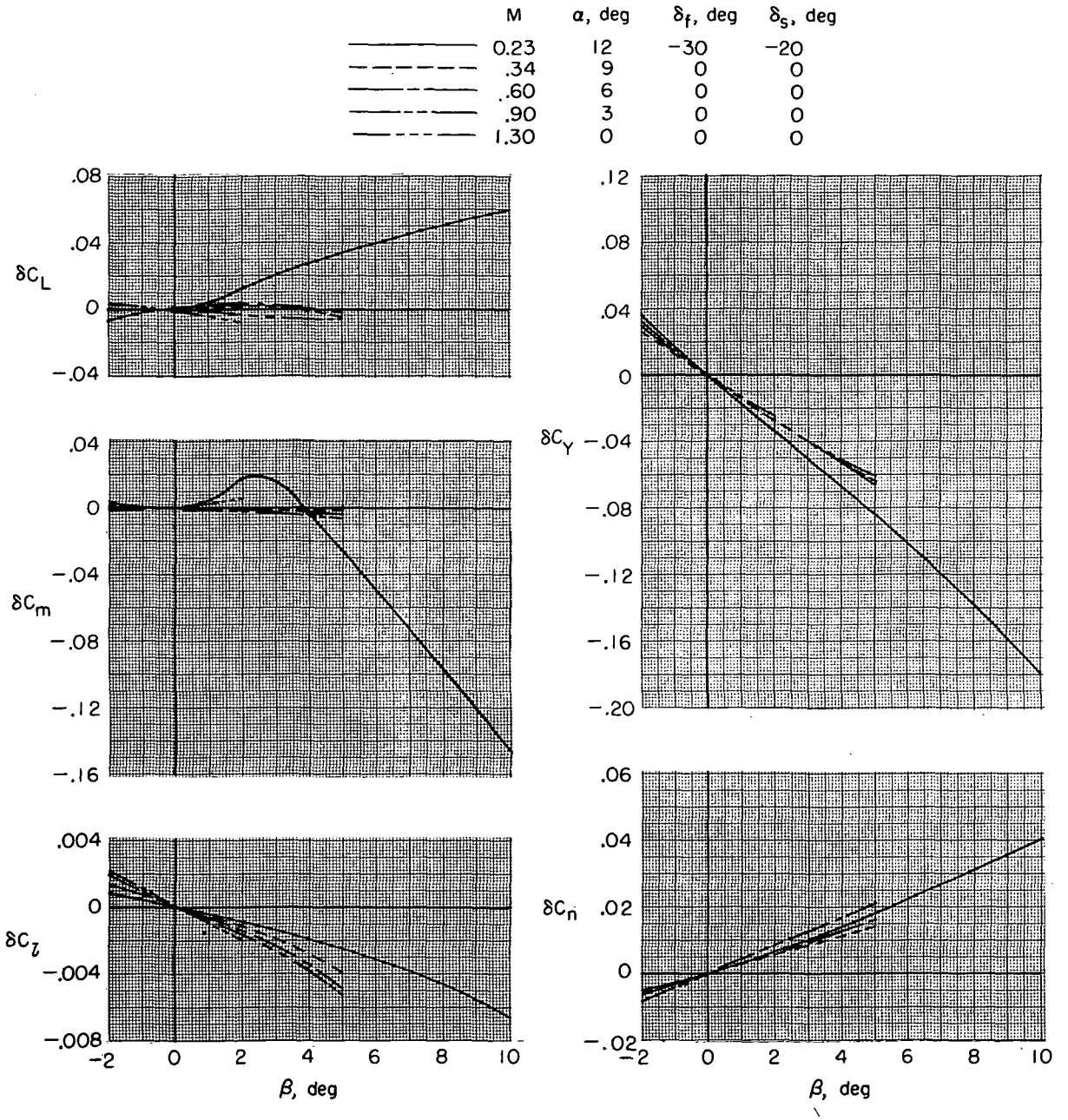

(a) Basic model.

Figure 52.- Variation of adjusted incremental aerodynamic characteristics with angle of sideslip for several Mach numbers at scheduled jet-total-pressure ratio. $\delta_t = 0^o$; $\delta_r = 0^o$; and military power.

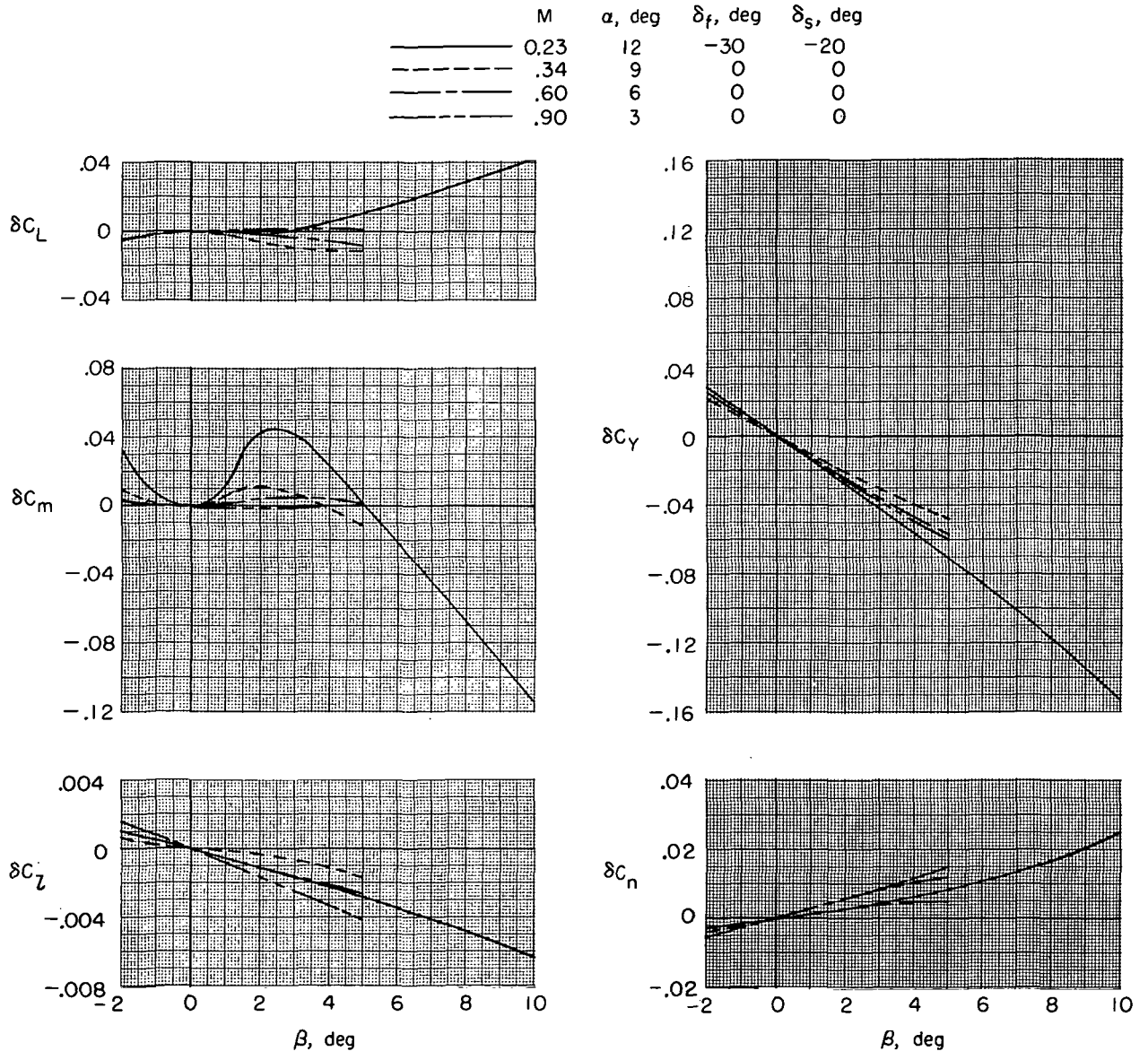

(b) TCU; $\delta_{du} = 32.5^{o}$; $\delta_{dl} = 52.5^{o}$; $\delta_{b} = 100$ percent.

Figure 52.- Concluded.

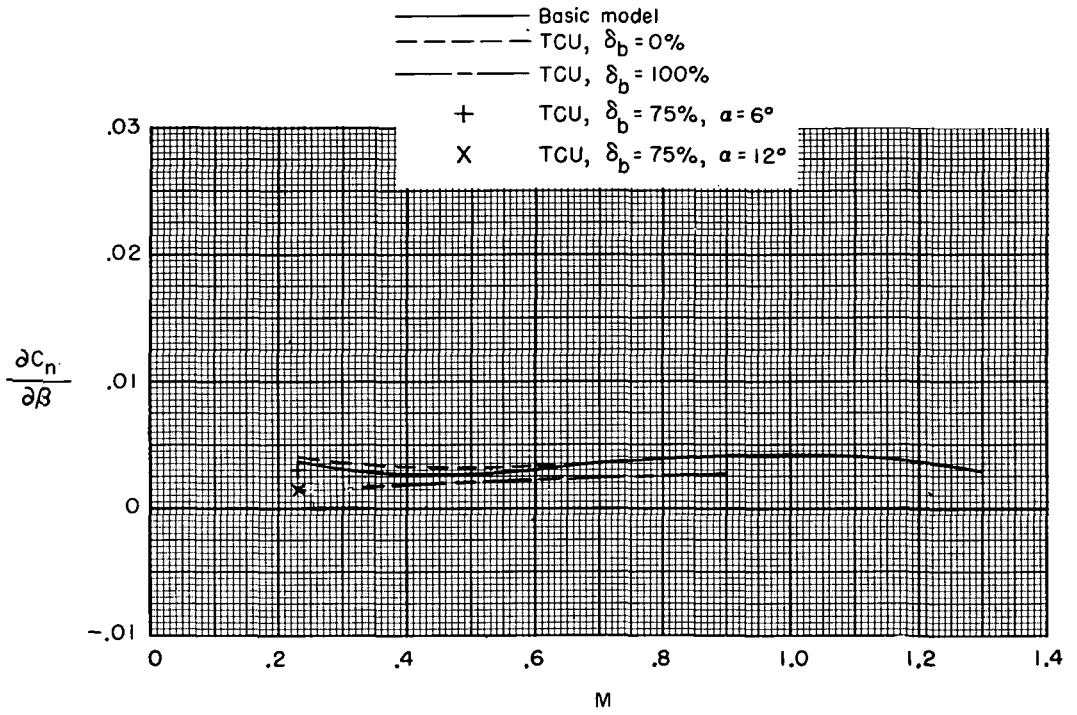

(a) Yawing moment.

Figure 53.- Directional stability derivatives for basic model and TCU (reverse-thrust mode). $\delta_{du} = 32.5^{o}$; $\delta_{dl} = 52.5^{o}$; and military power.

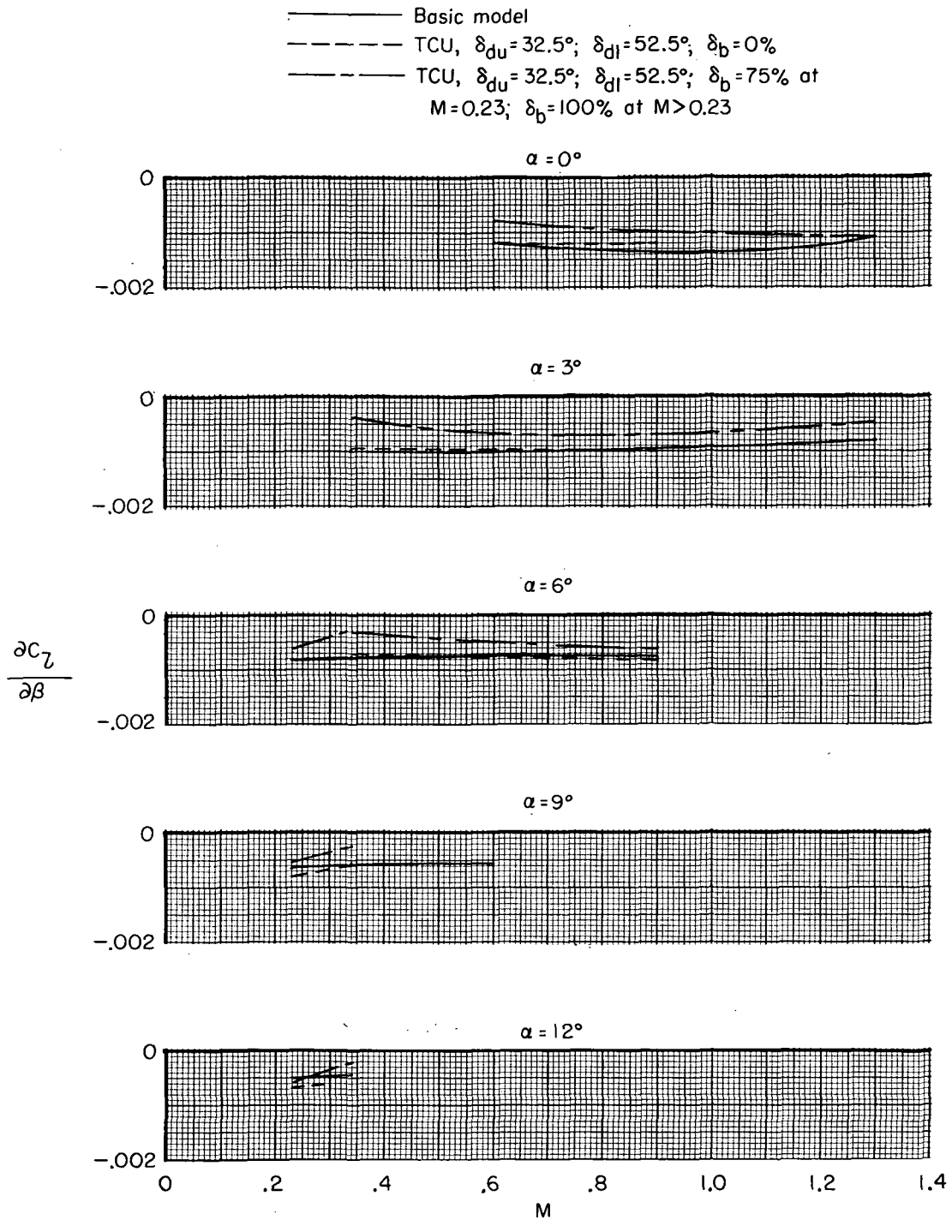

(b) Rolling-moment derivative.

Figure 53.- Concluded.

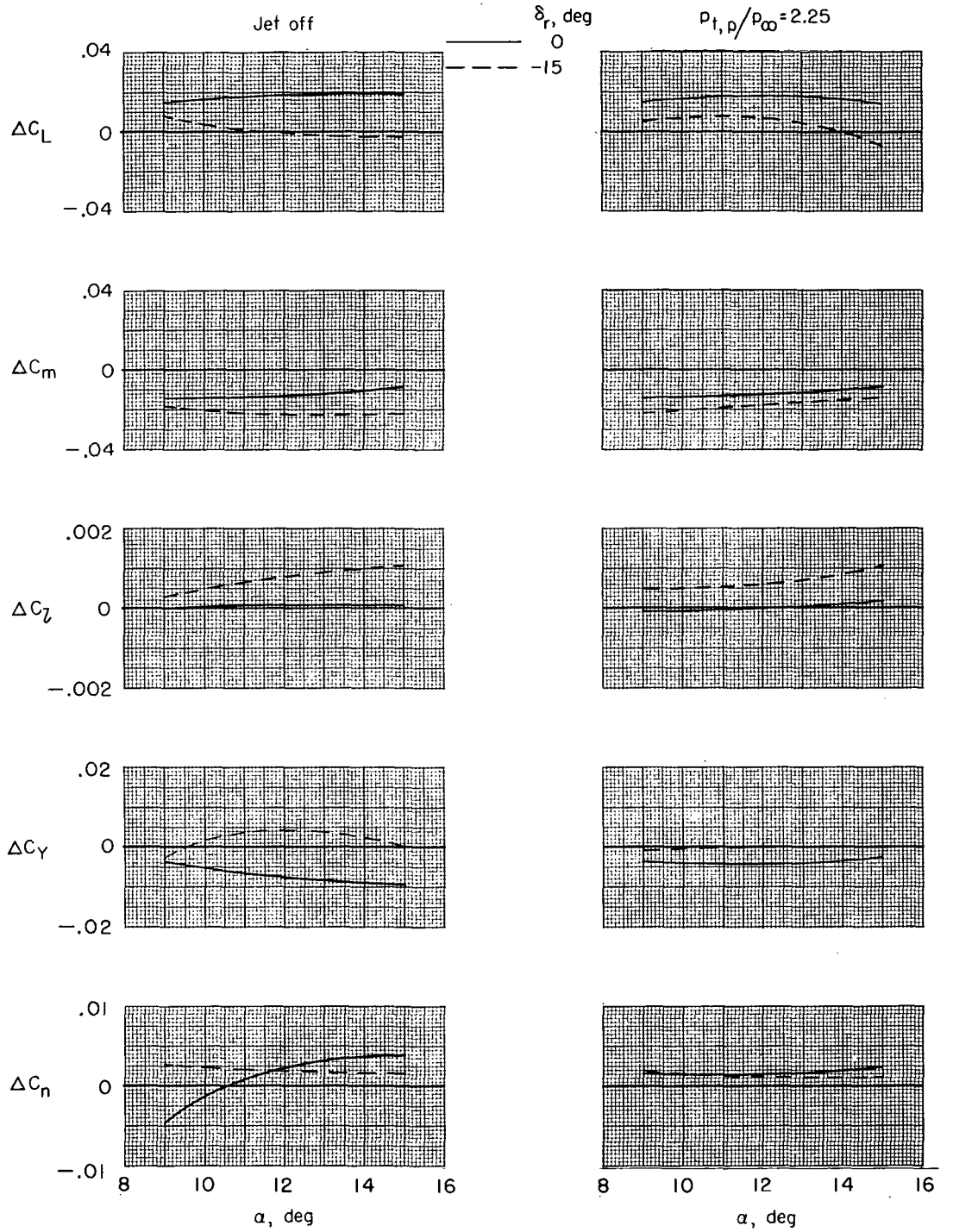

(a) M = 0.23; $\beta = 10^o$; $\delta_f = -30^o$; $\delta_s = -20^o$; $\delta_h = -10^o$.

Figure 54.- Effect of angle of attack on incremental aerodynamic characteristics of TCU for various rudder deflections. $\delta_{du} = 32.5^o$; $\delta_{dl} = 52.5^o$; $\delta_b = 0$ percent; and military power.

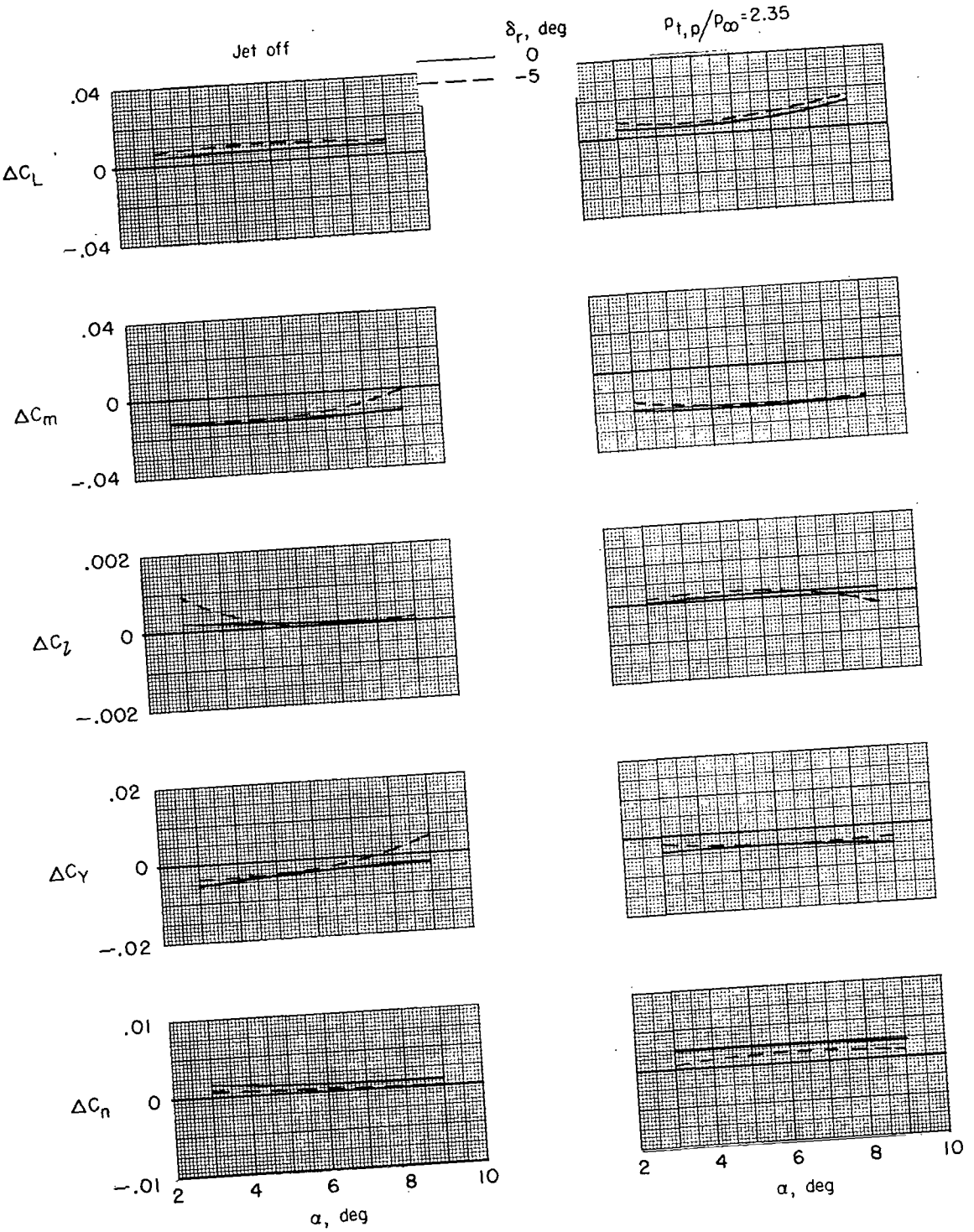

(b) M = 0.34; $\beta = 5^o$; $\delta_f = 0^o$; $\delta_s = 0^o$; $\delta_h = -1.5^o$.

Figure 54.- Continued.

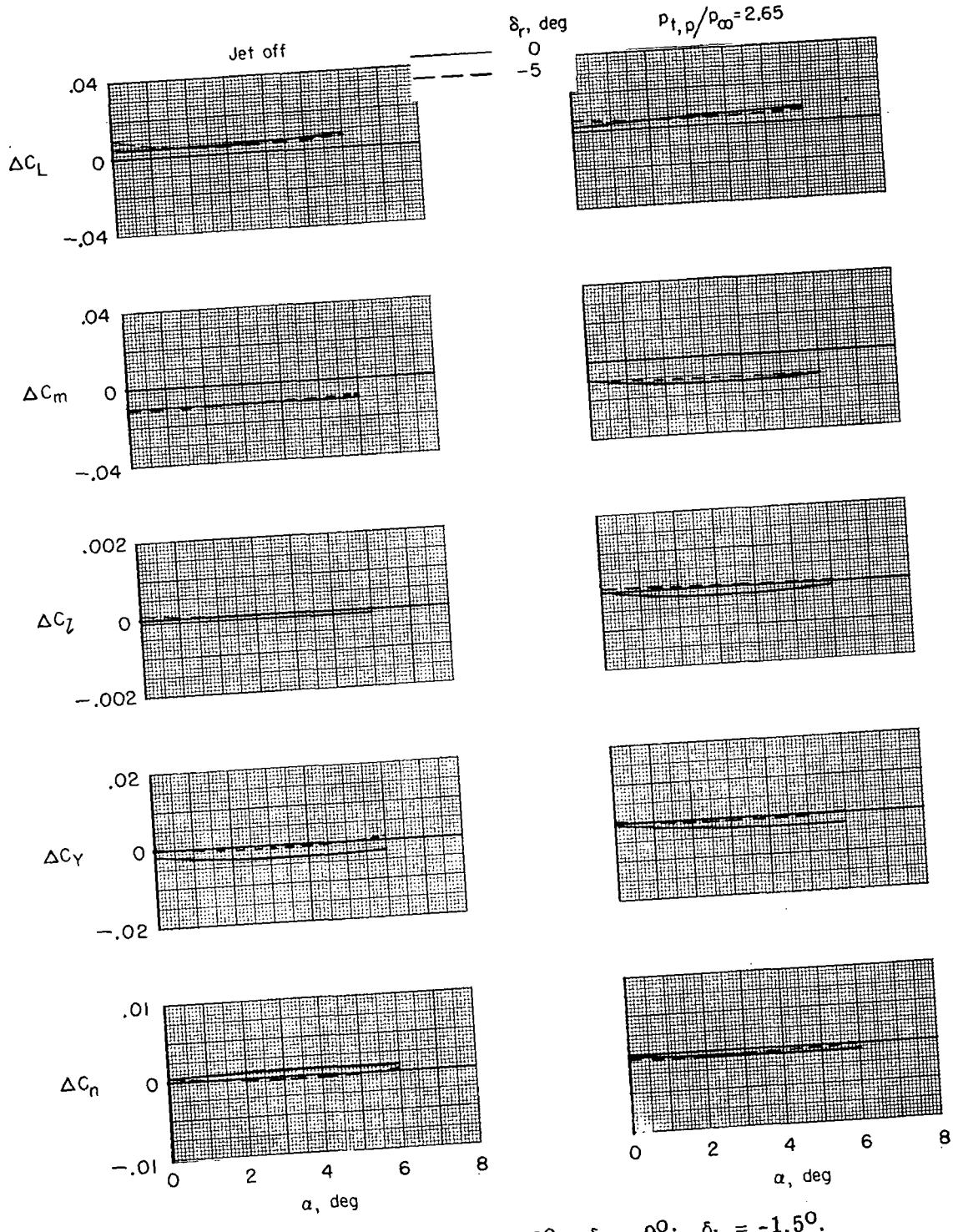

(c) M = 0.60; $\beta = 5^o$; $\delta_f = 0^o$; $\delta_s = 0^o$; $\delta_h = -1.5^o$.

Figure 54.- Concluded.

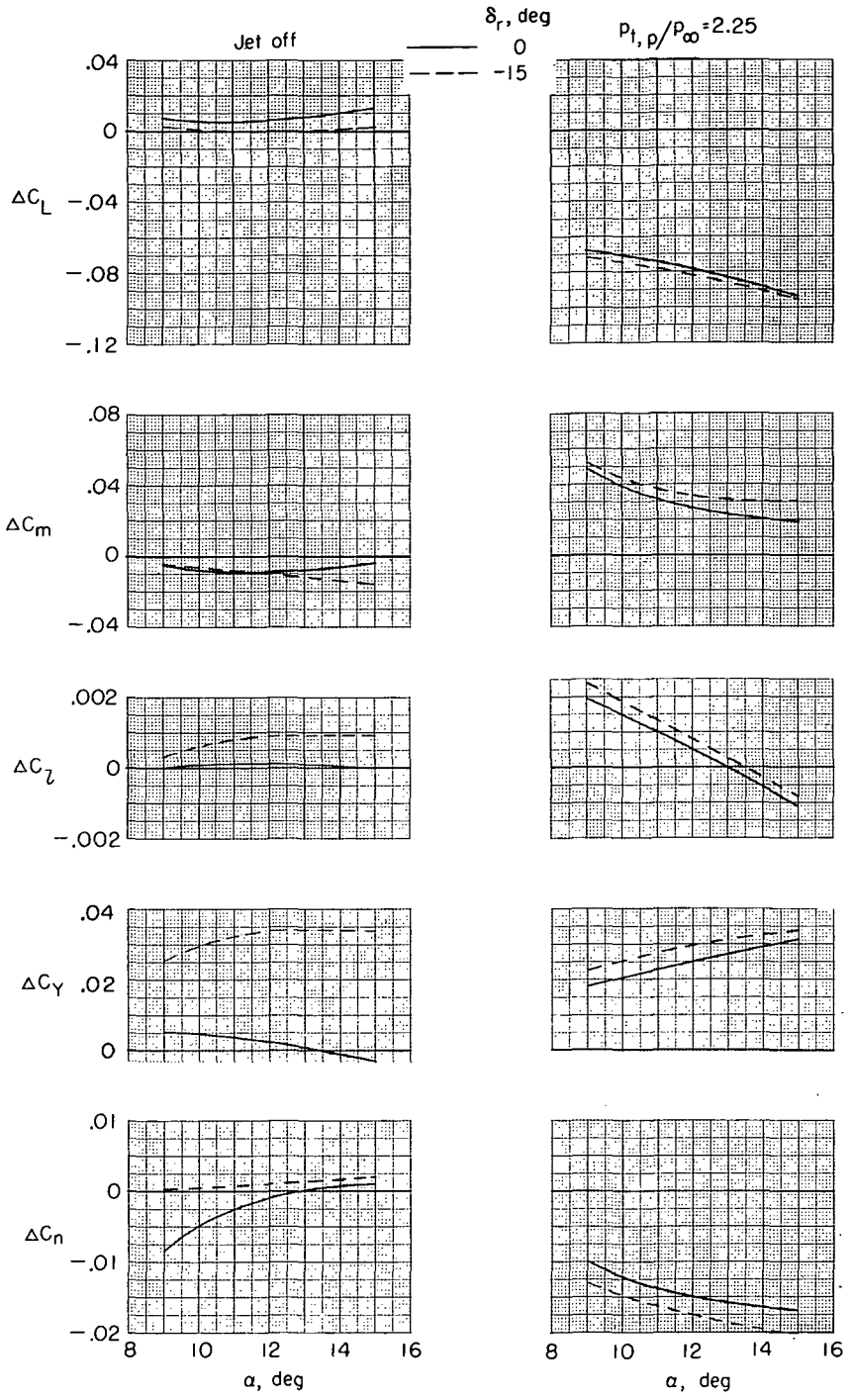

(a) M = 0.23; $\beta = 10^o$; $\delta_f = -30^o$; $\delta_s = -20^o$; $\delta_h = -10^o$; δ_b = 75 percent.

Figure 55.- Variation of TCU (reverse-thrust mode) incremental aerodynamic characteristics with angle of attack for various rudder deflections. $\delta_{du} = 32.5^o$; $\delta_{dl} = 52.5^o$; and military power.

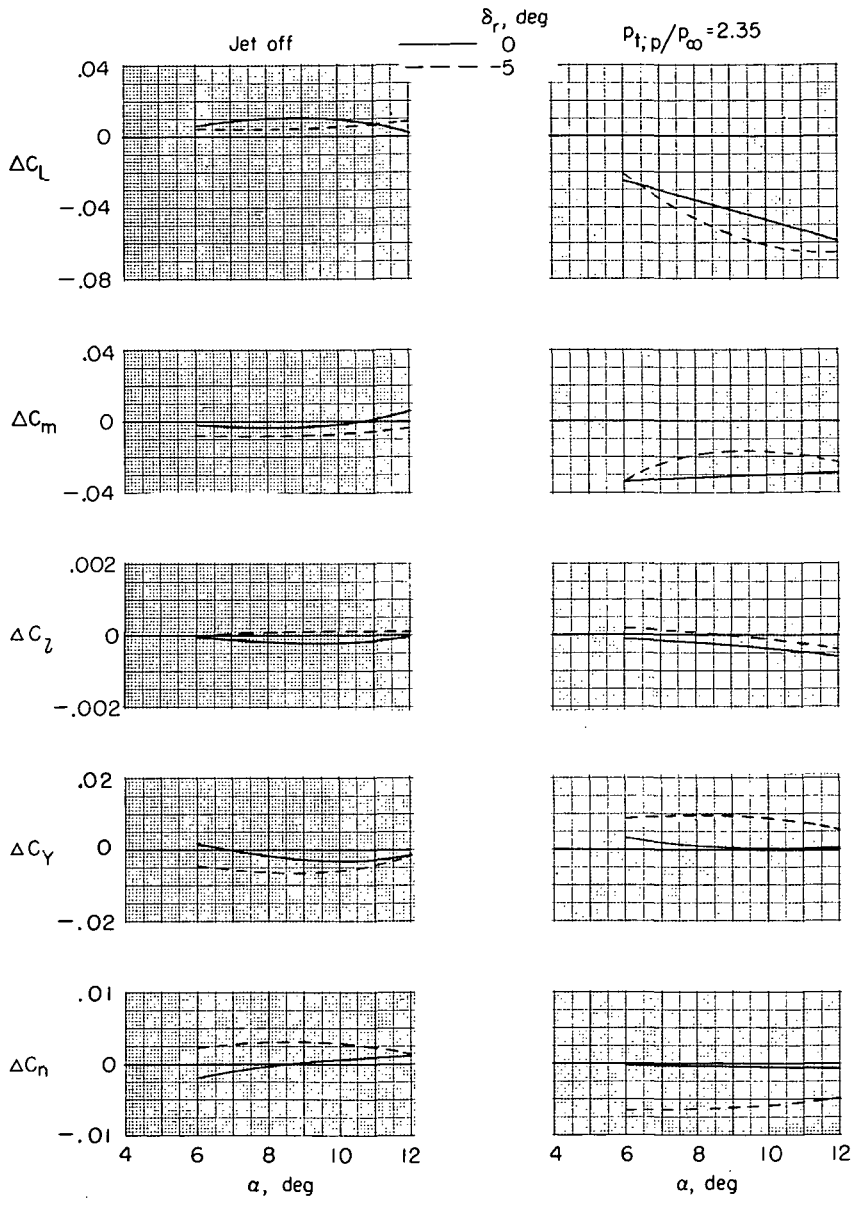

(b) M = 0.34; $\beta = 0^o$; $\delta_f = 0^o$; $\delta_s = 0^o$; $\delta_h = -1.5^o$; δ_b = 100 percent.

Figure 55.- Continued.

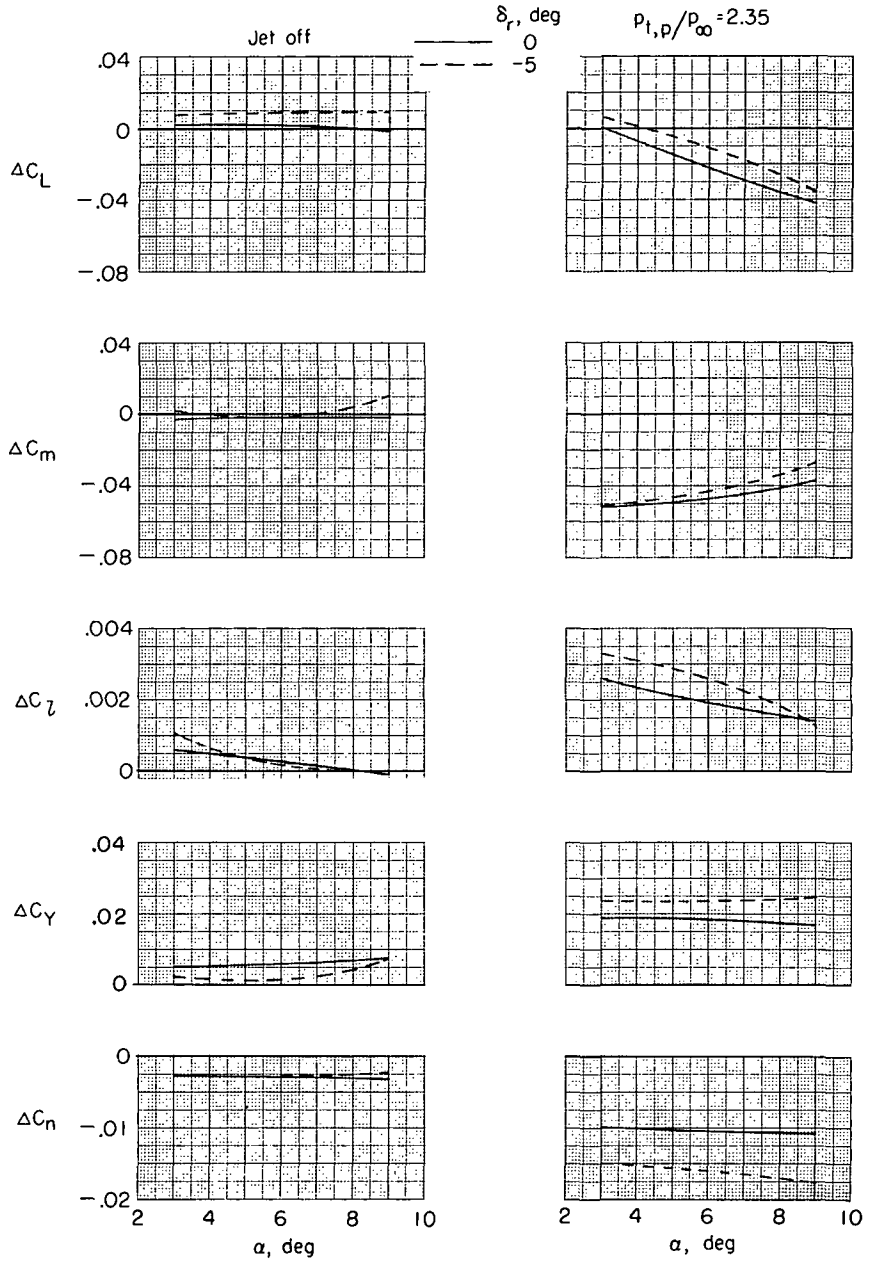

(c) M = 0.34; $\beta = 5^o$; $\delta_f = 0^o$; $\delta_s = 0^o$; $\delta_h = -1.5^o$; δ_b = 100 percent.

Figure 55.- Continued.

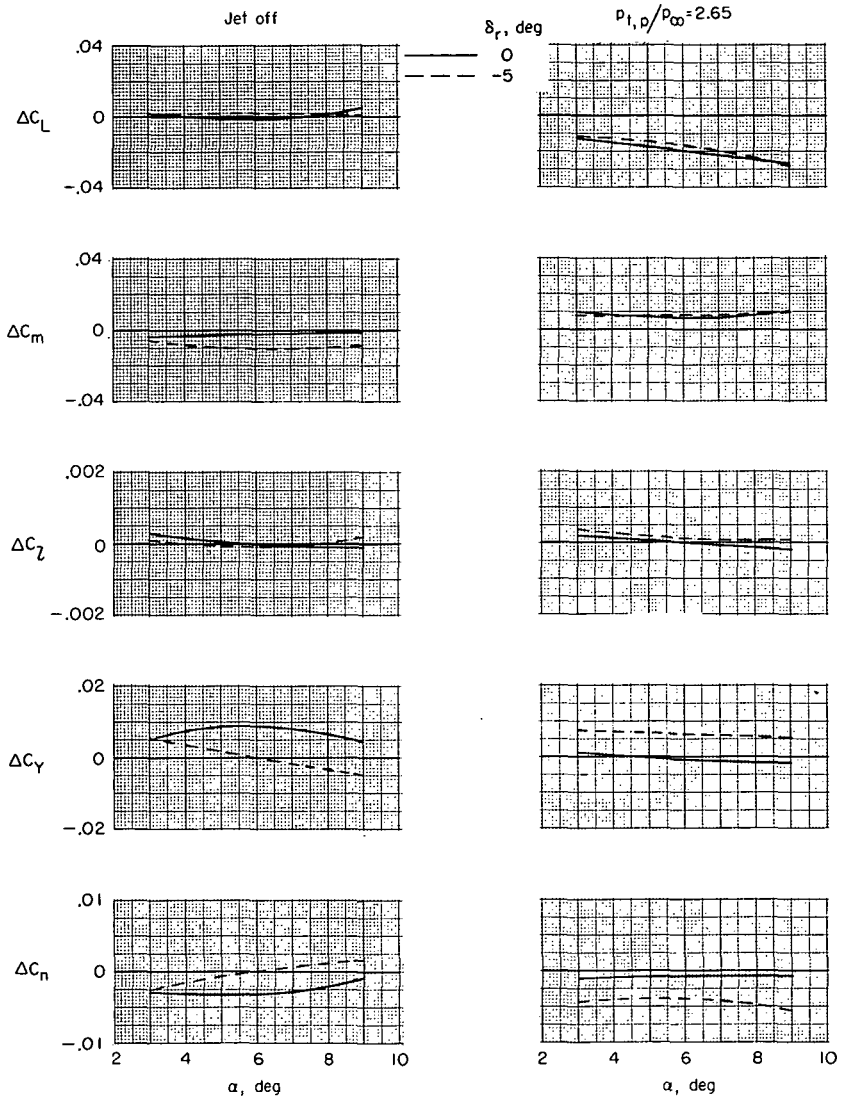

(d) M = 0.60; $\beta = 0^o$; $\delta_f = 0^o$; $\delta_s = 0^o$; $\delta_h = -1.5^o$; δ_b = 100 percent.

Figure 55.- Continued.

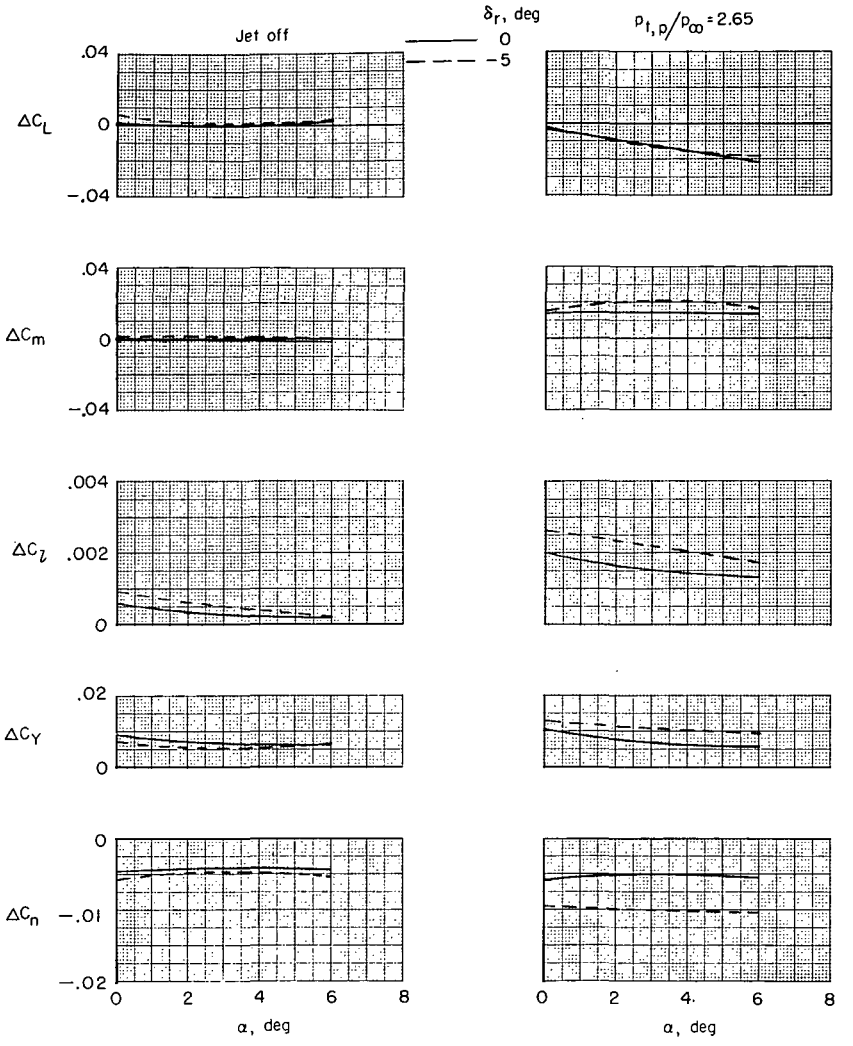

(e) M = 0.60; $\beta = 5^o$; $\delta_f = 0^o$; $\delta_s = 0^o$; $\delta_h = -1.5^o$; δ_b = 100 percent.

Figure 55.- Continued.

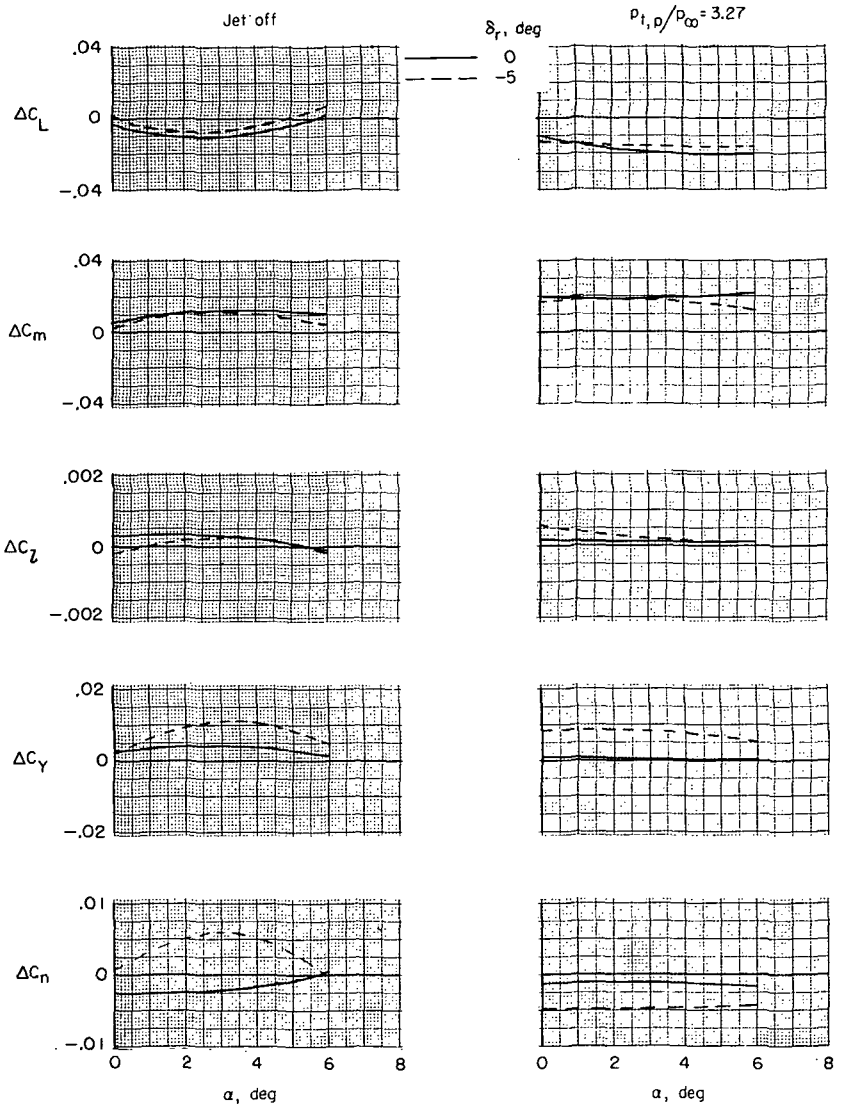

(f) M = 0.90; $\beta = 0^o$; $\delta_f = 0^o$; $\delta_s = 0^o$; $\delta_h = -1.5^o$; δ_b = 100 percent.

Figure 55.- Continued.

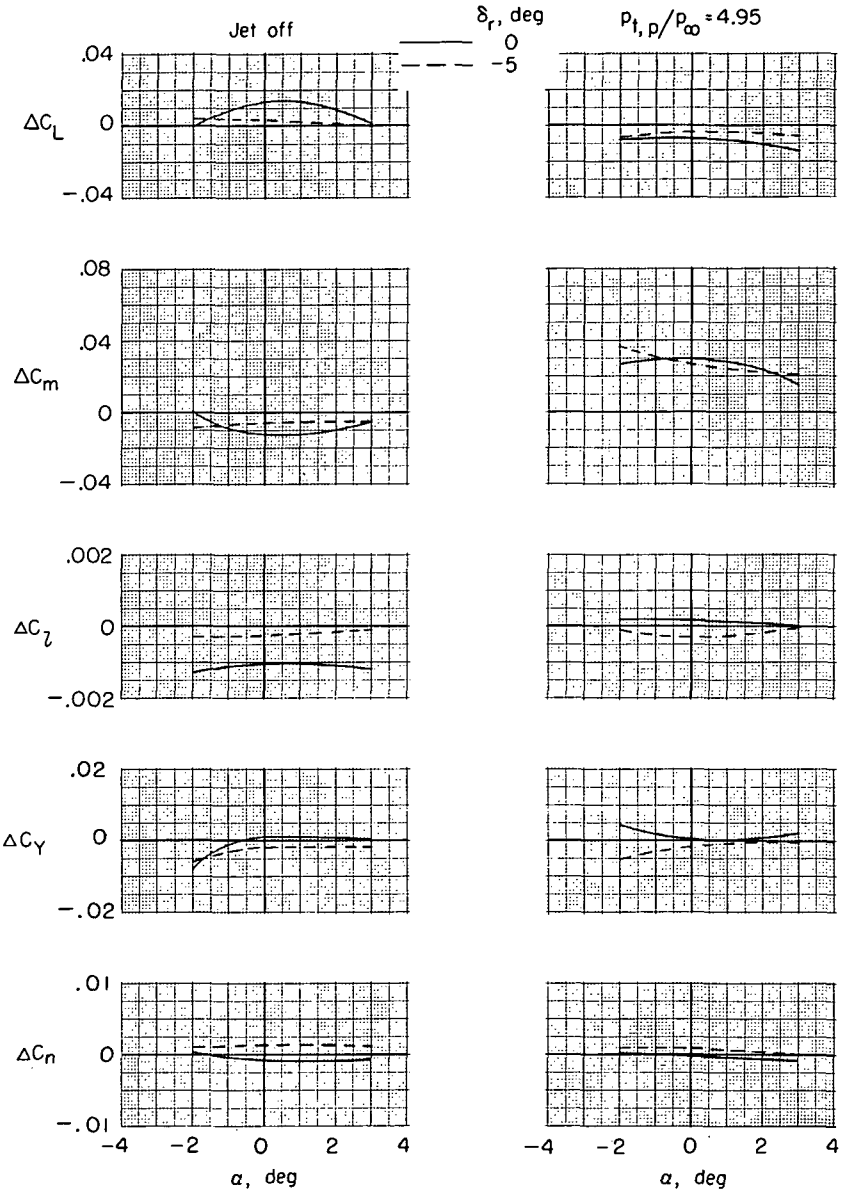

(g) M = 1.30; $\beta = 0^o$; $\delta_f = 0^o$; $\delta_s = 0^o$; $\delta_h = -1.5^o$; δ_b = 100 percent.

Figure 55.- Concluded.

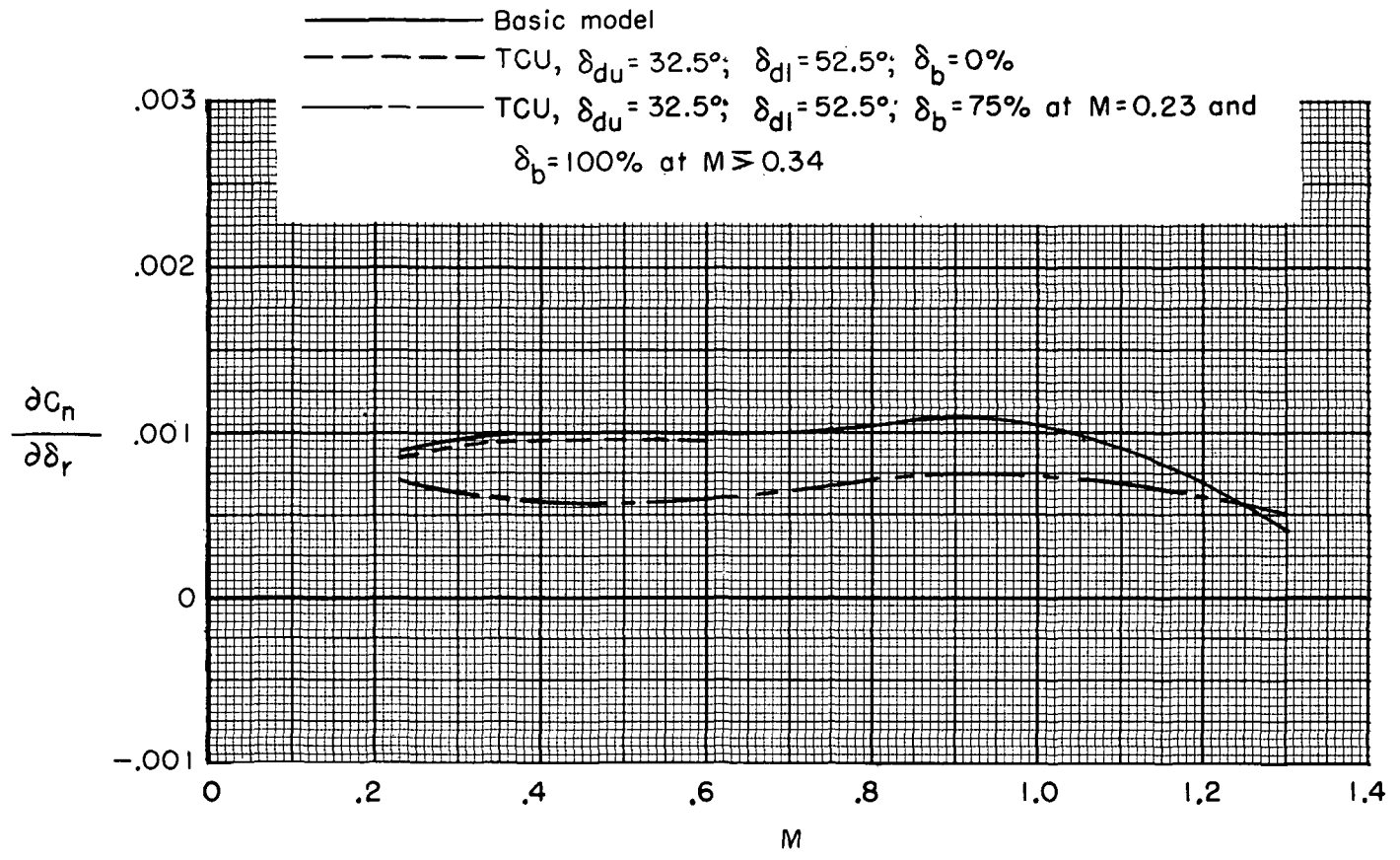

Figure 56.- Rudder effectiveness of basic model and TCU (reverse-thrust mode) for Mach range and at scheduled jet-total-pressure ratios. Military power.

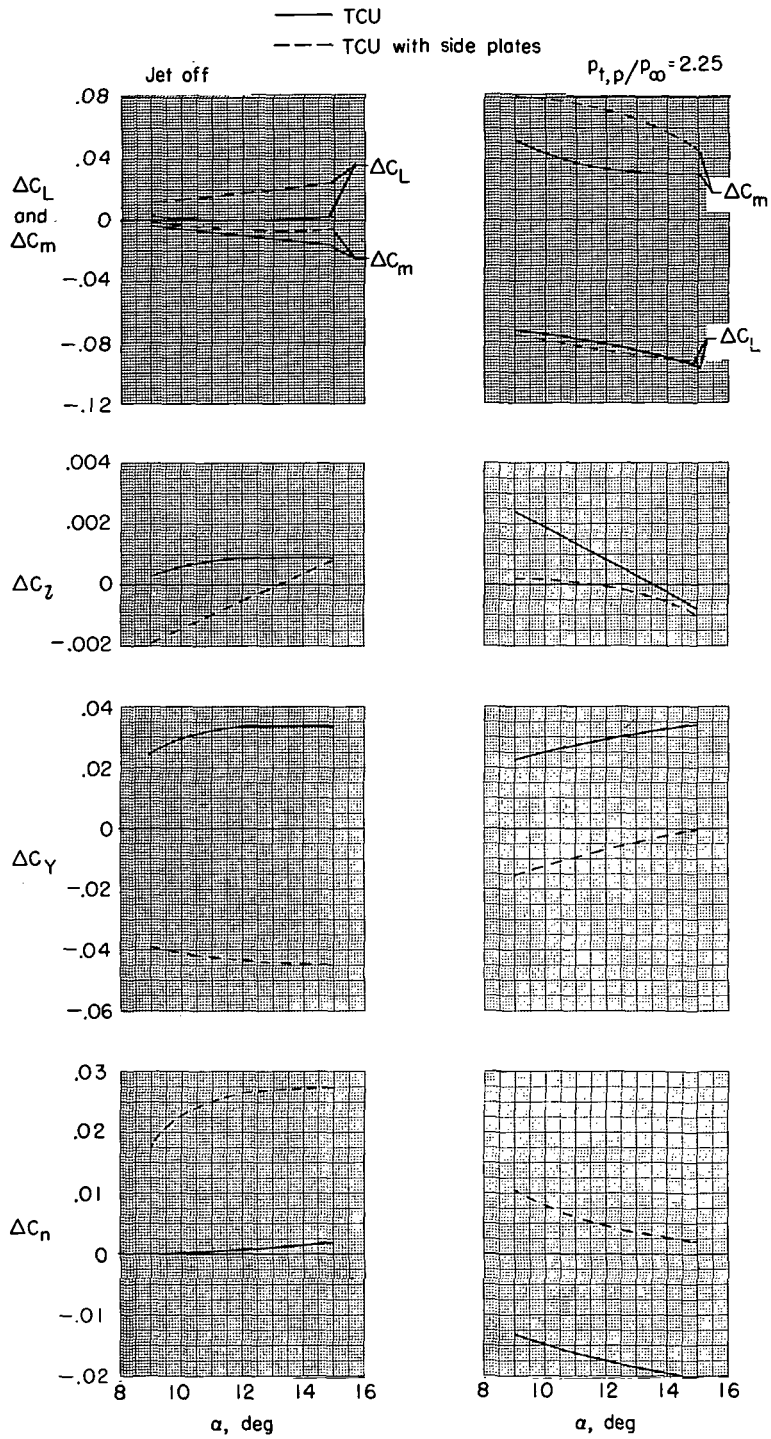

(a) M = 0.23; $\beta = 10^o$; $\delta_f = -30^o$; $\delta_s = -20^o$; $\delta_h = -10^o$; δ_b = 75 percent.

Figure 57.- Variation of incremental aerodynamic characteristics of TCU (reverse-thrust mode) with angle of attack for model with geometric fixes on upper deflector doors. $\delta_r = 0^o$; $\delta_{du} = 32.5^o$; $\delta_{dl} = 52.5^o$; and military power.

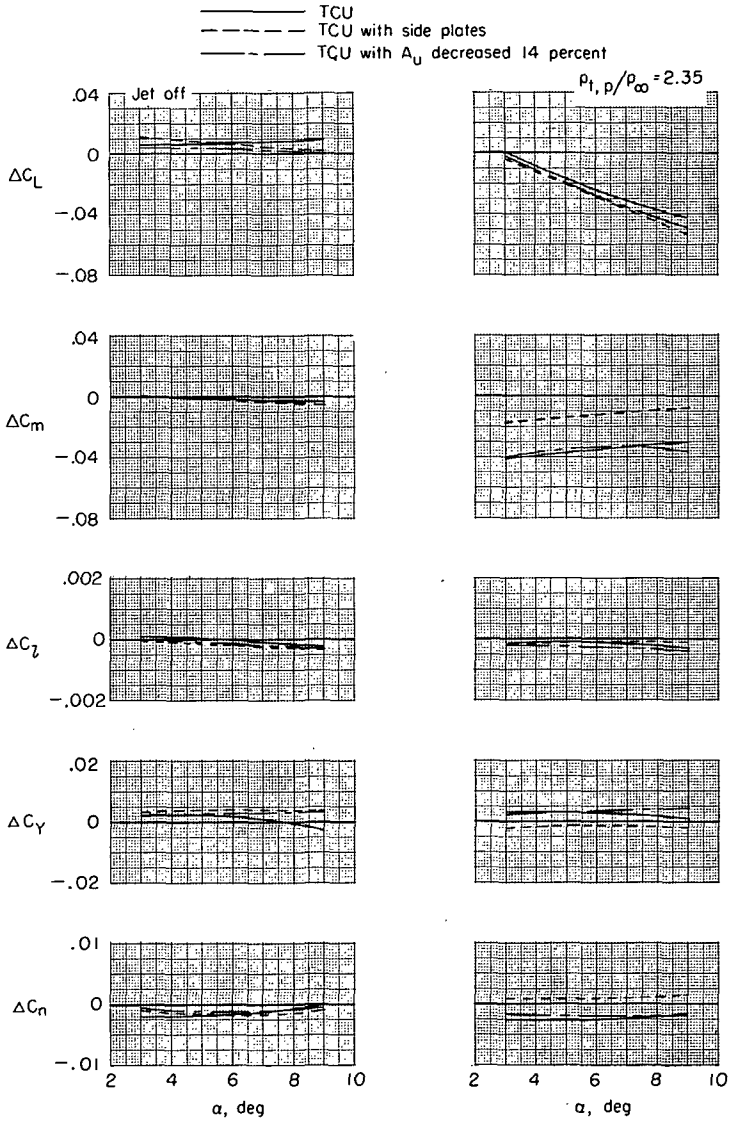

(b) $M = 0.34$; $\beta = 0^o$; $\delta_f = 0^o$; $\delta_s = 0^o$; $\delta_h = -1.5^o$; $\delta_b = 100$ percent.

Figure 57.- Continued.

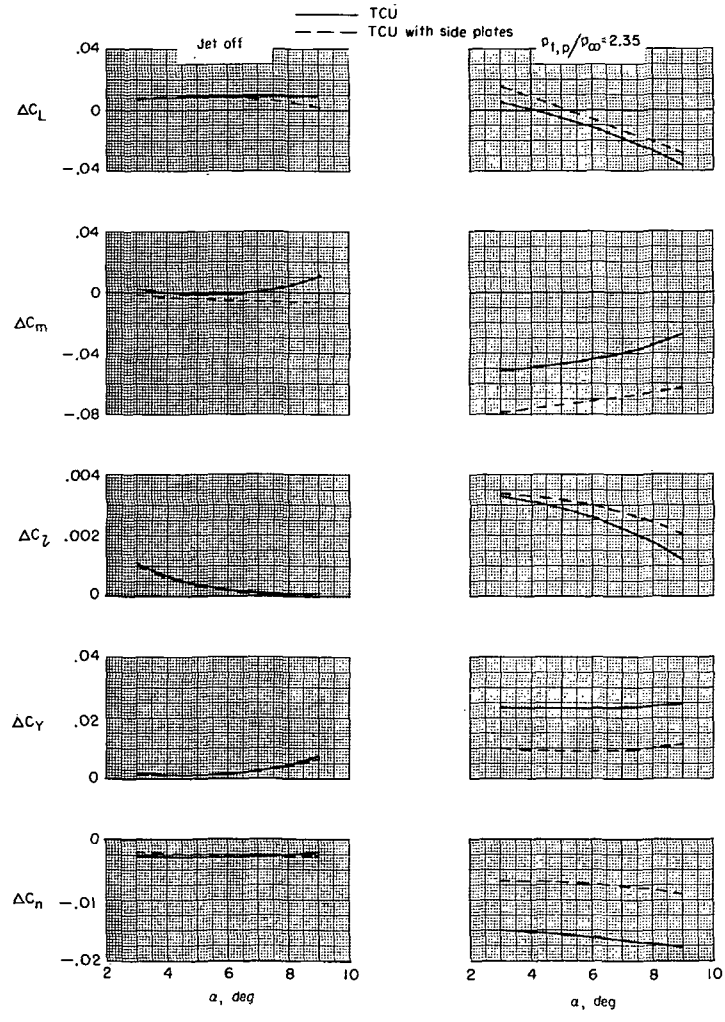

(c) M = 0.34; $\beta = 5^{o}$; $\delta_f = 0^{o}$; $\delta_s = 0^{o}$; $\delta_h = -1.5^{o}$; δ_b = 100 percent.

Figure 57.- Continued.

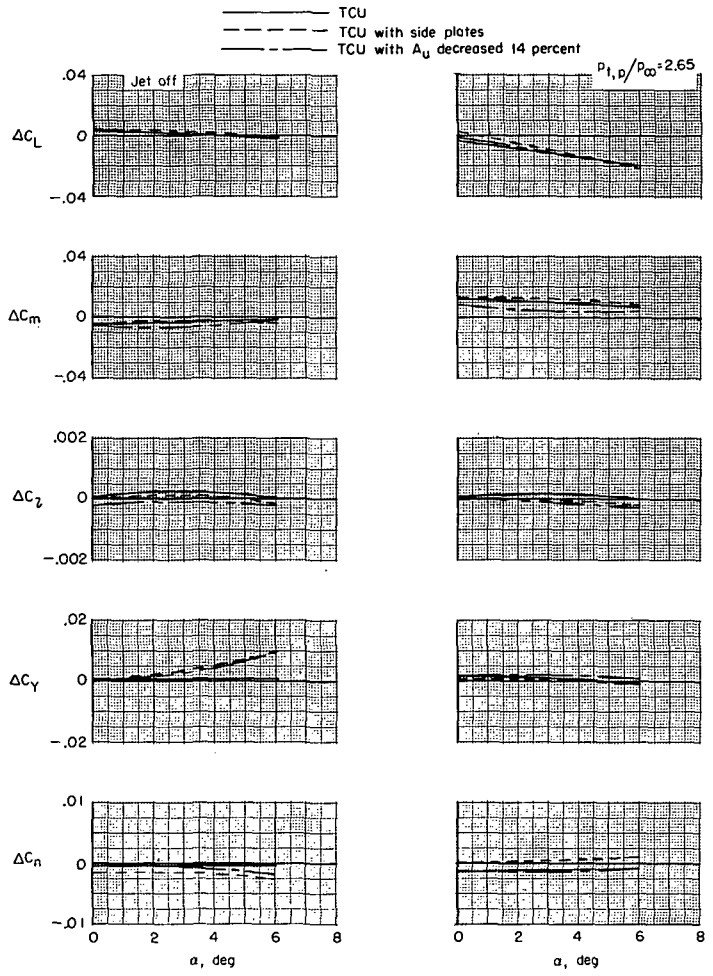

(d) M = 0.60; $\beta = 0^o$; $\delta_f = 0^o$; $\delta_s = 0^o$; $\delta_h = -1.5^o$; δ_b = 100 percent.

Figure 57.- Continued.

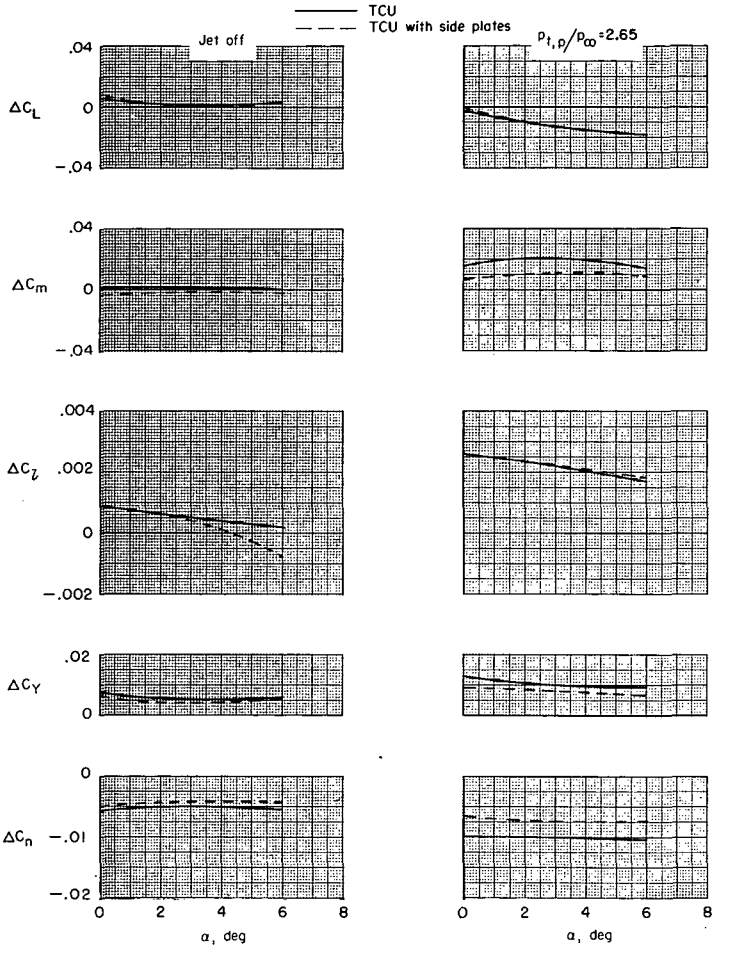

(e) M = 0.60; $\beta = 5^{o}$; $\delta_f = 0^{o}$; $\delta_s = 0^{o}$; $\delta_h = -1.5^{o}$; δ_b = 100 percent.

Figure 57.- Continued.

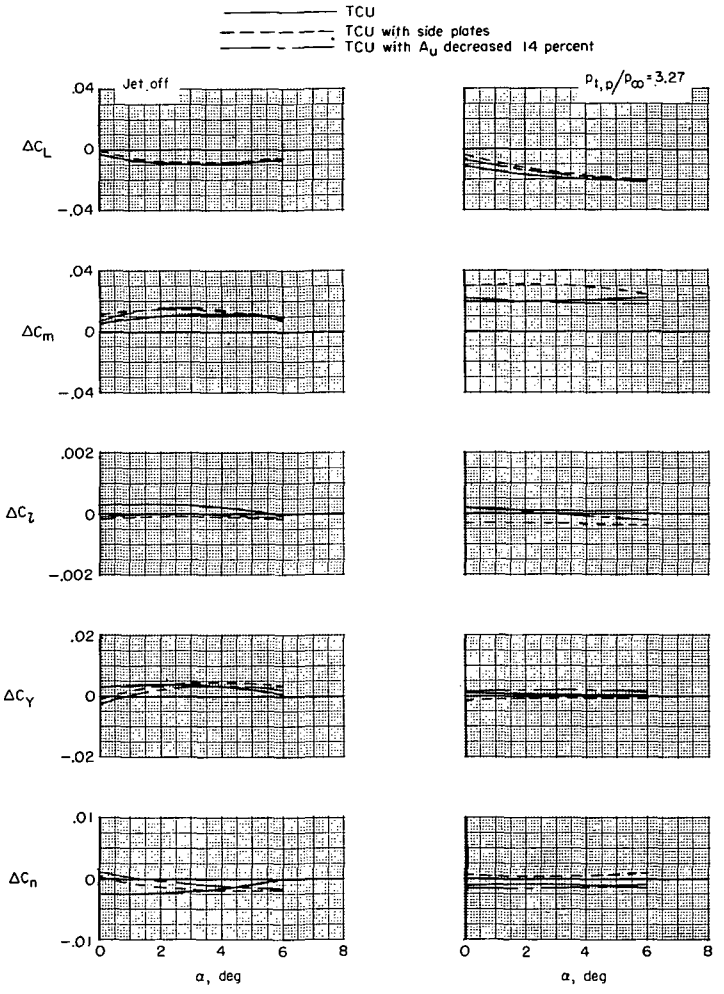

(f) M = 0.90; $\beta = 0^o$; $\delta_f = 0^o$; $\delta_s = 0^o$; $\delta_h = -1.5^o$; δ_b = 100 percent.

Figure 57.- Continued.

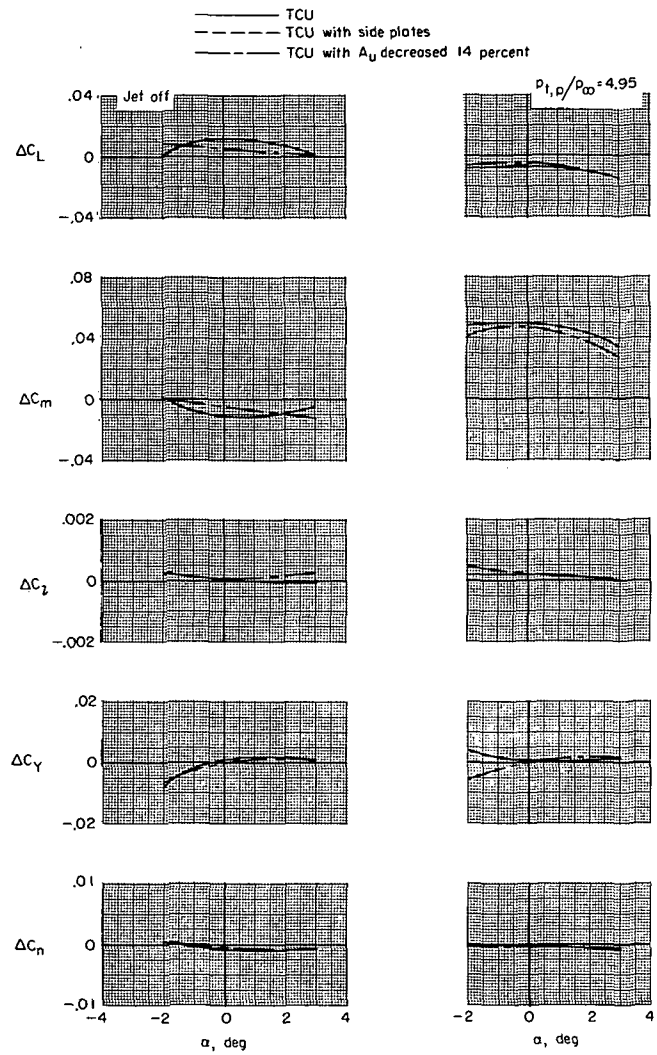

(g) M = 1.30; $\beta = 0^o$; $\delta_f = 0^o$; $\delta_s = 0^o$; $\delta_h = -1.5^o$; $\delta_b = 100$ percent.

Figure 57.- Concluded.

"The aeronautical and space activities of the United States shall be conducted so as to contribute . . . to the expansion of human knowledge of phenomena in the atmosphere and space. The Administration shall provide for the widest practicable and appropriate dissemination of information concerning its activities and the results thereof."

—NATIONAL AERONAUTICS AND SPACE ACT OF 1958

NASA SCIENTIFIC AND TECHNICAL PUBLICATIONS

TECHNICAL REPORTS: Scientific and technical information considered important, complete, and a lasting contribution to existing knowledge.

TECHNICAL NOTES: Information less broad in scope but nevertheless of importance as a contribution to existing knowledge.

TECHNICAL MEMORANDUMS: Information receiving limited distribution because of preliminary data, security classification, or other reasons. Also includes conference proceedings with either limited or unlimited distribution.

CONTRACTOR REPORTS: Scientific and technical information generated under a NASA contract or grant and considered an important contribution to existing knowledge.

TECHNICAL TRANSLATIONS: Information published in a foreign language considered to merit NASA distribution in English.

SPECIAL PUBLICATIONS: Information derived from or of value to NASA activities. Publications include final reports of major projects, monographs, data compilations, handbooks, sourcebooks, and special bibliographies.

TECHNOLOGY UTILIZATION PUBLICATIONS: Information on technology used by NASA that may be of particular interest in commercial and other non-aerospace applications. Publications include Tech Briefs, Technology Utilization Reports and Technology Surveys.

Details on the availability of these publications may be obtained from:

SCIENTIFIC AND TECHNICAL INFORMATION OFFICE

NATIONAL AERONAUTICS AND SPACE ADMINISTRATION

Washington, D.C. 20546